# Quantitative analysis and biomechanical modeling of the balance alteration during aging

Celia Amabile

## ▶ To cite this version:

Celia Amabile. Quantitative analysis and biomechanical modeling of the balance alteration during aging. Biomechanics [physics.med-ph]. Ecole nationale supérieure d'arts et métiers - ENSAM, 2016. English. NNT : 2016ENAM0031 . tel-01381264

## HAL Id: tel-01381264
## https://pastel.hal.science/tel-01381264

Submitted on 14 Oct 2016

**HAL** is a multi-disciplinary open access archive for the deposit and dissemination of scientific research documents, whether they are published or not. The documents may come from teaching and research institutions in France or abroad, or from public or private research centers.

L'archive ouverte pluridisciplinaire **HAL**, est destinée au dépôt et à la diffusion de documents scientifiques de niveau recherche, publiés ou non, émanant des établissements d'enseignement et de recherche français ou étrangers, des laboratoires publics ou privés.

2016-ENAM-0031

École doctorale n° 432 : Science des Métiers de l'ingénieur

## Doctorat ParisTech

# T H È S E

**pour obtenir le grade de docteur délivré par**

## l'École Nationale Supérieure d'Arts et Métiers

**Spécialité " Biomécanique "**

*présentée et soutenue publiquement par*


**Celia AMABILE**


le 27 septembre 2016

# Quantitative analysis and biomechanical modeling of the balance alteration during aging

Directrices de thèse : **Wafa SKALLI, Virginie LAFAGE**
Co-encadrement de la thèse : **Hélène PILLET, Bertrand MOAL**

**Jury**

| | |
|---|---|
| **M. David MITTON**, Professeur, Laboratoire de biomécanique et mécanique des chocs, IFFSTAR, Université de Lyon, Lyon | Président |
| **M. Hugues PASCAL-MOUSSELARD**, Professeur, Hôpital de la Pitié-Salpétrière, Paris | Rapporteur |
| **M. Andrew PHILLIPS**, Senior Lecturer, Department of Civil and Environmental Engineering, Imperial College London, Londres | Rapporteur |
| **M. Philippe GORCE**, Professeur, Laboratoire de biomodélisation et d'ingénierie des handicaps (HANDIBIO), Université de Toulon, Toulon | Examinateur |
| **M. Michel RITZ**, Médecin, Centre de l'Arche, Saint-Saturnin | Examinateur |
| **Mme Virginie LAFAGE**, Docteur, Hospital for Special Surgery, New York City | Examinateur |
| **Mme Hélène PILLET**, Maître de Conférences, Institut de Biomécanique Humaine Georges Charpak, Arts et Métiers ParisTech, Paris | Examinateur |
| **Mme Wafa SKALLI**, Professeur, Institut de Biomécanique Humaine Georges Charpak, Arts et Métiers ParisTech, Paris | Examinateur |
| **M. Bertrand MOAL**, Docteur, Institut de Biomécanique Humaine Georges Charpak, Arts et Métiers ParisTech, Paris | Invité |

T H È S E

**Arts et Métiers ParisTech - Campus de Xxxx**
**Institut de Biomécanique Humaine Georges Charpak**

*Le corps et l'esprit sont une même chose,*
*vue sous deux angles différents.*
*Et nul ne sait ce que peut le corps.*

*L'Éthique*
*Spinoza*

*Points Seuil, 1999*

# REMERCIEMENTS

Une thèse est le résultat de trois ans de travail riches en rencontres, échanges et collaborations. Beaucoup de personnes ont permis la réalisation de ce travail par leurs échanges, aides, expertises, collaborations et soutiens. J'ai enfin l'occasion de les remercier ici.

Je voudrais tout d'abord remercier l'ensemble des membres du jury pour leur participation à ce jury. Je remercie particulièrement le Pr Pascal-Mousselard et le Dr Andrew Phillips d'avoir accepté de rapporter ce travail de thèse. Je remercie le Pr Philippe Gorce, le Pr David Mitton et le Dr Michel Ritz d'avoir accepté de participer au jury en tant qu'examinateurs.

Je remercie l'ensemble de l'équipe encadrante de cette thèse: Wafa Skalli, Virginie Lafage, Bertrand Moal et Hélène Pillet.

Je remercie tout d'abord Wafa Skalli d'avoir dirigé cette thèse. Votre vision à long terme du projet dans lequel s'inscrit cette thèse et votre sens critique ont grandement influencé ce travail.

Je remercie vivement Virginie Lafage pour son expertise et expérience. Merci de m'avoir accueillie si naturellement dans l'équipe à NY, merci pour tous les moments partagés avec l'équipe là-bas. Enfin merci pour nos discussions autour du contexte clinique entourant ce travail.

Je remercie grandement Hélène Pillet d'avoir toujours été présente lors de cette thèse, d'avoir pu se rendre disponible pour n'importe quelle question. Merci de m'avoir encouragée à prendre du recul à chacune de nos discussions. Enfin merci pour ton soutien lors de ces 3 années.

Je remercie Bertrand Moal pour nos discussions autour des protocoles d'acquisitions IRM, pour la reconstruction musculaire et pour la valorisation de ces travaux.

Je remercie les financeurs du programme de chaires ParisTech BiomecAM en modélisation biomécanique personnalisée, porté par la Fondation ParisTech : la Société Générale, le Groupe COVEA, la Société PROTEOR et la Fondation Yves Cotrel pour la recherche en pathologie rachidienne, pour leur contribution à environnement scientifique qui m'a permis de conduire cette recherche dans les meilleures conditions.

Je remercie la Commission Fulbright d'avoir financé un séjour de 6 mois aux Etats-Unis lors de ma thèse. Merci particulièrement à Séverine Peyrichou et Emily Resnier pour leur patience et bienveillance au cours du processus de sélection mais aussi pendant mon séjour ainsi qu'à mon retour. Merci à Jennifer Skiba pour avoir facilité ce séjour aux Etats-Unis et pour sa réactivité à mes questions administratives américaines.

I thank deeply Philippe Rouch and Frank Schwab for their welcoming in their respective teams.

Je remercie l'ensemble des sujets et volontaires ayant accepté de participer aux collectes de données utilisées dans cette thèse.

Je remercie le Dr Bronsard et le Dr Antoine Iannessi du CHU de Nice pour avoir collecté les données IRM de jeunes asymptomatiques et pour nos échanges autour du traitement des données et de leur valorisation.

Je voudrais remercier le Pr Carlier et le Dr Marty ainsi que l'ensemble de leurs équipes à l'Hôpital Raymond Poincaré pour la collaboration mise en place autour d'une collecte de données EOS + IRM d'adultes vieillissants asymptomatiques.

I would like to thank José Raya from Hospital for Special Joint Diseases (NYU) for his expertise and advices on MRI acquisitions. I would like to thank all the NYU team and especially José Raya for the data collection of adults with spinal deformities during Bertrand Moal's PhD.

Je remercie le Pr Vital et le Pr Barrey pour notre collaboration autour de l'analyse de l'alignement postural de jeunes asymptomatiques dont les radiographies provenaient de la base de données de l'Institut.

Je remercie le Pr Le Huec pour nos travaux communs à partir de radiographies EOS précédemment collectées à Bordeaux, je remercie également Carolyn Anglin d'EOS Imaging pour son aide sur ce travail.

Merci au Dr Xavier Ohl pour son aide et sa convivialité lors de la collecte de données EOS de jeunes asymptomatiques à l'Institut.

Je remercie également Véronique Schmitt et son équipe du Centre de Recherche Paul Pascal à Bordeaux pour leur patience et leur expertise dans la fabrication de fantômes graisseux pour IRM.

I would like to thank Dr Schwab and Dr Lafage and the whole NYU and HSS teams for their incredible welcoming during my 6 months stay. Particularly thanks to Alexandra, Bart, Bassel, Bojana, Bradley, Hongda, Jeffrey, Jensen, Renaud and Ziad for the nice talks and moments during the work and outside. Thanks to all the HSS and NYU teams for the moments in San Diego and Minneapolis.

Je remercie Oussama Arous Chtara et Cédric Maillot avec qui j'ai eu le plaisir de travailler pendant ma thèse. Merci Cédric pour ton point de vue de médecin lors nos discussions autour du modèle et de ses possibles applications.

Je remercie Dominique Bonneau pour nos discussions passionnantes sur l'anatomie musculaire et squelettique. Merci pour vos cours d'anatomie d'une limpidité rare et pour nos conversations autour des rôles de muscles spécifiques. Enfin merci pour votre disponibilité afin de discuter de tout cela et votre bonne humeur lors de nos échanges.

Je remercie Vincent Pomero pour son aide sur le modèle musculo-squelettique et notamment pour sa réactivité afin de nous apporter son expertise dans l'adaptation de modèle. Le modèle a pu être adapté aux nouveaux algorithmes avec l'aide précieuse de Maxime Van den Abbeele, Sylvain Persohn et Aurélien Laville. Merci Maxime pour nos journées sans fin sur Matlab et pour ta patience lors de celles-ci. Merci Sylvain et Aurélien pour vos suggestions et vos idées toujours précieuses sur les questions de recalage et krigeage.

Merci à Cédric, Oussama et Hongda pour avoir reconstruit en 3D les muscles étudiés dans cette thèse. Merci Sonia pour ton expertise en reconstructions EOS et ta réactivité quand il a fallu dans l'urgence traiter les radios de plusieurs sujets. Merci Maria pour ton aide lors des essais pour calibration de la plateforme de force, et lors des collectes de données.

Je remercie particulièrement Brigitte Roux de la Fondation ParisTech pour son support permanent au sein de la Fondation.

Merci à Mohamed et Thomas sans qui cette thèse ne serait pas la même. Mohamed merci pour ta réactivité et ton professionnalisme pour trouver les articles introuvables et ce toujours dans les moments les plus pressés. Merci Thomas pour avoir sauvé mon manuscrit de thèse au moins trois fois. Merci aussi pour ton expertise sur le traitement des images EOS comme IRM.

Je voudrais très chaleureusement remercier Marine pour son efficacité, son aide tout au long des 3 ans, notamment pour toutes mes questions administratives et autres. Merci notamment d'avoir géré la partie administrative de la soutenance jusqu'au dernier moment, cela m'a permis de gérer les derniers jours avec une confiance totale dans la bonne organisation de cette journée. Je continue de penser que le labo tourne en grande partie grâce à toi. Merci pour ton aide sur la gestion de la cellule plus belle la vie du labo. Enfin merci pour ta bonne humeur, nos rires, nos discussions variées et tout le reste. Une vraie belle rencontre du labo !

J'ai eu la chance d'avoir été accueillie et chouchoutée dès mon arrivée par une dream team de doctorants: merci à Coralie, Guillaume, Léo, Lucas, Marianne, Marion, Mary et Rivka. Ça a été super d'arriver dans cette ambiance-là, de pouvoir participer tout de suite à la règle de nouvelle arrivée = gâteau (merci Rivka, Mary et Marianne), de pouvoir m'investir dans le labo avec une cellule vie de labo (merci Guillaume), de découvrir les gros appétits du labo (merci Léo et Lucas), de monter un plancher surélevé avec moquette au retour de vacances de Noël (merci Léo), de découvrir une chanteuse et sprinteuse de talent (merci Marion), de me découvrir une collègue anglaise de natation synchro (merci Coralie), de papoter sur tout et rien (merci Mary et Marianne). Pour tout ça, merci !

Merci à tous les membres de l'Institut qui ont accepté de me faire répéter pour la soutenance: merci pour votre patience, votre temps, vos corrections, suggestions et questions. J'espère que la version finale vous aura convaincus de l'utilité de ces répétitions. Une mention spéciale à Boris et ses incroyables connaissances en power point pour transformer des images: merci pour tes trucs et astuces, et ton expertise. J'espère par cette phrase ne pas provoquer un déluge de questions sur PPT de la part des gens du labo !

Je remercie très fortement mes collègues de bureau, Agathe, Anthony et Cheng, pour la convivialité, les discussions, échanges et moments précieux de décompression. Merci Anthony pour nos batailles navales, merci Cheng pour nos discussions variées. Merci Agathe pour ta bonne humeur, ton expertise pour tout ce qui touchait à EOS, aux figures Matlab. Merci pour ta gentillesse et ta générosité, le travail en équipe que l'on a pu réaliser ensemble et avec Julie reste une expérience à part dans la thèse. Merci pour tous nos échanges au-dessus de nos deux ordis et surtout pour nos longues discussions bien animées à 8h du matin !

Merci à Claudio, Clayton, Dominique, Jennyfer et Julie qui ont rendu mon arrivée au labo très sympathique. Merci Claudio pour toutes tes idées, ta patience et ton expertise lorsque j'avais une question. Merci pour ton soutien et nos échanges au sujet de mon sujet de thèse. Merci à Clayton pour nos discussions sympathiques et pour ta connaissance du disque inter-vertébral. Merci à Dominique pour m'avoir désignée pour reprendre la cellule plus belle la vie du labo, j'ai vraiment apprécié toutes nos discussions majoritairement autour de ce que l'on mangeait. Merci à Jennyfer pour ton enthousiasme et ta bonne humeur, merci pour tes encouragements tout au long de la thèse. Merci Julie pour notre travail ensemble, j'ai vraiment apprécié travailler en équipe avec quelqu'un d'aussi motivé et rigoureux. Merci pour tes encouragements et ton soutien, même au bout du monde !

Merci encore à Aurélien et Sylvain pour nos conversations matinales et notre partage fructueux des nouvelles internet du monde entier. Merci encore pour avoir partagé votre expérience et expertise dans des domaines très variés !

Merci à Maria et Sonia pour leurs gentillesses et leurs patiences. Merci d'être toujours disponibles et tout cela dans la bonne humeur.

Merci à ceux que j'ai brièvement croisé, avec qui les échanges ont toujours été sympathiques: Ayman, Sergio, Xavier. Merci à tous au labo pour l'ambiance très sympathique: Alice, Aurélien, Boris, Francois, Jérémy, Karine, Laura, Laurent, Louis, Léopold, Maxim, Maxime, Miassa, Nicolas, Shahin, Thomas, Valérie, Zoé.

Merci à Coralie et Joseph d'être toujours aussi enthousiastes lors de vos passages au labo, c'est toujours un plaisir de vous voir et ce depuis la manip de marche au CERAH !

Merci à tous les maîtres de conf et assimilés pour votre soutien, vos idées, vos suggestions et vos encouragements: Baptiste, Christophe, Damien, Hélène, Pierre-Yves Rohan, Rachele, Sébastien, et Xavier.

Enfin je remercie l'ensemble des membres de l'Institut pour la bonne ambiance qui y règne, ce fût un réel plaisir de venir travailler tous les jours dans un tel environnement.

Je remercie l'ensemble de mes amis de l'ESPCI, notamment Amaury, Axel, Bénédicte, Claire, Fanny, François M., François P., Hugo, Jean, Joachim, Lauriane, Léopold, Lucie, Marianne, Marine, Maya, Nicolas, Pascaline, Paul, Pauline, Perrine, Pierre, Rémi F., Rémi M., Ruben, Stéphane, Victor et plein d'autres ! Merci pour tous les moments passés ensemble lors de ces 3ans, toujours aussi sympa de pouvoir découvrir les boulots ou thèses aux antipodes de mon travail.

Merci Bénédicte, Fanny, Marianne et Pascaline pour tout ce que l'on partage depuis notre rencontre en 1ère année de PC.

Merci Pierre, Rémi et Ruben pour avoir constitué le meilleur groupe de tutorat de PC. Ruben, merci pour nos séances de TP en binôme qui restent un super souvenir.

Merci aux copines Claire, Maya et Perrine pour notre année londonienne et tout ce que nous avons partagé pendant cette super année.

Merci Joachim d'être un copain délégué de promo aussi cool !

Je remercie les copains marseillais pour nos rendez-vous pas assez fréquents mais toujours supers sympas: Alix, Aurélie, Fayçal, Laury, Manon, Nathanaël, Olivier et Quentin. Merci particulièrement à Alix et Laury d'être venue à la soutenance !

Je remercie ma famille et notamment oncles et tantes ainsi que les nombreux cousins. Merci d'avoir confronté mon travail à vos questions, un exercice de vulgarisation pas toujours facile. Avoir une famille si nombreuse ait une vraie chance et en être aussi proche est très important pour moi. Encore merci pour votre soutien au long de ces 3 ans.

Merci particulièrement à Philippe pour avoir suivi avec intérêt mon parcours dans le biomédical. Je pense que la fascination que j'avais petite pour les parapluies qui se déplient dans les vaisseaux sanguins (stents) sur lesquels tu travaillais, ont été pour beaucoup dans mes choix de carrières.

Je remercie mes grands-parents Jacques, Marie-Jeanne, Nelly et Silvio de m'avoir transmis tant de connaissances variées: de savoir-être, de savoir-faire, de livres, de recettes et d'histoire familiales. Merci d'être toujours aussi présents et attentifs.

Je voudrais remercier mes frères, Arno, Loris et Aurélien. Merci les garçons de me supporter, de m'avoir toujours soutenue et de s'être toujours intéressés à mon travail. Merci aussi pour vos passages réguliers à Paris lors de cette thèse.

Nicolas, je voudrais te remercier pour tout ce que tu m'as apporté depuis que l'on se connaît. Ton soutien quotidien pendant cette thèse a été essentiel pour présenter ce travail sous cette forme. Merci pour ta patience, tes encouragements et ton écoute lors de ces 3 ans.

Enfin je voudrais remercier mes parents. Merci d'être des coachs hors pair, et de vous intéresser autant à mon travail. Merci d'être toujours à l'écoute et ce depuis toujours. Enfin merci de m'avoir encouragée depuis toujours dans mes études, de m'avoir répété que même lorsque quelque chose paraissait inatteignable, on pouvait toujours y prétendre et parfois le décrocher. Bref que l'on peut mieux faire.

# Contents

# RÉSUMÉ LONG EN FRANÇAIS

## R - 1 Introduction générale

Le vieillissement mondial de la population (22% de personnes plus âgées que 60 ans dans le monde en 2020, contre 12% en 2015 (World Health Organization, 2008)) pose la question “comment bien vieillir ?” Le vieillissement impacte le corps localement et de façon globale, ce qui a des conséquences sur la vie quotidienne des personnes âgées. En particulier, on sait que les adultes âgés de plus de 65 ans sont plus sujets aux chutes (World Health Organization, 2008): alors qu'un jeune adulte peut restaurer son équilibre après l'avoir perdu, une telle tâche est plus difficile pour les personnes âgées, qui sont donc associées à des chutes plus fréquentes. Entre 28% et 35% des personnes âgées de plus de 65 ans chutent chaque année, contre 32% à 42% pour les adultes âgés de plus de 70 ans (World Health Organization, 2008). Comme le squelette est moins robuste pour les personnes âgées, les conséquences de ces chutes peuvent être dramatiques (37,3 millions de chutes par an nécessitent une intervention médicale (World Health Organization, 2008)), et peuvent conduire à la chirurgie, à de longs séjours hospitaliers et/ou la perte d'autonomie.

Les coûts des chutes pour la société ont été quantifiés: par exemple, pour la République de Finlande (respectivement l'Australie), pour les adultes âgés de plus de 65 ans, le coût moyen pour le système de santé par chute est de US$3611 (respectivement US$1049) (World Health Organization, 2008). Tout aussi important, la perte d'autonomie a également un impact sur la qualité de vie du patient et de sa famille. Cela reste un fardeau économique pour l'entourage: les pertes par ménage sont estimées à environ US$40 000 par an pour le Royaume-Uni (World Health Organization, 2008).

Parce que la perte d'équilibre est une des causes de la chute, le maintien d'un bon équilibre au cours du vieillissement apparaît comme un facteur clé dans la prévention des chutes. L'identification précoce des personnes à risque de vieillissement pathologique (conduisant à une possible perte d'équilibre et donc une éventuelle chute), permettrait la mise en place de programmes spécifiques pour améliorer l'équilibre de ces personnes: par exemple, des exercices pour renforcer des muscles particuliers, et retrouver l'amplitude de certains mouvements (Organisation mondiale de la santé: programme de vieillissement actif pour la prévention des chutes (World Health Organization, 2008)).

Cette identification nécessite la définition de biomarqueurs du vieillissement tels que des paramètres ou scores basés sur des examens cliniques et/ou issus d'analyse d'images médicales permettant la discrimination entre les personnes qui vont évoluer vers un vieillissement pathologique et ceux qui vont évoluer vers un vieillissement asymptomatique. Si plusieurs critères ont déjà été rapportés comme marqueurs fiables du vieillissement, aucun biomarqueur global simple n'a été trouvé à ce jour. Cela est dû à l'aspect multifactoriel de la perte de l'équilibre au cours du vieillissement (Tinetti *et al.*, 1994). En particulier il a été montré que lors du vieillissement la composition du disque inter-vertébral change (Adams *et al.*, 1996), conduisant à un dos moins souple et donc à une altération de la posture (Diebo *et al.*, 2015): en particulier un déplacement vers l'avant de la partie supérieure du tronc et une flexion du genou ont été rapportés (Barrey *et al.*, 2013; Diebo *et al.*, 2015). En outre, le système musculaire est également affecté, avec une perte de volume musculaire (sarcopénie) (Narici *et al.*, 2003; Frontera *et al.*, 2000), mais aussi avec une diminution de la force musculaire (Macaluso and De Vito, 2004). Les capacités cognitives peuvent également être modifiées (vision, audition ...) ce qui complique le maintien d'un équilibre efficace (Lacour *et al.*, 2008; Laughton *et al.*, 2003). Combiner l'étude des systèmes squelettique et musculaire dans la recherche de nouveaux biomarqueurs du vieillissement apparaît donc comme pertinent. Des recherches récentes dans les deux équipes d'accueil de cette thèse, l'Institut de Biomécanique Humaine Georges Charpak et Hospital for Special Surgery, ont mis au point de nouvelles techniques et nouveaux algorithmes combinant des informations squelettique et musculaire en 3D.

Le système EOS, par l'acquisition de radiographies bi-planes à basse dose, permet la reconstruction 3D du squelette (Dubousset *et al.*, 2010); tandis que l'analyse des images IRM combinée avec la méthode de déformation d'un objet spécifique paramétrique (DPSO) aboutit à la reconstruction 3D des muscles (Jolivet *et al.*, 2008). En outre, les deux équipes qui collaborent à travers cette thèse, sont experts dans l'analyse du système spino-pelvien (Lafage *et al.*, 2008; Schwab *et al.*, 2006; Skalli *et al.*, 2007; Moal *et al.*, 2015; Steffen *et al.*, 2010; Pomero *et al.*, 2004), et soulignent la nécessité d'une modélisation personnalisée du patient. Comme le vieillissement impacte l'ensemble du corps, les changements observés sont spécifiques à chaque sujet, et la personnalisation des modèles biomécaniques reste cruciale. Dans la littérature, peu d'études ont étudié à la fois le vieillissement du système squelettique et à la fois le vieillissement du système musculaire. Bien que quelques modèles aient été développés pour estimer les interactions entre les deux structures, la personnalisation de ces modèles reste complexe. L'objectif de cette thèse est donc d'étudier les changements dû au vieillissement et de modéliser les interactions musculo-squelettiques, à partir de l'analyse de radios EOS et d'images IRM, afin de chercher de nouveaux biomarqueurs du vieillissement.

Plus précisément, trois questions ont guidé le raisonnement scientifique de cette thèse:

- Comment change l'alignement postural avec le vieillissement ?
- Comment change le système musculaire avec le vieillissement ?
- Quel est l'impact de l'altération combinée de l'alignement postural et du système musculaire, sur la biomécanique de la colonne vertébrale ?

La première partie du travail personnel s'intéresse à l'étude d'adultes jeunes et âgés afin d'étudier les changements d'alignement postural dus au vieillissement, à l'aide de radiographies EOS. La seconde partie présentera des études portant sur le vieillissement du système musculaire à partir d'images IRM. La troisième partie traitera la question de l'interaction des muscles et de la posture permettant un équilibre efficace. Enfin, la dernière partie conclura sur les travaux réalisés durant ce doctorat et proposera des perspectives pour les travaux futurs.

## R - 2 Revue de littérature

La revue de littérature non détaillée ici a permis de faire une analyse des différentes approches utilisées dans la littérature pour étudier l'altération de l'équilibre au cours du vieillissement, en incluant à la fois les changements d'alignement postural mais aussi changements musculaires. L'étude de l'interaction complexe entre les deux systèmes squelettique et musculaire peut être réalisée avec un modèle biomécanique musculo-squelettique.

Tout d'abord, l'analyse de la revue de la littérature concernant l'alignement postural a permis de montrer l'utilité d'analyser cet alignement postural en 3D, de la tête aux pieds, en incluant le segment tête afin de quantifier sa position par rapport à d'autres segments et l'évolution de sa position au cours du vieillissement. Une telle analyse peut être réalisée en utilisant des radiographies bi-planes et des algorithmes de reconstruction 3D.

Deuxièmement, même si l'importance des muscles a bien été rapportée dans la littérature, peu d'études se sont concentrées sur l'analyse de la géométrie 3D des muscles qui semble être essentielle pour quantifier les changements qui se produisent au cours du vieillissement, en raison de mécanismes de compensation, ou de l'évolution d'une pathologie.

Troisièmement, si les modèles biomécaniques se sont développés ces dernières années, à notre connaissance, un seul modèle publié a permis une personnalisation de la géométrie 3D des os et des muscles comme données d'entrées (Pomero *et al.*, 2004). Les altérations de l'équilibre au cours du vieillissement étant personnelles et dépendantes du sujet, ce modèle apparaît approprié pour quantifier plus précisément l'effet du vieillissement sur la colonne vertébrale lombaire, les disques et les muscles.

Après cette revue de l'état de l'art, l'objectif de cette thèse a été d'apporter des éléments de réponse à trois questions:

- Comment change l'alignement postural avec le vieillissement ?
- Comment change le système musculaire avec le vieillissement ?
- Quel est l'impact de l'altération combinée de l'alignement postural et du système musculaire, sur la biomécanique de la colonne vertébrale ?

Trois parties distinctes répondront à chacune de ces trois questions. Tout d'abord, l'analyse de l'alignement postural de deux populations d'âges différents sera étudiée.

Deuxièmement, des coupes IRM axiales seront étudiées afin de caractériser le système musculaire de jeunes sujets asymptomatiques. Ces valeurs de référence seront utilisées pour quantifier la dégradation musculaire survenant pour des adultes avec déformations rachidiennes.

La troisième partie présentera le modèle musculo-squelettique choisi afin d'étudier les interactions entre l'activation musculaire et l'alignement postural chez des volontaires et patients de différents âges.

## R - 3 Changements de l'alignment postural au cours du vieillissement

### R - 3 - 1 Introduction

La première partie de cette thèse se concentre sur l'alignement postural d'adultes asymptomatiques. L'analyse a été réalisée à partir de radiographies EOS et visait à étudier les changements liés à l'âge en terme de posture.

Lors de l'étude de la posture et de l'analyse de l'équilibre, la tête est un segment de première importance vu que des récepteurs majeurs tels que les yeux et l'oreille interne y sont situés. Sa masse de 4 à 5 kg (Vital and Senegas, 1986) est supporté par une tige flexible, la colonne cervicale, suivi du segment thoraco-lombaire. Le dernier segment de la partie supérieure du corps est le bassin supportant le poids de la partie supérieure. L'alignement de ces trois segments doit être atteint pour fournir un équilibre économique (Dubousset, 1994). Cependant, inclure le segment tête dans les analyses radiographiques n'est pas encore courant, probablement en raison de la taille des cassettes à rayons X. Le développement récent d'un système rayons X produisant des radiographies bi-planes de la tête aux pieds, à faible dose a permis la visualisation du segment tête pour les études d'alignement postural (Dubousset *et al.*, 2010).

Avec le vieillissement, divers troubles de la colonne vertébrale peuvent apparaître et modifier l'alignement de la colonne et l'équilibre global. L'alignement du thorax a été largement étudié chez les patients avec différents paramètres, tels que l'axe vertical sagittal (SVA) et le rapport C7-plateau sacré sur la distance sacro-fémorale (Barrey *et al.*, 2011). En outre, les paramètres pelviens détaillés par Duval-Beaupère permettent la caractérisation de la morphologie pelvienne (incidence pelvienne), de la rétroversion pelvienne (version pelvienne) et de l'inclinaison pelvienne (pente sacrée) (Duval-Beaupère *et al.*, 1992). Cependant le vieillissement des sujets asymptomatiques est beaucoup moins étudié (El Fegoun *et al.*, 2005; Vialle *et al.*, 2005; Schwab *et al.*, 2006; Lafage *et al.*, 2008; Kim *et al.*, 2014), en particulier lorsque le segment tête est inclus dans l'analyse. Peu d'études ont rapporté, pour les adultes asymptomatiques, l'alignement de la tête avec la colonne vertébrale et/ou du bassin (Gangnet *et al.*, 2003; Le Huec *et al.*, 2014; Steffen *et al.*, 2010; Iyer *et al.*, 2016). Parmi ces études, très peu ont étudié l'effet du vieillissement sur l'alignement de la tête par rapport au bassin (Le Huec *et al.*, 2014; Iyer *et al.*, 2016).

L'objectif de cette étude était de décrire un groupe d'adultes asymptomatiques âgés de moins de 40 ans et un groupe de d'adultes âgés de plus de 49 ans, en s'intéressant particulièrement à l'alignement de la tête par rapport au bassin et aux mécanismes de compensation mis en place par les personnes de plus de 49 ans afin de corriger une éventuelle altération de l'alignement postural.

## R - 3 - 2 Matériels et méthodes

### R - 3 - 2 - 1 Sujets et collecte de données

Le groupe Jeunes comprenait 69 volontaires (32 hommes et 37 femmes) rétrospectivement inclus dans l'étude: les radiographies bi-planes ont été obtenues entre Février 2007 et Juillet 2014, après approbation par le comité d'éthique (Comité de Protection des Personnes CPP N°06036) et consentement éclairé de chaque sujet. Parmi les critères d'exclusion étaient: précédente chirurgie musculo-squelettique, ou pathologie concernant le(s) système(s) visuel et/ou auditif.

Les radiographies de 41 volontaires (24 hommes et 17 femmes) âgés de plus de 49 ans, ont été extraites d'études précédentes et ont été rétrospectivement inclus dans l'étude: les radiographies bi-planes ont été obtenues entre Juillet 2011 et Avril 2013, après approbation par le comité d'éthique (Comité de protection des Personnes CPP N° 2010/113 (32 sujets) et le CPP N° 06036 (12 sujets)) et consentement éclairé de chaque sujet. Les critères d'inclusion étaient: score d'Oswestry (ODI) inférieur à 20% (Fairbank *et al.*, 1980) et score EVA (échelle visuelle analogique) inférieur à 2 dans l'évaluation de la douleur au dos (y compris la douleur au cou) (Million *et al.*, 1982). Parmi les critères d'exclusion étaient: présence de douleurs au bas du dos ou lombalgie régulière, pathologie des membres inférieurs qui pourrait affecter la colonne vertébrale, précédente chirurgie des membres inférieurs, du bassin ou de la colonne vertébrale.

Les radiographies bi-planes ont été obtenues avec le système EOS, un système basse dose permettant l'acquisition simultanée de radiographies dans les plans sagittal et coronal du patient (avec deux sources à 90°), de la tête aux pieds (Dubousset *et al.*, 2010). Inclusion des radiographies EOS dans l'étude nécessitait la visibilité totale du bassin, fémur proximal et des vertèbres sur les deux radiographies.

Les sujets devaient respecter la Free Standing Position lors de l'acquisition des radiographies, position adaptée de Faro *et al.* (Faro *et al.*, 2004), avec les mains posées sur les mandibules (SRS Free Standing Position) et avec les pieds légèrement décalés comme décrit par Chaïbi *et al.* (Chaibi *et al.*, 2012) (Figure 1).

### R - 3 - 2 - 2 Traitement des radiographies

A partir des radiographies bi-planes, un modèle 3D personnalisé du sujet, comprenant la colonne vertébrale (de C3 à L5, avec ajout du point le plus supérieur de l'apophyse dentiforme de C2 (OD)), le bassin et les membres inférieurs; a été obtenu en utilisant des techniques de reconstructions validées

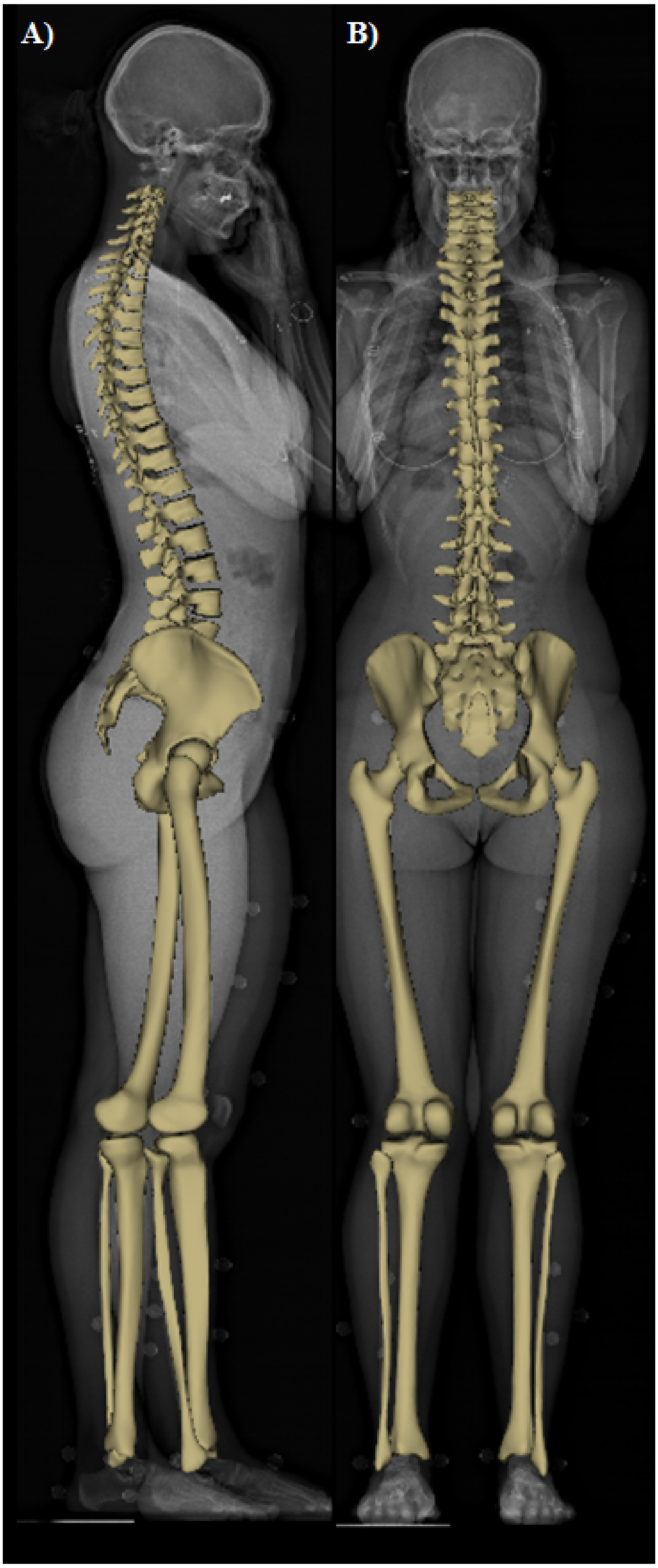


Figure 1. [Reconstruction 3D du squelette.]: Radiographies bi-planes avec le modèle 3D de la colonne vertébrale (C3 à L5), du bassin et des membres inférieurs. **A)** Vue sagittale. **B)** Vue coronale.

(Chaibi *et al.*, 2012; Humbert *et al.*, 2009a; Mitton *et al.*, 2006; Quijano *et al.*, 2013). En outre, comme décrit par Steffen *et al.* (Steffen *et al.*, 2010), lorsque les radiographies incluent le haut de la tête, deux points stéréo-radiographiques localisant les conduits auditifs externes ont été numérisés pour calculer leur centre (CAM).

### R - 3 - 2 - 3 Paramètres étudiés

Tous les paramètres ont été calculés dans le repère anatomo-gravitaire, qui est la repère du patient: le plan frontal est le plan vertical passant par les deux centres des cotyles, les plans transversal et sagittal sont perpendiculaires au plan frontal. L'origine du repère est le centre du segment bi-coxofémoral (point nommé HA). Les courbures rachidiennes (courbure cervicale, cyphose thoracique et lordose lombaire) et les paramètres pelviens (incidence pelvienne IP, version pelvienne VP, pente sacrée PS et overhang de S1) ont été calculés à partir de la reconstruction 3D. Ont également été calculés le sagittal vertical axis (SVA), l'angle de T1-pelvien (TPA) et les angles avec la verticale de différentes droites: CAM-HA, OD-HA, C7-HA et T9-HA.

L'inclinaison spinale (Incl Sp) a été calculée comme l'angle avec la verticale de la ligne qui passe le mieux (au sens des moindres carrés) par les points anatomiques suivants: milieu des centres des conduits auditifs (CAM), le point le plus supérieur de l'apophyse dentiforme de C2 (OD), tous les centres des corps vertébraux de C3 à L5, centre du plateau sacré (S1) et le milieu des centres de chaque cotyle (HA). Cette méthode de droite aux moindres carrés est un moyen robuste de calculer l'inclinaison globale de la colonne vertébrale. Le ratio C7PL/SFD, introduit par Barrey *et al.* (Barrey *et al.*, 2011), est le rapport entre la distance C7-$^{\text{post-sup}}$ S1 et la distance HA-$^{\text{post-sup}}$ S1.

### R - 3 - 2 - 4 Analyse statistique

Un test de normalité Lilliefors (Lilliefors, 1967) a été appliqué à chacun des paramètres. Les corrélations avec l'âge ont été étudiées, en utilisant des corrélations de Spearman (seuil fixé à 0,05).

### R - 3 - 2 - 5 Différences entre les jeunes et les adultes de plus de 49 ans

Une comparaison a été faite entre les adultes de plus de 49 ans et le groupe Jeunes de 69 volontaires asymptomatiques âgés de moins de 40 ans. Pour chaque paramètre, la moyenne M et l'écart type EC du groupe Jeunes de référence ont été utilisés pour classifier les valeurs pour l'adulte âgé de plus de 49 ans: cette valeur était qualifiée de **normale** si elle était comprise entre $M+/-1*EC$, **subnormale** *haute* entre $M+1*EC$ et $M+2*EC$ (*bas* entre $M-1*EC$ et $M-2*EC$) ou **anormale** quand hors de la gamme $M+/-2*EC$ (*haut* ou *bas*). La version pelvienne a été définie comme normale, subnormale ou anormale en fonction de la position du couple de points (version pelvienne; incidence pelvienne) sur la figure 2: la figure a été tracée à l'aide de la relation publiée par Vialle *et al.* (Vialle *et al.*, 2005).

### R - 3 - 2 - 6 Mécanismes de compensation

Pour les sujets présentant une version pelvienne anormale (valeur inférieure à moyenne-2*EC ou supérieure à moyenne+2*EC, tel que défini par la figure 2), les mécanismes de compensation ont été étudiés en s'intéressant particulièrement à l'inclinaison spinale et à la lordose cervicale. Plus précisément, l'alignement non compensé a été modélisé comme expliqué dans la figure 3: pour chacun de ces sujets, la version pelvienne théorique a été calculée à partir de l'incidence pelvienne en utilisant la relation fournie par Vialle *et al.* (2005). La différence entre la version pelvienne mesurée et théorique définit la compensation par rétroversion pelvienne, une rotation du bassin et de la colonne vertébrale (de cet angle de compensation par rétroversion) a été réalisée autour de HA afin de simuler un alignement sans cette compensation par rétroversion.

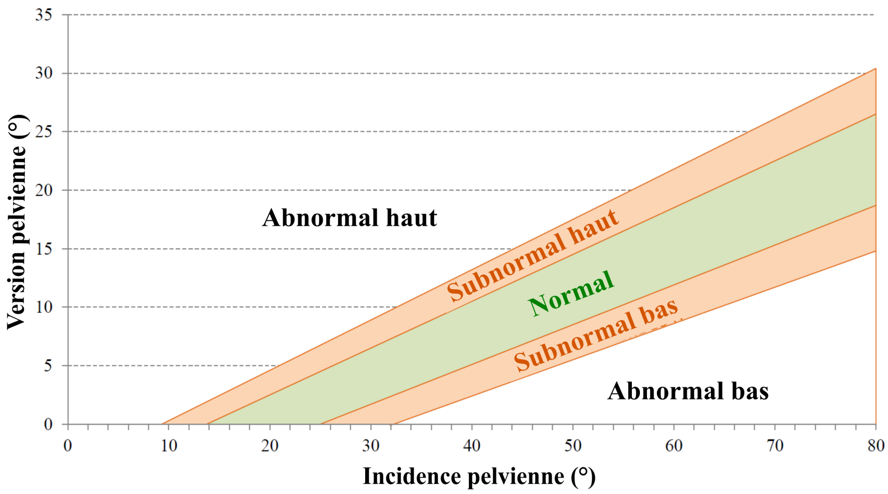


Figure 2. : Corridor de normalité pour la version pelvienne (VP) en fonction de sa relation avec l'incidence pelvienne (IP) issue de l'étude de Vialle *et al* (Vialle *et al.*, 2005): VP = 0,37 (+/- 0,03) * IP -7 (+/- 1,5)

.

La compensation au niveau cervical a été calculée comme la différence entre la lordose cervicale mesurée et la valeur de référence fournie par les adultes asymptomatiques âgés de moins de 40 ans. Une rotation de la colonne cervicale autour C7 a ensuite été appliquée pour supprimer la compensation au niveau cervical. Le nouvel alignement simulé, sans rétroversion pelvienne ou hyperlordose cervicale, permet le calcul d'une nouvelle valeur théorique CAM-HA non compensée (respectivement OD-HA), nommé CAM-$HA_{NC}$ (resp. OD-$HA_{NC}$) (Figure 3).

## R - 3 - 3 Résultats

### R - 3 - 3 - 1 Description des sujets

Pour le groupe Jeunes, l'âge moyen était de 26,3 ans (écart-type (EC): 4,7 ans). Les conduits auditifs n'étaient pas visibles sur 8 examens EOS sur les 69 examens des jeunes adultes. Pour le groupe de personnes âgées de plus de 49 ans, l'âge moyen était de 57,9 ans (EC: 7,9 ans) (Tableau 1).

| | **Agés (N=41)** | | **Jeunes (N=69)** | |
|---|---|---|---|---|
| | *** Age (ans)** | **IMC ($kg/m^2$)** | *** Age (ans)** | *** IMC ($kg/m^2$)** |
| **Moyenne** | 57.9 | 25.6 | 26.3 | 22.4 |
| **1 * Ecart-type** | 7.9 | 4.1 | 4.7 | 3.1 |
| **Minimum** | 49.0 | 18.6 | 20.1 | 16.6 |
| **Maximum** | 76.0 | 39.2 | 39.7 | 33.2 |

Table 1. Données démographiques des volontaires âgés de plus de 49 ans qui ont participé à l'étude (N=41) et de la population de référence (N=69). * signifie que le paramètre n'est pas issu d'une distribution normale.

Sur tous les paramètres utilisés pour étudier les corrélations, seulement 2 ont été trouvés comme non-issus d'une distribution normale (CAM-HA (p = 0,04) et l'âge (p = 0)). Moyennes et écarts-types ont été calculés pour tous les paramètres (figures 4 & 5).

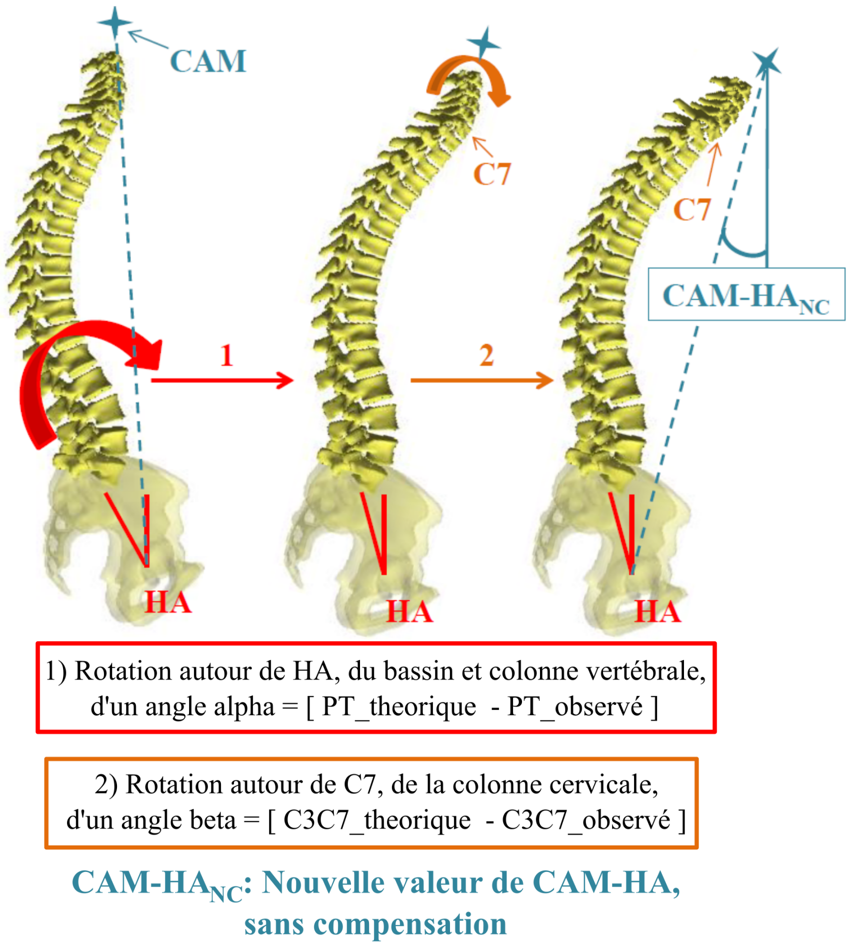


Figure 3. : Représentation schématique du calcul de la posture non compensée représentée sur la figure 6. PT _theorique se réfère à la valeur théorique de PT calculée à partir de PI comme indiqué par Vialle *et al.*, (Vialle *et al.*, 2005). C3C7_theorique se réfère à la valeur moyenne calculée pour les adultes asymptomatiques âgés de moins de 40 ans (6°). De même que pour CAM-HA$_{NC}$, une nouvelle inclinaison OD-HA$_{NC}$ a été calculée suivant les mêmes étapes.

Les inclinaisons avec la verticale, de la ligne joignant CAM et HA et de la ligne joignant OD et HA présentaient la variation interindividuelle la plus faible (EC de 2° pour les deux) et étaient le plus proche de la verticale: inclinaison de 3° pour les deux. Ces résultats étaient identiques entre les deux groupes Jeunes et Agés de plus de 49 ans. Concernant aux différents types d'alignement définis par Roussouly (Roussouly *et al.*, 2005), 27% des personnes âgées de plus de 49 ans présentent un type 1 ou 2 d'alignement, 59% présentent un alignement de type 3 et 15% présentent un alignement de type 4.

Les paramètres significativement corrélés avec l'âge, avec R> 0,3, sont: sagittal vertical axis (R = 0,48), l'inclinaison spinale (R = 0,46), l'angle T1-pelvien (R = 0,44), la version pelvienne (R = 0,35), overhang S1 (R = - 0,35) et la courbure cervicale (R = - 0,42).

### R - 3 - 3 - 2 Différences entre jeunes et adultes de plus de 49 ans

Aucune différence statistique n'a été observée entre les groupes Jeunes et Agés de plus de 49 ans pour les angles CAM-HA et OD-HA. Des différences significatives ont été observées entre les 2 populations pour plusieurs paramètres (figures 4 à 5), y compris (valeurs moyennes indiquées ci-après):

- lordose cervicale: -5° pour le groupe de personnes âgées de plus de 49 ans vs 6° pour le groupe Jeunes,
- incidence pelvienne: 56° pour le groupe de personnes âgées de plus de 49 ans vs 51° pour le groupe Jeunes,
- version pelvienne: 17° pour le groupe de personnes âgées de plus de 49 ans vs 11° pour le groupe Jeunes,
- SVA: 15mm pour le groupe de personnes âgées de plus de 49 ans vs -9mm pour le groupe Jeunes.

Dans l'ensemble, 44% des personnes âgées de plus de 49 ans, présentent une inclinaison spinale normale et 27% présentent une inclinaison spinale anormale haute (Figure 4). Seulement, 10% (resp. 12%) des personnes âgées de plus de 49 ans présentent un angle CAM-HA anormal (haut ou bas) (resp. OD-HA) (Figure 4).

#### R - 3 - 3 - 3 Mécanismes de compensation

9 personnes âgées de plus de 49 ans présentent une lordose cervicale anormale basse. 11 personnes âgées de plus de 49 ans présentent une version pelvienne anormale haute ou basse (selon la classification présentée dans la figure 2). 11 personnes âgées de plus de 49 ans présentent une inclinaison spinale anormale haute. Toutes ces personnes âgées de plus de 49 ans (N = 20) ont été étudiées plus en détail. Concernant les différents types d'alignement définis par Roussouly *et al.*, (Roussouly *et al.*, 2005) 30% de ces 20 personnes âgées de plus de 49 ans présentent un alignement de type 1 ou 2, 55% présentent un alignement de type 3 et 15% présentent un type d'alignement 4. Les angles CAM-HA$_{NC}$ et OD-HA$_{NC}$ ont été calculés pour ces sujets, sans compensation par rétroversion pelvienne et sans compensation cervicale (voir Figure 3).

Parmi ceux-ci, 13 personnes âgées de plus de 49 ans présentent un CAM-HA$_{NC}$ nouvellement calculé ou OD-HA$_{NC}$ supérieur à 3°, tandis que leur valeur initiale de CAM-HA ou OD-HA était en moyenne de -1° (EC de 3°). Les différents types d'alignement décrits par Roussouly se retrouvent chez ces 13 personnes âgées de plus de 49 ans, dans la même proportion que pour la population initiale (Roussouly *et al.*, 2005): 38% de ces 13 personnes âgées de plus de 49 ans présentent un alignement de type 1 ou 2, 54% présentent un type alignement 3 et 15% présentent un alignement de type 4.

Dans l'ensemble, ces 13 personnes âgées de plus de 49 ans présentent une grande rétroversion pelvienne: différence moyenne réelle PT avec PT théorique de 8° (EC: 5°). Ils présentent également une grande courbure cervicale: différence entre la valeur observée pour la lordose C3C7 et 6° (courbure C3C7 normale) de -19° (EC: 10°). L'apport de la rétroversion pelvienne et de l'hyperlordose cervicale dans la position compensée est illustré sur la figure 6 pour 3 de ces 13 personnes âgées.

### R - 3 - 4 Discussion

L'alignement postural des adultes asymptomatiques âgés de moins de 40 ans et d'adultes asymptomatiques âgés de plus de 49 ans a été étudié. L'alignement de la tête par rapport au bassin a été rapportée comme quasi-invariant chez les adultes asymptomatiques âgés de moins de 40 ans, et cette invariance a été conservée pour les personnes âgées de plus de 49 ans. Cela confirme l'intuition des praticiens cliniques, résumée par le concept de cône d'économie décrit par Dubousset (Dubousset, 1994). Bien que les deux angles CAM-HA et OD-HA soient apparus comme quasi-invariant pour des sujets asymptomatiques, étant ainsi des marqueurs potentiels de déséquilibre chez les sujets atteints de troubles rachidiens, OD-HA pourrait être d'un intérêt particulier en raison de la visibilité du point OD sur la plupart des radiographies, tandis que CAM peut ne pas être visible pour les personnes de grande taille en raison de la taille du système d'acquisition de radios bi-planes.

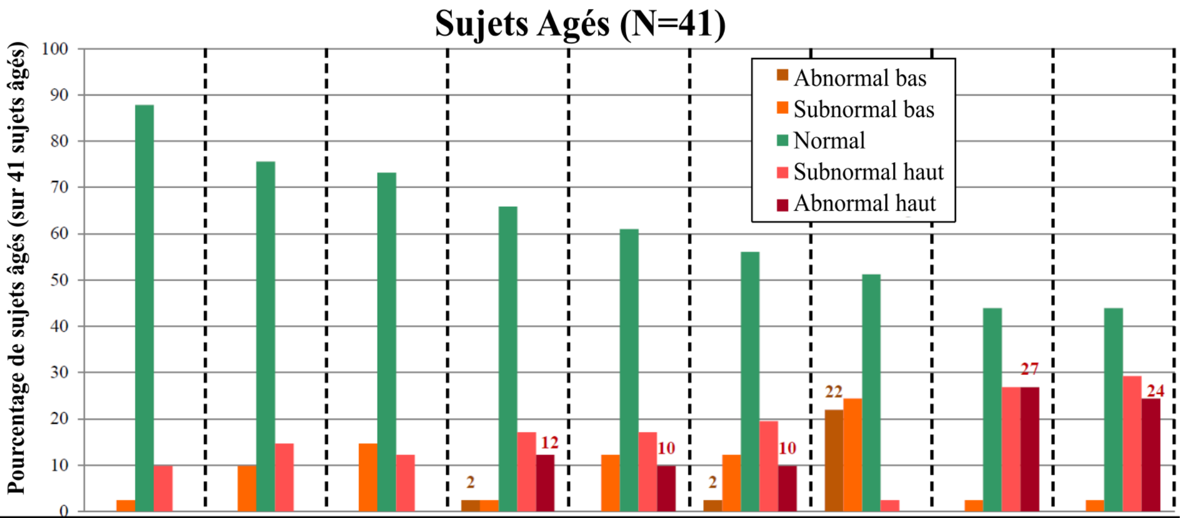


| Paramètre | L1S1 (°) | PS (°) | T1T12 (°) | IP (°) | CAM-HA (°) | OD-HA (°) | C3C7 (°) | Incl Sp (°) | SVA (mm) |
|---|---|---|---|---|---|---|---|---|---|
| Jeunes | -58 (13) | 41 (9) | 50 (13) | 51 (9) | - 2 (2) | - 2 (2) | 6 (12) | - 3 (3) | - 9 (22) |
| Agés | -55 (8) | 39 (7) | 51 (11) | 56 (11) | -2 (2) | -2 (2) | -5 (12) | 1 (3) | 15 (23) |
| Stats | | | | * | | | * | * | * |

Figure 4. : Répartition des valeurs de différents paramètres, pour les personnes âgées, par rapport aux corridors donnés par le groupe Jeunes: le pourcentage de sujets est calculé comme le pourcentage sur l'ensemble de la population (n = 41). T1T12 est la cyphose thoracique, L1S1 est la lordose lombaire et C3C7 est la courbure cervicale. Moyennes (1 * écart-type) pour les groupes Jeunes et personnes de plus de 49 ans. * Signifie que des différences significatives ont été observées entre les deux groupes.

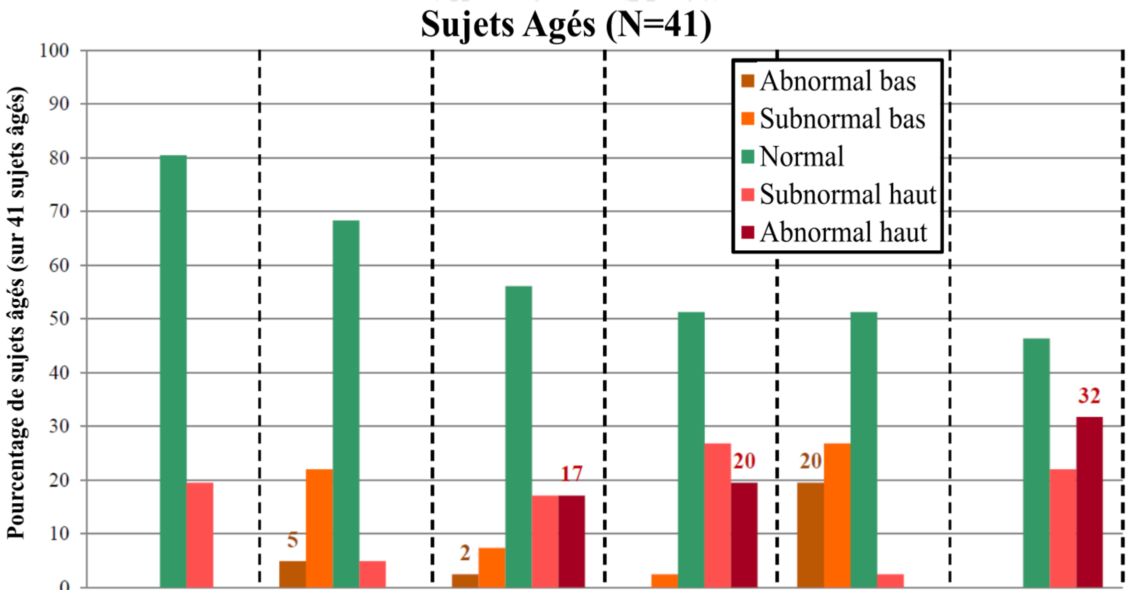


| Paramètre | C7PL/SFD | T9HA (°) | C7-HA (°) | T1-S1 (°) | S1 overhang (mm) | TPA (°) |
|---|---|---|---|---|---|---|
| Jeunes | 0(0) | - 10 (3) | - 4 (2) | - 4 (3) | - 20 (10) | 5 (6) |
| Agés | 0 (1) | - 12 (3) | - 3 (3) | - 1 (3) | -30 (12) | 13 (7) |
| Stats | * | * | * | * | * | * |

Figure 5. : Répartition des valeurs de différents paramètres, pour les personnes âgées, par rapport aux corridors donnés par le groupe Jeunes: le pourcentage de sujets est calculé comme le pourcentage sur l'ensemble de la population (n = 41). Moyennes (1 * écart-type) pour les groupes Jeunes et Agés de plus de 49 ans. * Signifie que des différences significatives ont été observées entre les deux groupes.

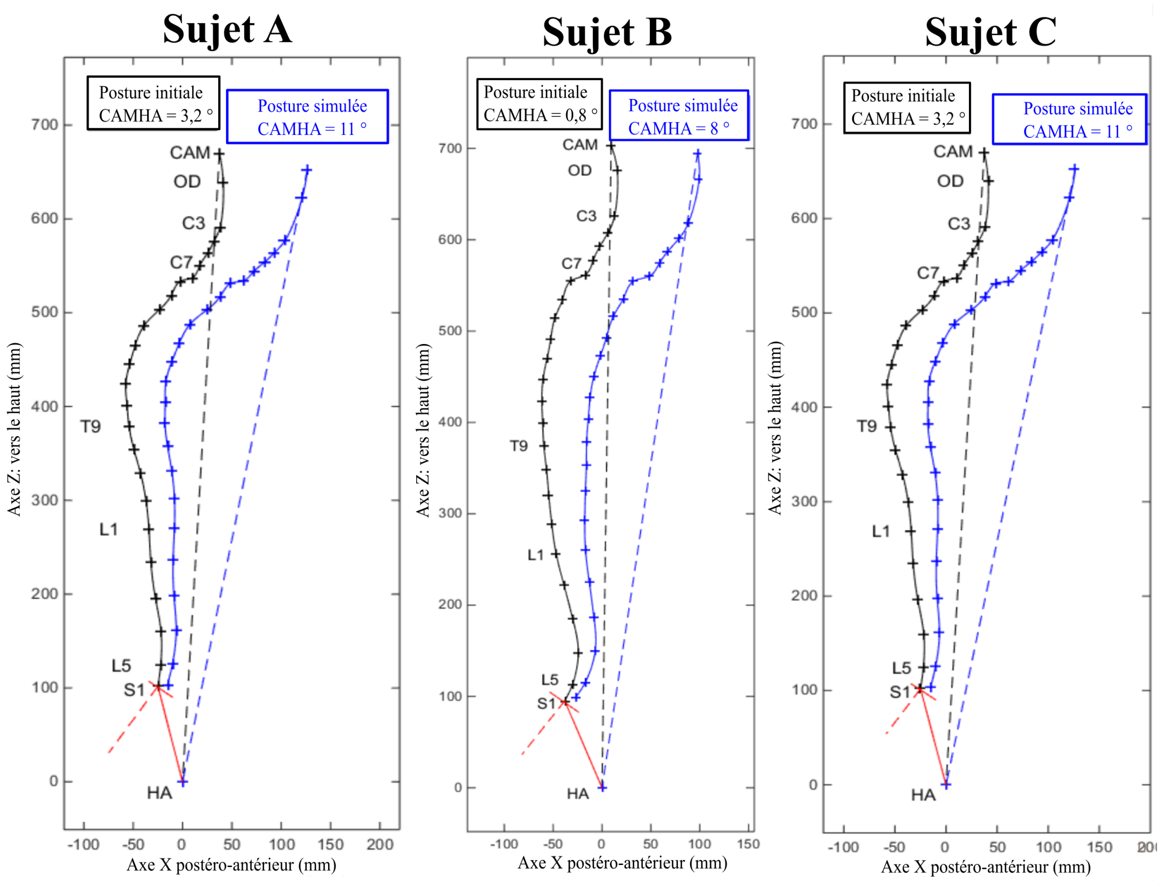


Figure 6. : Posture initiale (courbe noire) et posture simulée sans compensation aux niveaux pelvien et cervical (courbe bleue): la valeur théorique de la version pelvienne a été calculée à partir de l'incidence pelvienne (Vialle *et al.*, 2005) et la courbure cervicale a été fixée à 6°, cette valeur ayant été rapportée comme valeur moyenne pour les adultes asymptomatiques âgés de moins de 40 ans . Les lignes rouges représentent le plateau sacré et la droite liant S1 à HA pour représenter l'incidence pelvienne. Pour les adultes asymptomatiques âgés de moins de 40 ans, la valeur moyenne pour CAM-HA était -2°. Le sujet A (respectivement B; respectivement C) est une personne âgée de plus de 49 ans avec une incidence pelvienne supérieure à 60° (respectivement entre 44° et 60°; respectivement inférieure à 44°).

L'étude de la population des personnes âgées de plus de 49 ans était similaire aux études publiées. Ceux-ci présentaient une plus grande cyphose thoracique T1T12 et une lordose L1S1 plus petite que les adultes asymptomatiques âgés de moins de 40 ans. Cette perte de lordose et gain de la cyphose lors du vieillissement a été précédemment rapportée dans la littérature (Schwab *et al.*, 2006; Kim *et al.*, 2014).

Cette étude a portée sur l'altération de la posture, de personnes asymptomatiques âgées de plus de 49 ans, évaluée avec des paramètres différents: le sagittal vertical axis, le C7PL/SFD (Barrey *et al.*, 2011), et l'inclinaison spinale. Lorsque l'on étudie en détail les mécanismes de compensation, 13 personnes âgées de plus de 49 ans peuvent être identifiées avec un alignement de la tête par rapport du bassin conservé au détriment d'une importante rétroversion pelvienne et d'une augmentation lordose cervicale. En comparaison, 7 sujets ont été identifiés comme étant mal alignées sur la base du SVA, 10 sur la base de C7PL/SFD (Barrey *et al.*, 2011) et 6 en fonction de l'inclinaison spinale. Bien que SVA, C7PL/SFD et l'inclinaison spinale soient utiles dans l'évaluation d'altérations locales, la classification basée sur l'un de ces paramètres n'a pas permis d'identifier l'ensemble des 13 sujets identifiés dans cette étude comme sujets présentant une posture compensée. La population des adultes âgés de plus de 49 ans présentaient les différents types d'alignement décrits par Roussouly (Roussouly *et al.*, 2005), de même que les différents sous-groupes de cette population, analysés dans cette étude.

Certains de ces sujets sont apparus comme présentant une compensation maximale, par rapport à la réserve de compensation. Une étude longitudinale pourrait suivre l'évolution de leurs postures au fil du temps et évaluerait si des troubles posturaux se produiront plus tard pour ces sujets par rapport aux autres. Cela confirmerait les résultats de cette étude dans la définition d'un marqueur précoce de l'altération posturale.

Les points CAM et OD ont été choisis afin de représenter la position de la tête. Des études antérieures ont mis l'accent sur d'autres points spécifiques pour quantifier l'alignement de la tête avec la colonne vertébrale et bassin: comme la selle turcique (Le Huec *et al.*, 2014), McGregor ligne (Le Huec *et al.*, 2014), ou le centre de masse du crâne (milieu de la ligne nasion-inion) (Sugrue *et al.*, 2013). Comme dans cette étude, tous les points considérés sont censés être proches du vrai centre de masse de la tête afin de quantifier son alignement par rapport au bassin. Cependant, dans l'analyse des radiographies, une méthode fiable et précise, mais aussi facile à mettre en œuvre est nécessaire pour identifier les points d'intérêt (en particulier lorsque l'on travaille dans un environnement clinique). Voilà pourquoi dans cette étude, seuls les points directement identifiables sur le modèle 3D de la colonne vertébrale ont été considérés: pour la tête, cela ne comprenait que les points CAM et OD. On peut noter que toutes ces études, y compris celle-ci, ont conclu sur l'importance l'alignement de la tête par rapport au bassin (Le Huec *et al.*, 2014; Sugrue *et al.*, 2013).

#### R - 3 - 4 - 1 Limites et perspectives

En raison de la position dans la cabine EOS (pieds décalés), les paramètres mesurés concernant le fémur doivent être interprétés avec précaution. Les radiographies des âgés de plus de 49 ans ne comprenant pas complètement les jambes, l'analyse des membres inférieurs et de leur rôle dans les mécanismes de compensation ont été exclus de l'étude actuelle (Barrey *et al.*, 2013; Diebo *et al.*, 2015). Une autre limite concerne les contraintes liées à l'acquisition de l'image dans la cabine de l'EOS. Si la Free Standing Position a permis d'être aussi proche que possible de la posture naturelle, l'observation supplémentaire de la posture "de routine", hors de la cabine, pourrait être intéressant dans les études futures.

En outre, une étude plus approfondie sur un plus large éventail de sujets serait intéressante afin de confirmer ces résultats obtenus sur une population de taille raisonnable (41 personnes âgées de plus de 49 ans). Le potentiel biais concernant la sélection des sujets a été minimisé en fixant des critères d'exclusion similaires entre les deux groupes Jeunes et Agés de plus de 49 ans, en ajoutant des scores cliniques pour les personnes âgées de plus de 49 ans afin d'uniquement recruter des personnes asymptomatiques. De plus, la collecte et le traitement de données des deux groupes ont été effectués en suivant le même protocole. Inclure des patients dans une étude future serait d'un intérêt particulier pour évaluer si un seuil de degré de compensation apparaît comme permettant l'identification des patients souffrant de douleur ou d'invalidité. Il serait également intéressant d'étudier si un lien existe entre sévérité de la maladie (et/ou scores de qualité de vie) et recrutement faible des mécanismes de compensation.

### R - 3 - 5 Conclusion

Cette partie de la thèse s'est intéressée aux changements liés à l'âge de l'alignement postural du squelette. Plus précisément, il a fourni des réponses à deux des questions clés initialement introduites:

- comment évolue l'alignement postural au cours du vieillissement?
- est ce que l'alignement de la tête par rapport au bassin est maintenu pour les sujets âgés de plus de 49 ans ?

Le premier chapitre décrit une population de référence et a identifié la quasi-invariance de la position de tête au-dessus du bassin chez les adultes asymptomatiques jeunes. Le deuxième chapitre a présenté des résultats intéressants sur l'alignement postural des personnes de plus de 49 ans : la majorité d'entre eux maintient l'alignement de la tête au-dessus du bassin, même si une inclinaison antérieure globale du tronc a été observée. Cette inclinaison vers l'avant a été compensée en partie par l'augmentation de la lordose cervicale, et en partie par l'augmentation de la rétroversion pelvienne.

Des modèles spéciaux de compensation ont été confirmés par rapport à ceux rapportés dans la littérature, avec l'ajout de l'évolution de la position de la tête au cours du vieillissement. L'alignement de la tête par rapport au bassin est maintenue pour les sujets de plus de 49 ans qui recrutent déjà une compensation aux niveaux pelvien et cervical. Ce résultat confirme l'intuition de la plupart des praticiens cliniques lors de l'observation des patients en routine clinique (alignement de la tête au-dessus du bassin), même si la quantification de ces observations n'avaient pas été faite jusque-là. Si ces deux études ont permis d'établir l'invariance de la position de tête par rapport au bassin, de plus grandes cohortes doivent être envisagées afin d'affiner l'étude des mécanismes de compensation précoces, et afin de mieux représenter la population mondiale en termes d'âge, de sexe, et morphologie. Des études longitudinales pourraient évaluer l'évolution de la posture des sujets qui présentent déjà un alignement compensé.

Si la partie actuelle a mis en évidence les changements de posture qui se produisent avec le vieillissement, et leurs impacts sur la position neutre des sujets, on peut se demander quel va être le rôle des muscles dans la mise en place de tels mécanismes de compensation, et en les rendant les plus économes en énergie et durables possible. De plus, comme les muscles se dégradent au cours du vieillissement, il semble primordial d'inclure le système musculaire dans l'étude des altérations de la posture globale liée à l'âge. Ainsi, la deuxième partie de cette thèse se concentrera sur la quantification des volumes des muscles spino-pelviens dans différentes populations.

## R - 4 Changements du système musculaire au cours du vieillissement

### R - 4 - 1 Introduction

Cette partie se concentre sur la caractérisation des muscles spino-pelviens pour les jeunes adultes asymptomatiques et des personnes avec déformations rachidiennes.

Bien que l'alignement postural du squelette ait été largement étudié à partir de radiographies (Barrey *et al.*, 2013), la quantification de la dégradation musculaire n'est pas encore pleinement documentée. Comme la dégradation musculaire (principalement en terme de diminution de l'aire musculaire sur une coupe transversale) a été corrélée à la douleur dorsale (Gildea *et al.*, 2013; Lee *et al.*, 2008; Parkkola *et al.*, 1993; Rasch *et al.*, 2007) et au vieillissement (Ahmed *et al.*, 2005; Frontera *et al.*, 2000; Takahashi *et al.*, 2006; Takayama *et al.*, 2016), il est nécessaire d'analyser de façon quantitative le système musculaire en relation avec le vieillissement du squelette (dégradation osseuse et modifications de l'alignement postural). Dans un premier temps, afin de différencier les changements dus à une pathologie dans le système musculaire de ceux dus au vieillissement, il est important de donner des valeurs de référence pour les jeunes adultes asymptomatiques. Cependant la littérature manque de valeurs descriptives (en particulier sur les volumes) des muscles, en particulier sur la zone L1-genou (impliquée dans des mécanismes de compensation).

La géométrie musculaire a été explorée en utilisant la tomodensitométrie (CT) (Danneels *et al.*, 2000; Rasch *et al.*, 2007). Cependant, ceci implique une dose ionisante importante: couvrir de façon extensive une partie spécifique du corps (nombre important de coupes) implique une dose modérée à forte de rayonnement pour le patient (1.5mSv pour un scanner lombaire vs 0.02mSv pour une radiographie thoracique (Food and Drug administration, 2015)). Le plus souvent, pour CT, afin d'éviter les acquisitions répétées, seulement un ensemble réduit d'images est acquise, aux endroits d'intérêt uniquement (Danneels *et al.*, 2000; Rasch *et al.*, 2007).

Une autre méthode utilisée pour étudier les muscles est l'échographie (non-invasive). Cependant, les muscles profonds peuvent être plus difficiles à explorer car c'est une technique de surface. Les études l'utilisant ont principalement porté sur l'analyse de la contraction musculaire (Nuzzo and Mayer, 2013; Skeie *et al.*, 2015).

Enfin, la modalité d'imagerie la plus courante pour l'analyse du système musculaire est l'IRM (Crawford *et al.*, 2016; Fortin *et al.*, 2014, 2016; Gildea *et al.*, 2013; Kjaer *et al.*, 2007; Lee *et al.*, 2008; Niemeläinen *et al.*, 2011; Parkkola *et al.*, 1993; Pezolato *et al.*, 2012; Savage *et al.*, 1991; Takahashi *et al.*, 2006). Par exemple, les différentes études menées par Fortin *et al.* ont rapporté des valeurs d'aires musculaires et d'infiltration graisseuse (Fortin *et al.*, 2014, 2015, 2016) sur diverses populations. En particulier, ces études ont fourni des indications précieuses sur la relation entre l'asymétrie musculaire, l'infiltration graisseuse et lombalgie (Fortin *et al.*, 2015). La plupart de ces études ont rapporté des paramètres uniquement 2D tels que l'aire sur un coupe transversale (Fortin *et al.*, 2014; Gildea *et al.*, 2013; Lee *et al.*, 2009; Niemeläinen *et al.*, 2011; Parkkola *et al.*, 1993; Pezolato *et al.*, 2012; Savage *et al.*, 1991; Takahashi *et al.*, 2006), et/ou des informations sur l'infiltration graisseuse des muscles considérés (Crawford *et al.*, 2016; Fortin *et al.*, 2014, 2015; Kjaer *et al.*, 2007; Lee *et al.*, 2009; Parkkola *et al.*, 1993; Pezolato *et al.*, 2012; Valentin *et al.*, 2015). Le volume musculaire a été quantifié pour les composants du quadriceps fémoral (Barnouin *et al.*, 2014), muscles pelviens et/ou des membres inférieurs (Lube *et al.*, 2016; Handsfield *et al.*, 2014; Belavý *et al.*, 2011). Ces trois dernières études ont soit inclus un nombre limité de sujets (3 femmes et 3 hommes (Lube *et al.*, 2016)), soit un large éventail d'âge dans la population considérée (de 12 à 51 ans (Handsfield *et al.*, 2014)), ou ont mis l'accent sur l'effet du repos allongé (Belavý *et al.*, 2011) (cette étude n'est donc pas représentative d'une position quotidienne). Alors que l'infiltration graisseuse donne un aperçu de la qualité musculaire (Fortin *et al.*, 2014, 2015), la calibration reste un problème et cette étude se concentre donc seulement sur le calcul des volumes et des paramètres géométriques en 3D des muscles.

Le calcul du volume musculaire peut être effectué par interpolation ou reconstruction en 3D du muscle. En particulier, la reconstruction 3D à partir d'images IRM et méthode de calcul du volume ont été rapporté comme étant exacts (Jolivet *et al.*, 2008) et répétables (Moal *et al.*, 2014). Pourtant, l'analyse quantitative des images IRM peut prendre du temps. La méthode de déformation d'un objet spécifique paramétrique (DPSO) (Jolivet *et al.*, 2008, 2014) permet une reconstruction 3D exacte et précise de muscles individuels, à partir de segmentations du muscle sur un ensemble d'images IRM sélectionnées, conduisant à un calcul du volume précis en un temps assez court. Cette méthode a été utilisée sur des images IRM d'adultes avec déformations rachidiennes pour les muscles spino-pelviens (Moal *et al.*, 2014) et sur des volontaires âgés de moins de 40 ans, pour les muscles de la colonne cervicale (Li *et al.*, 2014) et pour les membres inférieurs (Hausselle *et al.*, 2014; Südhoff *et al.*, 2009). Si la méthode DPSO permet une réduction du temps en réduisant le nombre de coupes à examiner par muscle, ce procédé implique un traitement de différentes coupes pour chaque muscle ce qui peut encore être long lorsque de nombreux muscles sont pris en compte. En plus de quantifier les volumes des muscles spino-pelviens en 3D pour de jeunes volontaires asymptomatiques, et de comparer ces valeurs pour les adultes avec déformations rachidiennes, notre objectif est de proposer un modèle utilisant moins de 6 coupes IRM segmentées pour tous les muscles, afin de calculer de façon rapide le volume de groupes musculaires.

## R - 4 - 2 Méthodes

### R - 4 - 2 - 1 Conception de l'étude

Le groupe J était constitué d'adultes asymptomatiques âgés de moins de 24 ans. Les critères d'exclusion étaient la chirurgie sur les membres inférieurs ou la colonne vertébrale, la grossesse, les troubles posturaux, les contre-indications à un examen IRM (principalement liée au champ magnétique). Ceci est une étude mono-centrique prospective, les sujets ayant été recrutés entre Septembre 2014 et Mars 2015. Tous les participants ont signé un consentement préalable à l'examen IRM. Cette étude a été examinée et approuvée par Comité de Protection des Personnes (CPP 14.013).

Le groupe P inclus des femmes avec déformations rachidiennes de plus de 35 ans avec au moins un des critères suivants concernant la déformation rachidienne: angle coronal de Cobb thoraco-lombaire ou lombaire > 30 °, Sagittal Vertical Axis > 4 cm ou version pelvienne > 20 °. Le Groupe P a déjà été étudié dans une étude publiée en 2015 (Moal *et al.*, 2015).

### R - 4 - 2 - 2 Collecte de données

Les renseignements recueillis incluaient: l'âge, l'indice de masse corporelle (IMC), le sexe. L'historique des blessures musculo-squelettiques a également été documenté. Chaque sujet a subi un examen IRM (General Electric 1.5T, Fairfield, Etats-Unis), résultant en des images axiales depuis la vertèbre T12 jusqu'à l'extrémité distale du fémur. Le protocole utilisé est le même que celui qui a été décrit dans une étude précédente (Moal *et al.*, 2015). La machine IRM a été réglée avec les paramètres suivants: TR / TE = 427 / 11.3 ms, matrice d'acquisition = 416 * 416 pixels, phase de suréchantillonnage = 100%, résolution de plan = 0,82 × 0.82 $mm^2$, 8 blocs, 40 coupes par bloc, l'épaisseur de coupe = 5 mm, gap coupe = 0 mm, angle de bascule = 160 °, parallèle facteur d'accélération de l'imagerie (IPAT) = 2 , la bande passante = 391 Hz/pixel, l'espacement d'écho = 11.3 ms, temps d'acquisition par bloc = 7 min, temps d'acquisition total = 50 min.

La reconstruction 3D des muscles (à partir d'informations de toutes les coupes IRM) a été réalisée avec un logiciel développé dans l'Institut, en utilisant la méthode DPSO (Jolivet *et al.*, 2008; Moal *et al.*, 2014). Les muscles d'intérêt sont représentés sur la figure 7, l'analyse a été réalisée sur les muscles droit et gauche.

La frontière entre les muscles spécifiques pouvant être difficile à identifier, certains muscles ont été segmentés ensemble:

- l' "adductor" comprend adductor brevis, adductor longus, adductor magnus, ainsi que obturatorius internus et pectineus;
- les "érecteurs spinaux" comprend les tractus médial (multifidi et interspinales) et latéral (iliocostal et longissimus);
- l' "iliopsoas" comprend l'iliaque et le psoas;
- le "vastus lateralis inter" comprend les vastus lateralis et intermedius.

### R - 4 - 2 - 3 Analyse statistique

Pour chaque muscle (droit et gauche), le volume (V) et le rapport ($RV_{tot}$) du volume de chaque muscle sur le volume total du côté, ont été calculés.

Dans ce qui suit, les muscles ont été regroupés en groupes fonctionnels par articulation, respectivement fléchisseurs et extenseurs de la colonne vertébrale, de la hanche et du genou comme indiqué dans la figure 7. Pour chaque groupe, le volume musculaire total ($V^{gp}$) a été calculé. En outre, pour chaque articulation étudiée (colonne, hanche et genou), le ratio des fléchisseurs sur extenseurs, $R_{flex/ext}$, a été calculé comme étant le rapport du volume des fléchisseurs sur le volume des extenseurs de l'articulation.

Un test de normalité a été réalisé sur V, $RV_{tot}$, $V^{gp}$ et $R_{flex/ext}$ avec un test Lilliefors (Lilliefors, 1967) (seuil fixé à 0,05).

Pour chacun des paramètres, les valeurs ont été comparés entre les groupes J et P, et un test de Student a testé si les différences étaient significatives lorsque les données des groupes J et P étaient tirées d'une distribution normale (un test de Mann-Whitney a été utilisé si ce n'était pas le cas).

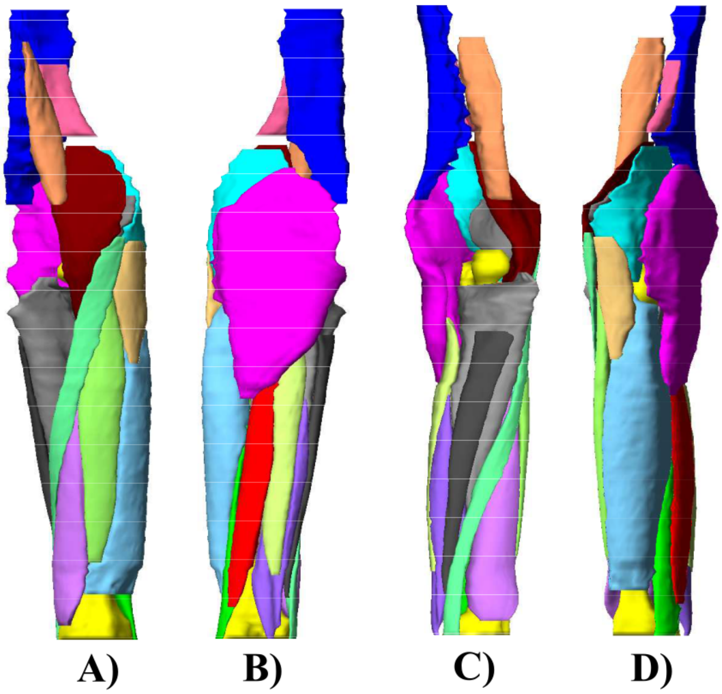


| F: fléchisseurs / E: extenseurs | Colonne F | Colonne E | Hanche F | Hanche E | Genou F | Genou E |
|---|---|---|---|---|---|---|
| Adductor | | | X | | | |
| Biceps femoris long | | | | X | X | |
| Biceps femoris short | | | | X | X | |
| Erectus spinae | | X | | | | |
| Femur | | | | | | |
| Gluteus maximus | | | | X | | |
| Gluteus medius | | | | | | |
| Gluteus minimus | | | | | | |
| Gracilis | | | X | | X | |
| Iliacus | X | | X | | | |
| Psoas | X | | X | | | |
| Quadratus lumborum | | X | | | | |
| Rectus femoris | | | X | | | X |
| Sartorius | | | X | | X | |
| Semi membraneous | | | | X | X | |
| Semi tendineous | | | | X | X | |
| Tensor Fascia Lata | | | X | | | |
| Vastus lateralis inter | | | | | | X |
| Vastus medialis | | | | | | X |

Figure 7. : Muscles considérés dans l'étude (figure obtenue avec la méthode DPSO (Jolivet *et al.*, 2008)), représentés sur une reconstruction 3D de la jambe gauche. **A)** Vue antérieure. **B)** Vue postérieure. **C)** Vue latérale. **D)** Vue médiale. Le tableau à droite décrit les groupes fonctionnels considérés pour l'analyse: Fléchisseurs de Colonne (Colonne F), Extenseurs de Colonne (Colonne E), Fléchisseurs de Hanche (Hanche F), Extenseurs de Hanche (Hanche E), Fléchisseurs de Genou (Genou F) and Extenseurs de Genou (Genou E).

### R - 4 - 2 - 4 Méthode de calcul du volume à partir de peu de coupes IRM

Un modèle a été mis au point permettant de calculer le volume à partir d'un ensemble réduit de coupes IRM segmentées afin de réduire le temps de segmentation et d'offrir un outil utilisable en routine clinique. Cette méthode a été développée uniquement sur le groupe J. Dans le but de quantifier le volume musculaire plus rapidement, le modèle construit considère un maximum de 5 coupes IRM segmentées.

Les volumes de tous les groupes fonctionnels ont été prédits à partir d'une régression multilinéaire en utilisant les informations d'un nombre limité de coupes (de 2 à 5 coupes). Les prédicteurs suivants ont été utilisés dans le modèle: âge, IMC, longueur du fémur et somme des aires des muscles contenus dans le groupe considéré, sur la coupe considérée. Une analyse en composantes principales (ACP) a été réalisée afin de ne conserver que les prédicteurs pertinents (combinaison linéaire de prédicteurs initialement considérés). Chaque prédicteur ACP calculé a été remplacé par le prédicteur initial le plus corrélé avec lui, afin d'obtenir une équation de prédiction claire et compréhensible. Même si la somme des aires des muscles n'a pas été retenue par cette procédure en tant que prédicteur, cette somme a été ajoutée en tant que tel pour sa pertinence comme un indicateur global.

Le modèle a été construit sur les données côté droit des sujets jeunes. Les coupes ont été numérotées vers le haut de 0 à 150: la coupe 0 est la première coupe où apparaît la partie postérieure des condyles fémoraux, et la coupe 100 est la dernière coupe proximale où la tête fémorale est visible.

Les fléchisseurs de colonne ($Col_{flex}$) et extenseurs de colonne ($Col_{ext}$) ont été segmentés sur des coupes IRM allant de T12 au grand trochanter ("coupes proximales"), tandis que les fléchisseurs et extenseurs de genou et hanche, ($Hanche_{flex}$, $Hanche_{ext}$, $Genou_{flex}$, $Genou_{ext}$), ont été segmentés sur des coupes IRM allant de S1 aux condyles fémoraux ("coupes distales"). Par conséquent, au moins 1 coupe des "coupes proximales " a été inclue dans les combinaisons de coupes. Une coupe a été considérée seulement si elle contenait les segmentations des muscles pour au moins 90% des sujets. Pour chaque coupe de la combinaison, chaque muscle du groupe fonctionnel, l'erreur moyenne quadratique (RMS) a été calculée comme la racine carrée de la moyenne du carré des différences (en % du volume réel) entre le volume prédit (avec méthode de leave-one-out) et volume réel (calculé avec la méthode DPSO).

Une analyse combinatoire a été effectuée afin de trouver la meilleure combinaison de "coupes proximales" (respectivement "coupes distales"), comme étant celle présentant l'erreur RMS la plus petite pour $Col_{ext}$ et $Col_{flex}$ (respectivement pour $Hanche_{flex}$, $Hanche_{ext}$, $Genou_{flex}$ et du $Genou_{ext}$). Enfin, la prédiction de ce modèle a été évaluée en calculant l'erreur de prédiction du volume pour chaque groupe fonctionnel.

## R - 4 - 3 Résultats

### R - 4 - 3 - 1 Démographie

Le groupe J comprenait 12 femmes et 11 hommes. L'âge (respectivement IMC) variait de 18 à 21 ans (resp. 17,4 à 24,8 kg/m$^2$). L'âge moyen était 19,3 ans (EC: 0,8). L'IMC moyen était de 20,9 kg/m$^2$ (EC: 2.0). Le groupe P incluait 19 femmes avec déformation rachidienne: âge moyen: 60,1 ans (EC = 12,7 ans); étendue: 37-80 ans.

### R - 4 - 3 - 2 Analyse statistique

Concernant le groupe J, aucune différence significative n'a été trouvée entre les côtés droit/gauche pour le volume musculaire des jeunes du groupe J, sauf pour: V et $RV_{tot}$ du qudartus lumborum, rectus femoris et semi-tendinosus. Cette différence entre les côtés droit et gauche pour ces muscles/paramètres était en moyenne inférieure à 11% de la valeur moyenne droite/gauche. Les valeurs ont été moyennées entre côtés droit/gauche quand aucune différence significative n'a été trouvée. La majeure partie des paramètres géométriques considérés étaient issus d'une distribution normale, sauf pour les muscles et les paramètres suivants: par exemple, le V de l'adductor droit, le $RV_{tot}$ du sartorius gauche.

Pour le groupe P, tous les volumes et ratios se sont révélés être issus d'une distribution normale à l'exception de:

- le volume V du gluteus maximus côté gauche ($p = 0{,}02$) et du gluteus minimus côté gauche ($p = 0{,}02$);
- le ratio $RV_{tot}$ du vastus lateralis inter côté droit ($p = 0{,}04$), biceps femoris breve côté droit ($p = 0{,}01$) et tensor fascia lata côté droit ($p = 0{,}04$).

Pour la plupart des muscles, les moyennes et écarts types ainsi que test de Student ont été utilisés pour la description de l'échantillon. Pour les muscles particuliers énumérés ci-dessus, les médianes, quartiles ainsi que le test de Wilcoxon ont été utilisés.

Les différences statistiques entre les sexes ont été trouvées pour tous les volumes musculaires avec des valeurs supérieures pour les hommes. Le ratio du volume d'un muscle donné sur le volume total ($RV_{tot}$) a été trouvée comme quasi-invariant pour tous les muscles (EC $<$1.2%).

Pour chaque groupe fonctionnel musculaire étudié, pour les hommes et les femmes séparément, aucune différence statistique entre les côtés droit et gauche, a été trouvé pour le volume $V^{gp}$ ($p > 0{,}05$ pour test t de Student ou test de Mann-Whitney en fonction de la normalité des données).

#### R - 4 - 3 - 3 Méthode de calcul du volume à partir de peu de coupes IRM

Figure 8 présente la meilleure combinaison de coupes. Deux coupes, bien choisies, au niveau du fémur et du bassin, a conduit à l'estimation du volume avec moins de 15% d'erreur. L'erreur de prédiction du modèle avec 5 coupes (en % du volume réel calculé à partir de la reconstruction 3D) variait de 6% ($\text{Knee}_{\text{flex}}$, $\text{Genou}_{\text{ext}}$ et $\text{Col}_{\text{flex}}$) à 11% ($\text{Col}_{\text{ext}}$), cette erreur étant autour de 9-10% pour $\text{Hanche}_{\text{flex}}$ et $\text{Hanche}_{\text{ext}}$.

#### R - 4 - 3 - 4 Comparaison entre les deux populations pour les groupes fonctionnels

**Volumes**
Des différences significatives entre les deux populations ont été trouvées pour les fléchisseurs de la colonne vertébrale côté gauche (différence moyenne de -13.6%) et extenseurs du genou (à droite: -18.1% ; gauche: -21.5%).

**Ratio du volume des fléchisseurs sur le volume des extenseurs: $\mathbf{R_{flex/ext}}$**
Une différence significative entre les deux populations a été trouvée pour le côté droit (15,1%) et côté gauche (22,3 %) du ratio flex/ext pour le genou.

#### R - 4 - 3 - 5 Comparaison entre les deux groupes pour chaque muscle individuel

**Volumes**
Lorsque l'on compare le groupe P au groupe J, tous les muscles présentent une perte de volume, sauf pour le gluteus medius côté droit (différence moyenne de +2,6%) et côté gauche (+1,5%); gluteus minimus côté droit (+8,6%) et côté gauche (12,4%); tensor du fascia lata côté droit (+2,9%) et côté gauche (+8,5%) et biceps femoris breve côté gauche (+0,4%).

**Ratio du volume sur volume total: $\mathbf{RV_{tot}}$**
Les différences statistiques ($p < 0{,}05$) ont été trouvés seulement pour le ratio $RV_{tot}$ des muscles individuels: gluteus medius côté droit et côté gauche ($p = 0{,}00$); gluteus minimus côté droit ($p = 0{,}02$); vastus lateralis intermedius côtés droit et gauche ($p = 0.00$); vastus medialis côté gauche ($p = 0{,}01$); rectus femoris côtés droit et gauche ($p = 0{,}00$).

### R - 4 - 4 Discussion

Cette étude quantifie les volumes musculaires pour des jeunes adultes asymptomatiques, fournissant des valeurs de référence pour les études futures. Le ratio d'un volume musculaire sur le volume de l'ensemble des muscles a été trouvé quasi-invariant chez les jeunes adultes asymptomatiques. Une comparaison a été faite avec des valeurs pour les adultes avec déformations rachidiennes.

Un ensemble réduit de 2 (respectivement 5) coupes IRM segmentées, bien choisies, peuvent être utilisées pour calculer le volume musculaire avec moins de 14% d'erreur (respectivement 11%) (figure 8).

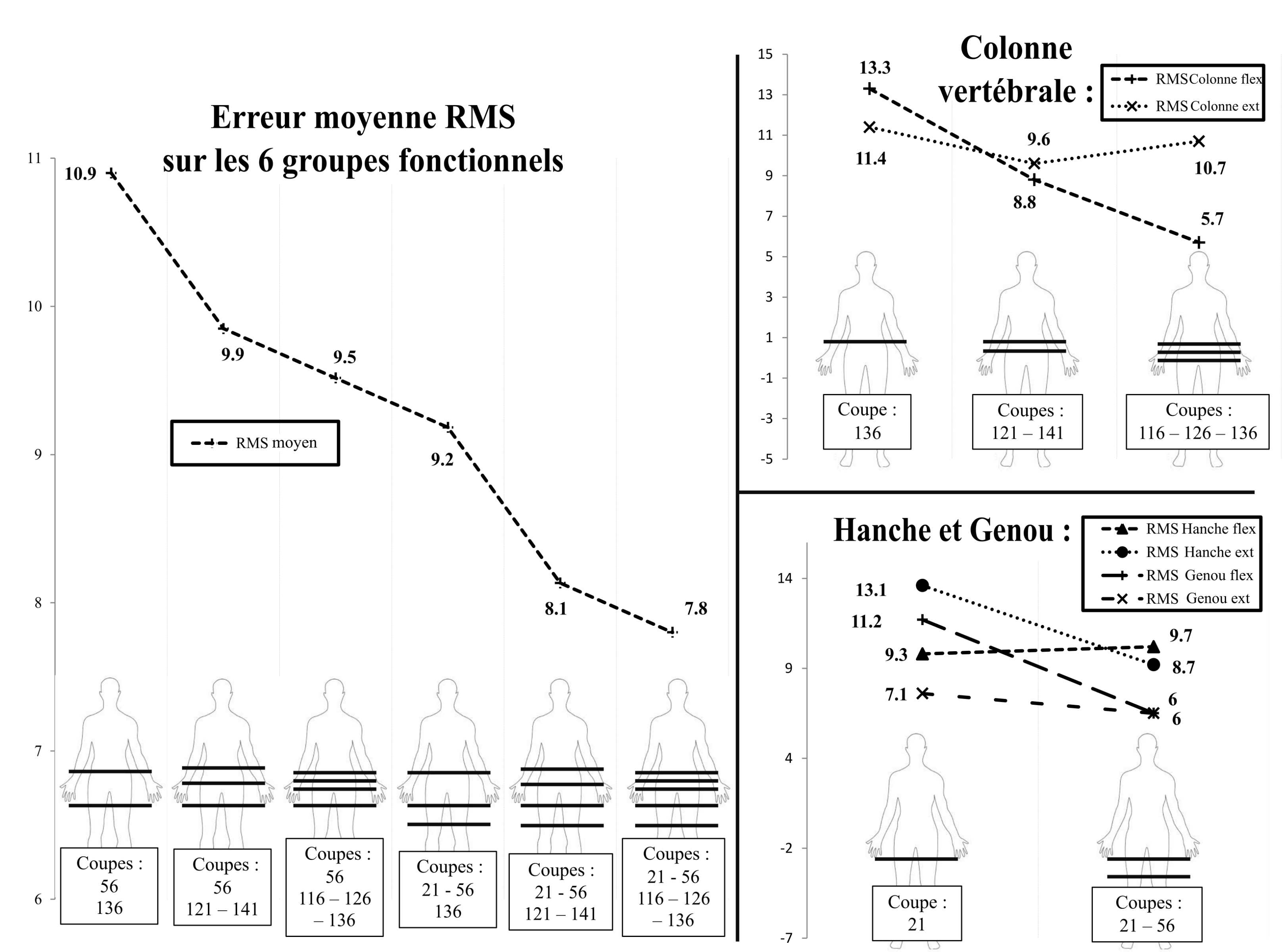


Figure 8. : Erreur de prédiction (RMS) pour chaque groupe fonctionnel, et moyenne sur les 6 groupes (« RMS moyen »), pour les différentes combinaisons de coupes IRM.

### R - 4 - 4 - 1 Limites

Ce travail comporte certaines limites. Premièrement, seuls 23 sujets jeunes ont été inclus dans l'étude mais comme ils étaient tous âgés entre 18 et 24 ans, et comme ils ont tous été recrutés dans le même environnement (étudiants en médecine), la variabilité entre leurs systèmes musculaires devrait être faible. La petite tranche d'âge étudiée était un objectif afin de mieux caractériser la population jeune asymptomatique, mais d'autres études devraient quantifier les changements liés à l'âge en recrutant des volontaires de différents groupes d'âge. Une seconde limite est de ne pas avoir étudié la qualité musculaire, mesurée par l'infiltration graisseuse qui reste un paramètre important pour décrire le système musculaire. L'infiltration graisseuse peut être évaluée à partir des images IRM acquises avec la méthode Dixon (Moal *et al.*, 2015), ce fut le cas dans notre étude et les données connexes sont actuellement en cours d'analyse.

Une troisième limite est l'analyse de l'aire sur une coupe transversale et non de l'aire physiologique: l'angle de pennation des muscles n'a pas été considéré ici, vu que seulement des coupes axiales ont été étudiées.

En outre, certains muscles ont été regroupés en raison du manque de visibilité de leurs contours. D'autres études ont aussi mis en avant cette difficulté de distinguer la frontière entre les vastus lateralis et intermedius (Barnouin *et al.*, 2014) suggérant de regrouper les deux muscles ensemble en raison de la fusion fréquente chez les jeunes adultes. Un regroupement similaire a été fait pour mettre en place le groupe adducteur, le groupe érecteurs spinaux et le groupe iliopsoas. Alors que le dernier groupe est largement considéré comme tel dans la littérature (Lube *et al.*, 2016; Sanchis-Moysi *et al.*, 2011; Ghiasi *et al.*, 2016), regrouper les muscles vient de la difficulté à identifier la frontière entre les muscles de ce groupe, cette difficulté est renforcée ici par l'inclusion de jeunes en bonne santé présentant peu de graisse entre les aponévroses de différents muscles (Barnouin *et al.*, 2014).

Cette étude n'a pas inclus les petites rotateurs externes de la hanche car le choix a été fait de considérer les muscles fréquemment utilisés dans le maintien postural sagittal dans le cadre d'un projet plus large. Ces petits muscles doivent cependant être inclus dans une étude future plus fine. Il faut garder à l'esprit cependant que regrouper des muscles réduira la capacité de quantifier précisément les caractéristiques de ces muscles et donc de fournir des valeurs de base pour la comparaison avec d'autres populations. Néanmoins, l'objectif de cette étude était de fournir une première base de données globale pour ces muscles, et un outil facile d'utilisation pour la clinique afin d'estimer le volume de groupes musculaires et d'estimer quantitativement les changements musculaires.

Le modèle utilisant un nombre réduit de coupes IRM segmentées a été construit sur des données du côté droit de sujets jeunes. Les équations du modèle ont été appliquées sur le côté gauche et ont abouti à des erreurs de prédiction similaires (moins de 1% de différence), sauf pour les fléchisseurs de la colonne vertébrale (13,5% pour le côté gauche vs 5,7% pour le côté droit).

Aucune information n'a été recueillie pour les patients (recrutés dans une étude précédente au cours de la thèse de Bertrand Moal) sur l'origine de la pathologie, aucune information était donc disponible pour établir si la déformation développée en raison de douleurs du dos ou à la suite de changements posturaux pour maintenir un équilibre statique.

### R - 4 - 4 - 2 Comparaison des deux populations

La sarcopénie est la perte volumique des muscles qui se produit avec le vieillissement. La population étudiée ici inclut des patients avec déformations rachidiennes plus âgés que la population de référence (âge moyen: 60 ans vs 19,3 ans). Par conséquent, les deux effets de la sarcopénie et de la dégradation due à la pathologie doivent être observés dans les résultats. L'utilisation du ratio volume sur volume total est donc intéressante dans l'analyse des résultats afin de s'affranchir de l'effet de la sarcopénie dans l'analyse des résultats.

**Extenseurs du genou**
Un volume significativement plus faible a été observé (pour le volume moyen du groupe P vs groupe J) pour les extenseurs du genou (pour les deux côtés) et est responsable du plus grand ratio $R_{flex/ext}$ pour le Groupe P: différence moyenne de 15.1% pour le côté droit et de 22,3% pour le côté gauche.

Le rectus femoris, vastus medialis et vastus lateralis inter résentent un volume nettement plus faible associé à un ratio volumique significativement plus faible. Pour ces muscles, les plus petits volumes peuvent être expliqués par l'effet de l'âge; tandis que le ratio plus petit est lié au déplacement antérieur de la partie supérieure du tronc pour les patients. En raison de cette flexion vers l'avant du tronc, ces muscles sont raccourcis, se contractent donc moins, un faible recrutement conduit alors à un ratio plus faible.

**Groupe des muscles fessiers**
Le groupe des muscles fessiers comprend le gluteus minimus, gluteus medius et gluteus maximus.

Un plus grand volume a été quantifié pour les gluteus minimus et medius. Les deux muscles peuvent être assimilés à des extenseurs de la hanche, même si leur fonction couramment admise est un contrôle latéral du mouvement du fémur dans le plan coronal.

Le troisième muscle du groupe des muscles fessiers est le gluteus maximus, aussi un extenseur de la hanche et qualifié comme un muscle de propulsion utilisé pour la locomotion et les mouvements de grande amplitude (en raison de sa grande longueur et son grand volume, et de son insertion distale sur le fémur). Les gluteus minimus et medius, en raison de leurs longueurs plus courtes et insertions plus proximales sur le fémur, semblent contribuer à la régulation de la position du bassin par de petits mouvements et non à la locomotion: à la fois gluteus medius et minimus peuvent être qualifiés de muscles du contrôle postural, contrôlant la rétroversion pelvienne.

La perte du volume observée pour le gluteus maximus (différence moyenne de -7.9% pour le côté droit et -10.3% pour le côté gauche) peut alors être interprétée comme l'effet de la sarcopénie et/ou comme un marqueur d'une activité réduite chez les patients (amplitude réduite des mouvements du fémur par rapport au bassin). L'augmentation de volume (gain de volume nominal et du ratio volumique) observée pour le gluteus medius et minimus suggère un besoin de régulation posturale de la position du bassin, avec des mouvements de faible amplitude du bassin par rapport au fémur.

### R - 4 - 4 - 3 Comparaison avec la littérature

Concernant le volume musculaire pour les jeunes adultes asymptomatiques, la comparaison peut être faite avec des études antérieures de la littérature (Barnouin *et al.*, 2014; Lube *et al.*, 2016; Handsfield *et al.*, 2014; Belavý *et al.*, 2011): dans l'ensemble nos résultats sont en accord avec ces résultats de la littérature. En regardant plus en détails l'iliopsoas, pour les hommes, nos résultats sont supérieurs à ceux du Lube *et al.* (Lube *et al.*, 2016) et Handsfield *et al.* (Handsfield *et al.*, 2014): 515 $cm^3$ vs entre 442 et 452 $cm^3$ pour ces études. Pour les femmes, nos résultats sont supérieurs (291 $cm^3$) à ceux de Lube *et al.* (252 à 268 $cm^3$) (Lube *et al.*, 2016) mais inférieurs à ceux de Handsfield *et al.* (452 $cm^3$) (Handsfield *et al.*, 2014). Les différences peuvent être dues à des différences dans la population étudiée (IMC plus élevé, plus large tranche d'âge, etc.): par exemple, Handsfield *et al.* ont rapporté des valeurs pour 24 participants en bonne santé (avec seulement 8 femmes) (Handsfield *et al.*, 2014), et l'étude de Lube *et al.* (Lube *et al.*, 2016) a seulement inclus 3 femmes et 3 hommes. Tous ces commentaires pourraient également être appliqués aux différences observées avec ces études pour le groupe adducteur et biceps femoris. Pour ce dernier, Lube *et al.* avaient déjà rapporté une grande variation du volume entre les différentes populations, la différence dans les participants de chaque étude pourrait expliquer ces différences (différence maximale de 47 $cm^3$ pour les hommes) avec les données de cette étude (Lube *et al.*, 2016).

Frontera *et al.* a quantifié en 2000, dans une étude longitudinale sur 12 ans, l'effet de la sarcopénie sur la cuisse et ses muscles: en 12 ans, la diminution de l'aire sur une coupe a eu lieu pour l'ensemble de la cuisse (-12,5%), pour tous les muscles de la cuisse (-14.7%), pour rectus femoris (-16.1%) et pour les muscles fléchisseurs du genou (-14,9%) (Frontera *et al.*, 2000). Des résultats similaires ont été trouvés ici pour le rectus femoris et les muscles fléchisseurs du genou en termes de volume: -25% pour le rectus femoris et -7.1% et -5.6% pour les muscles fléchisseurs du genou. Une plus grande diminution du volume a été trouvé ici pour le rectus femoris par rapport aux muscles fléchisseurs du genou: cela pourrait être le signe d'une compensation via une flexion du genou pour les patients présentant une flexion vers l'avant du tronc. Le plus petit volume pour le rectus femoris peut être causé à la fois par la sarcopénie et l'évolution de la pathologie vu que le ratio était aussi plus petit: ce muscle est l'un des premiers à se dégrader si le tronc part vers l'avant (une plus petite longueur de contraction pourrait impliquer de plus petites contractions, puis diminution du volume et du ratio).

En ce qui concerne le psoas et rectus femoris, Takahashi *et al.* (2006) a rapporté l'évolution de l'aire dans différents groupes d'âge de 20 à 80 ans, pour des femmes asymptomatiques. A titre de comparaison, quand on ne regarde que les sujets âgés de 20 à 29 ans par rapport à ceux âgés de 50 à 69 ans, l'évolution de l'aire au cours du vieillissement est similaire à l'évolution du volume quantifié dans notre étude. Le volume de l'iliopsoas présente une diminution de volume de 12,0% par rapport à une diminution de 19% pour le psoas tel que rapporté par Takahashi *et al.* (aire plus petite, passant de 991 $mm^2$ à 800 $mm^2$). En ce qui concerne le rectus femoris, un volume de 26% plus petit a été trouvé ici, par rapport à une aire 17% plus petite tel que rapporté par Takahashi *et al.* (aire plus petite passant de 4096 $mm^2$ à 3400 $mm^2$). Si, pour le psoas la différence est du même ordre de grandeur, ce n'est pas le cas pour le rectus femoris: ceci peut être expliqué par l'effet de l'état pathologique des patients du groupe P étudié ici, qui s'ajoute à l'effet du vieillissement, rapporté par Takahashi *et al.* (2006).

#### R - 4 - 4 - 4 Méthode de calcul du volume à partir de peu de coupes IRM

Parmi tous les modèles étudiés (de 2 à 5 coupes), le modèle 2 coupes fournit une estimation relativement bonne du volume musculaire (Figure 8: RMS moyen = 10,9%). Le modèle 5 coupes est un compromis entre la précision requise et le temps d'analyse (notamment dans un environnement de routine), alors que l'ensemble du modèle 3D pourrait être plus approprié pour la recherche, en particulier lorsque l'on considère les extenseurs de la colonne vertébrale (RMS $<$ 8% pour la moyenne sur les 6 groupes fonctionnels (Figure 8)). Ce modèle utilise une combinaison de 2 "coupes distales" et 3 "coupes proximales". 2 coupes "distales" sont nécessaires: l'une près de l'extrémité distale du fémur (coupe 21) pour estimer le volume de muscles spécifiques (semi-membranosus et biceps femoris breve par exemple); une au milieu de la diaphyse (coupe 56) afin de mieux évaluer les grands muscles de la cuisse (adducteurs, vastus, rectus femoris par exemple). Les trois "coupes proximales" (coupes 116, 126 et 136) sont situées entre le cotyle et T12 afin d'estimer le volume des fléchisseurs et extenseurs de la colonne vertébrale: ces coupes sont proches les unes des autres (10 coupes d'intervalle) afin de se concentrer sur une zone où les 3 muscles d'intérêt sont segmentés (iliopsoas, érecteurs spinaux et quadratus lumborum), mais aussi pour estimer le volume d'un petit muscle changeant rapidement de forme: le quadratus lumborum (carré des lombes). En outre, le modèle est peu sensible à la position exacte de la coupe proposée dans le modèle: utiliser une coupe positionnée +/- 5 coupes au-dessus ou au-dessous, modifie l'erreur RMS au maximum de 1,5%. Par conséquent, si elle est validée sur d'autres populations, cette méthode pourrait être mise en oeuvre en routine clinique pour caractériser le volume musculaire de groupes fonctionnels.

Cette nouvelle méthode permet un gain de temps lors de l'analyse des images IRM (temps de reconstruction assez réduit: 5 coupes segmentées vs plus de 120 coupes pour la reconstruction 3D totale).

Différents niveaux d'analyse peuvent être nécessaires pour caractériser la géométrie musculaire: en routine clinique, une méthode rapide pourrait fournir un aperçu global des muscles des patients, alors que dans la recherche, une méthode plus longue peut être considérée pour obtenir une analyse plus fine. Si la méthode DPSO est la méthode actuelle fournissant l'estimation la plus pertinente de la géométrie de chaque muscle individuel, une nouvelle méthode a été proposée ici pour une utilisation dans un environnement clinique: elle nécessite moins de temps d'analyse des images IRM et fournit encore une bonne estimation du volume musculaire des groupes fonctionnels.

Le modèle actuel semble prometteur pour une utilisation en routine clinique pour quantifier le volume musculaire des groupes fonctionnels. Ce modèle doit encore être validé sur d'autres populations (personnes âgées, patients) avant d'être utilisé comme outil en routine clinique.

## R - 4 - 5 Conclusion

Cette partie de la thèse a porté sur une analyse fine des muscles spino-pelviens de deux populations: une population de référence (jeunes adultes asymptomatiques) et une population de sujets avec déformations rachidiennes.

Tout d'abord, les valeurs de référence ont été rapportés pour les muscles spino-pelviens d'adultes asymptomatiques. Un modèle permettant de calculer avec précision le volume musculaire de groupes fonctionnels, à partir de moins de 6 coupes IRM segmentées, a été proposé. Cette méthode permet un calcul précis du volume dans une routine clinique.

Deuxièmement, les muscles spino-pelviens ont été décris pour des adultes avec déformations rachidiennes. Une comparaison a été faite avec la population de référence. Des différences significatives peuvent être identifiées comme étant liées aux mécanismes de compensation observés pour les patients avec déformations rachidiennes: la rétroversion pelvienne peut être liée aun plus grand volume observé des petit et moyen fessiers (gluteus medius et minimus); une flexion du genou peut être liée au rapport volumique plus faible des extenseurs du genou, et à la plus grande proportion volumique des fléchisseurs de genou.

Ces mécanismes de compensation se produisent afin de limiter l'effet du décalage antérieur du tronc observé chez ces patients, recrutant ainsi des muscles particuliers afin d'augmenter la stabilité de cette position, même si d'autres muscles sont donc moins stimulés que chez des adultes jeunes asymptomatiques.

Même si cette étude a tenté de tirer des conclusions à partir de ces résultats préliminaires, des données supplémentaires sont nécessaires afin de consolider ces conclusions et interprétations. Une cohorte plus large et plus diversifiée à l'avenir pourrait aider à confirmer ces résultats. Une étude plus poussée est nécessaire afin de différencier correctement les mécanismes de compensation liés au vieillissement asymptomatique et les troubles liés à l'évolution d'une déformation rachidienne. Une telle étude est actuellement en cours en collaboration avec Cédric Maillot lors de son projet de master.

Les recherches futures devront inclure la composante infiltration graisseuse pour les différentes populations afin d'évaluer la dégradation de la qualité musculaire avec l'âge et l'évolution d'une pathologie. Cette étude apportera des connaissances importantes sur la prévention de la dégradation musculaire chez les personnes âgées et les patients.

Cette partie se concentrant sur l'analyse de muscles à partir d'images d'IRM, a mis en évidence le lien entre altération posturale et changements musculaires. Si ces modifications et des changements ont été décrits dans les deux premières parties de cette thèse, les interactions entre les systèmes squelettique et musculaire ne peuvent être étudiées à partir de ces travaux. La modélisation biomécanique musculo-squelettique peut donner un aperçu de ces interactions lors de la régulation d'une posture afin de la rendre efficace.

La troisième partie de cette thèse présentera en conséquence l'adaptation et la personnalisation d'un modèle biomécanique musculo-squelettique pour étudier le schéma de recrutement musculaire pour différentes sujets/patients, pour différentes postures.

# R - 5 Modèle musculo-squelettique

## R - 5 - 1 Introduction

La quantification des changements de l'alignement postural et du système musculaire se produisant avec le vieillissement a été effectuée dans les deux premières parties de cette thèse. Si une forte interaction a lieu entre ces deux systèmes, il est difficile de tirer des conclusions sur la relation entre les deux, d'après les deux premières parties de ce manuscrit. La modélisation musculo-squelettique offre la possibilité de combiner des informations posturales et musculaires.

Pour atteindre cet objectif, un modèle de régulation musculaire est utilisé dans cette troisième partie. Il a été adapté à partir du modèle développé par Vincent Pomero au cours de son doctorat en 1999-2002 (Pomero *et al.*, 2002, 2004). L'hypothèse principale est que les muscles agissent pour protéger l'articulation intervertébrale en réduisant les forces et moments résultants au niveau du disque intervertébral à une limite acceptable, au cours d'activités quotidiennes.

Ce modèle de régulation musculaire vise à estimer, en utilisant une boucle de contrôle, le recrutement musculaire et les efforts intervertébraux (IV) résultants, compte tenu des forces et des moments résultant de la gravité s'appliquant au centre du disque intervertébral. Ici, l'axe X est l'axe postéro-antérieur; Y est l'axe médio-latéral, orienté vers la gauche du patient, et Z est l'axe caudo-crânien. Dans ce qui suit, Fx (respectivement Fy et Fz) désigne la force exercée sur l'axe X (respectivement Y et l'axe Z.); Mx (respectivement My et Mz) désigne le moment sur l'axe X (resp. Axes Y et Z). Dans ce qui suit, le terme efforts désigne les 6 composantes des efforts: la force de cisaillement postéro-antérieure (Fx), la force de cisaillement latéral (Fy), la force de compression (Fz), le moment d'inflexion latérale (Mx), le moment de flexion (My) et le moment de torsion (Mz).

Les efforts au niveau de l'articulation intervertébrale (appelés $E_{IV}$) sont égaux aux forces et moments dus à la gravité de la partie supérieure sur la section considérée ($E_{ext}$) auxquels sont soustraits les efforts résultant de l'action des muscles ($E_{muscles}$) (équation 8.1):

$$E_{IV} = E_{ext} - E_{muscles} \tag{1}$$

$E_{ext}$ sont les forces et moments dus à la gravité de la partie supérieure et peuvent être estimés à partir de données de plateforme de force par exemple. Les inconnues sont $E_{IV}$ et $E_{muscles}$.

Afin d'estimer les efforts générés par les muscles activés, une boucle de régulation est utilisée dans ce modèle (figure 9) qui vise à maintenir les efforts intervertébraux sous des valeurs seuils acceptables.

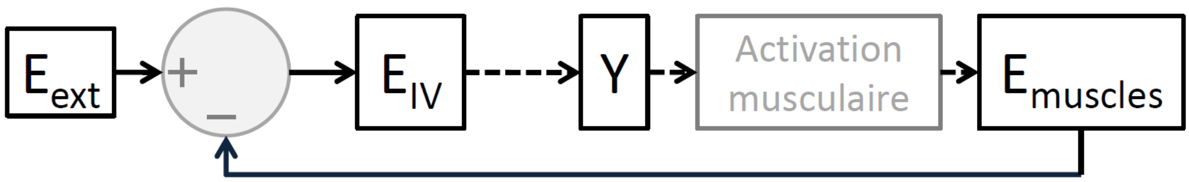


Figure 9. : Boucle de contrôle du modèle de régulation musculaire (MMR).

Le processus de régulation tient compte de deux aspects:

- en fonction des forces et des moments dus à la gravité, une fonction de régulation est calculée pour stimuler l'activation musculaire (équation 8.2). La fonction de régulation, Y, fixe la quantité d'activation musculaire requise: plus Y est grand , plus la demande en contraction musculaire sera grande afin de réduire considérablement les efforts résultants dans l'articulation intervertébrale.

$$Y = 10 * \frac{{E_{IV}}^3}{Seuil_I V^3} \tag{2}$$

- pour chaque muscle, suivant sa section sur la coupe transversale, sa ligne d'action et la position de son centroide par rapport à l'articulation intervertébrale, ce muscle présentera plus ou moins la capacité de réduire une ou plusieurs composantes des forces et moments appliqués au centre de l'articulation intervertébrale considérée. Par exemple, le quadratus lumborum (carré des lombes) génère un moment d'inflexion latérale et un cisaillement latéral par sa contraction et donc peut réguler ces deux composantes des efforts (figure 10).

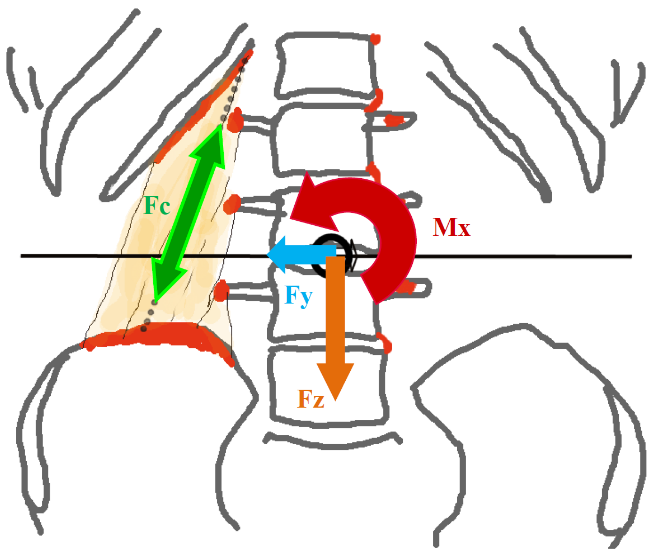


Figure 10. : La contraction du quadratus lumborum (carré des lombes) (Fc en vert) va générer un moment d'inflexion latérale (Mx en rouge) et un cisaillement latéral (Fy en bleu). La contraction musculaire génère également une force de compression (Fz en orange) [Adapté de (Pomero, 2002)].

Une première estimation des efforts générés par l'activation des muscles est calculée, ce qui conduit à une valeur plus faible des efforts dans l'articulation IV, d'après l'équation 8.1. Cette nouvelle valeur est ensuite utilisée comme donnée d'entrée pour calculer la deuxième estimation de $E_{muscles}$. Cela continue, jusqu'à ce que l'addition de contraction musculaire ne change plus beaucoup la valeur de $E_{IV}$.

L'algorithme du modèle a été décrit dans des articles publiés précédemment (Pomero *et al.*, 2002, 2004) et est inclus en annexe C. Les données d'entrée sont traitées dans Matlab® R2011b (The Mathworks Inc., Natick, MA, USA), avant passage dans Simulink® (The Mathworks Inc., Natick, MA, USA). Lorsqu'il a été développé en 2002, ce modèle nécessitait: l'utilisation d'une plateforme de force pour estimer les forces et moments dus à la gravité; des stéréoradiographies pour reconstruire en 3D les os, et des images IRM pour la saisie de la géométrie musculaire. Ce modèle a été appliqué sur quatre patients et un volontaire (Pomero *et al.*, 2002).

La principale contribution de cette thèse est de proposer un processus pour générer un modèle musculo-squelettique personnalisé à partir de radios EOS et d'images IRM, utilisant les nouveaux algorithmes de reconstruction 3D. La nouveauté réside dans le calcul des forces et moments dus à la gravité (directement à partir des radiographies EOS) et l'élaboration d'une géométrie 3D complète de la colonne vertébrale, du bassin et des muscles dans la position debout. Les chapitres suivants présenteront ce processus et les résultats obtenus lorsqu'il est appliqué sur 20 sujets d'âges différents, avec et sans déformations rachidiennes.

## R - 5 - 2 Matériels et méthodes

### R - 5 - 2 - 1 Modèle biomécanique

Le modèle de régulation musculaire (MMR) est basé sur des informations personnalisées du patient. La reconstruction 3D du squelette à partir d'images EOS et des muscles à partir d'images IRM sera utilisée pour accéder à des informations personnalisées du sujet au niveau intervertébral L3-L4. Le modèle MMR nécessite les données d'entrée suivantes:

- les valeurs seuils des efforts intervertébraux pour la boucle de régulation,
- les forces et moments dus à la gravité, s'appliquant au niveau de l'articulation intervertébrale,
- les caractéristiques des muscles:
  - la géométrie musculaire dans le plan axial passant par le centre du disque intervertébral: la section (CSA), les coordonnées du centroide du muscle ($Centroide\_i$, i = X, Y) et les coordonnées du vecteur ligne d'action ($Dir\_Muscle\_i$, i = X, Y, Z),
  - la contrainte maximale admissible du muscle en $N/cm^2$,

Les données de sortie du modèle sont les suivantes:

- les efforts résultants au niveau de l'articulation intervertébrale,
- les forces musculaires.

**Valeurs seuils pour efforts intervertébraux**
Comme les valeurs seuils peuvent être difficiles à obtenir *in vivo*, ces valeurs ont été fixées en fonction de celles utilisées par Vincent Pomero (Pomero, 2002), basées sur les données internes de l'Institut. Les valeurs seuils ont été fixées comme suit: 75N pour le cisaillement postéro-antérieur (Fx), 100N pour le cisaillement latéral (Fy), 1500N pour la compression (Fz) et 4.9N pour les différents moments (Mx, My, Mz).

**Forces et moments dus à la gravité, s'appliquant sur l'articulation intervertébrale**
Si la plupart des méthodes ont utilisé une plateforme de force pour obtenir les forces et moments dus à la gravité, ici le calcul a été effectué à partir de l'enveloppe externe reconstruite en 3D à aprtir des radios EOS, et d'un modèle de densité issu de la littérature.

La reconstruction 3D de l'enveloppe externe à partir de radios EOS est coupée par un plan axial au niveau du disque intervertébral L3-L4. Le centre de masse et le poids de chaque segment situé au-dessus de cette coupe peut être calculé à partir des volumes des différents segments (issus de l'enveloppe externe en 3D (Nérot *et al.*, 2015)), avec un modèle de densité (Figure 11). Ensuite, le centre de masse du haut du corps, sa masse et la force verticale associée résultant de la gravité, peuvent être facilement calculés.

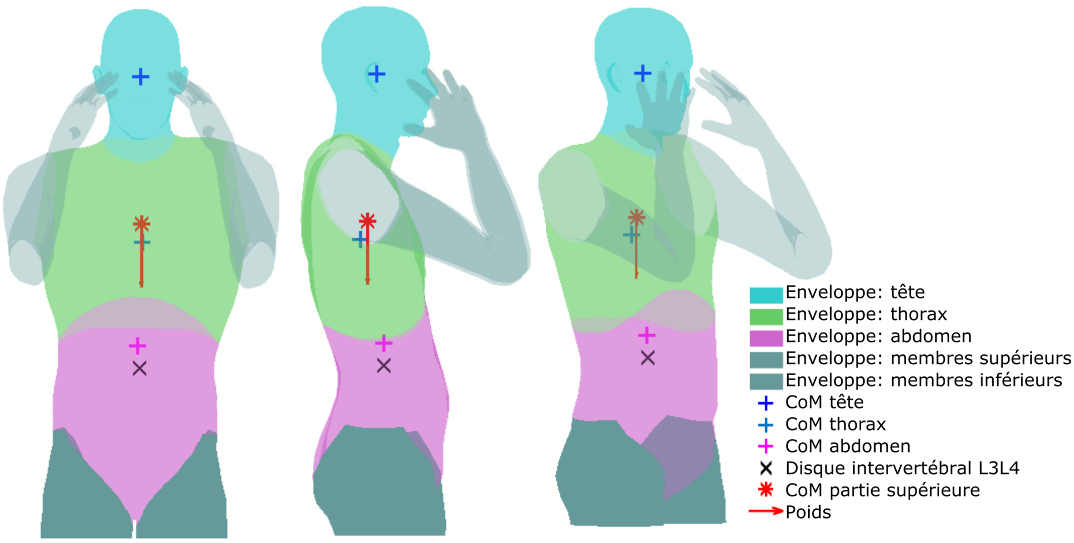


Figure 11. [Calcul des forces et moments dus à la gravité.]: Enveloppe 3D avec les différents segments et leurs centres de masse. A gauche: vue frontale. Au milieu: vue sagittale. A droite: vue globale. CoM signifie centre de masse.

Une attention particulière a été portée au modèle de densité classiquement utilisé, basé sur des études cadavériques (Dempster, 1955; Chandler *et al.*, 1975). Afin d'améliorer la précision de la densité du thorax pour la population, une étude spécifique a été menée au cours de cette thèse. Ce travail a été publié dans Journal of Biomechanics en 2016 (Amabile *et al.*, 2016c). L'objectif était d'affiner l'estimation de la densité du thorax en prenant en compte l'air présent dans les poumons.

Des radiographies bi-planes ont été acquises sur 58 participants, permettant la reconstruction 3D de la colonne vertébrale, de la cage thoracique et de l'enveloppe externe. Trois méthodes de calcul de la masse du thorax ont été comparées pour 48 sujets: (1) la méthode Dempster de densité uniforme, utilisant les données de densité publiées par Dempster (Dempster, 1955) actuellement utilisés dans la littérature, (2) la méthode personnalisée à l'aide de la description complète des différents éléments du thorax en se basant sur la reconstruction 3D de la cage thoracique et de la colonne vertébrale et (3) la méthode de densité uniforme améliorée en utilisant une densité de thorax uniforme issue de la méthode personnalisée. Pour 10 participants, une comparaison a été faite entre la masse totale du corps obtenue à partir d'une plateforme de force et celle obtenue en calculant la masse du thorax avec chacune des trois méthodes.

La méthode de densité uniforme Dempster présentait une erreur moyenne de 4,8% dans l'estimation de la masse totale par rapport à la plateforme de force vs 0,2% pour la méthode personnalisée et 0,4% pour la méthode de densité uniforme améliorée. La densité du thorax ajustée à partir de la reconstruction 3D était 0,74 g/cm$^3$ pour les hommes et 0,73 g/cm$^3$ pour les femmes. Cette valeur conduit à une meilleure estimation de la masse du thorax et de la masse totale par rapport à celle Dempster (0,92 g/cm$^3$).

Cette nouvelle densité du thorax apparaît comme pertinente pour affiner l'estimation des forces et moments dus à la gravité s'appliquant au centre du disque intervertébral.

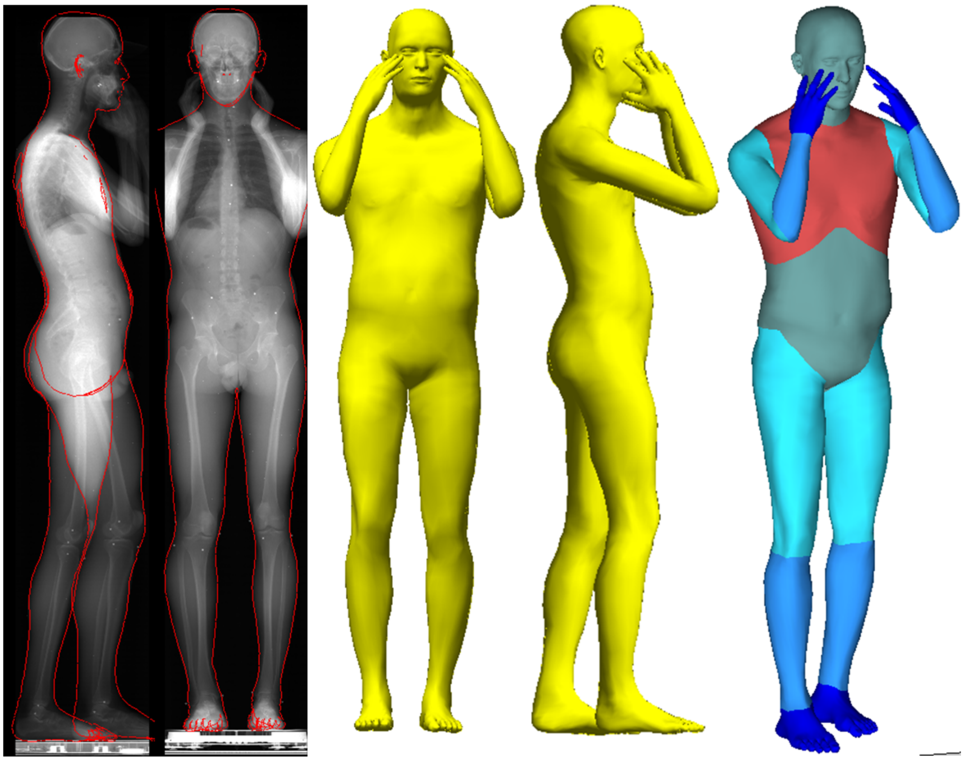

Figure 12. : Reconstruction 3D de l'enveloppe externe: projections sur les radiographies bi-planes et reconstruction 3D de l'enveloppe externe avec les 15 segments considérés (thorax en rouge).

**La géométrie de muscles dans le plan du disque intervertébral**

Le modèle MMR considère une section au niveau lombaire, précisément au niveau du disque intervertébral L3-L4 (Figure 13).

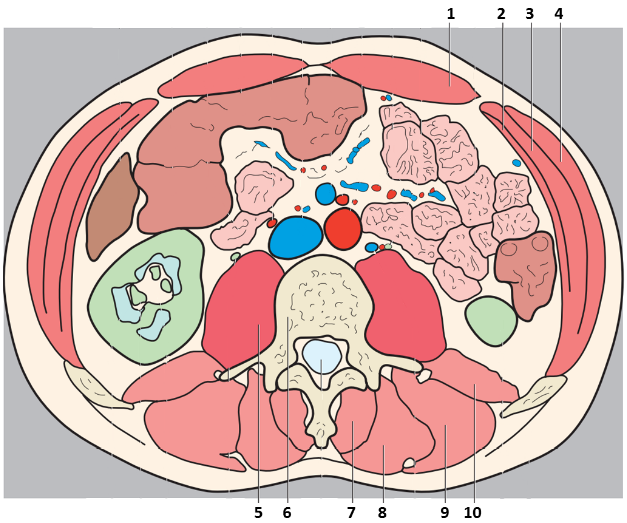


1. Rectus abdominis
2. Transversus abdominis
3. Obliquus internus
4. Obliquus externus
5. Psoas
6. Vertèbre lombaire
7. Multifidus
8. Longissimus dorsi
9. Iliocostalis
10. Quadratus lumborum

Figure 13. : Coupe axiale au niveau lombaire. [Adapté de (Moeller and Reif, 2001)]

Le modèle nécessite la géométrie musculaire détaillée au niveau intervertébral étudié. Cette information peut être extraite à partir d'images d'IRM, mais a besoin d'un traitement supplémentaire afin de représenter la géométrie des muscles dans la position debout, les patients étant en position couchée lors des acquisitions IRM. Tout d'abord, le patient subit un examen EOS dans la position debout, ce qui permet de reconstruire en 3D de la colonne vertébrale et le bassin. Ensuite, les muscles sont reconstruits en 3D à partir d'images IRM, en utilisant la méthode DPSO présentée précédemment. Enfin, les deux géométries 3D sont combinées comme expliqué ci-après.

## Transformer la reconstruction 3D des muscles en position debout

La méthode utilisée est similaire à celle publiée, sur les membres inférieurs, par Hausselle *et al.* (Hausselle *et al.*, 2014): d'une part, l'enveloppe externe et le squelette sont reconstruits en 3D en position debout (à partir de radiographies EOS), d'autre part les muscles et l'enveloppe externe sont reconstruits en 3D en position couchée (à partir d'images IRM) (Figure 14). Une transformation élastique est ensuite utilisée pour transformer les muscles en position debout et faire correspondre les deux enveloppes externes.

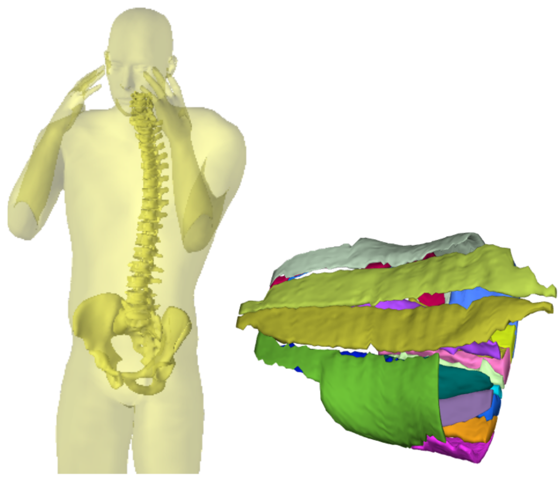

Figure 14. : A gauche, le bassin, la colonne vertébrale et l'enveloppe externe reconstruite en 3D dans la position debout. A droite: Les muscles reconstruits en 3D en position couchée. L'enveloppe externe 3D reconstruite à partir d'images IRM n'a pas été représentée pour plus de clarté.

Les tissus mous se déformant sous l'action de la gravité, une déformation spécifique de la reconstruction 3D des muscles doit être appliquée. Pour ce faire, des points de contrôle sont nécessaires sur les deux ensembles d'images pour faire correspondre les deux reconstructions 3D. Un choix a été fait ici d'inclure les points de contrôle suivants: des points de contrôle pelviens, des points de contrôle de la colonne vertébrale, et des points de contrôle de l'enveloppe externe.

La déformation de l'enveloppe et des muscles 3D issus des images IRM sur la reconstruction EOS 3D a permis d'obtenir la géométrie des muscles dans la position debout (Figure 15).

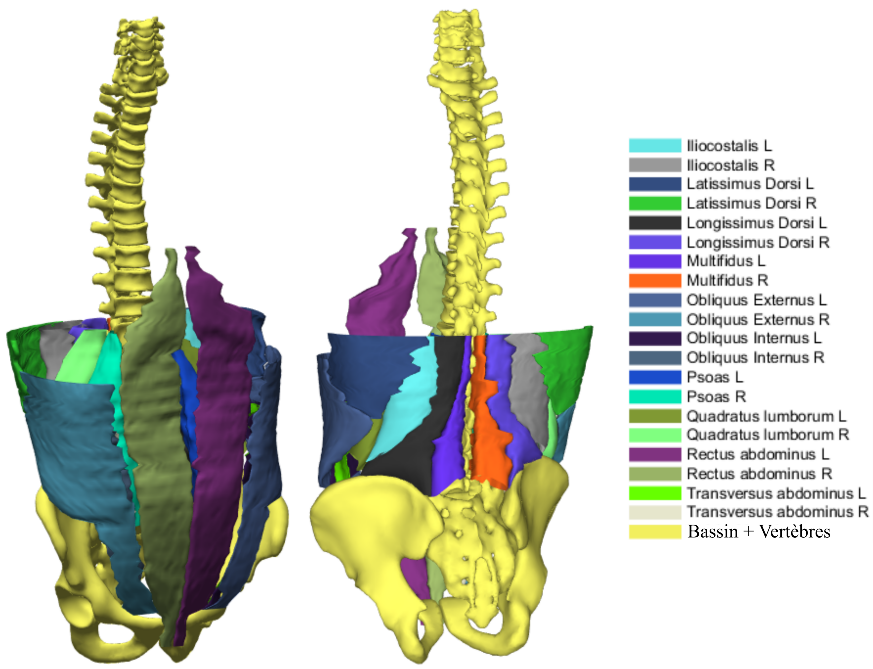


Figure 15. :. Reconstructions 3D des muscles obtenus à partir de segmentations d'images IRM, krigées sur la reconstruction 3D du squelette à partir de radios EOS.

### Coupe d'intérêt

Une fois que la reconstruction des muscles en 3D a été transformée dans la position debout, le modèle 3D est coupé par un plan axial passant par le centre du disque intervertébral L3-L4.

Ce plan axial, est défini par:

- sa normale, étant définie comme étant le vecteur vertical orienté vers le haut;
- le centre du disque intervertébral, étant défini comme étant le milieu entre le barycentre du plateau inférieur de la vertèbre supérieure et le barycentre du plateau supérieur de la vertèbre inférieure.

### Section musculaire sur la coupe axiale

Sur la coupe axiale obtenue, l'intersection des reconstructions 3D des muscles et le plan axial considéré, permet d'obtenir le contour de chaque muscle sur la coupe. L'aire du muscle sur la coupe est calculée à partir du nombre de pixels situés à l'intérieur du contour du muscle et de la taille du pixel. Cette aire est appelée aire sur la coupe (CSA).

### Centroide du muscle ($Centroide\_i$, i = X, Y)

La position du barycentre du contour du muscle est définie comme étant le centroide du muscle ($Centroide\_i$, i = X, Y).

### Vecteur ligne d'action

L'hypothèse principale est que, pour tous les muscles considérés, la force du muscle (et donc sa ligne d'action) est orientée parallèlement à la direction principale du muscle. Une spline cubique est calculée comme la spline cubique reliant les centroides successifs sur chacune des coupes axiales consécutives définissant le muscle étudié.

Le vecteur ligne d'action sur la coupe axiale considérée pour le modèle MMR est le vecteur orienté vers le haut qui suit la direction de la ligne qui passe au mieux (au sens des moindres carrés) par tous les centroides axiaux situés au-dessus du centroide de la coupe axiale considérée.

Un exemple de la géométrie musculaire obtenue peut être visualisé sur la figure 16: l'aire, le centroide, et la ligne d'action de chaque muscle sont représentés au niveau du disque intervertébral L3-L4.

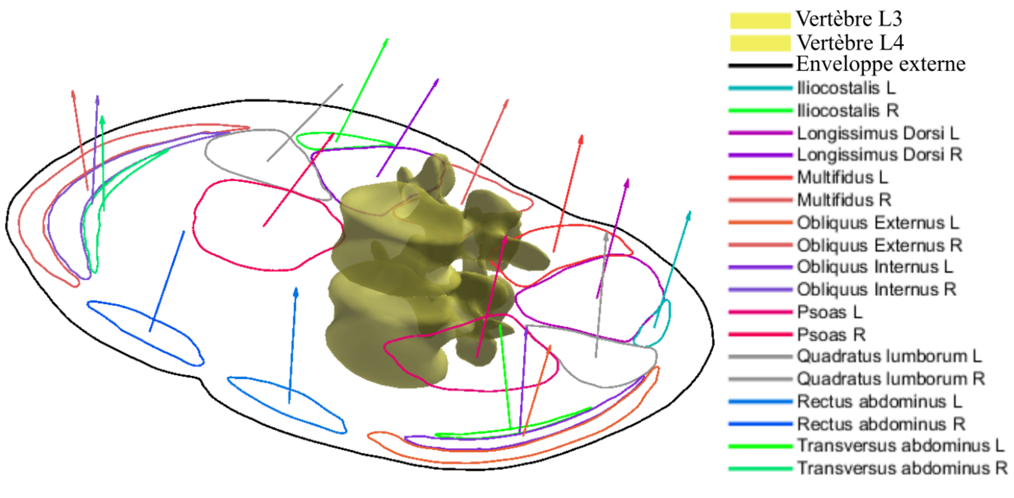


Figure 16. : Coupe axiale du disque intervertébral considéré (ici L3-L4), avec, pour chaque muscle: contour, centroide et vecteur de la ligne d'action.

**Contrainte maximale admissible du muscle**
La contrainte maximale admissible du muscle est liée à la force maximale par unité de surface que le muscle peut générer. Une valeur plus faible que les données normatives, représente une fatigue générale ou une blessure musculaire.

Les études de la littérature donnent des valeurs de 0,3 MPa à 1,0 MPa, ce qui équivaut à des valeurs de 30 $N/cm^2$ à 100 $N/cm^2$.

La valeur de $50N/cm^2$ a été choisie ici. Cette valeur a également été utilisée par Pomero *et al.* (Pomero *et al.*, 2002, 2004).

**Excitation des muscles antagonistes**
Les muscles antagonistes peuvent être activés pour contrôler une position et/ou un mouvement et pour protéger l'articulation en la stabilisant. Dans le cadre du contrôle postural, les muscles antagonistes sont d'un grand intérêt. La question est de savoir comment implémenter l'excitation antagoniste dans le modèle ?

La loi antagoniste publiée en 1996 par Zhou *et al.* (Figure 17), a été implémentée dans le modèle par Vincent Pomero en 2002 (Pomero *et al.*, 2002, 2004). Cette loi antagoniste fournit l'excitation des muscles antagonistes en fonction du moment résultant pour l'articulation considérée.

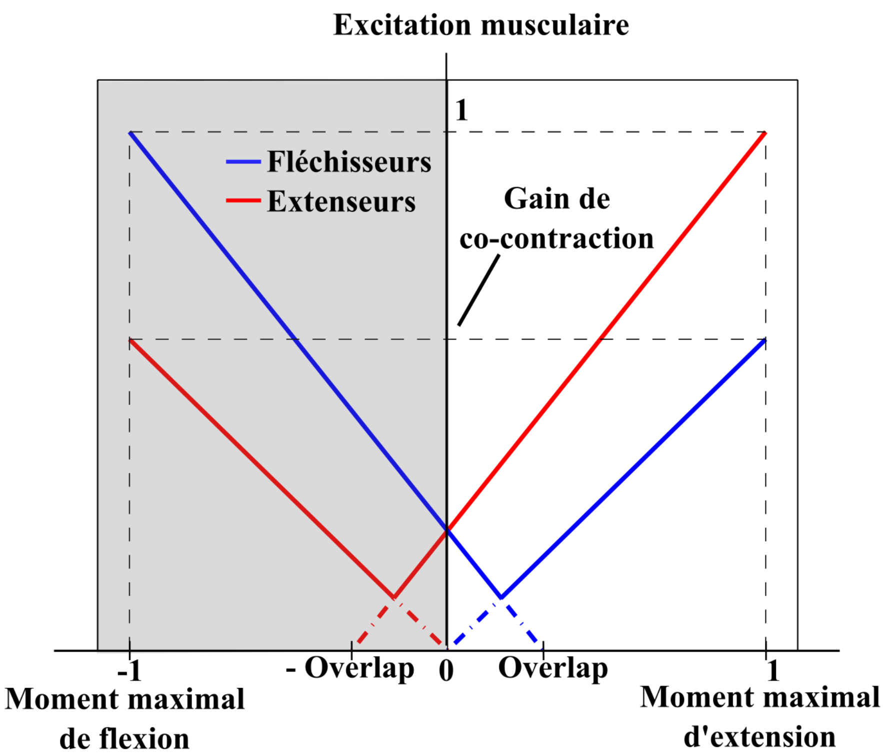


Figure 17. : Loi antagoniste (Zhou *et al.*, 1996).

Si le *Overlap* pour les deux muscles est fixé à 50%, "cela signifie que si l'entrée de la commande varie linéairement du moment de flexion maximale (-1) au moment d'extension maximale (+1), le muscle fléchisseur commence comme étant pleinement actif et son activité diminue linéairement, atteignant zéro à 50% de moment d'extension. A 50% en entrée de couple de flexion, l'extenseur est peu actif, et son activité augmente de façon linéaire jusqu'au couple d'extension maximale (+1).", cité de Zhou *et al.* (1996).

Le *Gain de co-contraction* est défini comme "la pente de la fonction linéaire d'activation antagoniste" cité de Zhou *et al.* (1996).

Les paramètres Overlap et Gain de co-contraction, ont été fixées après une étude de cas (Annexe D): la valeur de Overlap a été fixé à 25% tandis que le Gain de co-contraction a été fixé à 20%.

#### R - 5 - 2 - 2 Population

Trois groupes différents de sujets/patients ont été considérés, pour lesquels les radiographies EOS et images IRM ont été acquises:

- le Groupe **Contrôle**: jeunes adultes asymptomatique (N = 1),
- le Groupe des **Agés**: adultes asymptomatiques âgés de plus de 50 ans (N = 11),
- le Groupe des **Patients**: patientes avec déformations rachidiennes (N = 8).

Pour les groupes Contrôle et Agés, l'inclusion dans l'étude nécessitait: acquisition IRM tête aux pieds avec la méthode Dixon, radiographies EOS tête aux pieds, pas d'antécédents de chirurgie musculo-squelettique et aucune invalidité lors de l'étude. Pour le groupe des Patients, l'inclusion dans l'étude nécessitait: être plus âgé que 35 ans, aucun antécédent de chirurgie du rachis, aucune instrumentation et au moins l'un des paramètres radiographiques suivants: angle de Cobb coronal thoraco-lombaire ou lombaire supérieur à 30°, Sagittal vertical axis (SVA) supérieure à 4 cm, ou version pelvienne (PT) supérieure à 20° (pour plus de détails, voir l'étude de Moal *et al.* (Moal *et al.*, 2015)).

Tous les patients/sujets ont donné leur consentement avant de participer à l'étude (approbation CCP et IRB). Les données du sujet Contrôle ont été recueillies au cours de cette thèse. Les sujets du groupe Agés ont été recrutés prospectivement et les données ont été collectées à l'Hôpital Raymond Poincaré (Garches, France), au cours de cette thèse. Les sujets du groupe Patients ont été extraits d'une étude antérieure réalisée lors de la thèse de Bertrand Moal (Moal, 2014), à l'Hospital of Joint Diseases, (New York, États-Unis).

#### R - 5 - 2 - 3 Radiographies bi-planes

Tous les sujets/patients ont réalisé un examen EOS tête aux pieds. Les reconstructions 3D de la colonne vertébrale (C3-L5) (Humbert *et al.*, 2009b), bassin (Mitton *et al.*, 2006) et enveloppe externe (Nérot *et al.*, 2015), ont été réalisées.

#### R - 5 - 2 - 4 Imagerie par résonance magnétique

Tous les sujets/patients ont subi un examen IRM tête aux pieds. Les détails concernant l'acquisition IRM peuvent être trouvés dans une étude précédente (Moal *et al.*, 2015).

La reconstruction 3D des muscles spino-pelviens considérés a été réalisée avec la méthode DPSO (Jolivet *et al.*, 2014). Les muscles considérés sont: les muscles du dos (multifidus, longissimus, iliocostalis), latissimus dorsi, psoas, quadratus lumborum, externus olbiquus, internus obliquus, transversus abdominis, rectus abdominis. A partir de ces reconstructions ont été calculés pour chaque muscle: la position de son centroide sur la coupe L3-L4, le vecteur de sa ligne d'action et sa section (CSA).

Afin de quantifier l'infiltration graisseuse des muscles présents sur la coupe L3-L4 considérée, une méthode adaptée des travaux d'Antony *et al.* (Antony *et al.*, 2014) et Gilles (Gille, 2006) a été utilisée. Ceci a permis de quantifier l'infiltration graisseuse de chacun des muscles sur la coupe axiale L3-L4 par un système d'auto-calibration sur cette coupe des niveaux de gris.

### R - 5 - 2 - 5 Simulations

2 positions statiques différentes ont été étudiées:

- la position debout étant la Free Standing Position décrite par Chaibi *et al.* (Chaibi *et al.*, 2012) dans la cabine d'EOS, appelée position ***Neutre***;
- une position simulée avec une flexion antérieure du tronc de 30°, appelée position ***Flex30***.

La position ***Flex30*** a été simulée en changeant seulement l'estimation des forces et moments dus à la gravité: rotation de 30° vers l'avant (rotation autour de l'axe Y médio-latéral) du centre de masse de la partie supérieure du corps, par rapport au centre du disque intervertébral L3-L4.

Trois configurations différentes ont été testées pour chaque position:

- Tous les muscles ont été considérés comme non altérés (pas d'infiltration graisseuse), avec une contrainte musculaire maximale admissible de 50 $N/cm^2$, cette configuration est appelée ***Aucune altération***;
- Tous les muscles ont été considérés comme altérés en prenant en compte l'infiltration graisseuse personnalisée pour chaque muscle de chaque sujet/patient (infiltration graisseuse calculée à partir de la coupe IRM), avec une contrainte musculaire maximale admissible de 50 $N/cm^2$, cette configuration est appelée ***Altération***;
- Tous les muscles ont été considérés comme altérés en prenant en compte l'infiltration graisseuse personnalisée pour chaque muscle de chaque sujet/patient (infiltration graisseuse calculée à partir de la coupe IRM), et la contrainte musculaire maximale admissible a été réduite à 15 $N/cm^2$ pour simuler la fatigue musculaire, cette configuration est appelée ***Fatigue***.

Au total, 6 simulations ont été réalisées pour chaque patient (à savoir 2 positions * 3 configurations).

### R - 5 - 2 - 6 Analyse des résultats

Pour chaque simulation, les forces et les moments dus à la gravité seront comparés aux valeurs seuils: le rapport entre les deux définit la fonction de régulation Y qui conditionne la contraction musculaire (équation 8.2). Cela permettra d'évaluer à quel point la contraction musculaire est nécessaire pour maintenir la position considérée. Ensuite, les efforts résultants seront comparés aux forces et moments dus à la gravité pour évaluer l'effet de la contraction musculaire.

## R - 5 - 3 Résultats

Les caractéristiques de chaque groupe se trouvent dans le tableau 2.

La figure 18, présente l'enveloppe extérieure 3D, la position du centre de masse du corps supérieur et le centre commun intervertébral, pour un sujet du groupe Agés (A6).

| Groupe | N | Age (ans) | IMC (kg/m$^2$) | Infiltration graisseuse (%) |
|---|---|---|---|---|
| **Contrôle** | 1 | 28 | 24 | 2 (2) [0 - 9] |
| **Agés** | 11 | 63 (6) [52 - 71] | 25 (5) [20 - 38] | 4 (5) [0 - 35] |
| **Patients** | 8 | 63 (5) [54 - 70] | 22 (3) [20 - 28] | 6 (7) [0 - 36] |

Table 2. : Pour chaque groupe, âge, IMC et infiltration graisseuse sur l'ensemble des muscles. Moyenne (1*Ecart-type) [Etendue].

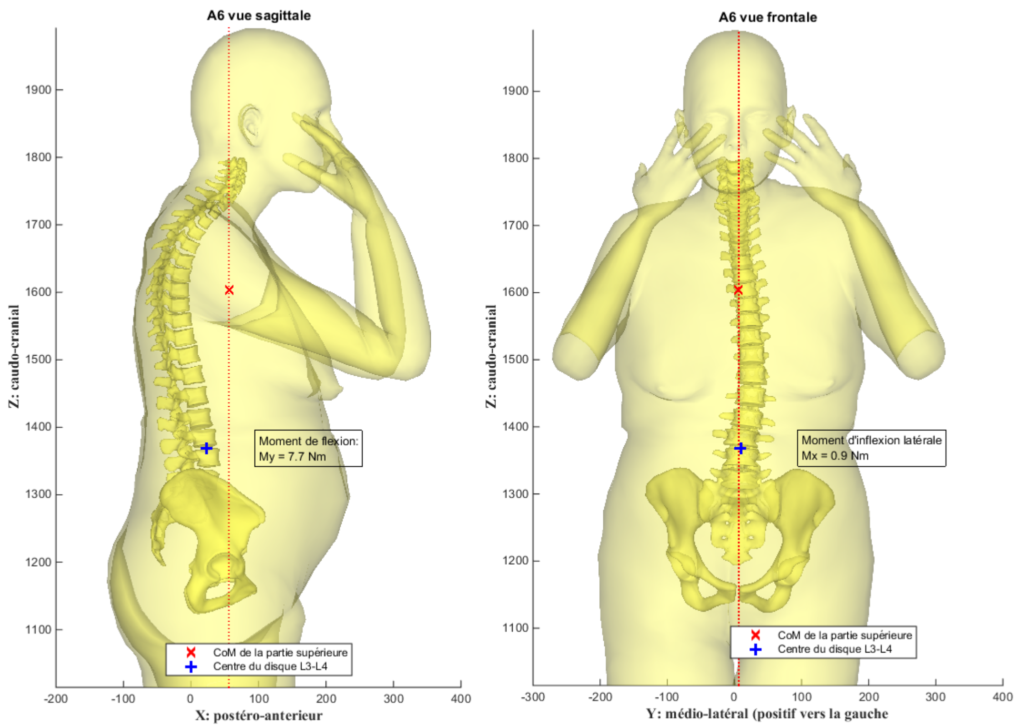


Figure 18. : Illustration du calcul des forces et moments dus à la gravité et s'appliquant au centre du disque intervertébral avec la position du centre de masse de la partie supérieure du corps pour sujet A6 du groupe Agés présentant les efforts suivants: - 40,2 N pour Fx; 0,3 N pour Fy; -232,5 N Pour Fz; 0,9 Nm pour Mx; 7,8 Nm pour My; -0,1 Nm pour Mz, dans la position ***Neutre***.

### R - 5 - 3 - 1 Position *Neutre*

Dans la position ***Neutre***, des valeurs pour les **forces et moments dus à la gravité** plus grands que les valeurs seuils ont été trouvées pour:

- le cisaillement postéro-antérieur: pour 2 du Groupe Agés (A3 et A9) et 1 du Groupe Patients (P8);
- le moment d'inflexion latérale: pour 1 du Groupe Agés (A2) et 1 du Groupe Patients (P7);
- le moment de flexion: pour le sujet contrôle (C1), 3 du Groupe Agés (A2, A6, A10) et de 2 du Groupe Patients (P1 et P2).

Pour le sujet contrôle (C1), cinq sujets du Groupe Agés (A2, A3, A6, A9, A10) et 4 patients du Groupe Patients (P1, P2, P7 et P8), la régulation était nécessaire par l'activation musculaire dans la position ***Neutre***. Pour tous les sujets/patients, pour les trois configurations simulées, l'activation musculaire a permis de réguler la composante au-dessus de la valeur seuil. Les schémas de recrutement musculaire sont représentés, pour un sujet et un patient, dans la figure 19.

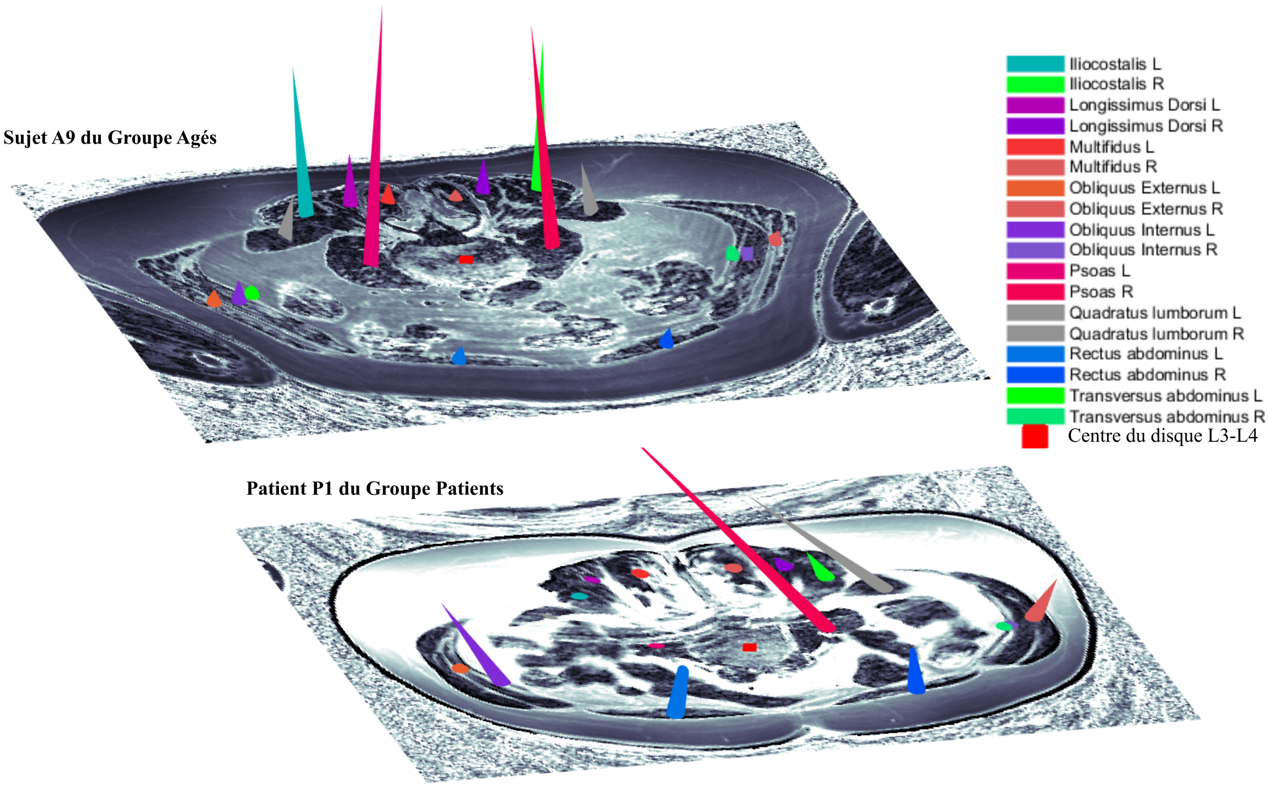


Figure 19. [Visualisation de l'activation musculaire pour le sujet âgé A9 et le patient P1.]: Coupe axiale IRM au niveau L3-L4 avec illustration de l'activation musculaire. La hauteur du cône est proportionnelle à l'activation du muscle. La position du centre de la base du cône est le centroide du muscle et la direction du cône est la ligne d'action du muscle. Sont représentés ici les schémas d'activation musculaire pour le sujet âgé A9 et le patient P1 dans la position ***Neutre***.

#### R - 5 - 3 - 2 Position *Flex30*

Dans la position ***Flex30***, des valeurs pour les **forces et moments dus à la gravité** plus grands que les valeurs seuils ont été trouvées pour:

- le cisaillement postéro-antérieur: pour 2 du Groupe Agés (A3 et A9) et 1 patient du Groupe Patients (P8);
- le moment latéral d'inflexion: pour 1 du Groupe Agés (A2) et 1 patient du Groupe Patients (P7);
- le moment de flexion, pour tous les sujets/patients de tous les groupes;
- le moment de torsion: pour 2 du Groupe Agés (A1 et A2) et 7 patients du Groupe Patients (P1, P2, P3, P5, P6, P7 et P8).

### R - 5 - 4 Discussion

Cette étude visait à étudier l'effet de différentes postures et d'altérations posturales sur le modèle de recrutement musculaire, en étudiant en détail les efforts intervertébraux résultants pour différentes positions et configurations musculaires.

### R - 5 - 4 - 1 Position *Neutre*

Pour la position ***Neutre***, toutes les composantes des efforts ont été régulées après activation musculaire. Ni l'altération de la qualité musculaire, ni l'effet de fatigue, n'a pas augmenté les efforts au-dessus des valeurs seuils. Cela a confirmé que la position debout neutre est économe en énergie, même si pour certains sujets du groupe Patients, le cisaillement latéral, et les moments de flexion et de torsion étaient plus élevés que dans les groupes Agés et Contrôle: comme les déformations rachidiennes de ces patients sont en 3D et principalement dans le plan coronal, le centre de masse de la partie supérieure du corps n'est pas été aligné avec le centre du disque intervertébral, en particulier dans le plan coronal, générant ainsi une force de cisaillement latéral et des moments associés (figures 18.

L'activation musculaire a permis de réduire les efforts par rapport aux forces et moments dus à la gravité. Cependant, lorsque l'on étudie l'effet de l'altération de la qualité musculaire avec ou sans effet de la fatigue, on peut noter que les efforts augmentent à cause d'une contraction musculaire moins efficace et performante.

Les valeurs de compression, pour la position ***Neutre***, s'étendent de 140 N à 476 N. Hajihosseinali *et al.* a rapporté des valeurs de compression de 420 N et 469 N, au niveau L4-L5, pour un adulte de 1.7 m pour 68 kg (Hajihosseinali *et al.*, 2014). Un sujet similaire a été considéré par Gagnon *et al.* qui a rapporté une valeur de compression de 475 N, au niveau L3-L4 (Gagnon *et al.*, 2011). Les sujets similaires dans notre étude sont les sujets A1 et A9 du Groupe Agés pour lesquels les valeurs de compression étaient comprises entre 217 N et 337 N. Les différences observées peuvent provenir de la compression initiale: les études de la littérature ont considéré une compression due à la gravité de 344 N alors qu'ici une compression due à la gravité de seulement 200N a été calculée. Cette différence, tout en observant des sujets similaires, peuvent provenir des différentes densités appliquées sur les segments lors du calcul du poids de la partie supérieure (Amabile *et al.*, 2016a) ou des différentes morphologies considérées. La force de compression due à la gravité utilisée dans cette étude a été directement calculée à partir de l'enveloppe externe personnalisée du sujet. Ces différences viennent aussi du fait que les bras n'ont pas été pris en compte dans le calcul des efforts dus à la gravité dans cette étude.

Des valeurs significativement plus élevées ont été rapportées pour la compression, allant de 800 N à 1600 N (Arshad *et al.*, 2016; Arjmand and Shirazi-Adl, 2006; Gagnon *et al.*, 2001; Granata and Wilson, 2001). Ces valeurs très grandes sont encore une fois influencées par la compression initiale (force due à la gravité) qui est autour de 350 N pour toutes ces études. Les différences dans la compression résultante peuvent aussi provenir des algorithmes qui régissent les modèles. Cependant, dans la position Neutre, on trouve ici un poids de la partie supérieure du corps allant de 14 kg à 45 kg ce qui semble raisonnable et plausible.

En ce qui concerne les valeurs de cisaillement postéro-antérieur, ceux-ci sont très dépendants du sujet car ils sont influencés par la posture initiale du patient, et plus particulièrement la répartition des différents segments au-dessus de la coupe considérée. Dans cette étude, les valeurs de cisaillement postéro-antérieur s'étendaient de -52 N à 61 N dans la position ***Neutre***. Les valeurs rapportées étaient 2 N et 36 N pour Hajihosseinali *et al.* (Hajihosseinali *et al.*, 2014); -21 N Pour Gagnon *et al.* (Gagnon *et al.*, 2011) et autour de 50 N pour Arshad *et al.* (Arshad *et al.*, 2016). Les sujets similaires dans cette étude (A1 et A9) ont présenté des valeurs comprises entre -33 N et -52 N en accord avec les valeurs rapportées dans la littérature. Ces valeurs de cisaillement postéro-antérieur dépendent de la position du centre de masse de la partie supérieure du corps par rapport au centre du disque intervertébral: parce que le plan du disque L3-L4 présente un angle positif avec le plan horizontal, la force de gravité génère une valeur négative pour le cisaillement postéro-antérieur. Seuls les sujets pour lesquels L3-L4 était en dessous de l'apex de la lordose (plan du disque orienté négativement par rapport à l'horizontale) ont présenté des valeurs de cisaillement postéro-antérieur positives.

Une étude a rapporté des valeurs de moment de flexion de 4.1 Nm, pour la position ***Neutre*** (Hajihosseinali *et al.*, 2014), en accord avec nos résultats actuels (de -4 à 3 Nm). Le signe positif ou négatif dépend de la position relative, dans le plan sagittal, du centre de masse de la partie supérieure du corps par rapport au centre du disque intervertébral.

#### R - 5 - 4 - 2 Position ***Flex30***

La position avec flexion du tronc vers l'avant, a été considérée pour stimuler une réponse musculaire plus élevée et une augmentation des forces et moments dus à la gravité par rapport à la position ***Neutre***. Comme prévu, le moment de flexion (My) est supérieur à la valeur seuil pour les forces et moments dus à la gravité pour tous les sujets; la demande de régulation est donc élevée ce qui conduit à une activation musculaire plus grande. Sur les 8 patients avec déformations rachidiennes, 7 (88%) ont présenté un moment de torsion plus élevé que la valeur seuil, soulignant la nature 3D des déformations rachidiennes de ces patients.

En ce qui concerne le moment de flexion (My), l'activation musculaire a permis de réduire ce moment en dessous de la valeur seuil, sauf pour 3 sujets du groupe Agés dans les configurations ***Aucune altération*** et ***Altération***. Tous ces sujets présentent une valeur élevée pour l'IMC (24-28 $kg/m^2$) sans présenter le plus grand IMC du Groupe Agés. Ces sujets ne sont pas ceux qui présentent la plus grande infiltration graisseuse dans les muscles du dos. Enfin leurs valeurs initiales de cisaillement latéral et moment de flexion étaient dans la gamme des valeurs d'autres sujets/patients.

Pour la configuration ***Fatigue***, plusieurs sujets n'étaient pas capables de réguler le moment de flexion (moment de flexion supérieur à 4,9 Nm). Fait intéressant, ces sujets/patients ne présentent pas une infiltration graisseuse plus élevée dans les muscles du dos que d'autres, mais tous présentent un IMC supérieur à 23 $kg/m^2$. La partie du corps supérieure à la coupe axiale étant plus lourde, un petit déplacement dans le plan axial de cette partie du corps introduit de grands moments dans l'articulation intervertébrale.

Seules 2 études à notre connaissance ont rapporté des valeurs pour les efforts intervertébraux résultants, pour une flexion du tronc de 30° du tronc sans port de charge. Arshad *et al.* a rapporté des valeurs de compression entre 800 et 1100 N, allant jusqu'à 1550 N pour un rythme spécifique de la colonne vertébrale (le rythme étant la distribution relative de la flexion lombaire pour les différents niveaux lombaires); des valeurs de cisaillement postéro-antérieur allant de -50 à + 50 N ou de 0 N à 100 N selon si la pression intra-abdominale a été prise en compte ou pas (Arshad *et al.*, 2016). Gagnon *et al.* a rapporté des valeurs de compression de 742 N et les valeurs de cisaillement postéro-antérieur de 68 N (Gagnon *et al.*, 2011). Les valeurs de cisaillement postéro-antérieur trouvées ici allaient de 11 N à 234 N et les valeurs de compression allaient de 342 N à 1291 N. Nos valeurs concordent globalement avec celles de la littérature, des valeurs plus élevées pour le cisaillement postéro-antérieur ont été trouvées chez les sujets avec forte infiltration graisseuse dans les muscles du dos (même si cette infiltration graisseuse ne dépasse pas 20%).

Étonnamment, le patient P7 présentant l'infiltration graisseuse la plus élevée pour les muscles du dos (iliocostalis, longissimus et multifidus) présente, dans la position ***Flex30***, une valeur de cisaillement postéro-antérieur de 72 N lors de la prise en compte de cette altération musculaire (vs 59 N sans altération). Le cisaillement postéro-antérieur atteint 93 N lorsque l'on considère la configuration de fatigue. Ce patient a réussi à limiter le cisaillement postéro-antérieur (même si la valeur seuil de 75 N a été dépassée) au détriment de plus grands moments dans l'articulation intervertébrale (moment de torsion de 1.9 Nm sans altération et avec altération par rapport à 2.8 Nm lorsque l'on considère la configuration de fatigue).

L'excitation des muscles antagonistes ayant été implémentée dans le modèle, les résultats prédisent une certaine quantité de co-activation des muscles abdominaux dans la position ***Flex30***. Cette co-activation est difficile à prédire avec des modèles d'optimisation (Arjmand *et al.*, 2009) mais a été rapportée dans des études utilisant des modèles avec EMGs (Gagnon *et al.*, 2001).

Ce modèle offre la possibilité d'étudier plus précisément l'activation musculaire pour chaque muscle comme indiqué dans la figure 19. Ce type de figure pourrait être utile pour visualiser les muscles qui doivent être renforcés pour limiter plus efficacement les efforts intervertébraux.

### R - 5 - 4 - 3 Perspectives et limites

Une amélioration future de ce modèle serait de prendre en compte les différences d'activation musculaire entre les adultes jeunes et plus âgés (Häkkinen *et al.*, 1998; Macaluso *et al.*, 2002). En particulier, la co-activité des muscles antagonistes a été montrée comme étant plus faible chez les personnes âgées, diminuant ainsi la stabilité de l'articulation (Häkkinen *et al.*, 1998).

Une autre étape vers une meilleure représentation serait de considérer les bras dans le calcul des forces et moments dus à la gravité car cela n'a pas été fait ici. Si les bras sont considérés comme étant pliés avec les mains sur les pommettes comme dans la Free Standing Position dans la cabine EOS (Faro *et al.*, 2004), tenir compte des bras augmenterait la compression ainsi que le cisaillement postéro-antérieur et le moment de flexion dus à la gravité. Il pourrait aussi être intéressant de considérer les bras le long du corps dans une position naturelle, comme lors de la marche par exemple, dans ce cas seulement la compression due à la gravité serait changée.

Une autre amélioration serait d'ajouter une déformation des muscles dans la position ***Flex30***, et de fournir la véritable géométrie 3D de la colonne vertébrale et du bassin dans une telle position. Cela conduirait à un calcul plus précis des forces et des moments dus à la gravité dans une telle position, et des effets de la contraction musculaire sur les efforts résultants dans l'articulation intervertébrale L3-L4. Une amélioration connexe serait de simuler la posture et la géométrie musculaire associée, pour une position non compensée pour les personnes âgées qui recrutent déjà des mécanismes de compensation, en utilisant le protocole décrit dans la figure 3 de la partie sur l'alignement postural.

Une limite de cette étude est le nombre limité de sujets dans le groupe de contrôle: étudier plus de jeunes sujets asymptomatiques permettrait de fournir des valeurs de référence pour les efforts au sein de l'articulation intervertébrale. Une autre limite réside dans la conception du modèle: actuellement, une seule coupe axiale est considérée pour la boucle de régulation. Par conséquent, la comparaison entre les différents niveaux intervertébraux ne peut pas être effectuée. Le niveau du disque L3-L4 a été choisi ici, car il est situé à l'apex de la lordose. Un autre choix intéressant pour les études futures serait de considérer le disque L5-S1, étant le dernier niveau avant la vertèbre pelvienne. Si la pente du sacrum est assez grande (grande pente sacrée), cela devrait conduire à des valeurs de cisaillement postéro-antérieur élevées nécessitant d'être régulées. Comme avec tous les modèles d'optimisation, il est difficile de valider ce modèle, sauf en le comparant à des valeurs EMG rapportées dans la littérature, et aux valeurs de pression intra-discale *in vivo* obtenues avec une sonde insérée dans un disque. Cependant cette comparaison peut être difficile en raison des différentes morphologies et postures des sujets étudiés.

## R - 5 - 5 Conclusion

Cette partie a porté sur le calcul des efforts intervertébraux pour des adultes de différents âges avec/sans déformations rachidiennes à l'aide d'un modèle biomécanique musculo-squelettique.

Tout d'abord, l'adaptation et la personnalisation des données d'entrée du modèle précédemment publié (Pomero *et al.*, 2004) ont été décrits. Les différentes étapes de préparation des données d'entrée à partir d'images médicales telles que des radiographies et des images IRM ont été détaillées. Le calcul des forces et des moments dus à la gravité, s'appliquant au centre du disque intervertébral L3-L4, a été présenté.

Deuxièmement, ce modèle a été utilisé pour calculer les efforts résultants au sein de l'articulation intervertébrale dans différentes positions (debout et avec flexion du tronc); et avec ou sans altération des muscles (infiltration graisseuse) ainsi que fatigue musculaire (diminution de la contrainte musculaire maximale admissible). Différentes populations ont été étudiées: un jeune adulte asymptomatique, des adultes asymptomatiques plus âgés et des adultes avec déformations rachidiennes.

Le schéma de recrutement musculaire varie pour chaque configuration, position, sujet/patient. Les efforts résultants sont donc des valeurs dépendantes du sujet. Les principaux résultats ont mis en évidence la capacité, pour tous, de régler les efforts intervertébraux résultants sous les valeurs seuils afin de protéger l'articulation, en position debout. Les sujets ayant une force de compression plus élevée (plus grand indice de masse corporelle), n'ont pas réussi à limiter le moment de flexion pour la position avec flexion du tronc, lorsque les muscles étaient altérés ou sous effet de fatigue.

Ces résultats fournissent de nouveaux éléments sur le travail requis par les muscles pour maintenir une posture efficace, tout en préservant les disques intervertébraux. Les modifications posturales ont un impact sur les efforts résultants dans l'articulation intervertébrale et les différentes positions ont donné lieu à des différences élevées dans les valeurs observées pour ces efforts.

Ce modèle permet d'identifier les muscles qui apparaissent comme essentiels pour le maintien d'une posture économique pour le sujet considéré. Ces résultats pourraient être utilisés pour la planification chirurgicale: pour un patient particulier, la meilleure approche pour la chirurgie peut être choisie comme celle minimisant la dégradation de ces muscles.

Cette partie se concentrant sur l'utilisation d'un modèle biomécanique musculo-squelettique, en utilisant des données 3D personnalisés des sujets, a souligné l'importance d'une telle personnalisation pour la prédiction des efforts résultants dans l'articulation intervertébrale afin de prévenir les lésions de la moelle épinière ou du disque intervertébral.

## R - 6 Conclusion générale

L'objectif de cette thèse était d'étudier les changements dû au vieillissement, de l'alignement postural et des muscles.

La première partie a porté sur les changements d'alignement postural au cours du vieillissement. Une première étude sur les jeunes adultes asymptomatiques a mis en évidence l'alignement quasi-invariant de la tête par rapport au bassin. Cette invariance fournit une bonne répartition des différents segments au-dessus de la vertèbre pelvienne, permettant une posture efficace en minimisant les dépenses d'énergie, et se situant à l'intérieur de cône d'économie, défini par Dubousset (Dubousset, 1994). L'analyse fine d'une population asymptomatique d'adultes de plus de 49 ans a permis de montrer une conservation de l'invariance de cet alignement dans la population plus âgée. Toutefois, pour 16 sujets sur 41, cette invariance était permise grâce à des mécanismes de compensation tels que la rétroversion pelvienne et l'hyperlordose cervicale. Une étude longitudinale pourrait évaluer si ces biomarqueurs permettraient l'identification précoce de sujets à risque de dégradation de l'alignement postural.

La deuxième partie de cette thèse a présenté le travail réalisé sur les muscles spino-pelviens à partir d'images IRM. Les valeurs de référence ont été calculées pour les adultes jeunes asymptomatiques. Une méthode rapide et précise a été proposée et validée afin d'estimer les volumes de groupes fonctionnels: cette méthode pourrait être mise en œuvre dans un environnement clinique. Un deuxième chapitre a étudié les muscles spino-pelviens de personnes plus âgées avec déformations rachidiennes. Le vieillissement pathologique a affecté les muscles par une perte de volume pour la plupart des muscles. Cependant, les muscles fessiers sont apparus comme particuliers, en effet les volumes et ratios volumiques des muscles fessiers étaient plus grands pour la population avec déformations rachidiennes comparés aux valeurs pour les jeunes adultes asymptomatiques. Cette augmentation de volume peut être le marqueur d'une stimulation accrue des muscles fessiers afin de réguler finement la position du bassin supportant tout le poids du corps situé au-dessus du bassin.

La troisième partie s'est intéressée à l'adaptation et la personnalisation d'un modèle musculo-squelettique de la colonne vertébrale et du bassin afin d'étudier la relation entre posture altérée et schéma de recrutement musculaire (et donc efforts résultants intervertébraux). En étudiant divers sujets en termes d'âge, de pathologie et de morphologie, il a été montré dans les résultats préliminaires, une variabilité dans le schéma de recrutement musculaire. La capacité à réguler la posture afin de limiter les efforts intervertébraux dépend du sujet et suggère que les études futures doivent intégrer une personnalisation des modèles musculo-squelettiques afin de prédire et analyser les efforts intervertébraux. Ce travail préliminaire a rapporté la difficulté de certains volontaires ou patients à limiter le moment de flexion lorsque le tronc est fléchi à environ 30 ° en avant, lorsque les muscles sont altérés (infiltration graisseuse quantifiée à partir d'images IRM) et dans le cas de fatigue musculaire. Ces résultats mettent en évidence l'importance de préserver les muscles durant l'évolution d'une pathologie ou le vieillissement, afin de résister à l'effet de la fatigue le plus longtemps possible et de compenser les modifications posturales.

Dans l'ensemble, cette thèse a établi des valeurs de référence pour les adultes asymptomatiques en termes d'alignement postural et de volumes musculaires. Ceci fournit une base de données pour comparaison lorsque l'on étudie l'effet du vieillissement ou de l'évolution d'une pathologie. Les changements liés à l'âge ont été quantifiés pour les systèmes squelettique et musculaire. L'impact d'une posture altérée a été étudié sur le volume musculaire et le recrutement musculaire. Une posture altérée peut être identifiée de façon précoce, avant d'être critique, par l'évaluation de l'alignement de la tête par rapport au bassin.

Si les deux premières parties de cette thèse ont quantifié les changements se produisant au cours du vieillissement, le modèle musculo-squelettique est un nouvel outil pour mieux comprendre l'interaction entre la posture, la colonne vertébrale et les muscles. Dans cette thèse, aucune conclusion claire et robuste ne peut être tirée sur qui des altérations posturales, ou des changements musculaires provoquent l'autre. Une plus grande cohorte et une étude longitudinale apporteraient des connaissances importantes sur les changements se produisant au cours du vieillissement ou lors de l'évolution d'une pathologie. En effet, ce modèle a été utilisé pour étudier le processus de vieillissement, mais pourrait également être utilisé afin d'étudier par exemple l'évolution de troubles rachidiens, le développement de douleurs lombaires, ou pour améliorer l'ergonomie de postes de travail. De même, étudier des patients atteints de diverses pathologies et symptômes tels que la lombalgie, idéalement dans une étude longitudinale, fournirait de nouveaux éléments sur la compréhension de ces pathologies.

Les perspectives à court terme comprennent la combinaison globale des différents résultats de cette thèse: la combinaison de marqueurs de l'altération de l'alignement postural avec la quantification de la dégradation musculaire dans le modèle biomécanique permettrait d'améliorer cette approche prometteuse et ouvrirait la voie à différentes utilisations. Simplifier le traitement des images médicales permettrait de mettre au point des outils faciles d'utilisation et utilisables dans les hôpitaux pour la routine clinique afin de quantifier l'alignement postural avec l'angle CAM-HA (ou angle OD-HA); la dégradation musculaire à partir d'images d'IRM; et les impacts sur le schéma de recrutement musculaire avec le modèle biomécanique. En particulier, le calcul des efforts résultants intervertébraux, pour les personnes âgées présentant des mécanismes de compensation aux niveaux pelviens et cervicaux, dans une position non compensée serait d'un intérêt particulier afin d'évaluer l'impact de ces mécanismes de compensation.

Les perspectives à long terme concernant la modélisation biomécanique concernent trois étapes différentes au cours le vieillissement: la première lors de la prévention, la seconde lors de la gestion des maux de dos lombaires et la troisième lors de la planification chirurgicale et de l'analyse post-opératoire.

Tout d'abord, à l'aide du modèle présentant le schéma de recrutement musculaire pour la position choisie, les équipes cliniques pourraient identifier les muscles spécifiques à renforcer, et ainsi prescrire des exercices appropriés pour tendre vers une posture efficace. Cela pourrait aussi être utilisé pour identifier les muscles spécifiques à renforcer avant une intervention chirurgicale afin d'améliorer la récupération et les résultats de la chirurgie.

Deuxièmement, la prise en charge des douleurs lombaires pourrait être améliorée en fournissant un aperçu réel des efforts intervertébraux et de l'activation musculaire. La différenciation entre efforts élevés pouvant à terme endommager le disque et hyperstimulation des muscles et donc leur fatigue, pourrait être faite pour améliorer le diagnostic, la prévention et la prise en charge à long terme.

Troisièmement, avec ce modèle biomécanique, différentes approches pour les interventions chirurgicales de la colonne vertébrale (approche antérieure, latérale ou postérieure) peuvent être simulées en reproduisant les dommages subis par les muscles dus à la procédure chirurgicale choisie. Cela pourrait donner un aperçu des efforts au niveau de l'articulation intervertébrale ou de l'implant après la chirurgie. La meilleure approche pour la chirurgie pourrait alors être choisie comme celle qui minimise ces efforts.

Ce modèle est original car il permet une vision 3D complète des muscles et du squelette. En fournissant les lignes d'action des muscles, l'impact de la chirurgie ou de l'exercice physique peut être directement imaginé et modélisé. Ce point de vue innovant du complexe spino-pelvien fournit un nouvel outil prometteur afin d'améliorer la prise en charge des patients avec déformations rachidiennes. Il ouvre aussi des perspectives pour l'aide à la réflexion lors de la planification chirurgicale de tels patients.

# GENERAL INTRODUCTION

Global aging of the population (from 12% of olders than 60 years old in the world in 2015, to 22% in 2050 (World Health Organization, 2008)) raises the question on "how to age well?" Aging has local and global impacts on the body with consequences on the daily life for elders. Particularly, it is well documented that adults older than 65 years old are more prone to falls (World Health Organization, 2008): while a young adult can restore his/her balance after losing it, such a task is more difficult for elders, who are therefore associated with more frequent falls. Between 28% and 35% of people older than 65 years old fall each year, versus 32% to 42 % for adults older than 70 years old (World Health Organization, 2008). As the skeleton is less robust for elders, the consequences of the fall can be dramatic (37.3 million falls per year, require medical attention (World Health Organization, 2008)), and can lead to surgery, long-time medical care needs and/or loss of autonomy.

The costs of falls for the society have been reported: for example, for the Republic of Finland (respectively Australia), for adults older than 65 years old, the average health system cost per fall injury is US$ 3611 (respectively US$ 1049) (World Health Organization, 2008). Just as important, loss of autonomy also impacts the quality of life of the patient and his family. It remains an economic burden for the relatives: lost earnings per household are estimated at around US$ 40 000 per year in the UK (World Health Organization, 2008).

Because loss of balance is one of the cause of falling, maintaining a good balance appears as a key factor in the prevention of falls. Early identification of people at risk of pathological aging (leading in the future to loss of balance and maybe falls), would allow the prescription of specific programs to tend towards a more efficient balance: exercise to reinforce specific muscles, and regain amplitude in movements for example (World Health Organization Falls Prevention for Active Aging Model (World Health Organization, 2008)).

Such identification requires the definition of aging biomarkers: parameters or scores based on clinical exams and/or medical images analysis allowing discrimination between people who will evolve towards pathological aging and people who will evolve towards healthy aging. If several criteria have already been reported as reliable markers of aging, no simple global biomarker has been found to date. This is due to the multi-factorial aspect of the problem of loss of balance during aging (Tinetti *et al.*, 1994). Particularly aging has been shown to induce changes in the inter-vertebral discs composition (Adams *et al.*, 1996), leading to a stiffer back and therefore to an altered posture (Diebo *et al.*, 2015): particularly a forward shift of the trunk and knee flexion have been reported (Barrey *et al.*, 2013; Diebo *et al.*, 2015). In addition, the muscular system is also impacted, with a loss of muscular volume (sarcopenia) (Narici *et al.*, 2003; Frontera *et al.*, 2000) but also with a decrease in muscular force (Macaluso and De Vito, 2004). Cognitive capacities can also be altered (vision, hearing...) complicating the maintenance of an efficient balance (Lacour *et al.*, 2008; Laughton *et al.*, 2003). Combining the skeletal and muscular systems in the search of new aging biomarkers appears to be a relevant task.

Recent research in the two laboratories hosting this PhD, Institut de Biomécanique Humaine Georges Charpak and Hospital for Special Surgery, proposed new techniques and algorithms combining skeletal and muscular information in 3D.

The EOS system, taking bi-planar low-dose radiographs, enables the 3D reconstruction of the skeleton (Dubousset *et al.*, 2010); while MRI images' analysis combined with the deformation of a parametric-specific object method (DPSO) results in the 3D reconstruction of muscles (Jolivet *et al.*, 2008). In addition, the two teams collaborating in this PhD, are expert in the analysis of the spino-pelvic system (Lafage *et al.*, 2008; Schwab *et al.*, 2006; Skalli *et al.*, 2007; Moal *et al.*, 2015; Steffen *et al.*, 2010; Pomero *et al.*, 2004), and are advocating the need for patient-specific modeling techniques. As aging impact the whole body, changes observed are specific to each subject, and personalization of these models remains crucial. In the literature, few studies reported combined aging analysis of both skeletal and muscular systems. While a few models have been developed to estimate interactions between the two structures, personalization of these models remains a difficult challenge. The objective of this PhD was therefore to investigate aging changes and model the musculo-skeletal interactions, from EOS and MRI images analysis, searching for new biomarkers of aging.

Specifically, three questions guided the scientific reasoning of this PhD:

- How does postural alignment change with aging?
- How do the muscular system's characteristics change with aging?
- What is the impact of the combined alteration of both postural alignment and muscular system, on the biomechanics of the spine?

After a review of the anatomical structures and imaging modalities studied in this PhD, an analysis of the literature will be presented.

The first part of the personal work reports the study of young and older adults to investigate age-associated postural alignment changes using EOS radiographs. The second part will present studies focusing on the aging of the muscular system from MRI images. The third part will address the issue of the combined work of muscles and posture to provide an efficient balance. Finally, the last part will conclude on the PhD findings and will suggest perspectives for future researches.

Figure 20. : The Tightrope Walker, 2002, photographed by Gilbert Garcin. Courtesy of Les filles du calvaire gallery, Paris. [from RENCONTRESARLES (`http://www.rencontres-arles.com`)].

## Part A

# Anatomy and Literature Review

# INTRODUCTION

The first chapter of this literature review will introduce the anatomy of the skeletal and muscular systems, based on anatomy books of Kamina (2006). In the second chapter, different ways to investigate changes in postural alignment will be presented. The third chapter will focus on studies of the muscular system's degradation. Finally, a review of the different existing biomechanical musculo-skeletal models will be introduced. Published studies will be presented to describe the global context of this PhD.

Anatomical planes of reference are presented in Figure 21. The sagittal plane is the plane separating right from left; the horizontal or axial plane is a plane parallel to the ground, separating the body into the upper and lower parts. The coronal or frontal plane is the plane perpendicular to the two others.

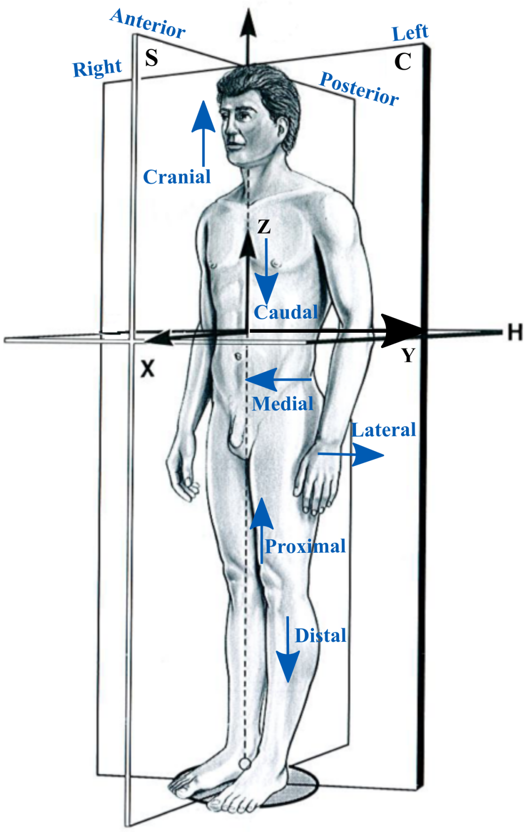


Figure 21. : Planes of study: **C:** Coronal plane. **S:** Sagittal plane. **H:** Axial plane. [Adapted from (Dubousset, 1994)].

# CHAPTER 1

# ANATOMY AND MEDICAL IMAGING

## 1 - 1 Skeleton

Balance alteration brings attention to the longitudinal skeleton in standing position. Upper limbs will not be considered here as the focus will be made on the static erected posture and as arms play a role in balance during dynamic movements. The skeleton involves different joints as illustrated in Figure 1.1, and detailed in Table 1.1.

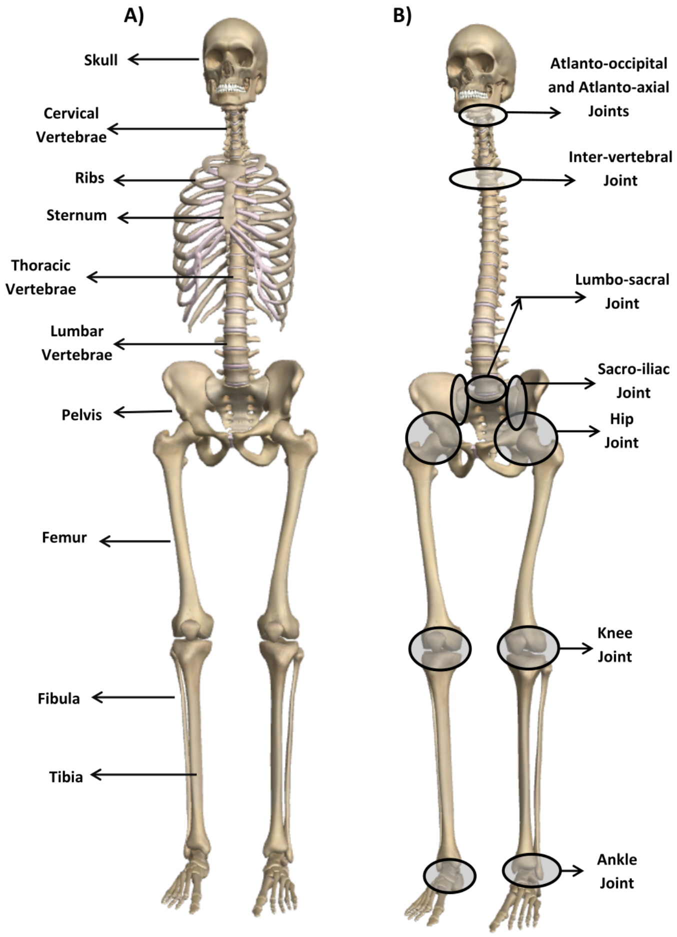


Figure 1.1. : 3D reconstruction of the skeleton.
**A):** Spine, rib cage, pelvis and lower limbs. **B):** Joints. [Adapted from ZYGOTE BODY (`http://zygotebody.com/`)]

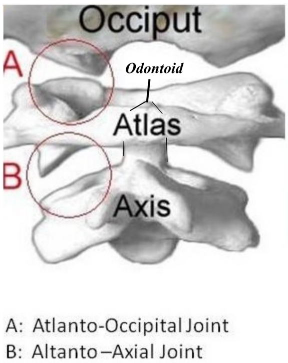


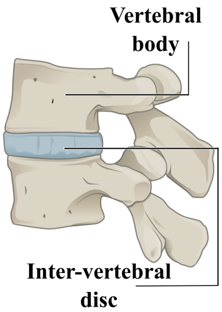


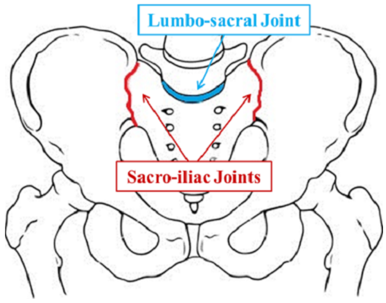


| **Name** | **Atlanto-occipital joint**[1] | **Atlanto-axial joint**[1] | **Inter-vertebral joint**[2] | **Lumbo-sacral joint**[3] | **Sacro-iliac joint**[4] |
|---|---|---|---|---|---|
| **Proximal Segment** | Occipital bone | Atlas | Vertebra | L5 | Sacrum |
| **Distal Segment** | Atlas | Axis | Adjacent inferior vertebra | Sacrum | Hip bones of the pelvis |
| **Joint** | Articulation of the head with the spine | Articulation of C1 with C2 | Articulation of two adjacent vertebrae with the inter-vertebral disc | Articulation of the spine with the pelvis | Articulation of the hip bones with the sacrum |

Table 1.1. : Different joints in the body. [Figures adapted from [1]STUDY BLUE (`https://www.studyblue.com`); [2]SPINE UNIVERSE (`http://spineuniverse.com`); [3]VECTOR STOCK (`https://www.vectorstock.com`); [4]FOOT LOGICS (`http://www.footlogics.com.au`)]

## 1 - 1.1 Head

The head is the segment containing the visual system and the inner ear; two of the sensory systems regulating balance. Because of its weight (4-5kg (Vital and Senegas, 1986)), and as the head is positioned on a flexible rod (i.e. the spine), the alignment of its center of gravity with the other segments is of primary importance. In addition, being the center of vision, specific alignment with the spine is required in order to maintain horizontal gaze (Figure 1.2). One study investigated the position of the center of gravity of the head and reported its position on the nasion-inion line, just above the center of acoustic meati (Vital and Senegas, 1986). In this PhD, the center of acoustic meati will be used to characterize the head position compared to other segments.

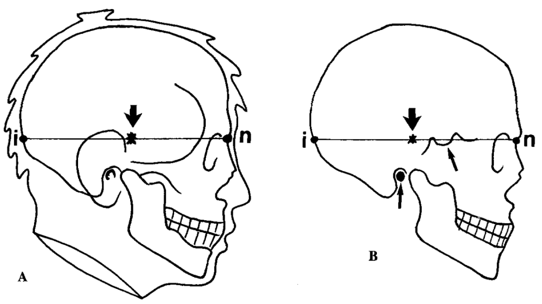


Figure 1.2. : Location of center of gravity **A** At the middle of the nasion-inion line. **B** Radiographic projection of this center behind the sella turcica, above and slightly in front of the external auditory meatus (point above the upward arrow). [Adapted from (Vital and Senegas, 1986)].

The atlanto-occipital and atlanto-axial joints are the joints permitting the 3D rotation of the head compared to the spine (Figure 1.1 and Table 1.1). The latter joint involves the dentiform apophyse of C2, which most superior point will be called Odontoid in the following. This point will be considered to characterize the position of the superior part of the spine, near the head, compared to other segments.

### 1 - 1.2 Spine

The inter-vertebral joint is the joint between two adjacent vertebrae (Table 1.1). The inter-vertebral disc is the flexible structure allowing for movement of one vertebra versus another (Figure 1.3). Facet joints on the vertebrae contribute to the limitation of movement, in order to protect the inter-vertebral disc and spinal cord (going through the neutral arch of vertebrae).

The behavior of “bag of fluid” of the inter-vertebral disc plays a role of shock absorber and is responsible for spinal flexibility (Dolan and Adams, 2001).

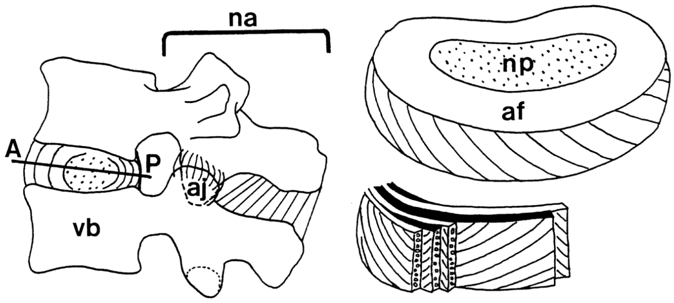


Figure 1.3. : Left: Lumbar motion segment consisting of two vertebrae and the intervening disc and ligaments. “Compressive” force acts perpendicular to the antero-posterior mid-plane of the disc (“A-P”). vb - vertebral body; aj - apophyseal joint; na - neutral arch. Upper right: In an inter-vertebral disc, the concentric lamellae of the annulus fibrosus (af) surround the soft nucleus polposus (np). Lower right: Expanded section of annulus showing the alternating direction of collagen fibers in successive lamellae. [Adapted from (Dolan and Adams, 2001)].

### 1 - 1.3 Rib Cage

Ribs are attached to the thoracic vertebrae and linked to the sternum (long flat bone in the center of the chest) (Figure 1.4). The rib cage function is to protect the vital organs such as the heart, liver and lungs. There are 12 pairs of ribs attached to vertebrae T1 to T12. The first seven pairs are called “true ribs” as the ribs are directly attached to the sternum. The following three pairs are known as “false ribs” as they are linked by cartilage to the sternum. The last two set of “false ribs” are “floating ribs” because they are not attached to the sternum (not shown in Figure 1.4).

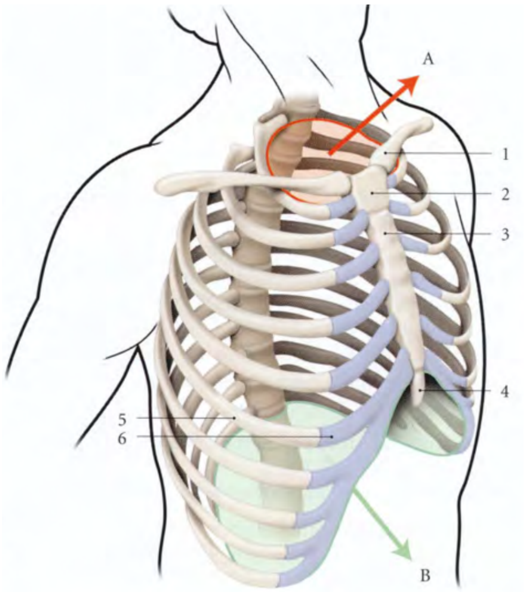


A Superior opening of rib cage

B Inferior opening of rib cage

1. Clavicle
2. Manubrium of the sternum
3. Sternum
4. Xiphoid process
5. Costal bone
6. Costal cartilage

Figure 1.4. : Ribcage [Adapted from (Kamina, 2006)].

Ribcage is particularly of importance when estimating the weight of the thorax, the larger part of upper body. Because of the different soft tissues in the ribcage, this estimation can be difficult and may not be accurate.

## 1 - 1.4 Pelvis

The pelvis is formed of three bones: the sacrum and coccyx at the back, and two hip bones (ilium, ischium and pubis) on each side (Figure 1.5). The pelvis is sometimes called the pelvic vertebrae because of its large mobility recruited to adapt and compensate the spine alignment above it. The lumbo-sacral joint allows mobility of the pelvis from the spine, while the sacro-iliac joint provides very little motion (Table 1.1).

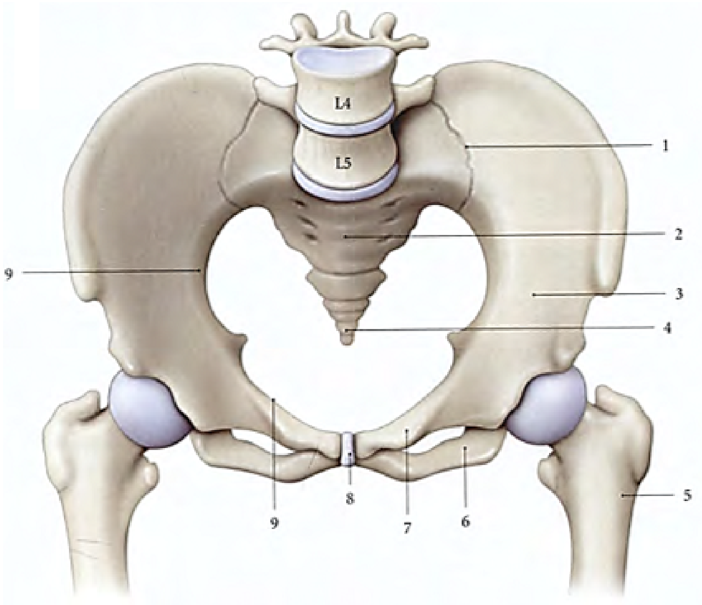


1. Sacro-iliac joint
2. Sacrum
3. Hip bone (os coxae)
4. Coccyx
5. Femur
6. Inferior ramus of pubis
7. Superior ramus of pubis
8. Pubic symphysis
9. Linea terminalis of the pubis

Figure 1.5. : Pelvis: Hip bones and sacrum [Adapted from (Kamina, 2006)].

## 1 - 1.5 Lower limbs

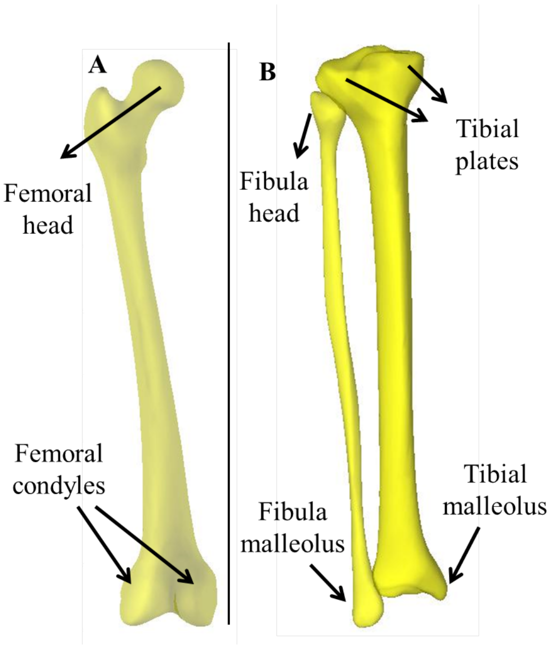


Figure 1.6. : Lower limbs: **A:** Femur. **B:** Tibia and Fibula.

Lower limbs include the femur, tibia and fibula (Figure 1.6). By providing locomotion they are of special interest when studying dynamic movements. In this PhD, as the objective was to quantify aging alterations in the setting of the static posture, they will not be extensively detailed here.

The femur is the thigh bone with the femoral head as proximal extremity and external and internal femoral condyles as the distal extremity.

The tibia associated with the fibula are the bones of the lower leg. The tibia's proximal extremity is formed by the tibial plates and the distal extremity by the medial malleolus. The fibula is attached on the tibia by its proximal head, its distal extremity is the lateral malleolus.

## 1 - 2 Muscles

Only skeletal muscles will be considered in this PhD as they are the ones responsible for movements of the skeleton by their contraction. A muscle can be characterized by its pennation angle, insertions points, length, cross-sectional area and composition. All these parameters can largely influence the muscular force generated during contraction.

The pennation angle is the angle of the fibers with respect to the principal muscle direction (Figure 1.7). A muscle with a large pennation angle will develop a larger muscular force, because the muscular contraction will result in a larger shortening of the muscle in its principal direction (Figure 1.7).

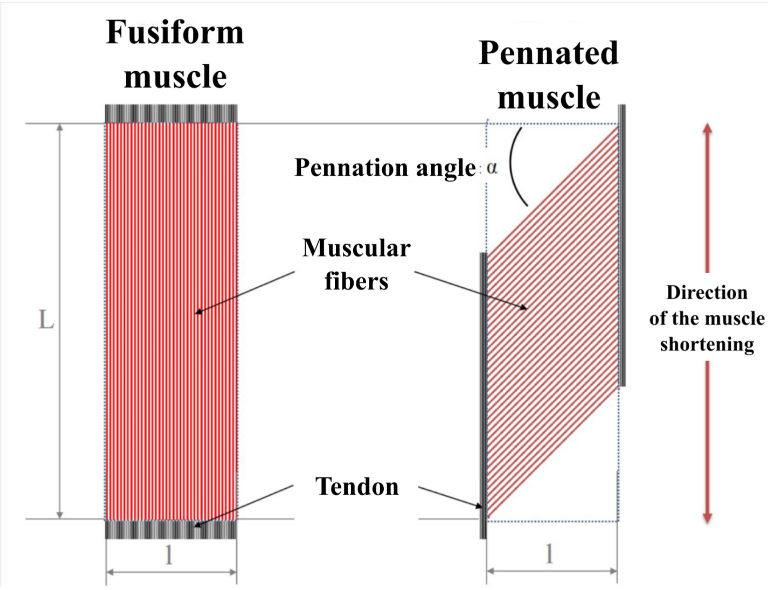


Figure 1.7. : Example of fusiform and pennated muscle. [Figure and legend from (Dubois, 2014)].

The insertion points will determine the lever arm of the muscle (i.e. its distance to the joint center). Muscles with large lever arms, for example lower limb muscles, will generate movements of large amplitude, while deep muscles in the spine (short lever arm) are responsible for spinal stability (linking two adjacent vertebrae together). The insertion points of the muscle are directly linked to the muscle's length. The insertion points, determining the lever arm of the muscle, also determine the moment generated at the joint by the muscular contraction.

The cross-sectional area of the muscle is directly correlated to the number of muscular fibers in the muscle, which is directly linked to the muscular force.

All these parameters are geometrical parameters characterizing the muscle, nevertheless the muscular composition is of primary importance. Different types of fibers can be identified in muscular fibers: type I fibers specialized in long duration contractile activities, and type II fibers for short explosive effort. Different distribution of these fibers will result in different muscular force. Another component of the muscle is the fat that can infiltrate the muscles during aging or during long periods without muscular stimulation.

The last important factor when considering muscles, is their activity and stimulation by the central nervous system: muscles can be activated to generate a movement (locomotion with lower limbs muscles), to stabilize a joint (during one leg stance for example), or to protect vulnerable structures (contraction of cervical muscles during whiplash after the brutal braking of a car).

In this PhD, as only medical images of EOS and MRI exams were analyzed, only geometrical characteristics of the muscle were considered, with the addition of the muscular activation. No analysis was made on the different types of fibers of the muscle, but insight into its quality (fat infiltration) was made. Spino-pelvic muscles considered in this PhD are detailed in Appendix A (Tables A.1, A.2, A.3 and A.4).

## 1 - 3 Aging of the musculo-skeletal system

As reported in the literature, aging induces changes in the musculo-skeletal system. Global aging of the postural alignment include an increased stiffness of the spine, losing flexibility. This rigidity is associated with a loss of lordosis, compensated by a backward rotation of the pelvis (pubis goes forward) (Figure 1.8). When this compensation is at its maximum, flexion of the knee can appear to maintain a global alignment inside the conus defined by Dubousset (Dubousset, 1994) (Figure 2.6).

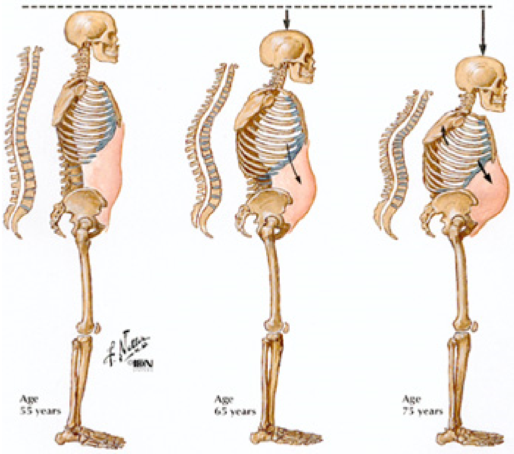


Figure 1.8. : Aging changes in the spine. Illustration by Netter. [Adapted from OSTEOPOROSIS SDW (http://osteoporosissdw.blogspot.fr/)].

Concerning the muscles, decrease has been reported in volume: -25% reported by Narici *et al.* (Narici *et al.*, 2003); and in muscular cross-sectional area: -40% between 20 and 80 years old (Porter *et al.*, 1995). The number of fibers decreases from 25 years old and type I and II fibers proportion can evolve in one way or another depending on the subject (Porter *et al.*, 1995). Different training programs have reported encouraging values on the re-gain of muscular strength and number of fibers for elders, such as stair climbing, or squats (Macaluso and De Vito, 2004). Muscle quality has been reported to deteriorate with age and has been associated with an increased fat infiltration: increase of fat signal fraction from 15% to 20% has been reported between 20 and 60 years old, for back muscles (Crawford *et al.*, 2016).

All these changes impacting the musculo-skeletal system can result in decreased activity and increased discomfort of elders in daily activities. In worst cases, these aging changes can result in spinal deformities or balance alterations leading to fall. Older adults are more subject to falls (up to 42% of olders than 70 years old experience fall each years vs up to 35% for olders than 65 years old (World Health Organization, 2008)) and these falls can require medical attention (37.3 million per year in UK (World Health Organization, 2008)). The consequences of a fall or spinal deformity can be surgery, long-time medical care and frequently loss of autonomy. This loss of autonomy decreases greatly the quality of life of the patient, and results in high costs for the patient as well as the society.

Therefore, it seems essential to study aging and investigate early markers of aging to identify the earliest possible, alterations possibly leading to loss of autonomy.

## 1 - 4 Clinical Imaging

Different types of imaging are used in clinical routine to diagnose and follow the evolution of pathology. The skeletal system can be investigated with long X-rays, Computed-Tomography, or bi-planar radiographs. The X-rays allow visualization of the bony structures and some soft tissues on a gray-scale image. Muscles and soft tissues in general can be investigated with the help of Magnetic Resonance Imaging and Ultrasound.

### 1 - 4.1 X-rays cassette

Conventional X-ray images consist in a long cassette placed in front of the X-ray tube allowing to acquire posture of the subject in one plane (Figures 1.9 and 1.10).

Figure 1.9. : Static Test, volunteer on the forceplate device for the frontal plane. [Adapted from (Schwab *et al.*, 2006)].

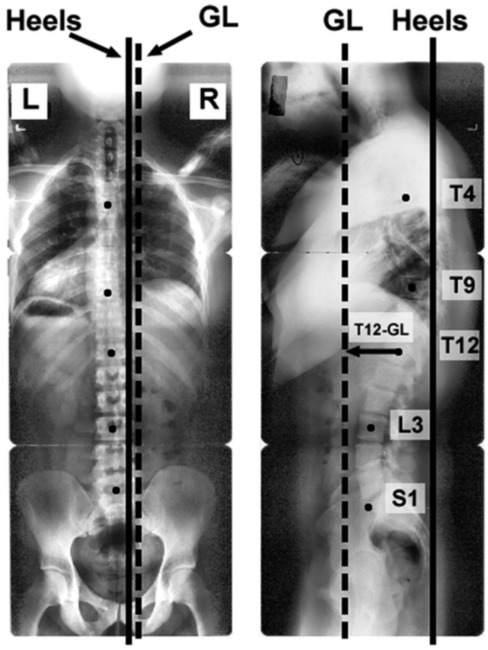


Figure 1.10. : Projection of anatomic landmarks, gravity line (doted line), and heel line on digital radiographs. The gravity line and heels line were detected with the help of a forceplate. [Adapted from (Schwab *et al.*, 2006)].

### 1 - 4.2 Computed Tomography

Computed tomography (CT) is a medical imaging method that uses tomography. Digital geometric processing is used to generate a three-dimensional image of an object from a large series of two-dimensional X-ray images taken around a single axis of rotation (Figure 1.11). CT produces a volume of data which can be manipulated in order to demonstrate various structures based on their ability to block X-ray radiation. CT images are commonly used for bones visualization in a clinical environment.

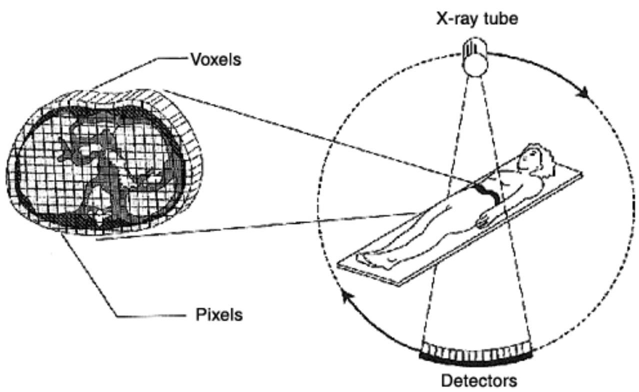


Figure 1.11. : Principle of CT-scan acquisition of 2D images. [Adapted from PHYSICS CENTRAL (`http://www.physicscentral.com/`)].

Main limitation in using CT, especially for volunteers, is that CT involves a moderate to high radiation dose for the subject: 1.5mSv for a lumbar spine CT vs 0.02mSv for a Chest X-ray (Food and Drug Administration, 2015).

### 1 - 4.3 Bi-planar radiographs

The EOS system is a bi-planar low dose radiography system developed from the work of Georges Charpak (Nobel Prize in1992) and now commercialized by EOS Imaging.

The specific advantage of the EOS radiographs relates to its ability to obtain full body X-rays in standing position (Figure 1.12).

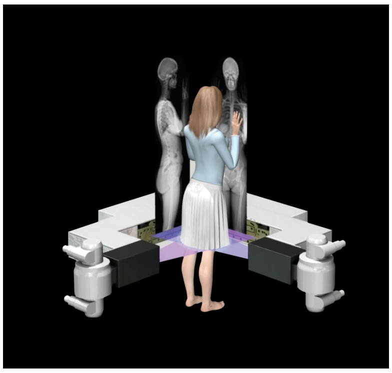

Figure 1.12. : Bi-planar standing radiographs from head to feet, acquired simultaneously. [Adapted from EOS IMAGING (http://www.eos-imaging.com/)]

The advantage of the standing position is that it reflects accurately the skeleton in the daily position, under the gravity effect (i.e. with joints compressed) (Dubousset *et al.*, 2005, 2008, 2010).

In addition to its large resolution (image pixel resolution of 254 $\mu$m (Illés and Somoskeöy, 2012)), 3D reconstruction of the skeleton has been developed, as bi-planar radiographs are taken simultaneously in a calibrated environment (Humbert *et al.*, 2009b; Quijano *et al.*, 2013) (Figure 1.13).

This technology permits not only to identify global and local postural alterations, but also to investigate compensatory mechanisms (ex: knee flexion, rotation of the pelvis) recruited by each individual in an effort to maintain an erected posture. The 3D reconstruction of the skeleton allows the characterization of the local alterations of vertebrae and/or discs; as well as the characterization of variations in lordosis and kyphosis.

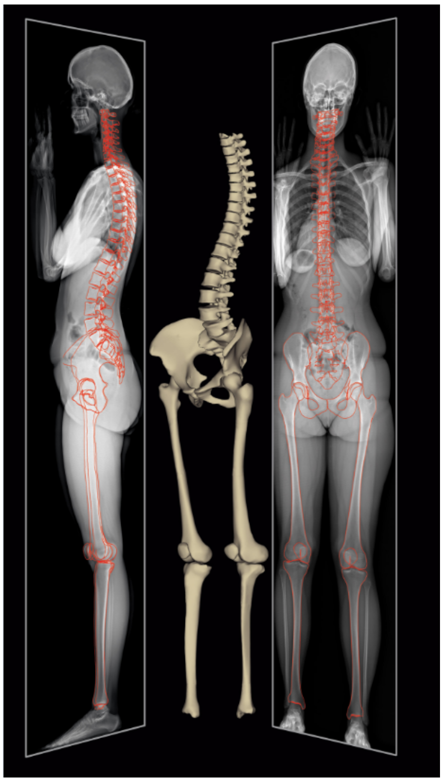

Figure 1.13. : EOS bi-planar radiographs and 3D reconstruction of the skeleton. [Adapted from EOS IMAGING (http://www.eos-imaging.com/)]

The EOS system involves a small amount of radiation: the effective dose of a EOS full spine examination is 290µSv (Damet *et al.*, 2014) (equivalent to 52 days of background radiation). When compared to a return flight London-Toronto whose effective radiation dose is 56µSv (Lewis *et al.*, 2001); in the end, a full spine examination with the EOS system is equivalent to 5 return flights from London to Toronto.

Because EOS images are associated with a low radiation dose and because it permits 3D reconstruction of the different bones, they will be used in this PhD to investigate the postural alignment changes during aging.

### 1 - 4.4 Ultrasound

The ultrasound is an easy to implement, non-invasive method, used to investigate soft tissues (Figure 1.14). It is based on the reflection by tissues of a sound wave: depending on the distance of the object from the source, the reflection wave, for this object, will be detected at a different time. The image is constructed based on the difference of reception time of the different reflection waves (one per object encountered) (Figure 1.15).

However, deep muscles can be more difficult to explore as it is a surface technique. Previous studies using ultrasound for muscles' investigation, mainly focused on the dynamic behavior of the muscle (muscles' contraction) as it is possible to capture multiple images during a movement (Nuzzo and Mayer, 2013; Skeie *et al.*, 2015). This method, to this day, is limited to 2D measure and does not give access to volumetric information. Still, ultrasound imaging is more and more used to investigate muscles, tendons and other internal organs.

Figure 1.14. : Acquisition of ultrasound image on the abdomen. [Adapted from MEDICAL NEWS TODAY (`http://www.medicalnewstoday.com/`)].

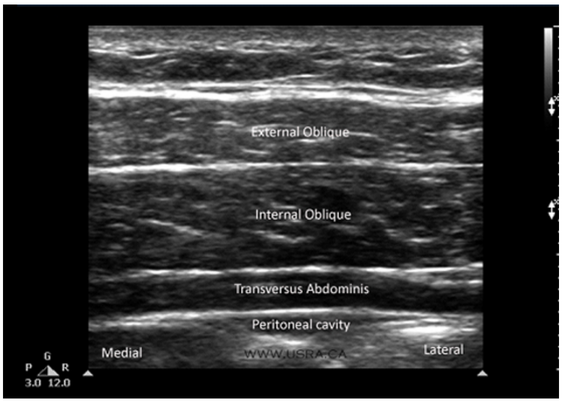


Figure 1.15. : Ultrasound image of the lateral abdominal wall. [Adapted from ULTRASOUND FOR REGIONAL ANESTHESIA (`http://www.usra.ca/`)].

### 1 - 4.5 Magnetic Resonance Imaging

Magnetic Resonance Imaging is a commonly used imaging system to investigate the muscular system (Gildea *et al.*, 2013; Kjaer *et al.*, 2007; Lee *et al.*, 2008; Parkkola *et al.*, 1993; Pezolato *et al.*, 2012; Savage *et al.*, 1991; Takahashi *et al.*, 2006) (Figure 1.16). It is a medical imaging technique that provides much greater contrast between different soft tissues structures than computed tomography (CT) (MRI was reported as more sensitive in demonstrating disc degeneration (Schnebel *et al.*, 1989)). Unlike CT, it uses no ionizing radiation, as MRI uses a powerful magnetic field to align the nuclear magnetization of hydrogen atoms in water contained in the body. MRI is commonly used to visualize muscles but other soft tissues as well: particularly for assessment of a disc pathology or disorder such as spinal cord compression, or hernia (Figure 1.17).

Figure 1.16. : Magnetic resonance imaging scanner. [Figure from HEALTHCARE SIEMENS (`http://healthcare.siemens.fr/`)].

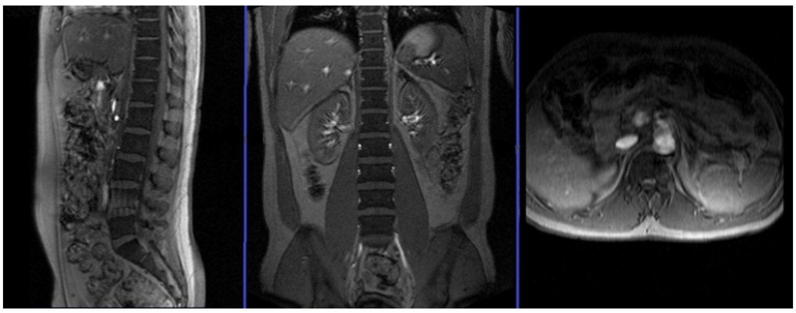

Figure 1.17. : Magnetic resonance images on the lumbar area in the three different planes: from left to right: sagittal plane, frontal plane and axial plane. T1 weighted low resolution images. [Figure from MRI MASTER (`http://mrimaster.com/`)].

Because MRI is the only non-invasive imaging technique allowing to compute the muscles' 3D geometry and because of the laboratory expertise in the MRI images processing (Südhoff *et al.*, 2009; Jolivet *et al.*, 2014; Moal *et al.*, 2014, 2015), the MRI technique will be used for muscles analysis in this PhD.

# CHAPTER 2

# STUDYING POSTURAL ALIGNMENT

## 2 - 1 Segments usually considered

The spine is a complex structure resulting from our adaptation to bipedalism, it has therefore been studied for a long time. The spine is characterized by the amplitudes of the three spinal curvatures: the cervical lordosis, the thoracic kyphosis and the lumbar lordosis (Stokes *et al.*, 1993; Vrtovec *et al.*, 2009) (Figure 2.1). Soon enough, the crucial role of the pelvis was highlighted in the postural alignment: in particular, Dubousset denoted the pelvis as the last vertebra supporting the upper body weight (Dubousset, 1994) (Figure 2.2).

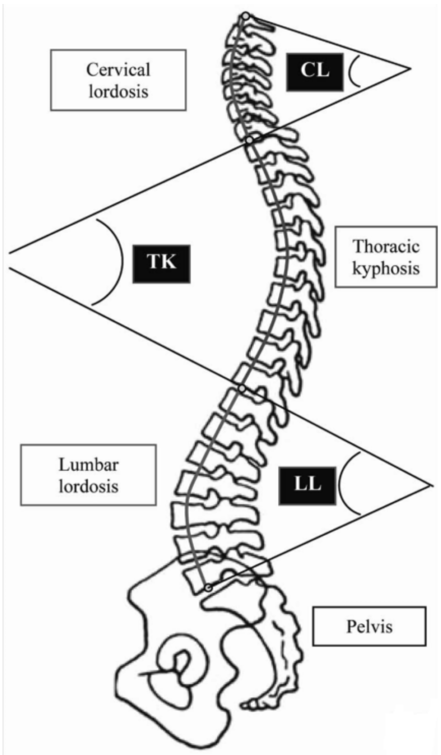


Figure 2.1. : Spinal curvatures: cervical lordosis, thoracic kyphosis and lumbar lordosis. [Adapted from (Berthonnaud *et al.*, 2005)]

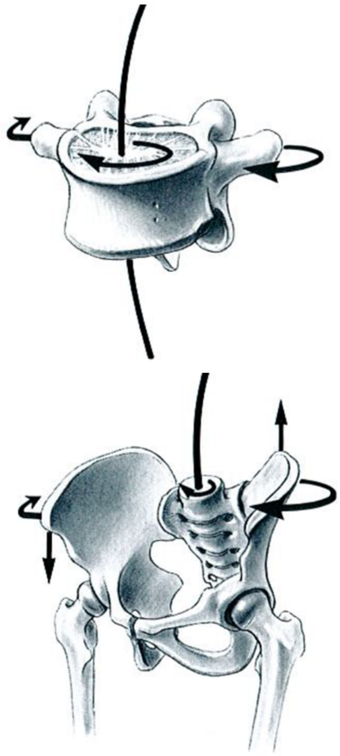

Figure 2.2. : The entire pelvis can be considered as one unique vertebra. [Figure and legend from (Dubousset, 1994)].

3 pelvic angles are used for characterization of the pelvis position and morphology (Figure 2.3): pelvic incidence (morphological parameter); pelvic tilt (pelvis position relative to the femoral heads) and sacral slope (pelvis inclination) (Duval-Beaupère *et al.*, 1992).

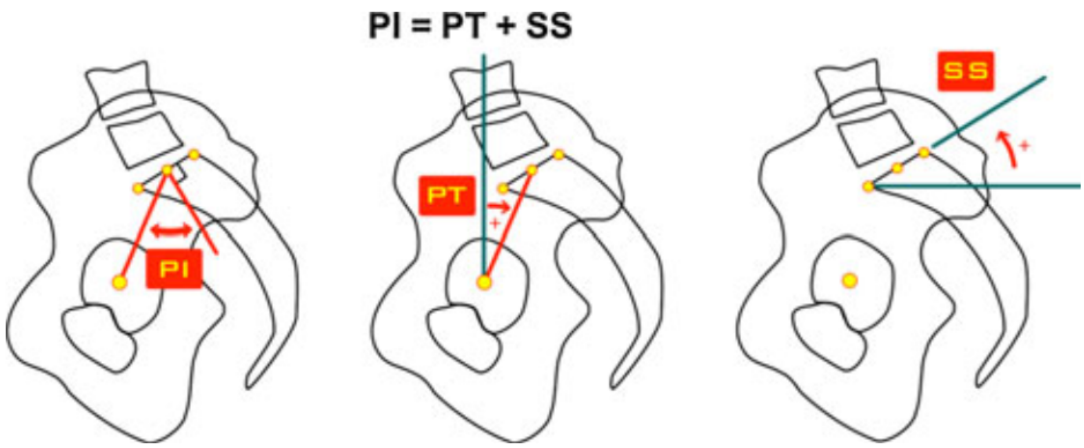


Figure 2.3. : Pelvic parameters. SS: Sacral slope (inclination of the sacral plate). PT: Pelvic tilt (retroversion of the pelvis). PI: Pelvic incidence (morphological parameter). [Adapted from (Mac-Thiong *et al.*, 2011)].

Reference values (Table 2.1) have been reported for these parameters, for various age groups of asymptomatic adults, as they provide baselines to quantify pathology's evolution and severity.

| in ° | **C2-C7 Cervical Lordosis** | **T4T12 Thoracic Kyphosis** | **L1-S1 Lumbar Lordosis** | **Pelvic Incidence** | **Pelvic Tilt** | **Sacral Slope** |
|---|---|---|---|---|---|---|
| **21-40 years old** | - | 38 (12) [a] | 60 (14) [a] | 52 (10) [a] | 13 (7) [a] | 39 (9) [a] |
| **41-60 years old** | - | 37 (9) [a] | 60 (8) [a] | 53 (8) [a] | 14 (6) [a] | 40 (7) [a] |
| **>60 years old** | - | 44 (12) [a] | 57 (11) [a] | 51 (9) [a] | 16 (6) [a] | 36 (9) [a] |
| **18-81 years old** | 5 (12) [b] | 41 (10) [c] | 43 (11) [c] | 55 (11) [c] | 13 (6) [c] | 41 (8) [c] |

Table 2.1. : Mean (Standard Deviation) reported in the literature for spinal curvatures and pelvic parameters, for asymptomatic adults of various ages. [a]Schwab *et al.* (2006). [b]Le Huec *et al.* (2014). [c]Vialle *et al.* (2005): lordosis was, for this paper, computed between L1 and L5.

Additional parameters have been introduced in the course of time, to better characterize the postural alignment. Among these, the most used are:

- the Sagittal Vertical Axis (SVA): anterior shift of C7 vertebra body's center from the most postero-superior point of the sacral plate (S1) (Figure 2.4),
- the Overhang of S1: postero-anterior distance between middle point of sacral plate (S1) and middle of bi-coxofemoral axis (middle of centers of femoral heads: HA) (Figure 2.4).

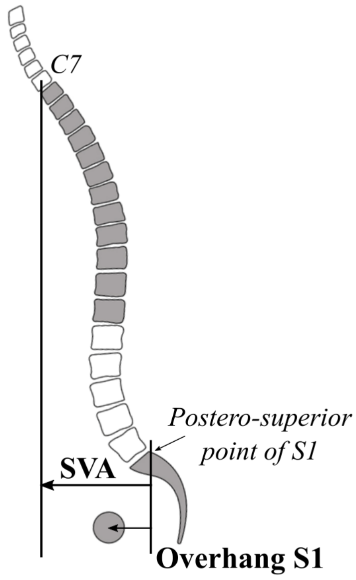


Figure 2.4. : Sagittal Vertical Axis (SVA) and Overhang of S1.

Reference values from the literature, for these parameters, are presented in table 2.2.

| in mm | SVA | Overhang S1 |
|---|---|---|
| **21-40 years old** | - 36 (33) [a] | 25 (16) [a] |
| **41-60 years old** | - 21 (40) [a] | 25 (14) [a] |
| **>60 years old** | - 11 (20) [a] | 32 (15) [a] |
| **20-84 years old** | - 44 (39) [b] | - |

Table 2.2. : Mean (Standard Deviation) reported in the literature for SVA and Overhang S1. [a]Schwab *et al.* (2006). [b]El Fegoun *et al.* (2005).

## 2 - 2 Lower limbs and head rarely considered

The other segments rarely included in the postural alignment studies are the head and the lower limbs. Concerning the lower limbs, they are of primary importance when considering compensatory mechanisms occurring during aging.

During aging, changes in the inter-vertebral disc (water loss (Adams *et al.*, 1996; Dolan and Adams, 2001)) and vertebra (bone remodling) can lead to loss of sagittal balance. Additionnaly, a loss of lumbar lordosis has been reported during aging (lumbar spine is less curved (Gelb *et al.*, 1995)), as well as a forward shift of the anterior part of the trunk (posture more bent).

In order to compensate for the forward flexion of the trunk due to the loss of lordosis, the pelvis rotates backwards (pelvis retroversion) (Barrey *et al.*, 2013; Diebo *et al.*, 2015; Fechtenbaum *et al.*, 2015). Aging is also associated with flexion of the knees and extension of the ankles to stabilize the postural global alignment (Barrey *et al.*, 2013) (Figure 2.5). Specific parameters have been reported in the literature to assess these compensatory mechanisms (Barrey *et al.*, 2013).

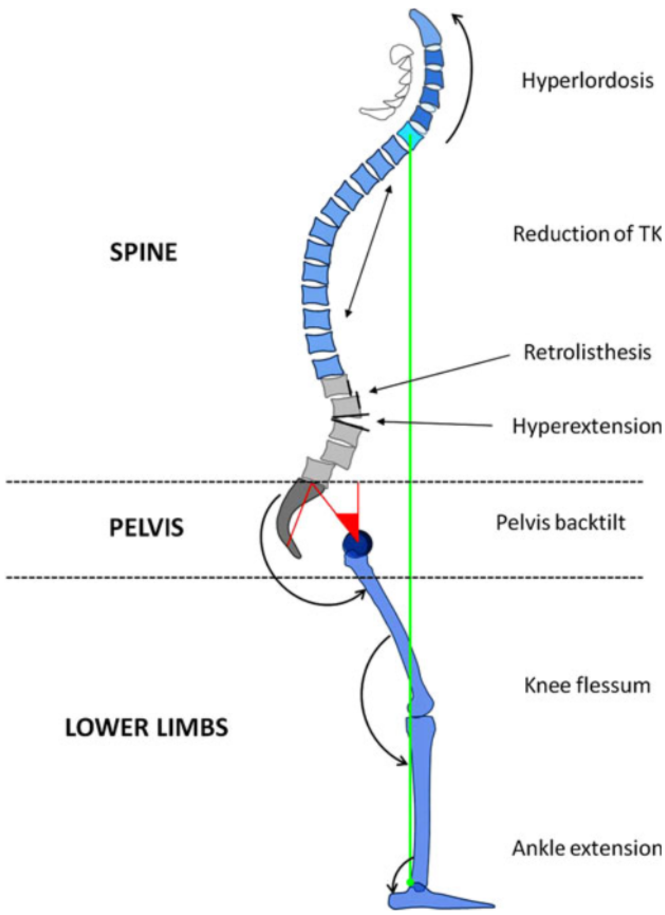


Figure 2.5. : Compensatory mechanisms occurring during asymptomatic/pathological aging [Adapted from (Barrey *et al.*, 2013)].

If the lower limbs have been studied in specific studies, they have rarely been included in postural alignment studies. Common parameters to characterize lower limbs' geometry are femoral and tibial torsions or femoral neck shaft angle (Table 2.3). Reference values for these parameters are presented in Table 2.3.

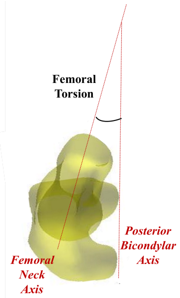


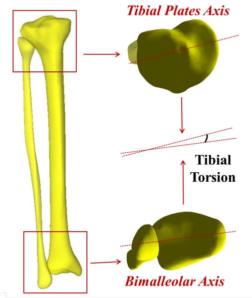


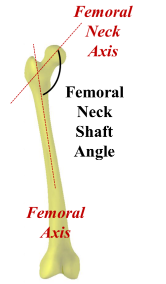


| in ° | **Femoral Torsion** | **Tibial Torsion** | **Femoral Neck Shaft Angle** |
|---|---|---|---|
| **Rubin *et al.* (1992)** | - | - | 122.9 (7.6) |
| **(Kim *et al.*, 2000)** | 16.6 (11.4) | - | - |
| **Seber *et al.* (2000)** | R: 6.5 (7.7) / L: 5.8 (8.4) | R: 30.9 (7.1) / L: 29.1 (6.9) | - |
| **Kristiansen *et al.* (2001)** | - | 37.8 (7.3) | - |
| **Kolta *et al.* (2005)** | - | - | 125.9 (6.4) |
| **Baudoin *et al.* (2008)** | - | - | 129.6 (2.5) |
| **Chaibi *et al.* (2012)** | 11.1 (3.9) | 27.9 (4.9) | 128.0 (1.9) |
| **Than *et al.* (2012)** | 17.1 (11.5) | 36.0 (8.4) | 128.4 (4.9) |

Table 2.3. : Mean (Standard Deviation) for lower limbs parameters from the literature. R (L): right (left).

Recent studies tend to include the lower limbs in the postural alignment analysis to quantify angles of the different lower limbs segments relative to another (knee flexion, ankle extension for example (Barrey *et al.*, 2013; Diebo *et al.*, 2015)). However these studies focused mainly on patients and not asymptomatic subjects (Table 2.5).

As for the head, this is a segment that needs special attention with regard to its weight (4-5kg) (Vital and Senegas, 1986) and position as it is far from the "pelvic vertebra" supporting the total upper body weight. Because the head is the segment with proprioceptive receptors (inner ear, eyes), its alignment compared to other body segments will be of great importance when monitoring an efficient and costless erected posture.

The head as individual segment has been studied in few studies (Lafage *et al.*, 2015; Le Huec *et al.*, 2014), and have rarely been included in previous postural alignment studies. Because the majority of radiographs stop between C5 and C7 to avoid eyes irradiation and because of the size of conventionally used X-ray cassette, the most superior point giving an idea of the position of the head was for a long time C7. More and more studies tend to include the cervical spine, as well as the head, in radiographs and studies, in order to get a broader look on the global postural alignment on the patient (Gangnet *et al.*, 2003; Steffen *et al.*, 2010; Le Huec *et al.*, 2014) (Table 2.5).

## 2 - 3 Plane considered for postural alignment analysis

Until recently, spinal deformities were studied in one plane only, either sagittal or coronal.

With development of new technologies and tools, and in particular of bi-planar radiographs and 3D reconstruction algorithms, the idea arose that spinal deformities are 3D deformations that need to be studied in 3D. Clinical routine however rarely included 3D analysis, even if it is particularly interesting for surgery planning in order to take into account the 3D geometry of the deformation (Dubousset, 1994; Dubousset *et al.*, 2010; Illés and Somoskeöy, 2012).

## 2 - 4 The need for head to feet analysis in 3D

As Dubousset eluded in 1994 (Dubousset, 1994), the head, thorax and pelvis needs to be aligned in order to provide horizontal gaze (i.e. vision) and keep the center of mass in a close area so the body remains balanced with minimal energy expenditure (Figure 2.6). Different studies reported parameters to characterize the position of the head and its morphology: such as the spino-cranial angle (SCA) or the cranial incidence (Le Huec *et al.*, 2014). One approach in modeling the conus of economy concept is the inverse pendulum (Figure 2.7): while ankle stiffness is greater than gravity load, the pendulum is at the equilibrium (El Helou, 2011).

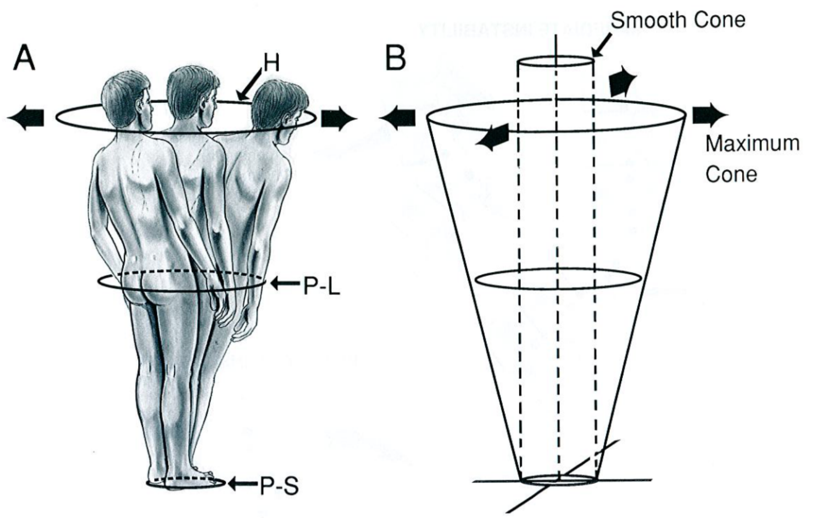


Figure 2.6. : **A:** When the human body is in a standing posture, the feet are located within a zone called the "polygon of sustentation" (P-S). The body, under the influence of muscle function, can move in a conical fashion without moving the feet. The maximum variable amplitude is at the pelvis level (P-L) and at the head (H). **B:** We can determine a maximum cone when muscles are working at their maximum to maintain balance and a smooth cone when muscles are working at their minimum to maintain balance. [Figure and legend from (Dubousset, 1994)].

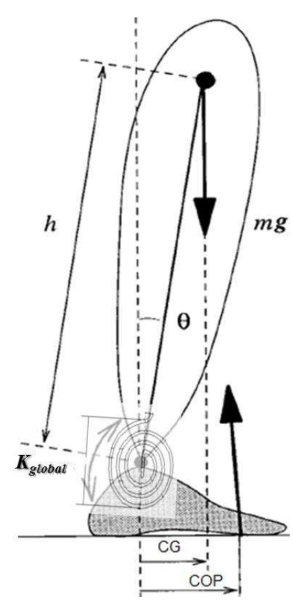


Figure 2.7. : Inverse pendulum illustration, controlled by the torsion stiffness ($K_{global}$) - adapted from (Morasso and Schieppati, 1999). [Figure and legend from (El Helou, 2011)].

As described before, the postural alignment analysis requires analysis of all segments from head to feet, as all are impacted during age-related postural alterations. Therefore, there is a need, for each subject, to acquire head to feet X-rays, in order to better understand compensatory mechanisms occurring during aging. For example, an elderly or patient with large pelvic backtilt and knee flessum will see his hip extension reduced, and therefore his length of step reduced. This could limit the ability to restore balance when missing a step for example.

Because postural alterations and compensatory mechanisms occurring during aging impact the skeleton in the different planes, 3D analysis of the skeleton over aging appears as of primary importance to take into account all the complexity of skeletal pathologies and postural alterations.

Thus, there is a strong need to characterize, for reference population (asymptomatic adults) of various ages, the global postural alignment, from head to feet, in 3D, in order to better appreciate the global condition of the subject/patient. Emphasis should be made on the head segment, too rarely studied in the literature.

Table 2.5 summarizes works published on the postural alignment, based on X-rays. In this table, studies focusing only on lower limbs or pelvis were not included (Mangione *et al.*, 1997; Pajarinen *et al.*, 2004; Baudoin *et al.*, 2008; Than *et al.*, 2012; Gaumétou *et al.*, 2014). In this table were reported studies focusing on the postural alignment in 2D or 3D: differentiation was made between asymptomatic and patients, according to age. The segments studied (head, spine, pelvis lower limbs) were reported. The majority of studies focused on the spine and pelvis, now clearly established as dependent segments. Some studies used a forceplate to estimate the gravity line and feet position (Vaz *et al.*, 2002; Gangnet *et al.*, 2003; El Fegoun *et al.*, 2005; Roussouly *et al.*, 2006; Schwab *et al.*, 2006; Steffen *et al.*, 2010; Lafage *et al.*, 2011).

The addition of the head or lower limbs in the study was rarely made (Gangnet *et al.*, 2003; Steffen *et al.*, 2010; Le Huec *et al.*, 2014; Diebo *et al.*, 2015). To our knowledge, no study combined both the head and lower limbs with spine and pelvis for 3D postural alignment analysis. When the head was included in the study, the study included only young adults (Gangnet *et al.*, 2003; Steffen *et al.*, 2010) or did not include the pelvis (Le Huec *et al.*, 2014). Only one studied combined analysis of the lower limbs with analysis of the spine and pelvis (Diebo *et al.*, 2015). This study reported results in 2D, only for patients, and did not include the head.

The studies on age-related changes in asymptomatic adults reported the effect of aging by reporting statistical difference between young and older groups for specific radiographic parameters (Kim *et al.*, 2014; Legaye, 2014), or correlations between age and radiographic parameters: most interesting correlations can be found in Table 2.4.

| Correlation coefficient (R) | TK | LL | PI | PT | SVA | Overhang |
|---|---|---|---|---|---|---|
| **El Fegoun *et al.* (2005)** | - | - | - | - | 0.31 | - |
| **Vialle *et al.* (2005) *** | 0.2 | 0.14 | 0.14 | - | - | - |
| **Schwab *et al.* (2006)** | 0.32 | - | - | - | - | - |
| **Mac-Thiong *et al.* (2007)** | - | - | - 0.21 | - 0.23 | - | - |
| **Lafage *et al.* (2008) *** | - | - | - | $<0.62$ | $<0.62$ | $<0.62$ |

Table 2.4. : Correlation coefficient (R) reported in the literature for correlation of radiographic parameters with age. * means that the study did not mention if the correlation found was significant. TK means thoarcic kyphosis, LL lumbar lordosis, PI pelvic incidence, PT pelvic tilt and SVA sagittal vertical axis.

These correlations are in line with clinical observation: aging is associated with an increased kyphosis, an increased pelvic tilt, an increased anterior shift of the upper part of the trunk. These changes have been reported as compensatory mechanisms or as pathological symptoms occurring during aging (Barrey *et al.*, 2013; Diebo *et al.*, 2015).

Overall, if several studies have investigated age-related changes in postural alignment, few studies included a 3D head to feet analysis of the postural alignment of asymptomatic adults, as seen in Table 2.5. The first part of this PhD thesis will address this need by the study of head to feet postural alignment, in the setting of young asymptomatic adults, and from head to hip for older adults.

| Study | N asymp. < 60years | N asymp. > 60years | N patients < 60years | N patients > 60years | Effect of aging ? | Head | Spine | Pelvis | Femur | Tibia | FP | 2D / 3D ? |
|---|---|---|---|---|---|---|---|---|---|---|---|---|
| **Duval-Beaupère *et al.* 1992a** | 17 | - | - | - | | | X | X | | | | 2D |
| **Legaye *et al.* 1998** | 49 | - | 66 [10yrs - 84yrs] | | | | X | X | | | | 2D |
| **Jackson *et al.* 2000** | 20 [26yrs-75yrs] | | 20 [26yrs - 73yrs] | | | | X | X | | | | 2D |
| **Rajnics *et al.* 2001** | 30 [30yrs - 39yrs] | | 0 | 0 | | | X | | | | | 2D |
| **Vaz *et al.* 2002** | 112 | - | - | - | | | X | X | | | X | 2D |
| **Gangnet *et al.* 2003** | 34 | - | - | - | | X | X | X | | | X | 3D |
| **Duval-Beaupère *et al.* 2004** | 47 [mean: 22yrs] | | - | - | | | X | X | | | | 2D |
| **Faro *et al.* 2004a** | 50 | - | - | - | | | X | X | | | | 2D |
| **Berthonnaud *et al.* 2005** | 160 [20yrs -70yrs] | | | | | | X | X | | | | 2D |
| **ElFegoun *et al.* 2005** | 41 [20yrs - 84yrs] | | 44 [24yrs - 88yrs] | | X | | X | X | | | X | 2D |
| **Roussouly *et al.* 2005** | 160 | - | - | - | | | X | X | | | | 2D |
| **Vialle *et al.* 2005** | 300 [20yrs - 70yrs] | | | | X | | X | X | | | | 2D |
| **Boulay *et al.* 2006** | 149 | - | - | - | | | X | X | | | | 2D |
| **Roussouly *et al.* 2006** | 153 | - | - | - | | | X | X | | | X | 2D |
| **Schwab *et al.* 2006** | 50 | 25 | - | - | X | | X | X | | | X | 2D |
| **MacThiong *et al.* 2007** | 341 | - | - | - | X | | X | X | | | | 2D |
| **Tanguay *et al.* 2007** | 60 | - | - | - | | | X | X | | | | 2D |
| **Lafage *et al.* 2008** | 66 [18yrs - 93yrs] | | 65 [18yrs - 93yrs] | | X | | X | X | | | X | 2D |
| **Legaye *et al.* 2008** | 42 | - | - | - | | | X | X | | | | 2D |
| **Lafage *et al.* 2009** | 125 [22yrs - 88yrs] | | - | - | | | X | X | | | | 2D |
| **Steffen *et al.* 2010b** | 23 | - | 93 [12yrs - 78yrs] | | | X | X | X | | | X | 3D |
| **Lafage *et al.* 2011** | - | - | 119 [mean: 52yrs; SD: 22yrs] | | | | X | X | | | X | 2D |
| **MacThiong *et al.* 2011** | 709 [18yrs - 81yrs] | | - | - | X | | X | X | | | | 2D |
| **Kim *et al.* 2014** | 342 [19yrs -23yrs and 53yrs-79yrs] | | - | - | X | | X | X | | | | 2D |
| **Legaye *et al.* 2014** | 71 | 18 | 149 | 51 | X | | X | X | | | | 2D |
| **LeHuec *et al.* 2014** | 106 [18yrs - ?] | | - | - | | X | X | X | | | | 3D |
| **Ryan *et al.* 2014** | - | - | 559 [mean: 53yrs] | | | | X | X | | | | 2D |
| **Diebo *et al.* 2015** | - | - | 161 [mean: 63yrs; SD: 13yrs] | | | | X | X | X | X | | 2D |

Table 2.5. : Summary of published studies on postural alignment from X-rays analysis. Asymp. means asymptomatic. N means number of patients/volunteers. A tick in the “FP” column means that a forceplate was used to record center of pressure position and ground forces. One can note the few studies including the head in the postural alignment analysis and the few studies using 3D reconstruction of the full skeleton. In blue are highlighted studies reporting a 3D analysis.

# CHAPTER 3

# STUDYING MUSCULAR SYSTEM

## 3 - 1 An additional tool in research: Electromyography

Electromyography (EMG) is a widely used technique to study dynamically the activity of muscles (Figure 3.1). Recording the electrical activity produced by the muscle (via surface electrodes or needle electrode placed inside the muscle), allows studying the muscular pattern recruitment during a movement (Figure 3.2). Are all muscles contracting at the same time? What is the extend of the contraction compared to the maximal voluntary contraction? Electromyography can provide materials to answer these questions.

Figure 3.1. : Surfacic electrodes for Electromyography. [Adapted from INNER SPORT (`http://innersport.com/`)].

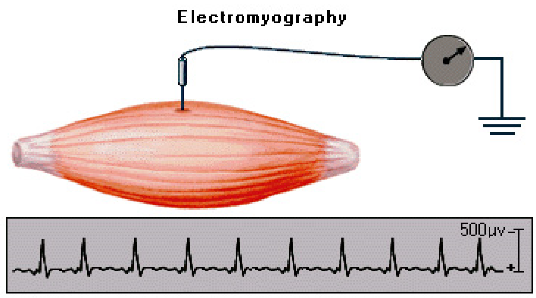


Figure 3.2. : Electromyography principle. [Adapted from HUMAN PHYSIOLOGY (`http://humanphysiology.tuars.com/`)].

EMG requires careful preparation of the skin before placing the electrodes, and careful placement of the electrode in order to record only one muscle and not a mixed signal of the contraction of 2 adjacent muscles (cross-talk issues). This technique does not provide any geometrical information on the muscles and is difficult to implement in a clinical environment as it requires time and room for testing different movements. This PhD project did not focus on the utilization of electromyography measures, because choice was made to only use clinical routine exams providing medical images in clinical routine such as MRI for example.

## 3 - 2 Muscles exploration in the literature

### 3 - 2.1 3D geometry of muscles

Most of the studies focusing on muscular system characterization from MRI images, computed the cross-sectional section area (CSA) and/or the fat infiltration percentage from different slices (see Table 3.1). If some studies computed the volume from CSA and slice thickness (Sanchis-Moysi *et al.*, 2011;

Beneck and Kulig, 2012; Valentin *et al.*, 2015), only 6 past studies reported a volume computed from a 3D geometry (Albracht *et al.*, 2008; Jolivet *et al.*, 2014; Li *et al.*, 2014; Moal *et al.*, 2014, 2015) (see Table 3.1).

From these 6 studies reporting 3D geometry of muscles, 2 different methods can be identified. The first one reported by Albracht *et al.* in 2008, is in two steps: first, segmenting axial contours on axial MRI slices; second, "a continuous B-Spline solid was created from the 3D- coordinates of the transversal contours" (Albracht *et al.*, 2008) (Figure 3.3).

The second method is a fast and semi-automatic technique, developed in the Institute. It enables the accurate and repeatable 3D reconstruction of the muscles from a reduced set of segmented MRI axial images (Jolivet *et al.*, 2014; Moal *et al.*, 2014) (Figure 3.4).

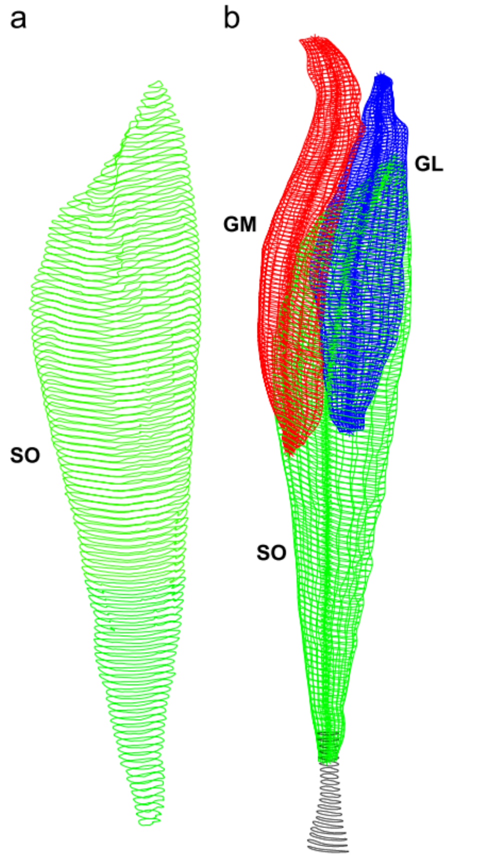


Figure 3.3. : (a) Segmented transversal contours of the soleus (SO) muscle. (b) B-Spline solid of the triceps surae muscles: soleus (SO), gastrocnemius medialis (GM) and gastrocnemius lateralis (GL). [Figure and legend from (Albracht *et al.*, 2008)].

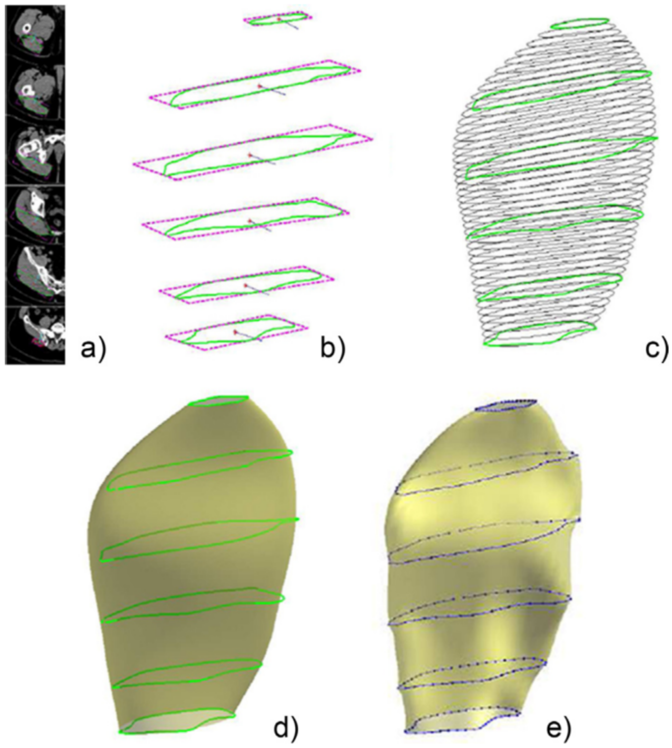


Figure 3.4. : Overview of the DPSO reconstruction method (Jolivet *et al.*, 2014): **a)** subset of MRI axial slices with manually segmented axial sections; **b)** contours approximated by ellipses [represented on the figure by a green rectangle whose length and width correspond to the major and minor axes of the ellipses]; **c)** cubic spline interpolation used to interpolate ellipses in all non-outlined slices covering the muscle; **d)** interpolated ellipses generated a 3D parametric object; **e)** non-linear deformation of the parametric object was deformed using the manual segmentations [from (Moal *et al.*, 2014)].

3D geometry of muscles can be of special interest when studying the compensatory mechanisms occurring during aging: as postural alignment changes over aging are in 3D, muscles will be impacted on the whole: on the volume, quality, CSA but also on the 3D geometrical shape.

Muscles of interest when focusing on balance alteration are primarily muscles in the lumbar, pelvic and knee areas. These joints are of special interest as compensatory mechanisms observed during aging impact these joints in particular (pelvic retroversion, knee flessum for example). These muscles will be called spino-pelvic muscles in the following.

### 3 - 2.2 Fat infiltration

Over aging and pathological evolution, muscles degrade both in terms of volume (sarcopenia (Narici *et al.*, 2003)) and in quality (increase of fat infiltration inside the muscle (Porter *et al.*, 1995)) (Figure 3.5). Access to the fat content of each muscle will help quantify the power / strength of the muscle considered. Associating this information with the loss or increase in volume will help better identify changes in the muscular system and hyper-recruitment of specific muscles, in case of postural mal-alignment or disorder.

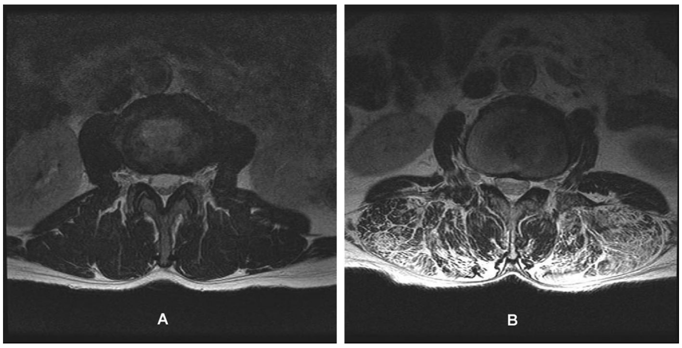


Figure 3.5. : Magnetic resonance imaging of a person with normal lumbar lordosis shows a healthy back extensor muscle (**A**), whereas that of a patient with a degenerative flat back deformity shows muscular atrophy and fat infiltration (**B**). [Figure and legend from (Lee *et al.*, 2008)].

Fat infiltration can be computed with different methods:

- by using semi-quantitative scale (Kjaer *et al.*, 2007) (see Figure 3.6),
- by detecting less bright pixels (Beneck and Kulig, 2012): either with a threshold (Figure 3.7), or with a sigmoid function on pixel intensity (Figure 3.8).

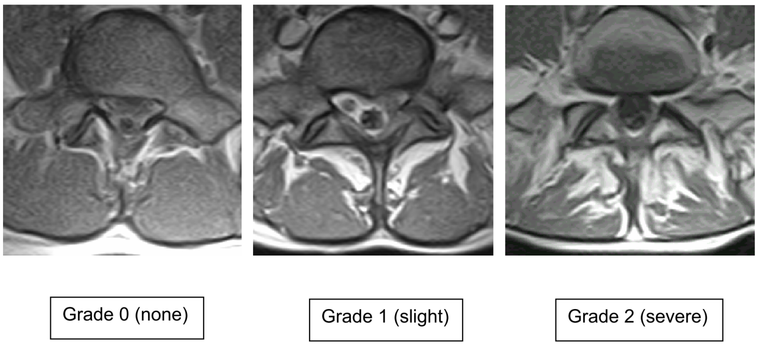


Figure 3.6. : Examples of amounts of fat in the lumbar multifidus muscles as seen on axial T1- weighted magnetic resonance imaging scans. These were rated as grade 0 if normal condition; grade 1 for slight fat infiltration (10–50%), and grade 2 for severe fat infiltration (>50%). [Figure and legend from (Kjaer *et al.*, 2007)].

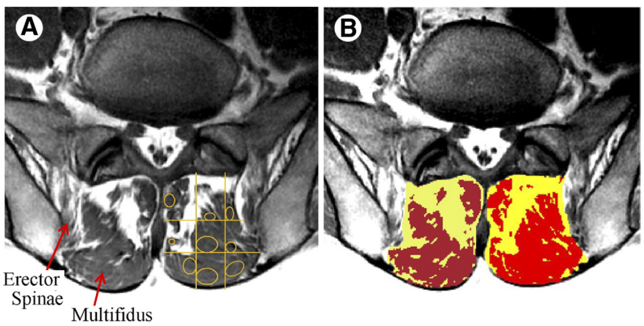


Figure 3.7. : Axial MR image at the L5-S1 level. (A) MR image before image quantification. (B) Color-coded regions distinguishing multifidus from non-muscle tissue. The crossbars and circles in the left multifidus in figure A illustrate the segmentation method used in this study. Note: the erector spinae size is typically small where it attaches to the sacrum and iliac crest. [Figure and legend from (Beneck and Kulig, 2012)].

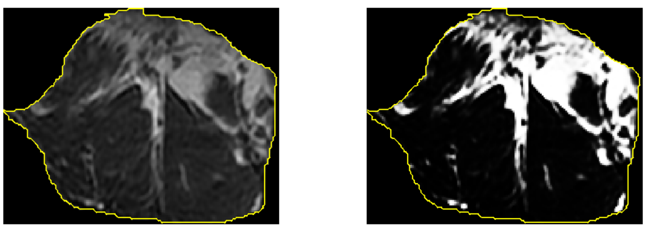

Figure 3.8. : Detected fatty region from the segmented muscle region (with threshold = 80 and softness = 0.1). [Figure and legend from (Antony *et al.*, 2014)].

A recent study (Moal *et al.*, 2015) demonstrated the potential of MRI in the quantification of the muscle fat infiltration based on Dixon images (Dixon, 1984). Dixon MRI sequence (Dixon, 1984) provides two identical images: the first one for which the intensity of the pixel is correlated to the amount of water contained (Water image) and the second one for which the intensity of the pixel is correlated to the amount of fat contained (Fat image) (Figure 3.9). By combining information of intensities of the same pixel from both images, and with calibration, fat percentage can be computed for each pixel (Dixon, 1984; Moal *et al.*, 2015).

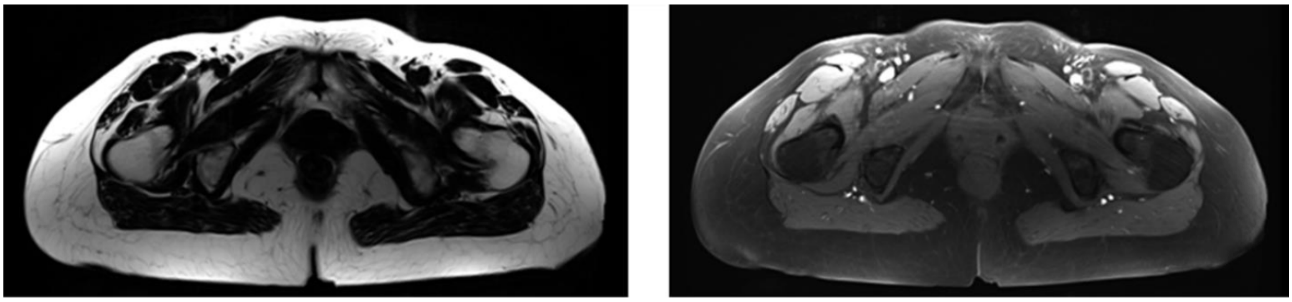

Figure 3.9. : Example of water (left) and fat (right) images with Dixon methods on a 64- year-old female adult spinal deformity patient. [Figure and legend from (Moal *et al.*, 2015)].

### 3 - 2.3 The need for 3D geometry database for reference population

As illustrated in the Table 3.1, the literature regarding muscle investigation based on MRI images is quite extensive as this modality can be used for diagnosis of muscular pathologies. Most the studies using MRI, only reported qualitative or semi-qualitative findings. This table focuses on research associated with either aging of the muscular system, fat infiltration and/or geometrical characterization of the muscles.

Only 6 studies reported 3D geometry for young asymptomatic adults, (Albracht *et al.*, 2008; Jolivet *et al.*, 2014; Li *et al.*, 2014; Moal *et al.*, 2014). Albracht *et al.* focused on calf muscles (Albracht *et al.*, 2008), while Li *et al.* looked into details the cervical muscles (Li *et al.*, 2014). On the other hand, Moal *et al.* and Jolivet *et al.* studied spino-pelvic muscles and thigh muscles (Jolivet *et al.*, 2014; Moal *et al.*, 2014). The two latter studies included less than 5 subjects as the purpose of each study was the validation of a new 3D reconstruction algorithm.

As seen in Table 3.1, few studies reported 3D description of spino-pelvic muscles for a reference population (young asymptomatic adults). There is, therefore, a strong need for reference values concerning spino-pelvic muscles 3D geometry, for young asymptomatic adults in order to better appreciate and quantify muscular age-related changes. This will be the purpose of the second part of this PhD.

| Author | MRI region of acquisition | | | | | | 3D / 2D ? | Effect of aging ? | Asymptomatic | | Patients | | CSA | Length | Pfat | Volume |
|---|---|---|---|---|---|---|---|---|---|---|---|---|---|---|---|---|
| | Cervical Spine | Thoracic Spine | Lumbar Spine | Pelvis | Thigh | Lower leg | | | N < 60years | N > 60years | N < 60years | N > 60years | | | | |
| **Savage *et al.* 1991** | | | X | | | | 2D | X | 68 | | 79 | | X | | | |
| **Parkkola *et al.* 1993** | | | X | | | | 2D | | 60 | | 48 | | X | | X | |
| **Marras *et al.* 2001** | | X | X | | | | 2D | | 30 | | | | X | | | |
| **Takahashi *et al.* 2006** | Not mentionned, probably lumbar spine to thigh | | | | | | 2D | X | 140 | 70 | | | X | | | |
| **Mengiardi *et al.* 2006a** | | | X | | | | 2D | | 25 | | 25 | | | | X | |
| **Kjaer *et al.* 2007** | | | X | | | | 2D | X | | | 854 | | | | X | |
| **Lee *et al.* 2008** | | | X | | | | 2D | | 10 | | 11 | | X | | X | |
| **Albracht *et al.* 2008** | | | | | | X | 3D | | 13 | | | | X | X | | X 3D |
| **Niemeläinen *et al.* 2011** | | | X | | | | 2D | | 126 | | | | X | | X | |
| **Sanchis-Moysi *et al.* 2011a** | | | X | X | | | 2D | | 29 | | | | | | | X computed |
| **Beneck *et al.* 2012** | | | X | X | | | 2D | | 14 | 14 | | | X | | | X computed |
| **Pezolato *et al.* 2012** | | | X | | | | 2D | | 30 | | 15 | | X | | X | |
| **Gildea *et al.* 2013** | | | X | X | | | 2D | | 8 | | 23 | | X | | | |
| **Fortin *et al.* 2014** | | | | | | | 2D | | 116 | | | | X | | X | |
| **Nam *et al.* 2014a** | | | X | | | | 2D | X | | | 112 | | | | X | |
| **Moal *et al.* 2014** | | | X | X | X | | 3D | | 2 | | | | X | X | X | X 3D |
| **Li *et al.* 2014** | X | X | | | | | 3D | | 16 | | | | | | | X 3D |
| **Mersmann *et al.* 2014** | | | | | | X | 3D | | 53 | | | | X | X | | X 3D |
| **Jolivet *et al.* 2014** | | | | X | X | X | 3D | | 4 | | | | | | | X 3D |
| **Valentin *et al.* 2015** | | | X | | | | 2D | X | 24 | | | | | | X | X computed |
| **Fortin *et al.* 2015** | | | X | | | | 2D | | 99 | | | | X | | X | |
| **Moal *et al.* 2015** | | | X | X | X | | 3D | X | | | 19 | | | | | X 3D |
| **Takayama *et al.* 2016** | | | X | | | | 2D | X | | | 100 | 60 | X | | X | |
| **Fortin *et al.* 2016** | | | X | | | | 2D | | | | 33 | | X | | X | |
| **Crawford *et al.* 2016** | | | X | | | | 2D | | 80 | | | | | | X | X computed |
| **Ghiasi *et al.* 2016** | | | X | | | | 2D | | 10 | | 6 | | X | | | |

Table 3.1. : Summary of published studies on muscular system from MRI images, reporting geometrical characterization of muscles, fat infiltration and effect of aging. N means number of patients/volunteers. CSA means cross-sectional area. Pfat means percentage of fat (i.e. fat infiltration). In blue are highlighted studies reporting a 3D analysis.

# CHAPTER 4
# STUDYING COMBINATION OF ALTERED POSTURAL ALIGNMENT AND ALTERED MUSCULAR SYSTEM

While the two previous chapters focused on age-related changes in postural alignment and muscular system, changes in composition of spinal structures occur as well, for example in the inter-vertebral disc (Adams *et al.*, 1996) or vertebra bone (osteoporosis), by change, among others, of the components' biochemistry.

The increased spine stiffness with age, is attributed to changes in the disc's mechanical properties, and particularly to its loss of water over aging: 80% water content for a young adult vs 65% for older adult (Nachemson, 1975). As a result, the inter-vertebral disc stress varies over aging, changing its ability to resist and support high loads in any direction (Figure 4.1).

The disc is one of the principal structures to support loads and particularly to support compression load while allowing some flexibility to the spine. In addition, other spinal structures can help support loads, such as facets joints to support high shear load for example (Figure 4.1).

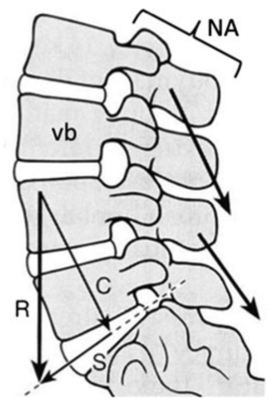


Figure 4.1. : Lumbar spine showing inter-vertebral discs lying between vertebral bodies (vb). Forces on the spine (arrows) arise mostly from gravity, and from tension in muscles attached to the neural arches (NA) of each vertebra. Spinal compression (C) and shear (S) are defined as those components of the resultant force (R) that act perpendicular to, and parallel to the mid-plane of each disc. [Figure and legend adapted from (Adams, 2015)].

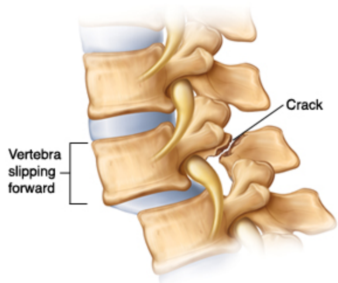


Figure 4.2. : Spondylolisthesis: slipping forward of a vertebra. [Adapted from FAIRVIEW (`http://www.fairview.org/`)].

Limiting loads in the inter-vertebral disc will limit injuries of the disc, such as for example inter-vertebral disc hernia resulting in compression of the spinal cord in the neutral arch, leading to pain.

By avoiding high loads in the inter-vertebral disc, the motion of the different vertebrae relative to each other is limited to protect the spinal cord: a spondylolisthesis (the sliding of one vertebra anteriorly (Figure 4.2)) will increase the shear load in the inter-vertebral disc and facets joints. At some point this load will not be supported anymore, and either facet fracture or inter-vertebral disc rupture will occur. This could lead to disc hernia and compression of the spinal cord.

One of the many roles of the spine is to protect the spinal cord, and this has been summarized by White *et al.* (White *et al.*, 1975) as they defined spinal stability "as the spine's ability under physiologic loads to limit patterns of displacement in order not to damage or irritate the spinal cord and nerve roots and to prevent incapacitating deformity or pain caused by structural changes" (cited from Izzo *et al.* (2013)).

In order to protect the spinal cord, spinal stability is governed by 3 different structures: the spine, the muscles and the central nervous system. The first one includes the bony structures of the spine (vertebrae), the inter-vertebral discs and the ligaments, and stabilizes the spine in a passive way. The muscles and tendons act as an active system and are activated by the central nervous system (CNS). The CNS is included in models via the strategy governing the model, while the spine and muscles are taken into account by their geometry.

The resulting loads in the inter-vertebral disc have been studied from direct measurement in the inter-vertebral disc with an inserted needle or instrumented inter-vertebral implant (Nachemson, 1975; Wilke *et al.*, 1999; Rohlmann *et al.*, 2014). Because these methods are invasive, biomechanical musculo-skeletal models have been developed to compute the inter-vertebral resulting loads and therefore identify critical situations that can lead to injury. These models need to include all the three structures involved in the regulation of spinal stability: the column, the muscles and tendons as well as the central nervous system.

There are, therefore, a lot of structures involved in the computation of inter-vertebral loads, as reported by Dreischarf *et al.*: "Since the number of unknown muscle forces exceeds that of available equilibrium equations, the problem is highly redundant and equilibrium equations cannot be solved deterministically" (Dreischarf *et al.*, 2016). This issue evoked by Winter *et al.* in 1990 (Winter *et al.*, 1990) is still relevant, and remains an issue as Dreischarf *et al.* mentioned recently (Dreischarf *et al.*, 2016). That is why different approaches can be found in the literature in order to reduce redundancy and solve the problem. Three types of models can be identified: the optimization driven models; the EMG driven models and hybrid models combining EMG and optimization approaches.

One common characteristic to all types of model is the computing of net reaction forces and moments on the inter-vertebral joint studied: it can be either calculated by inverse free body diagram from forceplate data (Figure 4.4) (tick in column "Use of forceplate" in Table 4.1), or from anthropometric data, estimating masses' distribution between segments (Dempster, 1955; DeLeva, 1996).

All these models aim to compute muscular forces to study muscular recruitment pattern (van Dieën *et al.*, 2003; Granata *et al.*, 2005), and resulting inter-vertebral loads for patients with different sagittal balances (Galbusera *et al.*, 2013).

# 4 - 1 Different types of biomechanical musculo-skeletal models

## 4 - 1.1 Optimization driven models

Optimization driven models aim to reduce the redundancy of the problem by modeling the central nervous system's strategy as a cost-function that should be optimized. Different cost functions have been proposed, the majority of them focusing on minimizing the muscular stress at different powers (Table 4.1). In these models, muscular forces are computed from the muscular area and muscular stress (force per unit of surface).

Models using optimization can include the 2D or 3D geometry of the spine and muscles such as finite element models, models derivated from OpenSim (Bruno *et al.*, 2015) or Anybody (AnyBody Technology A/S, Aalborg, Denmark) (Arshad *et al.*, 2016; Han *et al.*, 2013; Christophy *et al.*, 2012; Wong *et al.*, 2011).

They can also focus on a single-slice level with muscular geometry computed from the inter-vertebral joint center (Figures 4.3,4.4) (Table 4.1).

Multi-levels models, can compute the load at different inter-vertebral disc levels during dynamic tasks, while single-level musculo-skeletal models focus on quasi-static posture position and compute resulting loads in one inter-vertebral disc.

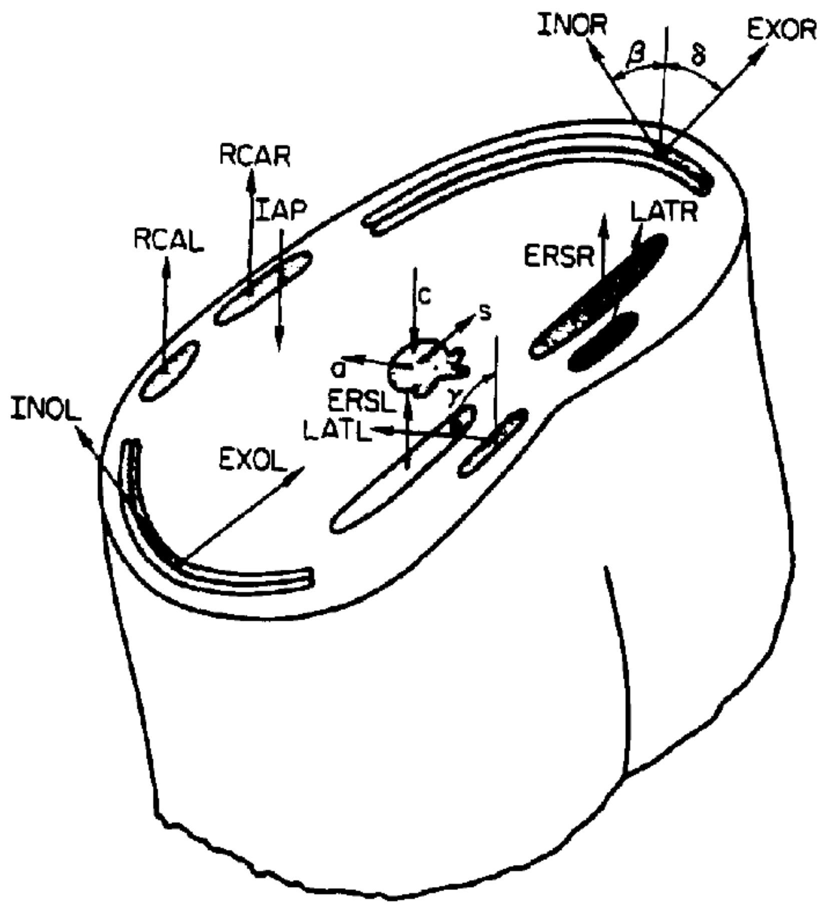


Figure 4.3. : Cross-sectional view of 10 trunk muscles and their moment arms used in the current model. Angles $\beta$, $\delta$, $\gamma$ are all assumed to be 45°. Reproduced from Schultz *et al.* (1982) [Figure and legend adapted from (Marras and Sommerich, 1991)].

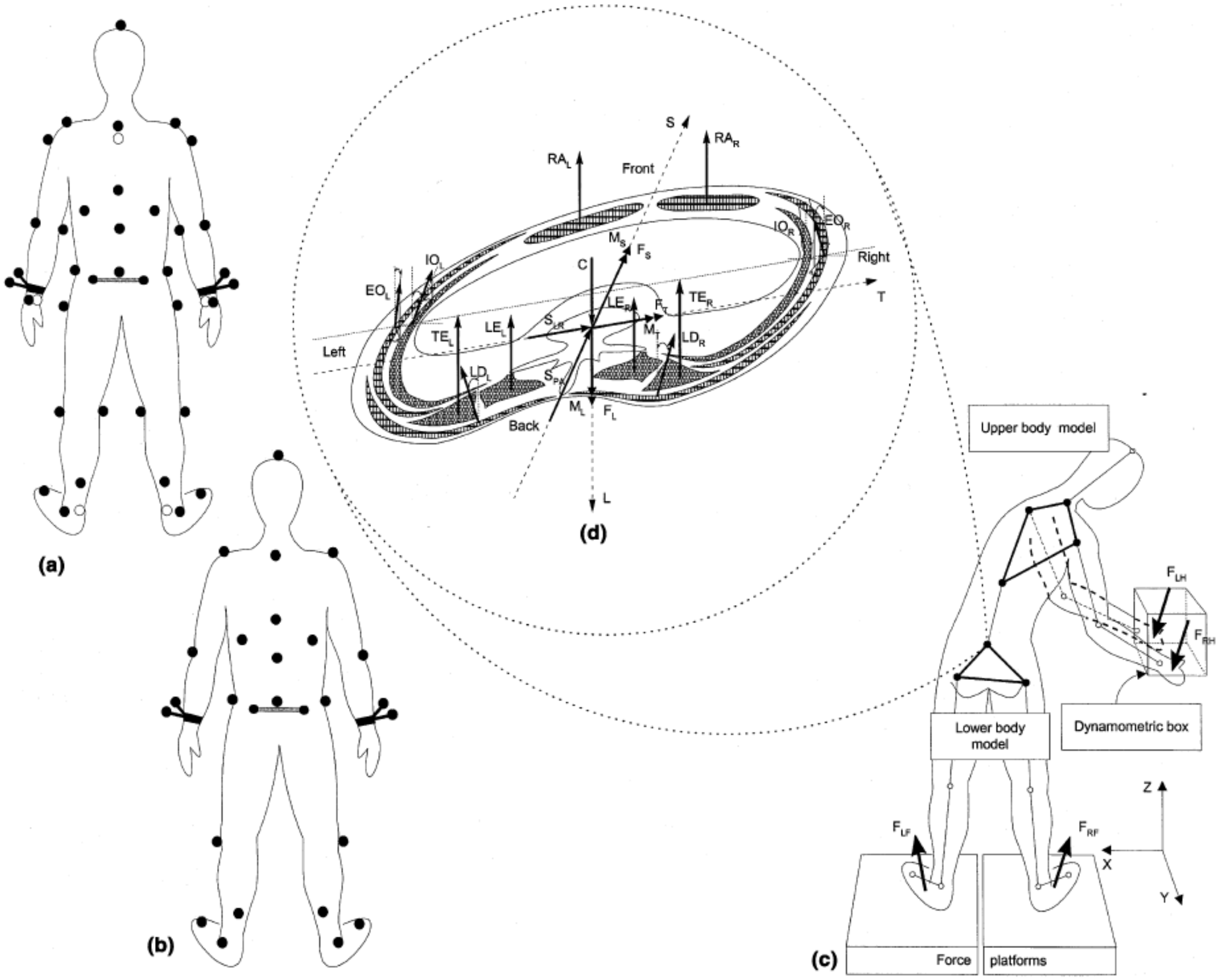


Figure 4.4. : Schematic representation of the procedure to construct the geometric, linked lumbar spine models. From the 44 surface markers used for anatomical calibration (a), 27 were tracked during task performance (b) to allow the reconstruction of a full body geometric model (14 segments) subdivided into *lower body* and *upper body* linked dynamic models (c) using respectively external forces at the feet ($F_{LF}$ and $F_{RF}$ measured by two force platforms) and the hands ($F_{LH}$ and $F_{RH}$ measured through a dynamometric box) as input. The lumbar spine model (d) was built from an imaginary plane cutting at the L5/S1 joint. [Figure and legend adapted from (Gagnon *et al.*, 2001)].

Multi-levels models are based on a scaled basic musculo-skeletal model: either from open-source models such as Open-Sim (Figure 4.5) or AnyBody (Figure 4.8); either from a previous literature study.

Another way to reduce significantly the number of unknowns to simplify the problem is to reduce the spine geometry to a 2D or 3D inverted pendulum (Figure 4.6) and to consider groups of muscles as a unique cable (Granata and Wilson, 2001; Granata and Orishimo, 2001): for example the erector spinae groups the multifidus and longissimus (Figure 4.6). By using optimization, a solution can be found. Even though the principal limitation of this model is its simplicity, it is still used and appreciated to get a roughly estimate of inter-vertebral load (particularly at the L5-S1 joint, supporting the whole upper body), in ergonomics for example (Essendrop *et al.*, 2002).

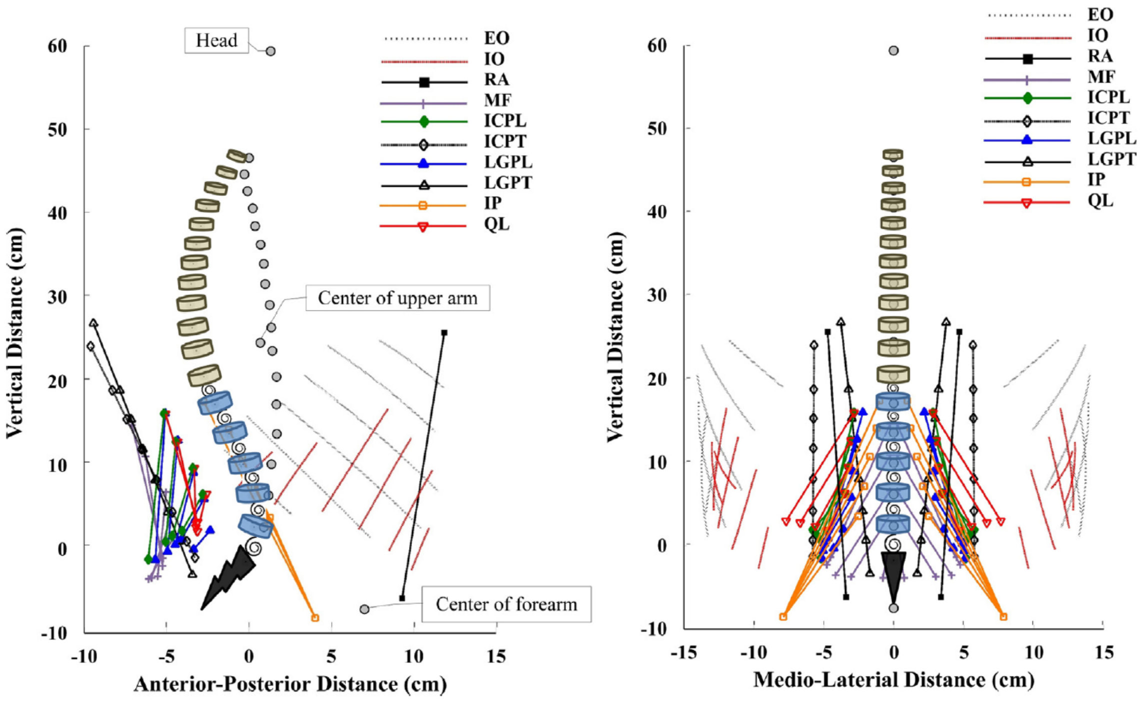


Figure 4.5. : The sagittally symmetric trunk model in the upright standing posture under gravity loading represented in both sagittal and coronal planes. 46 bilateral local muscles attached to lumbar vertebrae (ICPL: iliocostalis lumborum pars lumborum, LGPL: longissimus thoracis pars lumborum, MF: multifidus, QL: quadratus lumborum, and IP: iliopsoas) and 30 bilateral global muscles attached to thoracic spine and cage (global back muscles: ICPT: iliocostalis lumborum pars thoracic and LGPT: longissimus thoracis pars thoracic. Global abdominal muscles: IO: internal oblique, EO: external oblique, and RA: rectus abdominus) are considered (note that axes are not to the same scale). [Figure and legend adapted from (Hajihosseinali *et al.*, 2014)].

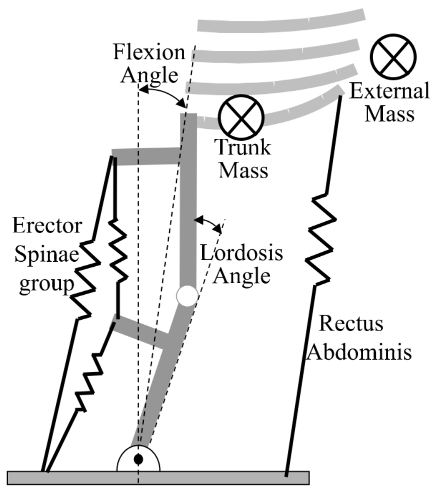


Figure 4.6. : Schematic representation of the stability model included a 3D inverted double-pendulum supported by 12 muscles (six bilateral muscle groups). Trunk mass and external load were applied at fixed vector locations relative to the superior surface of the upper vertebra. For clarity, the external oblique and internal oblique muscles have been omitted from the figure but were included in the computational analyses. [Figure and legend adapted from (Granata and Wilson, 2001)].

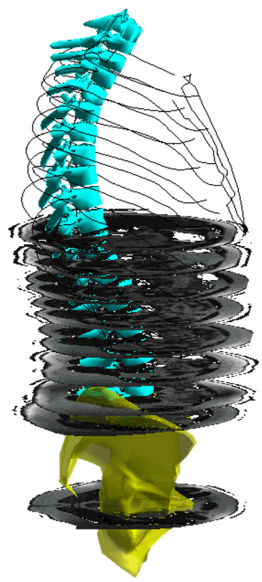

Figure 4.7. : Musculo-skeletal model with personalized 3D geometry of the spine, pelvis and muscles. Illustration of the positioning of the axial MRI slices within the 3D-reconstruction frame of the subject. [Figure and legend adapted from (Pomero, 2002)].

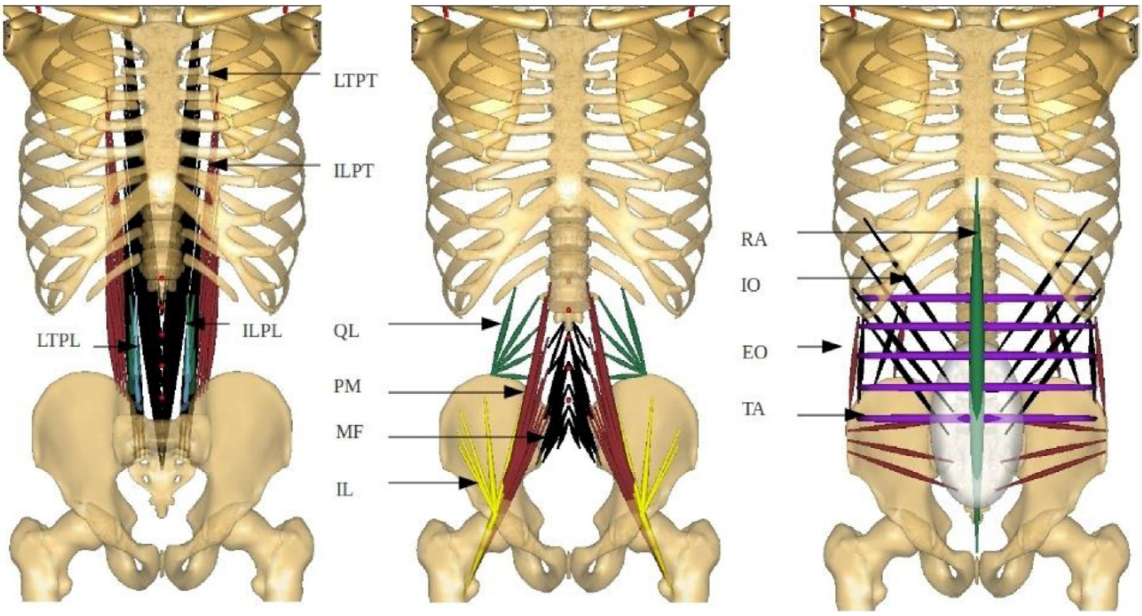


Figure 4.8. : Trunk musculature in AnyBody standing model. Global muscles (RA: rectus abdominis, IO: internal oblique, EO: external oblique, ILPT: iliocostalis lumborum pars thoracic, LTPT: longisimus thoracis par thoracic) and local muscles (ILPL: iliocostalis lumborum pars lumborum, LTPL: longisimus thoracis pars lumborum, PM: psoas major, IL: iliacus, MF: multifidus, QL: quadratus lumborum). [Figure and legend adapted from (Arshad *et al.*, 2016)].

A reported limitation of the optimization approach is the difficulty to predict antagonist co-activity (Stokes and Gardner-Morse, 2001; El Ouaaid *et al.*, 2013). As muscular contraction adds compression, the risk of this non-prediction of the antagonist activity, would be to under-estimate the resulting compression in the inter-vertebral joint. For example Cholewicki *et al.* reported, between optimization based and EMG-based predictions, an underestimation of the compression ranging from 23 to 43% (Cholewicki and McGill, 1996). However, different studies reported various strategies to solve this issue, in particular the addition of a lower limit for the muscle force when non activated (Hughes *et al.*, 1995), the design of a specific cost-function to differentiate between agonist and antagonist muscles (El Ouaaid *et al.*, 2013), the use of a quadratic cost-function (Modenese *et al.*, 2011) or the addition of stability requirements as equations (Brown and Potvin, 2005; Granata and Wilson, 2001; Stokes and Gardner-Morse, 2001; Hajihosseinali *et al.*, 2014).

Table 4.1 summarizes the principal studies reporting musculo-skeletal models using the optimization approach. Some things need to be highlighted from this table's reading. Firstly, the cost function used is, in most cases, related to the muscles' stress or force. Only few studies reported a cost function minimizing the resulting load in the inter-vertebral joint (Arjmand and Shirazi-Adl, 2006; Kiefer *et al.*, 1998; Christophy *et al.*, 2012; de Zee *et al.*, 2007; Pomero *et al.*, 2002).

Secondly, it is worth noting that most of the studies imported muscular geometry from cadaveric studies or medical images of few subjects, and sometimes scaled this geometry. In Table 4.1, study based on MRI or CT images (column "MRI or CT" in "Geometry of muscles" in the table), means that a generic model based on few people's images (MRI or CT scans) was used, except for two models (Pomero *et al.*, 2002; Han *et al.*, 1995). If Han *et al.* personalized muscular geometry from CT scans (Han *et al.*, 1995); Pomero *et al.* used as input MRI images at multiple level and in addition, personalized the posture from radiographs (Pomero *et al.*, 2002). Both studies reported a low number of subjects but provided the only results based on personalized geometry of the muscles only (Han *et al.*, 1995) and of muscles and posture for Pomero *et al.* (Pomero *et al.*, 2002). The only study, over all presented in Table 4.1, that included a large number of subjects was conducted by Han *et al.* in 2013. They did not include personalization for each subject, as a generic model was scaled for 7 different weights and 10 different heights to simulate 70 different virtual subjects (Han *et al.*, 2013).

| Author | Cost function for optimization | | | | | | Access to IV joint | | | | | | Geometry of muscles | | | | Number of subjects | Personalization | | |
|---|---|---|---|---|---|---|---|---|---|---|---|---|---|---|---|---|---|---|---|---|
| | muscular stress | muscular activation | Compression force | normalized forces | others load related | others muscle related | Anybody | Open Sim CT | Finite Element | Single-level: Slice | Use of forceplate | Others | Anybody | MRI or CT | Cadaveric study | Theoritical data | | Scaling | Published data | Personalization for each subject |
| **Arshad, …, Dreischarf, ... 2016** | | | | | | | X | | | | | | X | | | | 1 | X | | |
| **Shahvarpour, Shrazi-Adl, & Larivière 2016** | 3 | | | | | | | | X | | X | | | X | X | | 1 | | X | |
| **Bruno, Bouxein & Anderson 2015** | | 3 | | | | | | X | | | | | | X | | | 1 | X | | |
| **Hajihosseinali, …, Shirazi-Adl, … 2014** | 3 | | | | | | | | X | | | | | X | X | | 1 | X | | |
| **Han, Rohlamnn, ... 2013** | | X | | | | | X | | | | | | X | | | | 70 | X | | |
| **Christophy *et al.* 2012** | | | | X | | | X | | | | | | X | | X | | 1 | | X | |
| **Wong, …, DeZee, … 2011** | 3 | | | | | | X | | X | | | | | X | X | | 1 | X | | |
| | 2 | | | | | | | | | | | | | | | | | | | |
| **Arjmand, …, Shrazi-Adl, & Larivière 2010** | 3 | | | | | | | | X | | X | | | X | X | | 1 | | X | |
| **Arjmand, …, Shrazi-Adl, & Larivière 2009** | 3 | | | | | | | | X | | X | | | X | X | | 1 | | X | |
| **DeZee *et al.* 2007** | | | | X | | | X | | | | | | X | X | X | | 1 | X | | |
| **Arjmand & Shirazi-Adl 2006** | 3 | | | | | | | | X | | | | | X | X | | 1 | X | | |
| | 2 | | | | | | | | | | | | | | | | | | | |
| | | | | | | X | | | | | | | | | | | | | | |
| | | | | | | X | | | | | | | | | | | | | | |
| | X | | | | | | | | | | | | | | | | | | | |
| | | | | | | X | | | | | | | | | | | | | | |
| | | | X | | | | | | | | | | | | | | | | | |
| | | | | | | X | | | | | | | | | | | | | | |
| **VanDieen *et al.* 2005** | | 3 | | | | | | | | X | X | | | X | X | | 1 | | X | |
| **Pomero *et al.* 2002a** | Control loop approach | | | | | | | | | | | X | | X | | | 2 | | | X |
| **Shirazi-Adl *et al.* 2002** | | | | | X | X | | | X | | | | | X | X | | virtual loads | | | |
| **Gagnon, Larivière, ... 2001** | | | | | | X | | | | X | X | | | X | | X | 1 | | X | |
| **Granata *et al.* 2001** | 3 | | | | | | | | | | X | | | X | | | 1 | | X | |
| **VanDieen *et al.* 1999** | | | | | | | | | | X | | | | | X | | 1 | | X | |
| **Kiefer,Shirazi-Adl, … 1998** | | | X | | | | | | X | | | | | X | X | | 1 | X | | |
| **Cholewicki, McGill, ... 1995** | X | | X | | | | | | | | | X | | X | | | 1 | X | | |
| **Gardner-Morse & Stokes, … 1995** | | | | | X | | | | X | | | | | | X | | 1 | | X | |
| **Han *et al.* 1995** | 3 | | | | | | | | | X | X | | | X | | | 5 | | | X |
| **Stokes *et al.* 1995** | | | | | X | | | | X | | | | | | | | 1 | | X | |
| **Hugues, Chaffin, ... 1994** | 3 | | | | | | | | | X | | | | X | X | | 1 | X | | |
| | 2 | | | | | | | | | | | | | | | | | | | |
| | | | X | | | | | | | | | | | | | | | | | |
| | | | | | | X | | | | | | | | | | | | | | |
| **Bean, Chaffin, ... 1988** | | | | | | X | | | | | | X | | | | X | 1 | | X | |

Table 4.1. : Musculo-skeletal model using optimization approach. The column “Access to IV joint” refers to how is accessed the inter-vertebral joint under study: some studies use complete 2D or 3D geometry of the spine (column “AnyBody” and “Finite Element”); while others use only muscular geometry computed in a slice from the inter-vertebral joint center (column “Single-level: Slice”). The column “Use of forceplate” identifies studies for which a forceplate has been used to compute the external load at the inter-vertebral joint center.

### 4 - 1.2 EMG driven models

EMG-driven models (examples in Table 4.2) use as inputs the EMG signals recorded from the subjects during dynamic or quasi-static positions. One major difficulty with this type of model is the need to find an accurate relationship between the EMG signal and the force delivered by the muscle studied. In fact, the input in the model is the muscle force computed from the muscle's electrical activity recorded by EMG. Different relationships have been modeled in the literature (Anders *et al.*, 2008).

As detailed in section 3 - 1, one shortcoming of the EMG use is the need for careful placement of electrode to avoid cross-talk issue (Disselhorst-Klug *et al.*, 2009). Another shortcoming is the fact that it is limited to superficial muscles only. Deep muscles, such as the psoas for example, cannot be studied with the EMG. Those muscles are, therefore, either grouped with other muscles in the model or neglected. This simplification can however hide the true and complex recruitment pattern of the muscles.

All these limitations are well counter-balanced by the fact, that, up to now, only the EMG data can provide a validation set for these musculo-skeletal models. EMG is the only technique providing information of the in-vivo contraction of specific muscles over time, with different intensity. The muscular pattern given by the EMG can be either used as an input for EMG-driven models, or used for validation of the model outputs (whichever the type of the model is).

| Authors | Type | | Cost function for optimization | | Access to IV joint | | | | | Geometry of muscles | | | Team signing the study | | | | | | |
|---|---|---|---|---|---|---|---|---|---|---|---|---|---|---|---|---|---|---|---|
| | EMG driven | EMG optim | resultant moment | others muscle related | Anybody | Finite Element | Single-level: Slice | Use of forceplate | Others | MRI - CT | Cadaveric study | Given article | Marras | Shirazi-Adl | Granata | Vandien | Larivière | McGill | Other |
| **Dufour *et al.* 2013** | X | | | | | | | X | X | X | | | X | | | | | | |
| **Jia *et al.* 2011** | X | | | | X | | | X | | X | X | | | | | | | | X |
| **Gagnon *et al.* 2011** | | X | | X | | X | | X | | X | X | | | X | | | X | | |
| **Arjmand *et al.* 2009** | | X | X | | | | | X | | X | X | | | X | | | X | | |
| **Arjmand *et al.* 2010** | | X | X | | | | | X | | X | X | | | X | | | X | | |
| **Granata *et al.* 2005** | | X | X | | | | | X | | X | | | | | X | | | | |
| **VanDieen *et al.* 2005** | X | | | | | | X | X | | X | X | | | | | X | | | |
| **Gagnon *et al.* 2001** | X | | | | | | X | X | | X | | X | | | | | X | | |
| | | X | X | | | | X | X | | X | | X | | | | | X | | |
| **Cholewicki *et al.* 1996** | | X | X | | | | | | X | | X | | | | | | | X | |
| **Cholewicki *et al.* 1995** | X | | | | | | | | X | | X | | | | | | | X | |
| | | X | X | | | | | | X | | X | | | | | | | X | |
| **Granata *et al.* 1995** | X | | | | | | X | X | | | X | X | X | | X | | | | |
| **Marras *et al.* 1991** | X | | | | | | X | | | | | X | X | | | | | | |

Table 4.2. : Summary of published studies presenting musculo-skeletal models electromyography driven (EMG driven) or with a hybrid approach (combining EMG and optimization approaches). The column "Access to IV joint" refers to how is accessed the inter-vertebral joint under study: some studies use complete 2D or 3D geometry of the spine (column "AnyBody" and "Finite Element"); while others use only muscular geometry computed in a slice from the inter-vertebral joint center (column "Single-level: Slice"). The column "Use of forceplate" identifies studies for which a forceplate has been used to compute the external load at the inter-vertebral joint center.

A difference worth to highlight is the fact that the optimization approach satisfies the equilibrium of the system, while the EMG driven models do not. In order to compensate, hybrid models combining the two approaches have been proposed in the literature.

### 4 - 1.3 Hybrid models

Models combining muscular activity (EMG data) as input with optimization have been reported as hybrid models (Gagnon *et al.*, 2011; Arjmand *et al.*, 2010, 2009; Granata *et al.*, 2005). This type of models combines the advantage to use real data as input (EMG signals) and to satisfy equilibrium equations (use of optimization). However, the use of EMG can be difficult to implement, and interpret (uncertainty on the EMG signal-muscle force relationship).

Table 4.2 summarizes studies on EMG-driven models and hybrid models. Comparison between these models have been made in the literature suggesting that hybrid models are highly dependent on the optimization approach chosen and on the EMG signal-muscle force relationship (Mohammadi *et al.*, 2015; Dreischarf *et al.*, 2016).

### 4 - 1.4 Personalization of models

In the three different types of models, the question of the personalization of the posture and muscles is a concern. Few models attempted to import geometrical input from medical imaging for each subject, thus going towards a personalized geometry. However this method was never implemented on a large number of subjects, and has been mostly used to enhance a generic model by scaling or to refine the estimation of level arm of muscles for example (Hajihosseinali *et al.*, 2014; Arjmand *et al.*, 2010; Gagnon *et al.*, 2011; Han *et al.*, 1995).

Concerning the muscles' representation, these models represent muscles as a cable, not taking into account the 3D shape of muscles (Arjmand and Shirazi-Adl, 2006; de Zee *et al.*, 2007). Because muscular contraction is isovolumic; during contraction, the muscle will shorten and the maximal cross sectional area will increase. Two muscles side by side will therefore interact with each other, during contraction. This effect is neglected in such models as most of them model muscles as cables only. This issue remains unsolved in currently used models, by the complexity it introduces in the algorithm (additional contact forces required).

Only one published model, implemented patient specific 3D geometry of the skeleton and muscles from medical imaging (Figure 4.7) (Pomero *et al.*, 2002). This model uses a control loop approach to maintain the cubed inter-vertebral loads in the IV disc under defined thresholds. The assumed strategy of the central nervous system is to protect the inter-vertebral disc from high loads by activating specific muscles. 3D geometry of the spine was derivated from subject-specific 3D reconstructions based on bi-planar radiographs and muscles' geometry from Visible Human Project. This muscular generic model was then deformed to match muscles' insertions between 3D skeleton reconstruction and 3D reconstructions of muscles.

This personalization appears as a key issue in the observation and quantification of different postural alterations and static positions, on the muscular recruitment pattern and on the resulting inter-vertebral loads.

## 4 - 2 Summary of published musculo-skeletal models

Different approaches to model the spine stability and the resulting loads in the inter-vertebral discs have been reported with, for each type of model, limitations.

If the principal advantage of the EMG driven models is the true activation pattern from EMG signals, its application is limited to superficial muscles and requires appropriate signals force relationship.

Because the greatest advantage of EMG driven models is the link with in-vivo muscular activation, EMG has been widely used as a validation tool for optimization driven models. Optimization models have the advantage to model as many muscles as possible, but still personalization of these models is rarely made, resulting in only global estimation of spinal loads. A global shortcoming that applies on all these models with exception of two (Hajihosseinali *et al.*, 2015; Han *et al.*, 2013) is the non-modification of the anatomy when studying specific postures such as flexed positions or lateral bending. Similarly, studies focusing on postural alterations in patients, only changed net reaction forces and moments applied on the inter-vertebral discs, but did not modify accordingly the muscular geometry (except when input is the personalized 3D geometry of spine and muscles (Pomero *et al.*, 2002)).

Only one “optimization driven” model (more precisely a control-loop based model) to this date reported the use of 3D personalized geometry of the spine, and muscles from medical images (Pomero *et al.*, 2002). If this model considers only quasi-static positions, it has the great advantage to study the effect of an altered posture and altered muscles (alteration not modeled but implemented from 3D reconstructions of EOS and MRI images). The cost function used in this model is quite different from most other cost functions used, as the model minimizes the inter-vertebral loads by activating agonist and antagonist muscles. The central nervous system strategy modeled here is to protect the inter-vertebral disc, even if this leads to maximal recruitment of muscles and therefore high compression loads. With these advantages and limitations, this model has been chosen as the best to study patient-specific alteration of the posture by using personalized input data from medical images.

# CONCLUSION

This chapter summarized the different approaches used in the literature to study balance alterations occurring during aging, from postural alignment changes to muscular changes. The study of the complex interaction between both the skeletal and muscular systems can be realized with a biomechanical musculo-skeletal model.

Firstly, from the literature review emerged a strong need for 3D, head to feet, analysis of the postural alignment, especially including the head to quantify its relative position to other segments and its position's evolution over aging. Such analysis can be performed using bi-planar simultaneous X-rays and 3D reconstruction algorithms developed accordingly.

Secondly, even if the importance of muscles has been well reported in the literature, few studies reported 3D geometry of muscles which seems to be essential to quantify changes occurring during aging, due to compensatory mechanisms, or pathological evolution.

Thirdly, if biomechanical models underwent a significant development over the last years, to our knowledge, only one published model allowed personalized 3D geometry of the bones and muscles as inputs (Pomero *et al.*, 2004). Because balance alterations over aging are subject-specific, this model appears of primary importance when quantifying more precisely the effect of aging on the lumbar spine, discs and muscles.

In light of this state-of-the-art, the objective of this PhD was to answer three questions:

- How does postural alignment change with aging?
- How do the muscular system's characteristics change with aging?
- What is the impact of the combined alteration of both postural alignment and muscular system, on the biomechanics of the spine?

Three distinctive parts will answer each one of these three questions. Firstly, postural alignment analysis on two groups of different ages will be investigated.

Secondly, MRI axial slices will be studied in order to characterize the muscular system of young asymptomatic subjects. These reference values will be used to quantify muscular degeneration occurring in elders with spinal deformities.

The third part will present the musculo-skeletal model chosen to further investigate interactions between muscles' activation and postural alignment in volunteers, and patients of various ages.

# Part B

# Age-related postural alignment changes

# INTRODUCTION

The first part of this PhD focuses on postural alignment of asymptomatic adults. Analysis was carried out based on EOS images and aimed to investigate age-related changes in terms of posture.

Firstly, a population reference of young asymptomatic adults (i.e. 18-40 years old) has been studied in order to report reference values of postural alignment. Volunteers' radiographies were retrospectively included from an extensed existing database in the Institute built from previous studies. This work has been accepted for publication in the *European Spine Journal* (Amabile *et al.*, 2016c).

Secondly, a population of older asymptomatic adults (i.e. greater than 50 years old) has been studied following the same protocol. Subjects' radiographies were retrospectively included from a research cohort previsouly recruited in the Hospital of Bordeaux by Professor Jean-Charles Le Huec. Results were compared to those of the reference population and differences were investigated in order to identify compensatory mechanisms associated with aging.

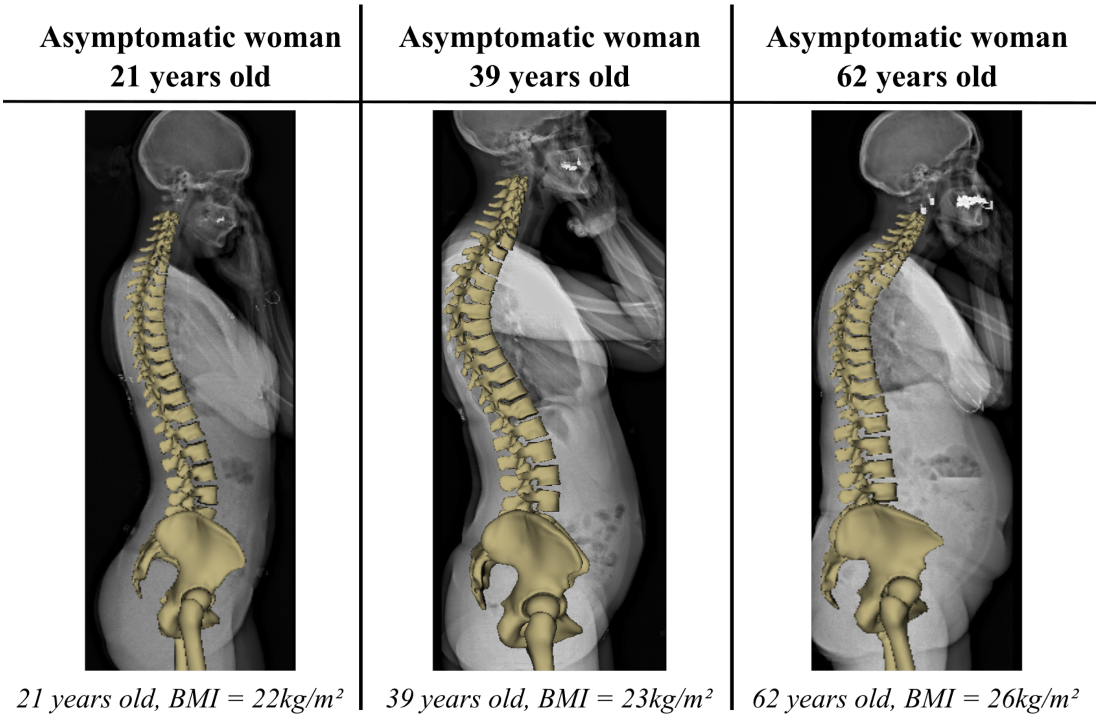


Figure 4.9. : Sagittal view of the 3D skeleton of women of different ages.

# CHAPTER 5

# POSTURAL ALIGNMENT OF YOUNG ASYMPTOMATIC ADULTS

This chapter was accepted for publication in European Spine Journal in 2016 (Amabile *et al.*, 2016c), under the title:

### A NEW QUASI-INVARIANT PARAMETER CHARACTERIZING THE POSTURAL ALIGNMENT OF YOUNG ASYMPTOMATIC ADULTS.

**Authors:**

Celia Amabile[a, b], Hélène Pillet[a], Virginie Lafage[b], Cédric Barrey[c], Jean-Marc Vital[d], Wafa Skalli[a].

**Affiliations:**

[a] Arts et Métiers ParisTech, LBM/Institut de Biomécanique Humaine Georges Charpak, Paris, France;
[b] Spine Service, Hospital for Special Surgery, New York, NY 10021, USA;
[c] Department of Neurosurgery and Spine Surgery, P. Wertheimer Hospital, Hospices Civils de Lyon, University Claude Bernard Lyon 1, Lyon, France;
[d] Department of Orthopaedics and Spine Surgery, University Hospital of Bordeaux, Bordeaux, France.

**Conflict of interest statement:**
The authors have no conflicts of interest to declare.

**Acknowledgments:**
Authors thank the ParisTech BiomecAM chair program on subject-specific musculo-skeletal modeling, and in particular COVEA and Société Générale.

# 5 - 1 Abstract

## 5 - 1.1 Purpose

Our study aims to describe the postural alignment of young asymptomatic subjects from head to feet from bi-planar standing full-body X-rays, providing database to compare to aging adults. Novelty resides in the inclusion of the head and lower limbs in the erected posture's analysis.

## 5 - 1.2 Methods

For 69 young asymptomatic subjects (18 to 40 years old) 3D reconstructions of the head, spine, pelvis and lower limbs segments were performed from bi-planar full-body X-rays. Usual studied spinal, pelvic and lower limbs' parameters were computed in 3D, sagittal and frontal planes of the patient. Relationships between these parameters were investigated. Inclinations of different lines were studied to characterize the erected posture.

## 5 - 1.3 Results

Values found for spinal curvatures, pelvic parameters and lower limbs geometrical parameters agreed with the literature: thoracic kyphosis, lumbar lordosis, pelvic incidence, pelvic tilt and sagittal vertical axis were respectively in average of 26.9° (SD: 7.2°), 30.5° (SD: 7.5°), 51.0° (SD: 9.4°), 11.1° (SD: 5.6°) and -8.9mm (SD: 21.6mm). The angle between the vertical and the line joining the most superior point of dentiform apophyse of C2 (OD) and the center of the bi-coxofemoral axis (HA) was the less variable one (SD: 1.6°).

## 5 - 1.4 Conclusions

This study on 3D postural alignment reports the geometry of the spine, pelvis and lower limbs, of the young asymptomatic adult. The less variable angle is the one of the line OD-HA with the vertical, highlighting the vertical alignment of the head above the pelvis. This study provides a basis for future comparisons when investigating aging populations.


**Keywords:** Skeleton's postural alignment; 3D; Asymptomatic young adults; Head to feet; Spinal alignment.

## 5 - 2 Introduction

Dubousset first introduced the concept of the “conus of economy” describing the economic standing posture (Dubousset, 1994). Failure to maintain the center of gravity in this conus would trigger compensatory mechanisms to restore a stable posture. Postural alignment is maintained in order to stay in this “conus of economy”: alignment of all segments above the pelvis (torso and head) is needed to provide the best posture at the least energy expense. Particularly, keeping the head aligned with the whole body is important to provide horizontal gaze, but also accurate sensory inputs (i.e. inner ear). Adding that the head weight is approximately 4 to 5kg (Vital and Senegas, 1986), its global position in space appears of prior importance when considering posture and balance.

However, during aging, degradation of the musculo-skeletal system, due to disc degeneration, osteoporosis and loss of muscular volume, contributes to the degradation of postural alignment, leading to potential severe osteoarticular damages (Barrey *et al.*, 2013). In addition, postural malalignment increases the risk of loss of balance and fall that are associated to societal costs (for example, US$ 17,483 mean cost of hospitalization for fall-related injury in the US (Roudsari *et al.*, 2005)). In order to maintain this postural alignment, different strategies, involving the whole body from head to feet, are followed depending on the subject’s functional capabilities. In an effort to maintain the alignment of different body’s segments (head, torso, pelvis, lower limbs) objective, young subjects have the capacity to regulate their spino-pelvic alignment by fine-tuning the curvature of their spine and adjusting the orientation of their pelvis. In comparison, it has been demonstrated that older subjects recruit preferably mechanisms of compensation at the pelvis and lower limbs levels (Diebo *et al.*, 2015).

Evaluation of the posture has been made in the past by studying the spine and pelvis on sagittal X-rays (Boulay *et al.*, 2006; Legaye *et al.*, 1998; Rajnics *et al.*, 2001; Vialle *et al.*, 2005). To our knowledge, only two studies reported the alignment of the head with the rest of the body, stating that the inclination of the head compared to the pelvis could be a good indication of the postural trouble (Steffen *et al.*, 2010; Sugrue *et al.*, 2013) while others only focused on the alignment of C7 with the rest of the spine and pelvis (Kim *et al.*, 2014; Le Huec *et al.*, 2014). Previous clinical studies included the lower limbs, massively in 2D (not relevant for torsion values for example) (Seber *et al.*, 2000). However reference values, in 2D and 3D, of the complete global alignment of the normal young adult from a whole body (head to feet) exam are not yet available.

The aim of the current study was to study the postural alignment of young asymptomatic subjects including head, spine, pelvis and lower limbs, in 2D and 3D. Possible invariant parameters of the young adults’ posture were investigated.

## 5 - 3 Materials and Methods

### 5 - 3.1 Volunteers and data selection

69 volunteers (32 males and 37 females) were retrospectively included in the study: bi-planar X-rays radiographs were obtained between February 2007 and July 2014 after approval by the Ethics Committee (Comité de Protection des Personnes CPP N°06036) and written informed consent. Bi-planar X-rays were obtained with the EOS system, a low dose system allowing acquiring simultaneously radiographs in the sagittal and coronal planes of the patient (with two sources at 90°), from head to feet (Dubousset *et al.*, 2010).

Inclusion of the EOS radiographs in the study required total visibility of the lower limbs bones and vertebrae on both views. Among exclusion criteria were previous musculo-skeletal surgery, previous surgery or pathology concerning the visual and/or the hearing system(s). Patients were asked to stand up in the standardized free standing position, adapted from Faro *et al.* (Faro *et al.*, 2004), with the hands resting on the mandibles (SRS modified free standing position) and with shifted feet positioned as described by Chaïbi et al (Chaibi *et al.*, 2012) (Figure 5.1).

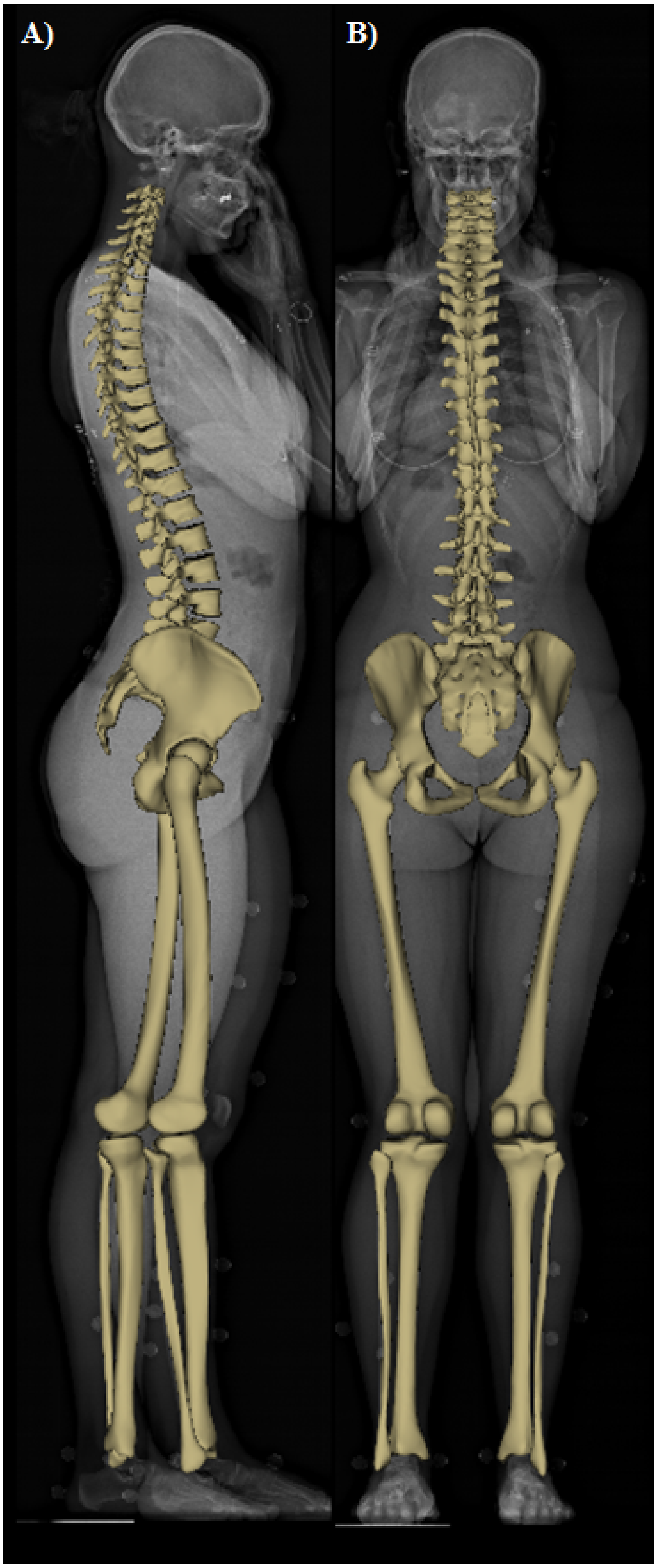


Figure 5.1. : Bi-planar radiographs with 3D model of the spine (C3 to L5), pelvis and lower limbs. **A)** Sagittal view. **B)** Coronal view.

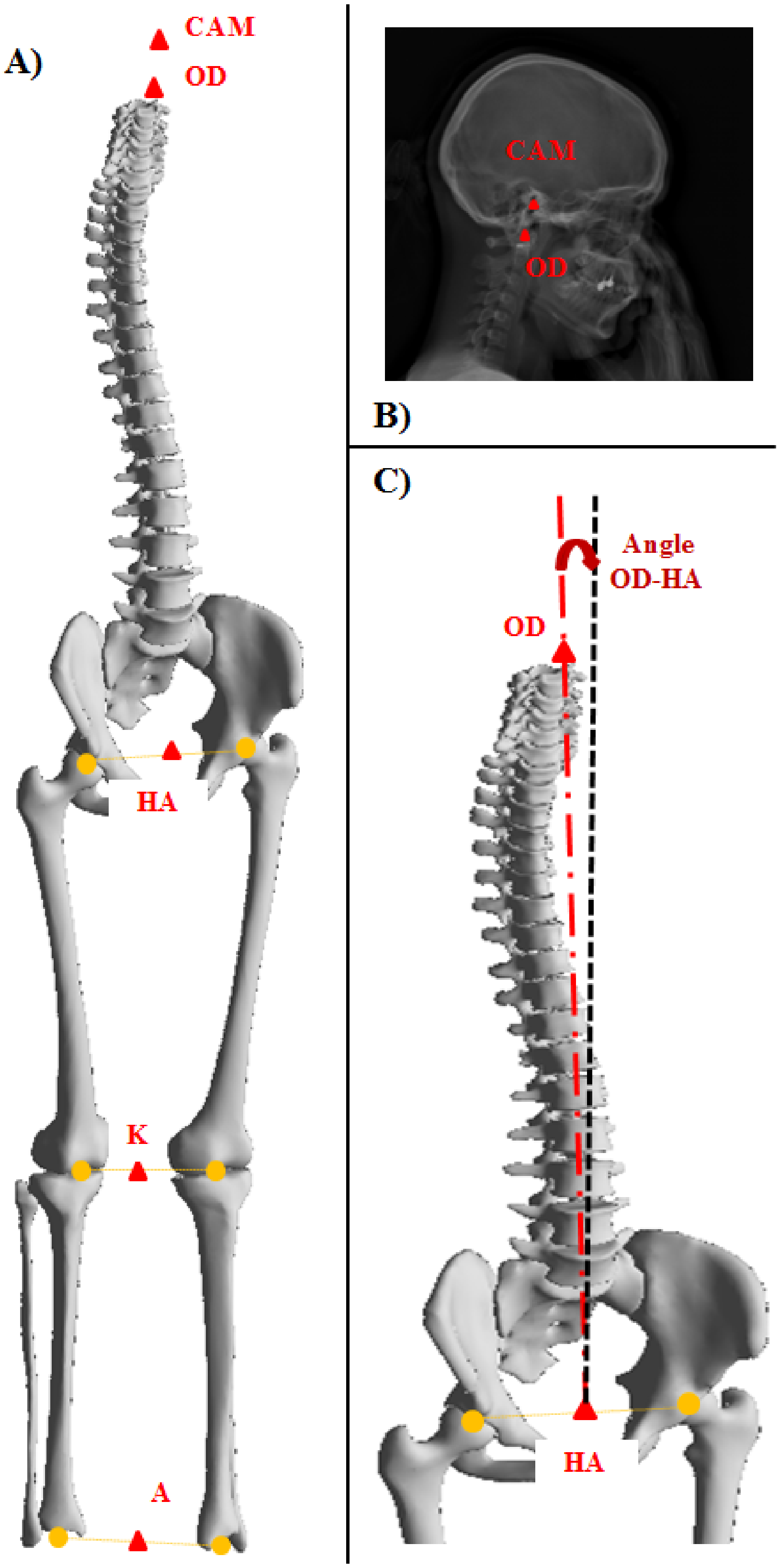


Figure 5.2. : **A)** 3D model of the spine (C3 to L5), pelvis and lower limbs: Identification of the center of the acoustic meati (CAM), the most superior point of dentiform apophyse of C2 (OD), the center of the bi-coxofemoral axis (HA), the middle of both knees points (K), and the middle of both ankles (A). **B)** Detailed identification of CAM and OD points on the sagittal radiography. **C)** Example of OD-HA parameter: angle with the vertical of the line joining the points OD and HA.

## 5 - 3.2 Imaging Data processing

From bi-planar X-rays, a 3D patient-specific model including the spine (from C3 to L5, with addition of the most superior point of dentiform apophyse of C2 (OD)), the pelvis, and the lower limbs; was obtained using validated reconstructions techniques (Chaibi *et al.*, 2012; Humbert *et al.*, 2009a; Mitton *et al.*, 2006; Quijano *et al.*, 2013) (Figure 5.2). In addition, as described by Steffen *et al.* (Steffen *et al.*, 2010), when visible, two stereo-corresponding points localizing the acoustic meati were digitized to each reconstruction to compute their center (CAM) (Figure 5.2).

## 5 - 3.3 Studied parameters

All the parameters were calculated in the anatomo-gravital frame, which is the patient frame: the frontal plane is the vertical plane going through both acetabulum centers', transversal and sagittal planes are orthogonal to the frontal plane. The origin of the frame is the center of the bi-coxofemoral segment (point named HA). Parameters' definitions are detailed in Tables 5.2, 5.3 and 5.4.

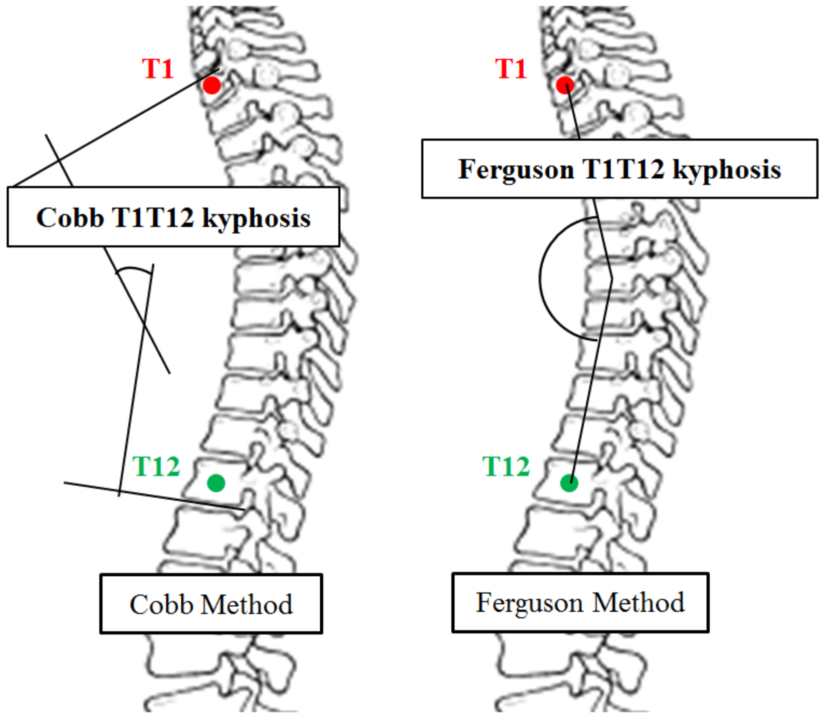


Figure 5.3. : Differences between Cobb Method and Ferguson Method to calculate spinal curvatures (example of kyphosis T1T12).

Pelvic (pelvic incidence, pelvic tilt and sacral slope) and lower limbs parameters were calculated from 3D reconstruction. Spinal curvatures (cervical lordosis, thoracic kyphosis and lumbar lordosis) were calculated using both Cobb and Ferguson methods (Figure 5.3).
Angles of the vertical with specific lines going through various landmarks (Figure 5.2) were also calculated.

Two global alignment lines were defined, searching for the most invariant one among subjects (defined as the one with the smallest standard deviation). The first line was defined as the line that best fits (in the least square sense), the following anatomical landmarks: middle of the centers of acoustic meati (CAM), the most superior point of dentiform apophyse of C2 (OD), all the vertebral bodies' center from C3 to L5, center of the sacral plate (S1) and middle of the centers of each acetabulum (HA). The second line was defined similarly without including the CAM point in the landmarks considered.

As proposed by Steffen *et al.* (Steffen *et al.*, 2010), offsets of the following points were calculated: CAM, T1, T4, T9, L3, and S1. We also considered the most superior point of dentiform apophyse of C2 (OD), the center of the knees (K) as the middle point of right and left middle points between condyles' centers and tibial plates' centers. The center of ankles (A) was also considered as the middle point of right and left centers of bimalleolar axis. Figure 5.2 presents all the points considered for offsets analysis. The offsets were calculated, in 3D, and in both directions of the transversal plane (postero-anterior and medio-lateral), as the distance between these points and the vertical going through HA.

The reliability of each point was already described elsewhere (Humbert *et al.*, 2009a) except for the OD location. For this parameter, 2 operators digitized the points two times for 12 patients on two distinct set of radiographs for each (48 repetitions per operator): 95% confidence interval was respectively of 2.0mm for X, antero-posterior direction; of 1.2mm for Y, medio-lateral direction; and of 2.2mm for Z, superior direction.

### 5 - 3.4 Statistical analysis

A paired-sample t-test was run on lower limbs' parameters to find if there was any statistical difference between right and left sides (McDonald, 2009). A Lilliefors normality test (Lilliefors, 1967) was run on all parameters. Correlations were searched for using pairwise Spearman correlations (significance level was set at 0.05).

## 5 - 4 Results

### 5 - 4.1 Description of the sample

Mean age was 26.3 years old (standard deviation (SD): 4.7 years old) (Table 5.1). The acoustic meati were not visible on 8 EOS exams out of the 69. Over all parameters used to study correlations, 13 were found to not be drawn from a normal distribution (Tables 5.2 and 5.3). As these parameters' distributions were found, by the operators, to be close to a bell-shape, means and SD were reported for all parameters (Tables 5.2, 5.3 and 5.4).

| | * Age (years) | * BMI (kg/m$^2$) |
|---|---|---|
| **Mean** | 26.3 | 22.4 |
| **1 * Standard deviation** | 4.7 | 3.1 |
| **Min** | 20.1 | 16.6 |
| **Max** | 39.7 | 33.2 |

Table 5.1. Demographic data of the volunteers who participated in the study. * means that the parameter was not found to be drawn from a normal distribution.

In average, pelvic incidence, pelvic tilt, and sacral slope were respectively of 51.0° (SD: 9.4°), 11.1° (SD: 5.6°) and 40.5° (SD: 8.7°). As for the spine curvatures, the 3D T1T12 thoracic kyphosis was in average of 26.9° (SD: 7.2°) versus 30.5° (SD: 7.5°) for the L1S1 lumbar lordosis.

| Abbreviation | Name | Mean (1*SD) |
|---|---|---|
| **PI** | Pelvic Incidence (°) | 51.0 (9.4) |
| **SS** | Sacral Slope (°) | 40.5 (8.7) |
| **PT** | Pelvic Tilt (°) | 11.1 (5.6) |
| $\mathbf{S1_{ov}}$ | Overhang of S1 (postero-anterior distance between S1 and HA) (mm) | 19.6 (10.2) |
| **SVA** | Sagittal Vertical Axis (postero-anterior distance between C7 and $^{\text{post-sup}}$S1) (mm) | - 8.9 (21.6) |
| **TPA** | T1 Pelvic Angle (angle between line T1 to HA and line S1 to HA) (°) | 5.3 (5.7) |
| *** PR** | Pelvic Rotation (Angle between the frontal plane of the acquisition system and the frontal plane of the anatomo-gravital frame) (°) | 3.2 (2.5) |
| **PO** | Pelvic Obliquity (Angle between the bi-coxofemoral axis and its projection on the horizontal plane) (°) | - 0.3 (2.5) |
| ˆ $\mathbf{Cov_{ext}}$ | External coverture angle (°) | R: 29.6 (5.6) |
| | | L: 29.8 (5.3) |
| ˆ **Cov%** | Acetabular coverage (%) (Humbert *et al.*, 2008) | R: 46.5 (3.5) |
| | | L: 46.0 (3.5) |
| ˆ $\mathbf{Incl_{acetab}}$ | Acetabular Inclination (°) | R: 34.1 (3.4) |
| | | L: 33.8 (2.9) |
| ˆ $\mathbf{Abd_{acetab}}$ | Acetabular Abduction (°) | R: 57.4 (4.4) |
| | | L: 57.0 (3.9) |
| $\mathbf{Antev_{acetab}}$ | Acetabular Anteversion (°) | R: 15.5 (3.5) |
| | | L: 16.7 (3.6) |

Table 5.2. Reference values for pelvic parameters: Mean (SD). S1: Centre of sacral plate; HA: middle of the centers of each acetabulum; C7: Center of vertebral body of C7; T1: Center of vertebral body of T1; $^{\text{post-sup}}$S1: Most posterior point of the superior plate of S1. R (L) is for the Right (Left) side. * means that the parameter was not found to be drawn from a normal distribution. ˆ means that for the correlation study, the values were averaged between right and left sides (as no statistical differences were reported by the paired t-test ran).

| Abbreviation | Name | Mean (1*SD) | |
|---|---|---|---|
| *** HKS** | Hip-Knee centers-femoral shaft angle (°) | R: 5.5 (1.3) | L: 5.2 (1.5) |
| **ˆ TMA** | Tibial mechanical angle (°) | R: 87.2 (2.2) | L: 87.4 (2.0) |
| **ˆ FMA** | Femoral mechanical angle (°) | R: 92.9 (1.7) | L: 92.6 (2.2) |
| **ˆ FT** | Femoral torsion (°) | R: 12.9 (9.6) | L: 13.8 (10.8) |
| **ˆ TT** | Tibial torsion (°) | R: 37.1 (6.0) | L: 35.9 (6.7) |
| $\mathbf{L_F}$ | Femoral length (mm) | R: 426.4 (24.6) | L: 427.5 (24.4) |
| **ˆ** $\mathbf{L_T}$ | Tibial length (mm) | R: 368.0 (21.9) | L: 368.3 (22.0) |
| $\mathbf{L_{Tot}}$ | Lower limb length (mm) | R: 798.9 (45.6) | L: 800.2 (45.9) |
| ***ˆ FTR** | Femoro-tibial Rotation (°) | R: 6.3 (3.9) | L: 6.6 (5.7) |
| ***ˆ FTMA** | Femoro-tibial Mechanical Angle (°) (also called HKA) | R: 174.7 (3.1) | L: 174.9 (2.6) |
| **ˆ FNSA** | Femoral Neck Shaft Angle (°) | R: 128.3 (4.4) | L: 128.0 (3.7) |
| **ˆ FO** | Femoral Offset (3D distance between the center of femoral head and the proximal diaphyseal axis) (mm) | R: 40.1 (5.5) | L: 40.6 (4.2) |
| *** FI** | Femoral inclination (angle with vertical of femoral mechanical axis) (°) | 3D: R: 6.3 (3.3) | 3D: L: 8.3 (3.5) |
| | | Fr: R: - 0.7 (1.9) | Fr: L: 0.6 (1.9) |
| | | Sag: R: 5.7 (3.8) | Sag: L: 8.0 (3.6) |
| **TI** | Tibial inclination (angle with vertical of tibial mechanical axis) (°) | 3D: R: 4.5 (2.0) | 3D: L: 5.0 (2.7) |
| | | Fr: R: - 2.5 (2.2) | Fr: L: 2.3 (2.0) |
| | | Sag: R: 1.4 (3.4) | Sag: L: 3.6 (3.3) |

Table 5.3. Reference values for lower limbs parameters: Mean (SD). R (L) is for the Right (Left) side. * means that the parameter was not found to be drawn from a normal distribution. ˆ means that for the correlation study, the values were averaged between right and left sides (as no statistical differences were reported by the paired t-test ran). 3D means 3D value; Sag means value for the sagittal plane; Fr means value for the frontal plane.

| Abbreviation | Description of the line | 3D | Frontal Plane | Sagittal Plane |
|---|---|---|---|---|
| * $\mathbf{L_{C3\text{-}C7}}$ | C3-C7 Lordosis (°) # 6.2 (11.6) | 8.6 (4.5) | 2.6 (5.2) | - 0.9 (8.5) |
| * $\mathbf{K_{T1\text{-}T12}}$ | T1-T12 Kyphosis (°) # 49.7 (13.1) | 26.9 (7.2) | - 1.1 (5.4) | 26.7 (7.3) |
| * $\mathbf{K_{T4\text{-}T12}}$ | T4-T12 Lordosis (°) # 35.6 (11.6) | 19.2 (6.1) | 1.5 (5.4) | 18.6 (6.6) |
| * $\mathbf{L_{L1\text{-}L5}}$ | L1-L5 Lordosis (°) # - 47.0 (12.0) | 21.8 (5.9) | -3.5 (6.6) | - 20.7 (5.6) |
| * $\mathbf{L_{L1\text{-}S1}}$ | L1-S1 Lordosis (°) # - 58.26 (12.9) | 30.5 (7.5) | 0.4 (10.1) | - 30.1 (7.6) |
| $\mathbf{A_{Pelvis\text{-}Fem}}$ | Angle between the bi-coxofemoral axis and the bi-condylar axis. (°) | R: 16.4 (8.4)<br>L: 15.4 (7.7) | R: 38.3 (175.0)<br>L: 74.2 (162.8) | / |
| **Incl_1** | Global Inclination: Angle between the vertical and the line that best fits[a]: CAM, OD, all the vertebral body' centers from C3 to L5, and S1. (°) | 3.1 (1.9) | - 0.5 (1.1) | - 2.3 (2.6) |
| **Incl_2** | Global Inclination: Angle between the vertical and the line that best fits[a]: OD, all the vertebral body' centers from C3 to L5, and S1. (°) | 3.5 (2.1) | - 0.5 (1.3) | - 2.8 (2.7) |
| *** CAM-HA** | Angle between the vertical and the line that connects CAM to HA. (°) | 2.9 (1.7) | - 0.3 (1.0) | - 2.4 (2.1) |
| **OD-HA** | Angle between the vertical and the line that connects OD to HA. (°) | 2.9 (1.6) | - 0.4 (1.2) | - 2.3 (2.0) |
| **C7-HA** | Angle between the vertical and the line that connects C7 to HA. (°) | 4.3 (1.9) | - 0.2 (1.4) | - 4.0 (2.1) |
| **CAM-C7** | Angle between the vertical and the line that connects CAM to C7. (°) | 6.8 (4.2) | - 1.0 (2.7) | 4.1 (6.3) |
| *** OD-C7** | Angle between the vertical and the line that connects OD to C7. (°) | 8.0 (4.5) | - 1.7 (3.4) | 5.6 (6.3) |
| **T1-HA** | Angle between the vertical and the line that connects T1 to HA. (°) | 5.5 (2.0) | - 0.1 (1.4) | - 5.3 (2.1) |
| **T9-HA** | Angle between the vertical and the line that connects T9 to HA. (°) | 10.6 (2.8) | 0.1 (1.7) | - 10.4 (2.8) |
| **T1-S1** | Angle between the vertical and the line that connects T1 to S1. (°) | 4.5 (2.2) | - 0.2 (1.4) | - 4.1 (2.7) |

Table 5.4. Reference values for spinal parameters and inclinations in 3D/sagittal plane/frontal plane: Mean (SD). [a] means in the least square sense; CAM: middle of the points describing the acoustic meati; C7 / HA / S1: See legend of Table 5.2. For the spinal curvatures, the values in the second column following the # symbol are the values computed with the Cobb Method. R (L) is for the Right (Left) side. * means that the parameter was not found to be drawn from a normal distribution.

### 5 - 4.2 Analysis of the least variant parameter(s)

The inclinations, with the vertical, of the line joining CAM to HA and of the line joining OD to HA had the lowest variation with a SD respectively of 1.7° and of 1.6° and were the closest to the vertical: mean inclination of 2.9° for both. In comparison, means (SD) of C7-HA, T1-HA and T9-HA were respectively of 4.3° (1.9°); 5.5° (2.0°) and 10.6° (2.8°).

As for the lines that could possibly represent the global inclination of the spine, the less variable inclinations between subjects were, when using the two following combinations of points for the calculation of the least-squared line: 1) CAM, OD, centers of C3 to L5 vertebral bodies (line called Incl_1), and S1; 2) OD, centers of C3 to L5 vertebral bodies, and S1 (line called Incl_2). Values are reported in Table 5.4.
When considering the offsets between HA and different plumblines (Figure 5.4) dropped from the specific anatomical landmarks (CAM, OD, T1, T4, T9, L3, S1, K, A), the average distances ranged from 70.3 to 10.7mm posterior to HA (SDmax=24.1mm) and from 5.1 medial to 2.3mm lateral to HA (SDmax=14.2mm). The distance in the transverse plane ranged from 17.9 to 71.5mm (SDmax=21.2mm). The center of the sacral plate S1, versus HA, presented the lowest variable offset across subjects, in the transverse plane (mean: 20.9mm; SD: 9.4mm). On average, the knee's center and ankles' center were posterior to HA in average less than 6cm (SD<2cm) and were lateral to HA in average less than 1cm (SD<1.5cm).

### 5 - 4.3 Statistical analysis

As, the paired-sample t-tests revealed that specific parameters (Tables 5.2 and 5.3) presented no statistical differences between both sides, the value kept for analysis was the mean of the right and left values. Cobb versus Ferguson relationship for spinal curvatures was strong ($R^2 = 0.96$) and significant (p-value<0.05) (Equation 5.1).

$$Cobb_{sag} = 1.90 * Ferguson_{sag} - 2.34 \tag{5.1}$$

The pairwise correlations found to be significant (p-value<0.05) are the following ones:

- L1S1 lordosis with sacral slope ($R^2$=0.87),
- L1S1 lordosis with pelvic incidence ($R^2$=0.62),
- L1S1 lordosis with thoracic kyphosis (T4T12: $R^2$=0.48; T1T12: $R^2$=0.36);
- overhang of S1 with pelvic tilt ($R^2$=0.97).

No significant correlation was found between spinal and lower limbs parameters.

## 5 - 5 Discussion

Erected posture of 69 young asymptomatic adults was described from head to feet in 3D and 2D. If, compensatory mechanisms of the pelvis and lower limbs have been documented in the literature, few have been reported for the cervical level: studying the skeleton postural alignment from head to feet allows for a complete view of the possible compensatory mechanisms. For example, Sugrue *et al.* is one study of the few to include points at the head level (cranial center of mass of the head and C2) (Sugrue *et al.*, 2013). Overall, our findings match the ones previously reported in the literature, with new information regarding the global postural alignment from head to feet, and in particular the position of the head relative to the pelvis.

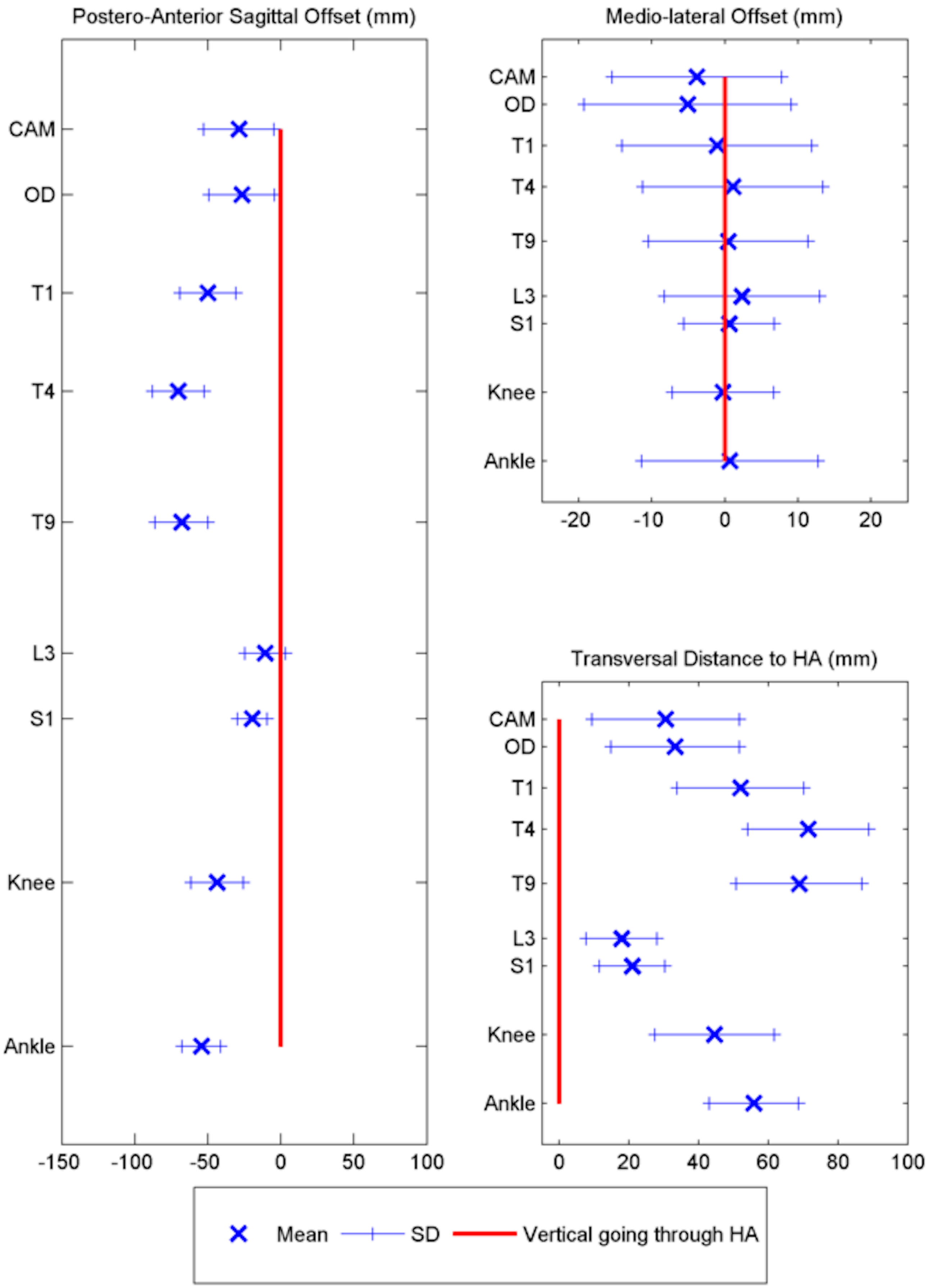


Figure 5.4. : Offsets from the vertical going through the center of the bi-coxofemoral axis (HA) (mean +/- 1*SD).

### 5 - 5.1 Spinal and pelvic parameters

Agreement with the literature was found for the hip joints' parameters (Cov%, $Abd_{acetab}$, $Antev_{acetab}$) (Humbert *et al.*, 2008; Seber *et al.*, 2000), and for spinal and pelvic parameters (Boulay *et al.*, 2006; Chaibi *et al.*, 2012; Legaye *et al.*, 1998; Rajnics *et al.*, 2001; Schwab *et al.*, 2006; Vaz *et al.*, 2002; Vialle *et al.*, 2005), particularly with the studies conducted by Vialle et al (Vialle *et al.*, 2005) and by Schwab et al (Schwab *et al.*, 2006). The correlations found between spinal curvatures and pelvic parameters are similar to the correlations reported in the literature (Boulay *et al.*, 2006; Legaye *et al.*, 1998; Rajnics *et al.*, 2001; Vaz *et al.*, 2002; Vialle *et al.*, 2005). In particular, Vialle *et al.* found a strong correlation between the L1L5 lordosis and the sacral slope ($R^2$=0.76) and a strong correlation between the L1L5 lordosis and the pelvic incidence ($R^2$=0.68) (Vialle *et al.*, 2005). These correlations highlight the influence of the morphology of the pelvis on the lumbar spinal curvature. As for Cobb versus Ferguson values, the relationship found is consistent with the literature (Stokes *et al.*, 1993).

### 5 - 5.2 Lower limbs parameters

For the lower limbs geometrical parameters (HKS, ˆ TMA, ˆ FMA, ˆ FT, ˆ TT, LF, ˆ LT, LTot, ˆ FTR, ˆ FTMA, ˆ FNSA, FO), the values found match values reported in studies using computer tomography in the supine position and in studies evaluating lower limbs' geometry on 3D model built from bi-planar radiographs (Chaibi *et al.*, 2012; Kolta *et al.*, 2005).

### 5 - 5.3 Global alignment parameters

The inclination of the line joining CAM and HA and the line joining OD and HA are the less variable among subjects (respectively SD=1.7° and SD=1.6°). The line with the OD point is less variable between subjects and more robust when it comes to digitizing the point on the radiographs.

Few studies reported values for inclinations: values similar to those reported in the literature were found for inclinations of the line going through T9 and HA (T9-HA); of the line going through T1 and S1 (T1-S1); of the line going through T1 and HA (T1-HA) and of the least square line going through OD, all the vertebral bodies from C3 to L5 and S1 (Incl_2) (Duval-Beaupère and Legaye, 2004; Rajnics *et al.*, 2001). Another alignment parameter is the T1 pelvic alignment (TPA) reflecting the inclination of the trunk and pelvic retroversion (accounting for both SVA and PT). Ryan *et al.* reported a value of TPA less than 15.9° for patients with adult spinal deformities well aligned (Ryan *et al.*, 2014), proposing a surgical target of 10° for TPA. For young asymptomatic adults (well aligned), mean TPA is 5.3° (SD=5.7°), which means that 66% of the population ranges between -0.4° and 11.0°. Some have subnormal values, between mean-2*SD and mean-1*SD (respectively between mean+1*SD and mean+2*SD) which can reach -6.1° (respectively 16.7°). This shows that the target set by Ryan *et al.* (Ryan *et al.*, 2014) could be adjusted to identify abnormalities.

For the global inclinations, the least squared line going through the points CAM, OD, centers of vertebral bodies from C3 to L5 and S1 (Incl_1) in Table 5.4 presented an inclination of 3.1° in average (SD: 1.9°) versus 3.5° in average (SD: 2.1°) for the second least-squared line (Incl_2), going through OD, centers of vertebral bodies from C3 to L5 and S1. The line used in Incl_1 is more vertical and less variable between subjects but the weaker digitization of CAM makes it less robust. The C7 point can be useful when CAM and/or OD are not visible on the radiographs. The C7-HA inclination is slightly greater than CAM-HA (4.3° versus 2.9°) and only very slightly more variable (SD: 1.9° versus 1.7°). It will be interesting to investigate whether this parameter is more variable in older subjects.

The CAM-HA or OD-HA parameter will be useful to assess the global alignment taking into account the cervical part of the spine contrary to the SVA and C7-HA parameter. Depending on the use and interpretation, studies could use CAM, OD or C7 points to characterize global alignment with CAM-HA, OD-HA, SVA and C7-HA that appear as complementary parameters. In addition, it will be interesting to further investigate changes for pathological and aging population, in the newly described parameters (CAM-HA and OD-HA) compared to SVA and C7-HA.

CAM and OD points were chosen to account for the head position. Previous studies have focused on other specific points to quantify alignment of the head with the spine and pelvis: such as the sella turcica (Le Huec *et al.*, 2014), McGregor line (Le Huec *et al.*, 2014), or cranial center of mass (as the midpoint of the nasion-inion line) (Sugrue *et al.*, 2013). Commonly to the current study, all considered points supposed to be close to the true center of mass of the head in order to quantify its alignment compared to the pelvis. However, in analyzing radiographs, a reliable and accurate but also easy-to-implement method is needed to identify points of interest (particularly when working in a clinical environment). That is why in this study, only points directly identifiable on the 3D model of the spine were considered: for the head, this included only the points CAM and OD. It can be noted that all these studies including this one, concluded on the importance of the position of the head above the pelvis in the global postural alignment (Le Huec *et al.*, 2014; Sugrue *et al.*, 2013).

Variability between subjects (SD) was comparable between the angles, measured in the sagittal planes: CAM-HA (SD=2.1°), OD-HA (SD=2.0°) and C7-HA (SD=2.1°). Inter-subject variability was greater for the angle corresponding to SVA: angle with the vertical of the line joining through C7 and $^{\text{post-sup}}$S1 (SD=2.8°). This suggests that the use of the point $^{\text{post-sup}}$S1 accounts for the inclination of the pelvis as well in this angle, when compared to the angle C7-HA using the point HA. Comparison of the angles CAM-HA, OD-HA and C7-HA highlighted that, for asymptomatic volunteers, these data variability are similar. It would be particularly interesting to assess changes occurring during aging and/or pathological conditions.

### 5 - 5.4 Offsets

Studies' reported offsets used the gravity line as the reference line (Gangnet *et al.*, 2003; Schwab *et al.*, 2006; Steffen *et al.*, 2010), using a forceplate simultaneously to the X-ray acquisition. Experimental setup did not provide forceplate data, thus we decided to use the vertical going through the center of the bi-coxofemoral axis (HA) as the reference line and not the heels as done in Schwab *et al.* (Schwab *et al.*, 2006) as, here, the feet's positions were not found to be consistent enough between all subjects to be used as a reference line. Despite these differences, our values are of the same order of magnitude as the literature's (Gangnet *et al.*, 2003; Schwab *et al.*, 2006; Steffen *et al.*, 2010). In addition, it can be noted that offsets of both knees' and ankles' centers were found to be relatively close to HA in the transverse plane (less than 6cm): this provides a baseline for comparison with older subjects.

### 5 - 5.5 Limitations

One limitation is the non-uniform age distribution: more subjects between 30 – 40 years old might highlight some correlations between all the parameters that were hidden here. Another limitation resides in the position of the subject in the X-ray cabin. Particularly, the position of the hands on the mandibles might have affected the volunteer's posture by shifting backwards the upper body in order to make room for the arms flexed. In addition, the shift between the feet must be controlled to be consistent between subjects. Monitoring more precisely the patient's position would lead to more reliable results characteristics of the true subject's erected posture.

## 5 - 6 Conclusion

In conclusion, a description of the postural alignment in 3D, and in sagittal and frontal planes of the young healthy adult has been reported. As hypothesized, the head is, for each subject, placed above the pelvis (line CAM-HA little variable). In this control group, the spine is globally vertical as the parameter Incl_1 and Incl_2 are close to 0°. We described the postural alignment and the geometry of the following segments: spine, pelvis, lower limbs. This study on young healthy adults (18 - 40 years old) would allow future comparisons for older population.

# CHAPTER 6

# POSTURAL ALIGNMENT OF ASYMPTOMATIC ELDERS

The previous chapter reported reference values for postural alignment of asymptomatic adults younger than 40 years old. An invariant has been identified as the position of the head above the pelvis. In order to investigate how postural alignment changes with aging, this chapter presents a similar study conducted on older adults. Particularly the position of the head relative to the pelvis is investigated in order to evaluate if this invariant was maintained in the aging population. Compensatory mechanisms were also investigated.
This chapter was submitted for publication in European Spine Journal in 2016, under the title:

## Invariance of head-pelvis alignment and compensatory mechanisms for asymptomatic adults older than 49 years old.


**Authors:**

Celia Amabile[a], Jean-Charles LeHuec[b], Wafa Skalli[a].

**Affiliations:**

[a] Arts et Métiers ParisTech, LBM/Institut de Biomécanique Humaine Georges Charpak, Paris, France;
[b] Université Bordeaux, Orthospine Department 2, 146 rue Leo Saignat, 33076, Bordeaux Cedex, France;



**Conflict of interest statement:**
The authors have no conflicts of interest to declare.

**Acknowledgments:**
Authors thank the ParisTech BiomecAM chair program on subject-specific musculo-skeletal modeling, and in particular COVEA and Société Générale.

## 6 - 1 Abstract


### 6 - 1.1 Purpose

The aim was to quantify the postural alignment of asymptomatic elderly, in comparison to a reference population, searching for possible invariants and compensatory mechanisms.

### 6 - 1.2 Methods

41 volunteers (49-76 years old) underwent bi-planar X-rays with 3D reconstructions of the spine and pelvis. Alignment parameters were compared to those of a reference group of asymptomatic subjects younger than 40 years old, with a particular focus on center of acoustic meati (CAM) and odontoid (OD) with regard to hip axis (HA). Possible markers of compensation were also investigated.

### 6 - 1.3 Results

No significant difference among groups appeared for CAM-HA and OD-HA parameters. 24% of elders had an abnormally high SVA value and 27% an abnormal global spine inclination. Increased pelvic tilt and cervical lordosis allowed maintaining the head above the pelvis.

### 6 - 1.4 Conclusions

CAM-HA and OD-HA appeared quasi-invariant even in asymptomatic elderly. Some subjects exhibited alteration of spine alignment, compensated at the pelvis and cervical regions.


**Keywords:** Postural alignment; 3D reconstruction; Asymptomatic elderly.

## 6 - 2 Introduction

In posture and balance analysis, the head is of primary importance as major receptors such as eyes and inner ear are located in the head. Its mass of 4 to 5 kg (Vital and Senegas, 1986) is supported by a flexible rod, the cervical spine, followed by the thoraco-lumbar construct. The last segment of the upper body is the pelvis supporting the upper body weight. Alignment of these three segments needs to be reached to provide an economic balance (Dubousset, 1994). However, inclusion of the head segment in radiographic analyses is not yet the standard of care, probably due to the size of the X-ray cassettes. Recent development of head to feet low dose bi-planar X-Rays system permitted visualization of the head segment for postural alignment studies (Dubousset *et al.*, 2010).

A recent study reported the relative position of the head with respect of the pelvis by introducing the center of acoustic meati point (CAM), the upper extremity of C2 dentiform apophyse (OD) and the center of hip axis (HA) (Amabile *et al.*, 2016c). Angles with the vertical, of both lines joining CAM to HA (CAM-HA) and OD to HA (OD-HA) were found invariant, confirming the intuitive alignment of the head above the pelvis for asymptomatic adults younger than 40 years old (Amabile *et al.*, 2016c). With aging, various spine disorders may appear with an impact on spinal alignment and global balance. Alignment of the thorax has been widely investigated on patients, with various parameters, such as the sagittal vertical axis (SVA) and the ratio of C7 plumbline over the sacro-femoral distance (Barrey *et al.*, 2011). In addition, pelvic parameters detailed by Duval-Beaupère allowed for characterization of pelvic morphology (pelvic incidence), retroversion (pelvic tilt) and inclination (sacral slope) (Duval-Beaupère *et al.*, 1992). However aging of asymptomatic subjects is much less investigated (El Fegoun *et al.*, 2005; Vialle *et al.*, 2005; Schwab *et al.*, 2006; Lafage *et al.*, 2008; Kim *et al.*, 2014), particularly when including the head. Few studies reported, for asymptomatic adults, alignment of the head with the spine and/or pelvis (Gangnet *et al.*, 2003; Le Huec *et al.*, 2014; Steffen *et al.*, 2010; Iyer *et al.*, 2016). Out of these studies, very few reported the effect of aging on the alignment of the head and the pelvis (Le Huec *et al.*, 2014; Iyer *et al.*, 2016).

The objective of this study was to describe a group of asymptomatic elderly in comparison to a younger population of asymptomatic adults younger than 40 years old, with a specific focus on investigating the alignment of the head above the pelvis and the compensatory mechanisms recruited to overcome spine alignment alteration.

## 6 - 3 Materials and Methods

### 6 - 3.1 Subjects and data selection

Volunteers older than 49 years old were extracted from separate studies and were retrospectively included in the study: bi-planar X-rays radiographs were obtained between July 2011 and April 2013 after approval by the Ethics Committee (Comité de Protection des Personnes CPP N°2010/113 (32 subjects) and CPP N°06036 (12 subjects)) and written informed consent. Bi-planar X-rays were obtained with the EOS system, a low dose system permitting the simultaneous head to feet acquisition of sagittal and coronal X-rays (Dubousset *et al.*, 2010).

Inclusion criteria were any subject presenting an Oswestry Disability index (ODI) score lower than 20% (Fairbank *et al.*, 1980) and an EVA score (visual analog scale) lower than 2 in assessing the back pain (including neck pain) (Million *et al.*, 1982). Among exclusion criteria were the presence of low back pain or regular low back pain, lower limbs pathology that could affect the spine, previous surgery on lower limbs, pelvis or spine.

Subjects were asked to stand up in the standardized free standing position, adapted from Faro *et al.* (Faro *et al.*, 2004), with hands resting on the mandibles (SRS modified free standing position) and with shifted feet (Chaibi *et al.*, 2012). A medical practitioner familiar to EOS radiographs and not involved in the study blindly reviewed all subjects' radiographs to label and rejected radiographs of subjects with incorrect posture (3 on 44). A total of 41 volunteers (24 males and 17 females) with a mean age of 57.9 years old (SD 7.9) were included (Table 6.1).

| | **Elderly (N=41)** | | **Young adults (N=69)** | |
|---|---|---|---|---|
| | *** Age (years)** | **BMI ($kg/m^2$)** | *** Age (years)** | *** BMI ($kg/m^2$)** |
| **Mean** | 57.9 | 25.6 | 26.3 | 22.4 |
| **1 * Standard deviation** | 7.9 | 4.1 | 4.7 | 3.1 |
| **Min** | 49.0 | 18.6 | 20.1 | 16.6 |
| **Max** | 76.0 | 39.2 | 39.7 | 33.2 |

Table 6.1. Demographic data of the volunteers who participated in the study (N=41), and of the reference population younger than 40 years old (N=69) (Amabile *et al.*, 2016c). * means that the parameter was not found to be drawn from a normal distribution.

### 6 - 3.2 Imaging Data processing

From bi-planar X-rays, a 3D patient-specific model including the spine (from C3 to L5, with addition of the most superior point of dentiform apophyse of C2 (OD)), the pelvis, and the lower limbs was obtained using validated reconstructions techniques (Chaibi *et al.*, 2012; Mitton *et al.*, 2006; Humbert *et al.*, 2009a; Quijano *et al.*, 2013). In addition, two stereo-corresponding points localizing the acoustic meati were digitized on each reconstruction to compute their center (CAM) (Steffen *et al.*, 2010).

### 6 - 3.3 Studied parameters

All parameters were calculated in the anatomo-gravital frame (Amabile *et al.*, 2016c). Spinal curvatures (cervical curvature, thoracic kyphosis and lumbar lordosis) and pelvic parameters (pelvic incidence, pelvic tilt and sacral slope, overhang S1) were calculated from 3D reconstruction. Were also calculated the sagittal vertical axis (SVA), the T1-pelvic angle and angles with the vertical of different lines: CAM-HA, OD-HA, C7-HA and T9-HA.

Spinal inclination was computed as the angle with the vertical of the line that best fits the following anatomical landmarks: middle of the centers of acoustic meati (CAM), the most superior point of dentiform apophyse of C2 (OD), all the vertebral bodies' center from C3 to L5, center of the sacral plate (S1) and middle of the centers of each acetabulum (HA). This method of best fitting line is a robust way to compute the global inclination of the spine. C7PL/SFD, introduced by Barrey *et al.* (Barrey *et al.*, 2011), is the ratio between the distance C7 to $^{\text{post-sup}}$S1 and the distance HA to $^{\text{post-sup}}$S1.

A Lilliefors normality test (Lilliefors, 1967) was run on all parameters. Correlations with age were investigated, using pairwise Spearman correlations (significance level was set at 0.05).

### 6 - 3.4 Differences between young reference population and elders

Comparison was made with a young reference group of 69 asymptomatic volunteers younger than 40 years old (Amabile *et al.*, 2016c). For each parameter, the mean M and standard deviation SD of the young reference group were used to class elderly as **normal** if within M +/− 1*SD range, **subnormal** *high* between M+1*SD and M+2*SD (*low* between M-1*SD and M-2*SD) or **abnormal** when out of the range M +/− 2*SD (*high* or *low*). Pelvic tilt was defined as normal, subnormal or abnormal depending on the position of the couple of points (pelvic tilt; pelvic incidence) on Figure 6.1: the figure was plotted with help of the relation published by Vialle *et al.* (Vialle *et al.*, 2005).

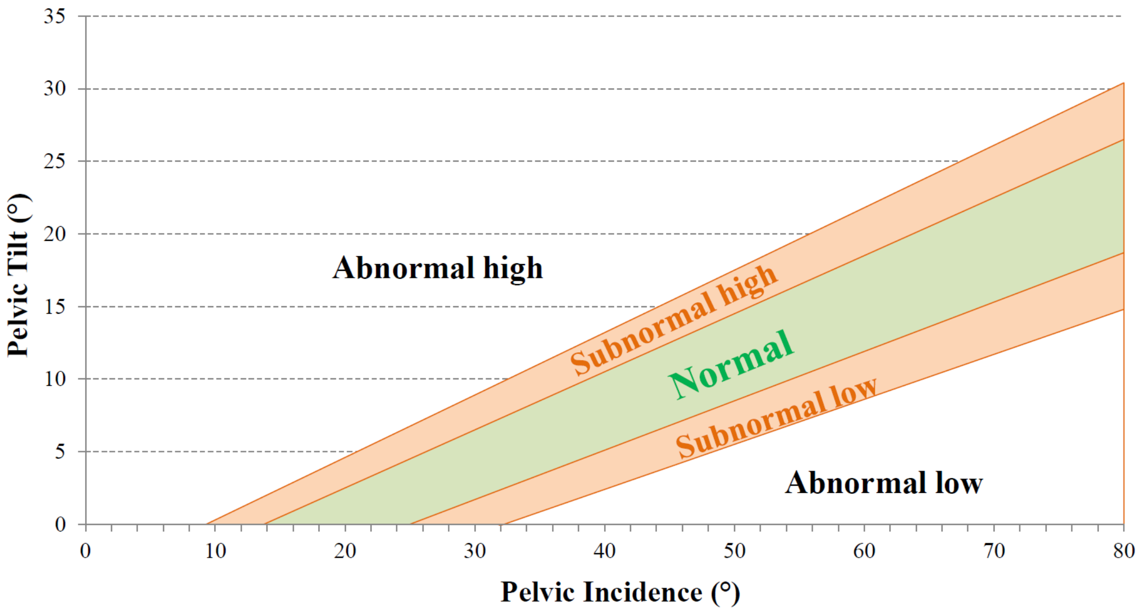


Figure 6.1. : Normality corridor for the pelvic tilt (PT) based on its relation with pelvic incidence (PI) provided by Vialle *et al.* (Vialle *et al.*, 2005): PT = 0.37 (+/-0.03)*PI -7(+/-1.5).

### 6 - 3.5 Spinal alignment alteration

As the Sagittal Vertical Axis parameter (SVA: postero-anterior distance between C7 and the most postero-superior point of S1) is widely used to characterize the postural alignment from radiographs, subjects were grouped according to their SVA value when compared to the reference values given by asymptomatic adults younger than 40 years old. Group 1 included subjects with a SVA value identified as normal, subnormal low or abnormal low. Group 2 included subjects with a SVA value identified as subnormal high or abnormal high.

### 6 - 3.6 Compensatory mechanisms

For those subjects who had abnormal pelvic tilt (value smaller than Mean-2*SD or larger than Mean+*2SD, as defined by the Figure 6.1), compensatory mechanisms were investigated with a particular focus on global spinal inclination and cervical lordosis. More specifically, the non-compensated alignment was modeled as explained in Figure 6.2: for each of these subjects, the theoretical pelvic tilt was computed from pelvic incidence using the relation provided in Vialle *et al.* (2005). The difference between the measured pelvic tilt and the theoretical one defined the compensation retroversion, then a rotation of the pelvis and spine was performed around the hip axis to simulate an alignment without such compensation retroversion.

The cervical compensation lordosis was computed as the difference between the measured cervical lordosis to the reference value provided by the asymptomatic adults younger than 40 years old (6°) (Amabile *et al.*, 2016c). A second rotation of the cervical spine around C7 was then applied to suppress the cervical lordosis compensation. The new simulated alignment, without pelvic retroversion or cervical hyperlordosis, allowed for the computation of a new theoretical non-compensated CAM-HA (respectively OD-HA), named CAM-$\mathrm{HA_{NC}}$ (resp. OD-$\mathrm{HA_{NC}}$) (Figure 6.2).

## 6 - 4 Results

### 6 - 4.1 Sample description

Over all parameters used to study correlations, only 2 were found to not be drawn from a normal distribution (CAM-HA ($p=0.04$) and Age ($p=0$)). Means and SD were reported for all parameters (Figures 6.3 & 6.4).

The inclinations with the vertical, of the line joining CAM to HA and of the line joining OD to HA had the lowest variation (SD of 2° for both) and were the closest to the vertical: mean inclination of 3° for both. The spinal inclination presented a similar mean (3°) and SD (2°). In comparison, means (SD) of C7-HA and T9-HA were respectively of 4° (2°) and 12° (3°). Following the different types of alignment defined by Roussouly (Roussouly *et al.*, 2005), 27% of the elderly presented a type 1 or 2 alignment, 59% presented a type 3 alignment and 15% presented a type 4 alignment.

Parameters significantly correlated with age with $R > 0.3$, are: sagittal vertical axis ($R=0.48$), spinal inclination ($R=0.46$), T1-pelvic angle ($R=0.44$), pelvic tilt ($R=0.35$), overhang S1 ($R = -0.35$) and cervical curvature ($R = -0.42$).

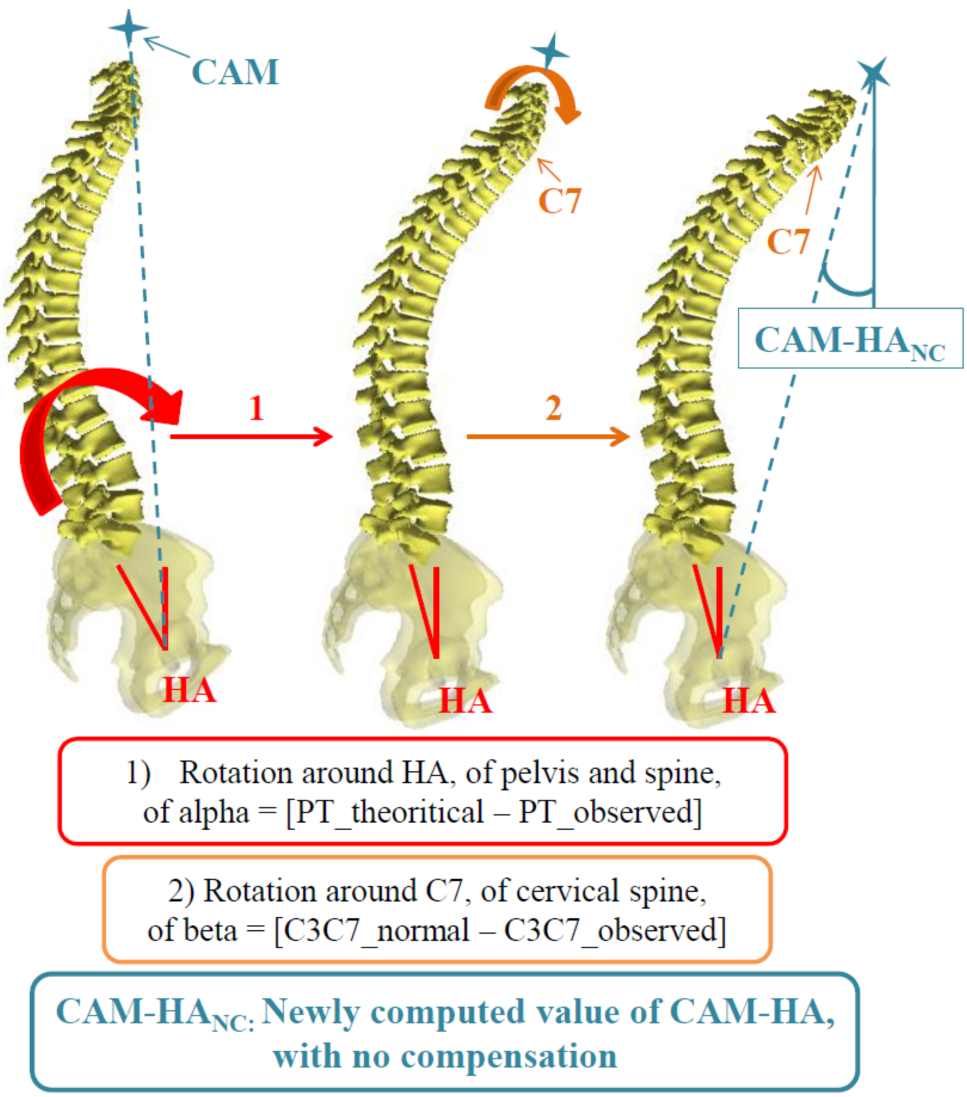


Figure 6.2. : Schematic representation of the computation of the non-compensated posture represented in Figure 6.6. PT_theoretical refers to the theoretical value of PT computed from PI as given by Vialle *et al.* (Vialle *et al.*, 2005). C3C7_normal refers to the mean value reported for asymptomatic adults younger than 40 years old which is 6° (Amabile *et al.*, 2016c). Similarly to CAM-HA$_{NC}$, a newly inclination OD-HA$_{NC}$ was computed following the same steps.

### 6 - 4.2 Differences with asymptomatic subjects younger than 40 years old

Comparison between Elderly and Young groups is presented in Figures 6.3 & 6.4. In the following Young group (respectively Elderly group) refers to asymptomatic adults younger than 40 years old (respectively older than 49 years old). No statistical differences were found between groups regarding CAM-HA and OD-HA angles. Significant differences were observed between groups for several parameters (Figures 6.3 to 6.5), including (mean values given in the following):

- C3C7 lordosis: -5° for the elderly group vs 6° for the young group,
- pelvic incidence: 56° for the elderly group vs 51° for the young group,
- pelvic tilt: 17° for the elderly group vs 11° for the young group,
- SVA: 15mm for the elderly group vs -9mm for the young group.

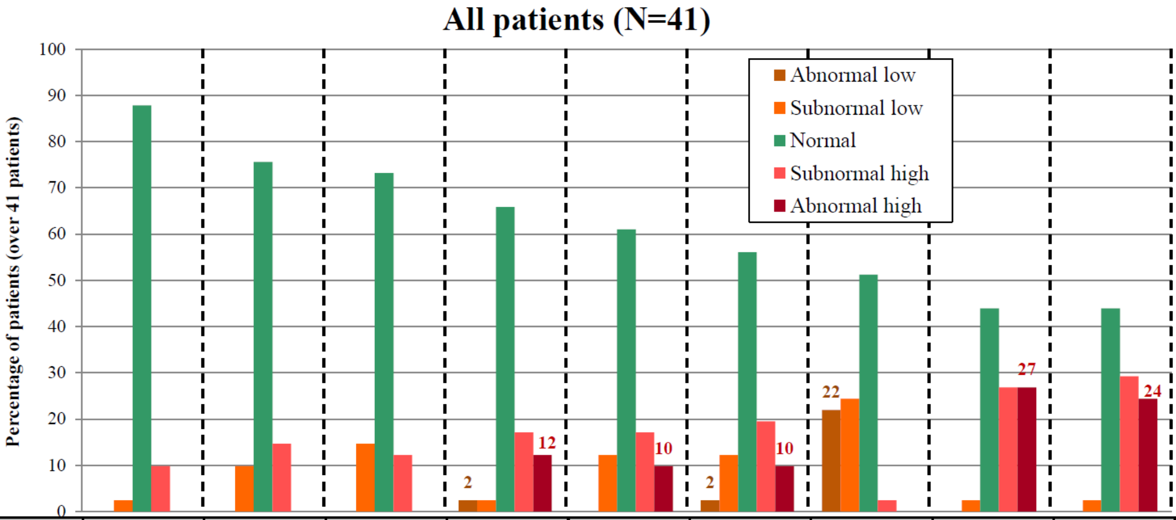


| Parameter | L1S1 (°) | SS (°) | T1T12 (°) | PI (°) | CAM-HA (°) | OD-HA (°) | C3C7 (°) | Spinal Incl (°) | SVA (mm) |
|---|---|---|---|---|---|---|---|---|---|
| Young Adults | -58 (13) | 41 (9) | 50 (13) | 51 (9) | - 2 (2) | - 2 (2) | 6 (12) | - 3 (3) | - 9 (22) |
| Elderly | -55 (8) | 39 (7) | 51 (11) | 56 (11) | -2 (2) | -2 (2) | -5 (12) | 1 (3) | 15 (23) |
| Stats | | | | * | | | * | * | * |

Figure 6.3. : Distribution of different parameters' values, for elderly, compared to corridors given by the young Group (Amabile *et al.*, 2016c): Percentage of subjects is computed as the percentage over the whole population (N=41). T1T12 is the thoracic kyphosis, L1S1 is the lumbar lordosis and C3C7 is the cervical curvature. Means (1*standard deviation) for Young Group (Amabile *et al.*, 2016c) and Elder Group. * means that significant differences were found between both groups.

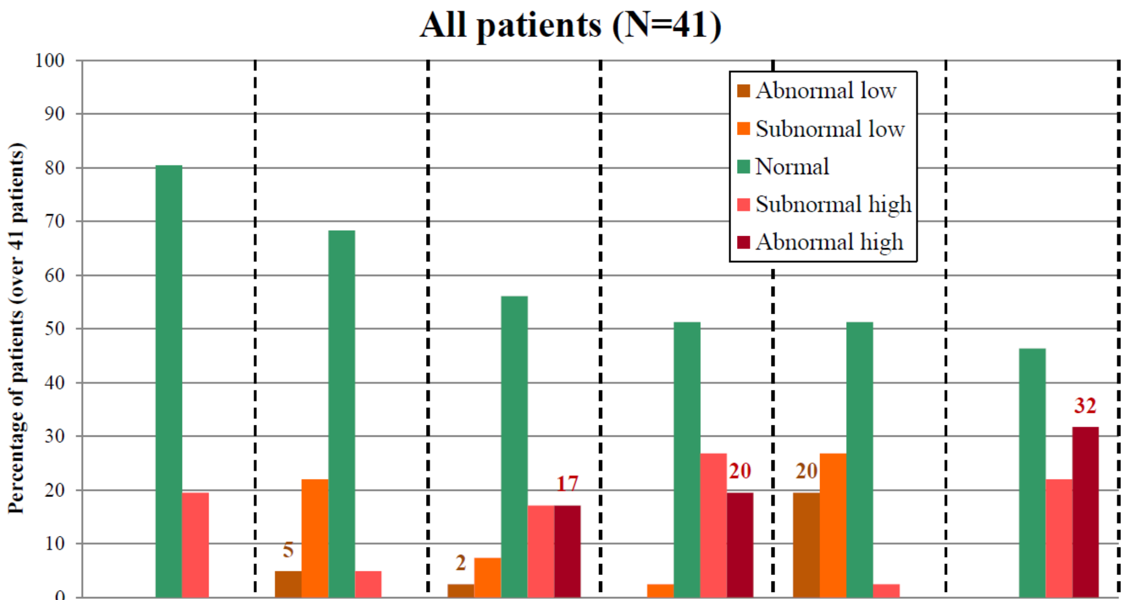


| | C7PL/SFD | T9HA (°) | C7-HA (°) | T1-S1 (°) | S1 overhang (mm) | TPA (°) |
|---|---|---|---|---|---|---|
| Young Adults | 0(0) | - 10 (3) | - 4 (2) | - 4 (3) | - 20 (10) | 5 (6) |
| Elderly | 0 (1) | - 12 (3) | - 3 (3) | - 1 (3) | -30 (12) | 13 (7) |
| Stats | * | * | * | * | * | * |

Figure 6.4. : Distribution of different parameters' values, for elderly, compared to corridors given by the young Group (Amabile *et al.*, 2016c): Percentage of subjects is computed as the percentage over the whole population (N=41). Means (1*standard deviation) for Young Group (Amabile *et al.*, 2016c) and Elder Group. * means that significant differences were found between both groups.

### 6 - 4.3 SVA subgroups analysis

Group 1 (N=19) included elderly with a normal or subnormal low SVA value. Group 2 (N=22) included elderly with subnormal high or abnormal high SVA value (Figure 6.3).

Overall, 44% of subjects presented a normal spinal inclination and 27% presented an abnormal high spinal inclination (Figure 6.3). Only, 10% (resp. 12%) of subjects presented an abnormal (high or low) CAM-HA (resp. OD-HA) (Figure 6.3).

Figure 6.5 and Table 6.2 present for each Group 1 and 2, comparison with reference values for: pelvic incidence, sacral slope, pelvic tilt, spinal inclination, OD-HA, CAM-HA.

| **Parameters** | **M (1*SD) Young** | **M (1*SD) Group 1** | **Young vs Group 1** | **M (1*SD) Group 2** | **Young vs Group 2** | **Group 1 vs Group 2** |
|---|---|---|---|---|---|---|
| **Age (yrs)** | 26 (5) | 57 (6) | X | 59 (9) | X | |
| **BMI (kg/m²)** | 22 (3) | 26 (5) | X | 26 (3) | X | |
| **PI (°)** | 51 (9) | 55 (8) | | 56 (13) | X | |
| **SS (°)** | -41 (9) | -39 (7) | | -39 (7) | | |
| **PT (°)** | 11 (6) | 16 (5) | X | 17 (10) | X | |
| **Spinal Inclination (°) (sagittal plane)** | -3 (3) | -2 (2) | | 3 (2) | X | X |
| **OD-HA (°) (sagittal plane)** | -2 (2) | -3 (2) | | 0 (2) | X | X |
| **CAM-HA (°) (sagittal plane)** | -2 (2) | -3 (2) | | 0 (2) | X | X |
| **C3C7 curvature (°)** | 6 (12) | -1 (10) | X | -8 (13) | X | |
| **SVA (mm)** | -9 (22) | -5 (12) | | 32 (15) | X | X |

Table 6.2. Results of statistical tests to assess differences between the Young Group (Amabile *et al.*, 2016c), Group 1 (N=19 subjects with SVA values subnormal low or normal) and Group 2 (N=22 subjects with SVA values subnormal high or abnormal high). M means mean and SD means standard deviation.

### 6 - 4.4 Compensatory mechanisms

In groups 1 and 2, elderly presenting an abnormal low cervical lordosis were identified: 5% in Group1 and 36% in Group2. Elderly presenting an abnormal high or low pelvic tilt (with respect of the classification presented in Figure 6.1) were labeled: 16% in Group1 and 36% in Group2. Elderly presenting an abnormal high spinal inclination were identified: 50% for Group2. All of these elderly (N=20) were studied in more details. Following the different types of alignment defined by Roussouly *et al.* (Roussouly *et al.*, 2005), 30% of these 20 elderly presented a type 1 or 2 alignment, 55% presented a type 3 alignment and 15% presented a type 4 alignment. CAM-$HA_{NC}$ and OD-$HA_{NC}$ inclinations were computed for these subjects, without pelvic tilt compensation and without cervical compensation (see Figure 6.2).

Among these, 13 elderly presented a newly computed abnormal CAM-HA$_{NC}$ or OD-HA$_{NC}$ greater than 3° while their initial value of CAM-HA or OD-HA was in average of -1° (SD of 3°). These 13 elderly presented all the different alignment types described by Roussouly (Roussouly *et al.*, 2005) in the same proportion as the initial population: 38% of these 13 elderly presented a type 1 or 2 alignment, 54% presented a type 3 alignment and 15% presented a type 4 alignment.

Overall, these 13 elderly presented a large pelvic retroversion: mean difference real PT with theoretical PT of 8° (SD: 5°). They also presented a high cervical curvature: mean difference between real C3C7 lordosis and 6° (normal C3C7 curvature): -19° (SD: 10°). Influence of the pelvic tilt and cervical curvature in the compensated posture of 3 of these 13 elderly is illustrated in Figure 6.6.

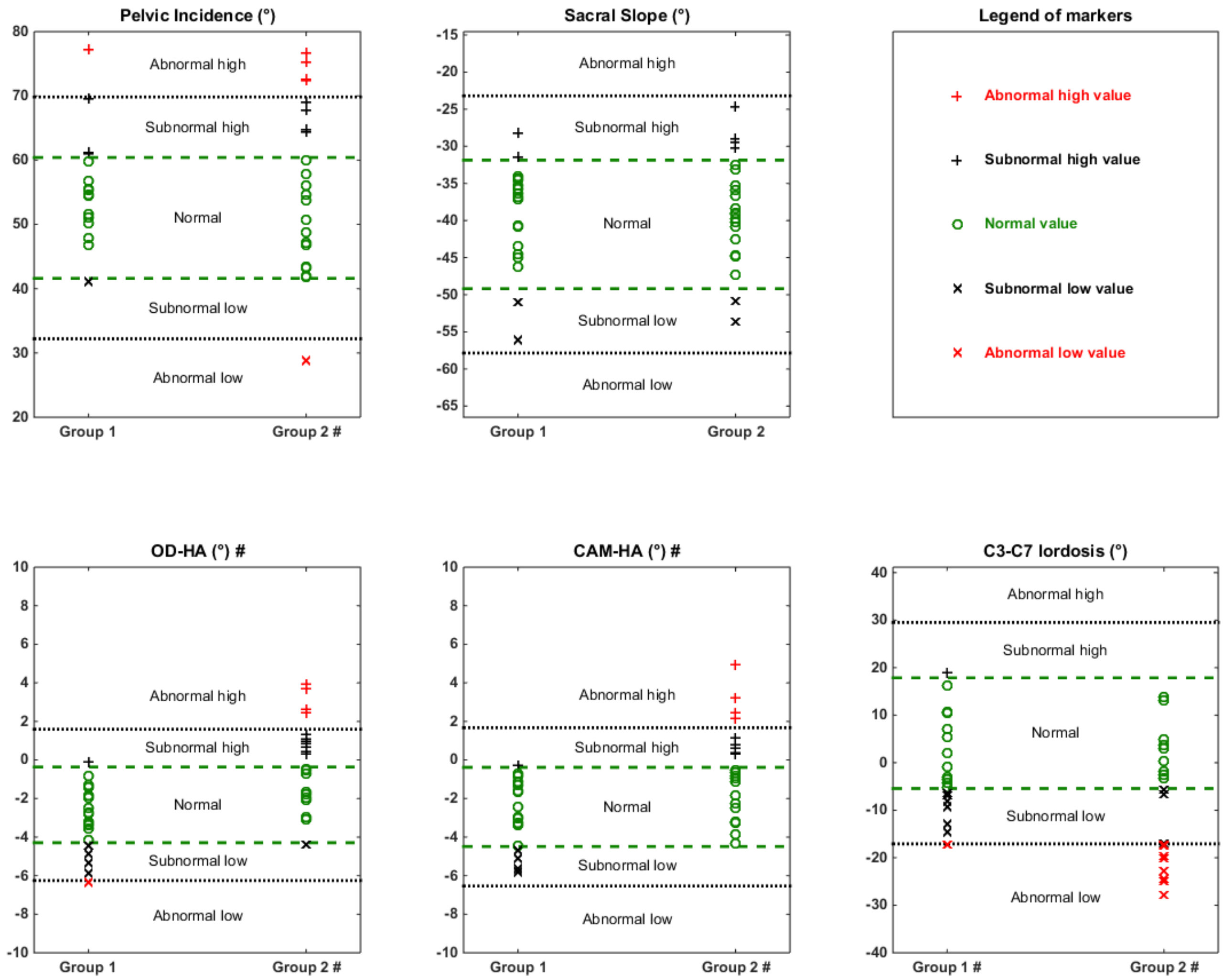


Figure 6.5. : Repartition of parameters' values for Group 1 (N=19 subjects with SVA values subnormal low or normal) and Group 2 (N=22 subjects with SVA values subnormal high or abnormal high), compared to intervals (dashed green and black lines) given by mean (M) and standard deviation (SD) of reference population (Amabile *et al.*, 2016c). # in the title means a significant difference between Groups 1 and 2. # next to Group1 (resp. Group 2) means a significant difference with the Young Group.

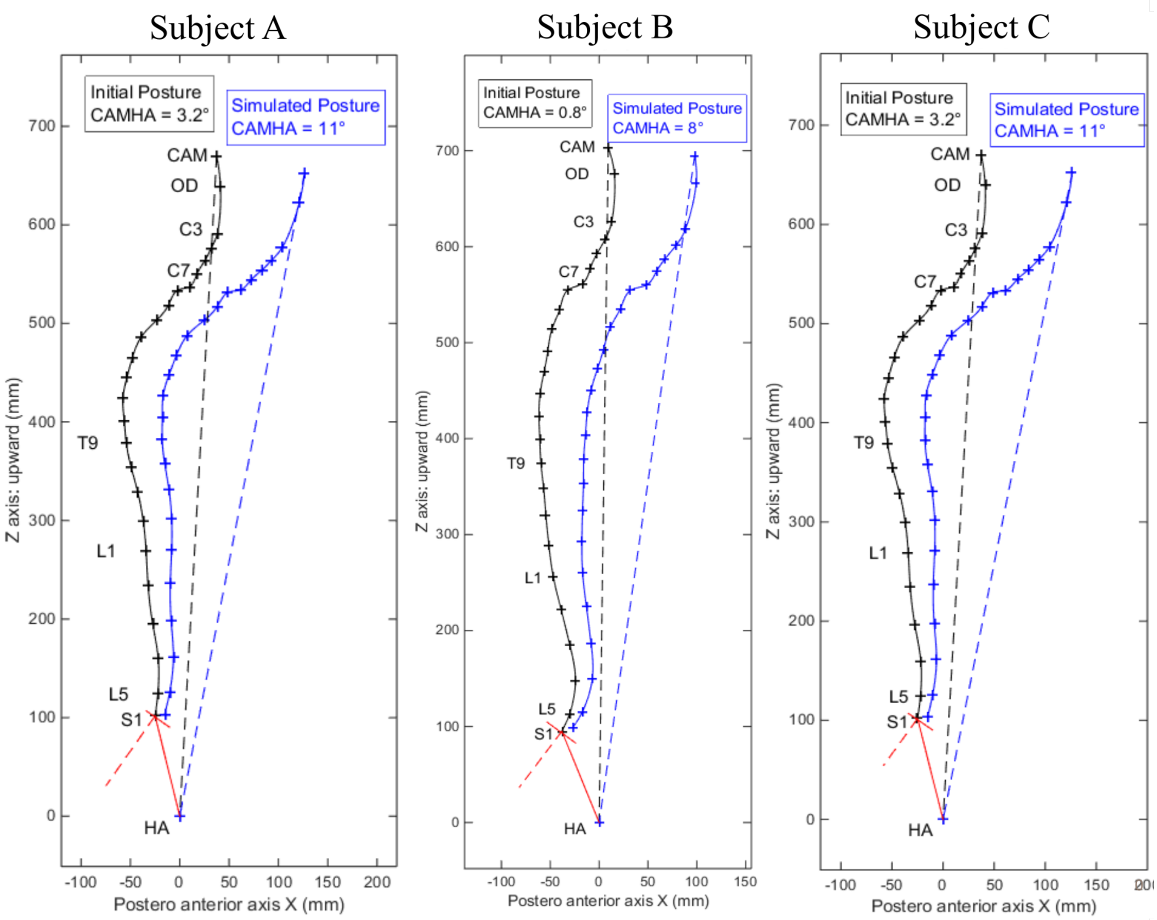


Figure 6.6. : Initial posture (black curve) and posture simulated without compensation at the pelvic and cervical levels (blue curve): theoretical value of the pelvic tilt was computed from the pelvic incidence (Vialle *et al.*, 2005) and cervical curvature was fixed at 6°, this value was reported as the mean value for asymptomatic adults younger than 40 years old (Amabile *et al.*, 2016c). The red lines represent the sacral plate and the link from S1 to HA to account for pelvic incidence. For asymptomatic adults younger than 40 years old, mean value for CAM-HA was -2°. Subject A (resp. B, resp. C) is an elderly with pelvic incidence higher than 60° (resp. between 44° and 60°; resp. lower than 44°).

## 6 - 5 Discussion

Postural alignment of asymptomatic adults older than 49 years old was investigated and compared to reference values from asymptomatic adults younger than 40 years old (Amabile *et al.*, 2016c). Quasi-invariance of the head-position above the pelvis, has been previously reported in asymptomatic adults younger than 40 years old (Amabile *et al.*, 2016c), and was conserved for elderly. This confirms the intuition of clinicians, summarized by the concept of conus of economy described by Dubousset (Dubousset, 1994). While both CAM-HA and OD-HA appeared as quasi-invariant on asymptomatic subjects, thus being potential markers of imbalance in subjects with spinal disorders, OD-HA could be of particular interest because of its visibility on most X-rays, while CAM-HA could not be visible for tall people because of the size of the bi-planar X-ray system.

Observation of the elderly was similar to the published studies. They presented a greater T1T12 thoracic kyphosis, and a smaller L1S1 lordosis than the asymptomatic adults younger than 40 years old (Amabile *et al.*, 2016c). This loss of lordosis and gain of kyphosis with aging has been previously reported in the literature (Schwab *et al.*, 2006; Kim *et al.*, 2014).

This study focused on the postural alteration of asymptomatic elderly assessed with different parameters: the Sagittal Vertical Axis, the C7PL/SFD (Barrey *et al.*, 2011), and the spinal inclination. When studying in details the compensatory mechanisms, 13 elderly can be identified with the head above the pelvis at the expense of an increased pelvic retroversion and increased cervical lordosis. In comparison, 7 subjects were identified as malaligned based on SVA, 10 based on C7PL/SFD (Barrey *et al.*, 2011) and 6 based on the spinal inclination. Although SVA, C7PL/SFD and spinal inclination are useful in the assessment of specific alterations, classification based on one of these parameters did not identify all the 13 subjects labeled in this study as subjects presenting a compensated posture. The population of elder adults represented the different types of alignment described by Roussouly (Roussouly *et al.*, 2005), as did the different sub-groups of elders analyzed in this study.

Some of these subjects appeared with maximal compensation, relative to the range of possible compensation. A longitudinal study following-up their postural evolution over time would assess if postural disorders will occur earlier for these subjects compared to the others. This would confirm the results of this study in the definition of an early marker of postural alteration.

### 6 - 5.1 Limitations and Perspectives

Due to the position in the EOS cabin (shifted feet), the measured parameters of the thigh must be interpreted with precaution. As most of the radiographs did not completely include the lower legs, the analysis of the lower limbs and their role as compensatory mechanisms were excluded from the current study (Barrey *et al.*, 2013; Diebo *et al.*, 2015). Another limitation relates to the constraints associated with the image acquisition in the EOS cabin. While standardized Free Standing Position allowed to be as close as possible to the natural posture, additional observation of routine relaxed posture, out of the cabin, could be interesting in future studies.

Additionally, further investigation on a wider range of subjects would be interesting to confirm these results obtained on reasonable sample size (41 elderly) split in two subgroups of around 20 subjects each. Potential bias regarding the subjects' selection was removed as exclusion criteria were similar between both populations, with the addition of clinical scores for the elderly in order to only recruit asymptomatic elderly. In addition, both groups' data collection and image processing followed the same protocol. Including patients in a future study would be of special interest to assess if a threshold of degree of compensation appears allowing for identification of patients with increased pain or disability. It would also be interesting to test for a special link between severity of the disease (and/or quality of life scores) and lack of compensation.

## 6 - 6 Conclusion

Postural alignment of asymptomatic adults older than 49 years old was studied. The position of the head above the pelvis appears as quasi-invariant in elderly. Despite the non-pathological condition of the subjects, in nearly 32% of them, this invariance is maintained at the expense of compensatory mechanisms at the pelvis and cervical level. Future investigation of those compensatory mechanisms, in longitudinal studies, could lead toward early assessment of subjects at risk of postural alteration, possibly leading to spinal disorders impacting quality of life.

# CONCLUSION

This part of the PhD thesis focused on the age-related changes of the postural alignment of the skeleton. More specifically, it provided answers to two of the key questions initially introduced:

- how does postural alignment evolve during aging?
- is the head maintained above the pelvis for older subjects?

The first chapter described a population of reference and identified the quasi-invariance of the head position above the pelvis. The second chapter reported valuable results on the postural alignment of older adults: the majority of them maintained the head above the pelvis, even if a global anterior inclination of the trunk was observed. This forward inclination was compensated in part by increasing the cervical lordosis, and in part by increasing the retroversion of the pelvis.

Identification of special patterns of compensation have been confirmed and compared to the literature, with addition of the head position's evolution over aging. Alignment of the head above the pelvis is maintained even for older subjects already recruiting compensation at the cervical and pelvic levels. This result confirms the intuition most of clinical practitioners reported when observing patients in clinical routine (alignment of the head above the pelvis), even though quantification of these observations was not available so far. While these two complementary studies permitted to establish the invariance of the head position above the pelvis, larger cohorts need to be considered in order to refine the study of early compensatory mechanisms, and to best represent the global population in terms of ages, genders, and morphologies. Longitudinal studies could assess postural evolution of subjects who already presented a compensated alignment.

While the current part highlighted the postural changes occurring with aging, and their impacts on the neutral position of subjects, one can envision the particular role of the muscles in this configuration: by allowing such compensatory mechanisms, and by rendering those the most economic and efficient possible. In addition, as muscles degrade during aging, it seems of primary importance to include the muscular system in the study of age-related alterations of the global posture. As such, the second part of this PhD will focus on the quantification of spino-pelvic muscles' characteristics in different populations.

# Part C

# Age-related changes in the muscular system

# INTRODUCTION

This part focuses on the characterization of the spino-pelvic muscles for both young asymptomatic adults and older adults with spinal deformities.

Firstly, a population of reference of young asymptomatic adults (i.e. 18-24 years old) has been studied in order to report reference values for the asymptomatic muscular system. Volunteers were prospectively recruited for MRI exams in Nice by Dr Bronsard during this PhD. This work has been accepted for publication in the journal *Surgical And Radiologic Anatomy* (Amabile *et al.*, 2016b).

Secondly, a population of older adults with spinal deformities (older than 30 years old) was studied following the same protocol used for the reference population. MRI acquisitions for patients were retrospectively analyzed in this PhD, but were previsouly collected and partly analyzed during the PhD of Bertrand Moal in NYU. Results were compared to those of the population of reference and changes were investigated in order to identify changes due to aging and due to pathological condition of the patients.

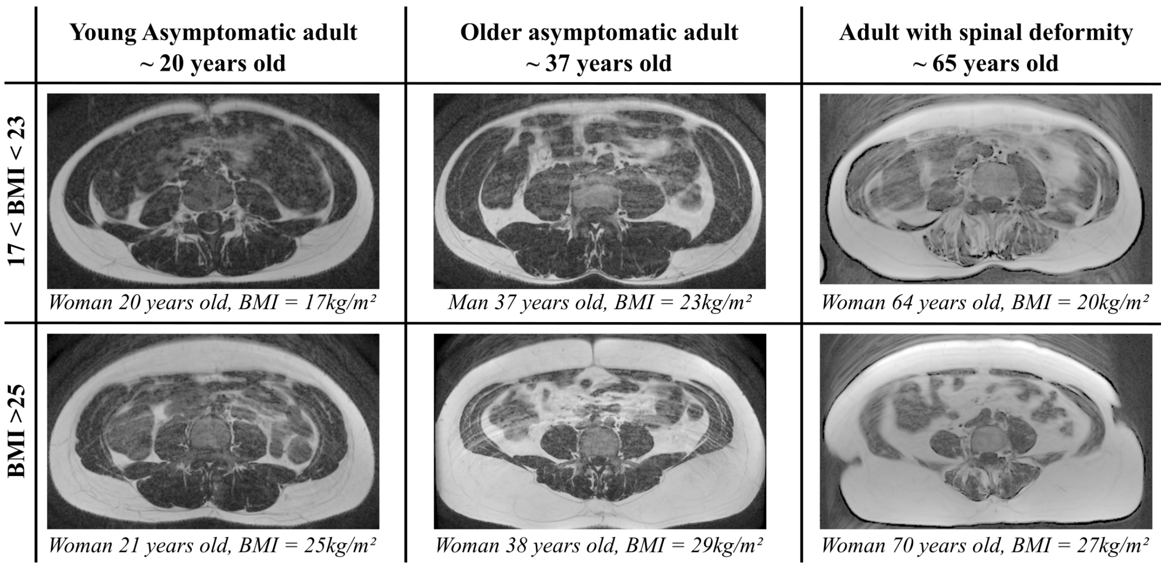


Figure 6.7. : Axial MRI slices, at the L4 level, of adults from 20 to 75 years old with different body mass index (BMI in kg/m$^2$), with/without spinal deformity.

# CHAPTER 7

# SPINO-PELVIC MUSCLES OF YOUNG ASYMPTOMATIC ADULTS

This chapter is currently under revision in Surgical and Ragiologic Anatomy in 2016 (Amabile *et al.*, 2016b), under the title:

## Estimation of spino-pelvic muscles' volume in young asymptomatic subjects: a quantitative analysis.

**Authors:**

Celia Amabile[a, b], Bertrand Moal[a], Oussama Arous Chtara[a], Hélène Pillet[a], Jose G. Raya[c], Antoine Iannessi[d], Wafa Skalli[a], Virginie Lafage[b], Nicolas Bronsard[e].

**Affiliations:**

[a] Arts et Métiers ParisTech, LBM/Institut de Biomécanique Humaine Georges Charpak, Paris, France;
[b] Spine Service, Hospital for Special Surgery, New York, NY 10021, USA;
[c] Center for Biomedical Imaging, Department of Radiology, New York University Langone Medical Center, New York, NY, USA;
[d] Department of Radiology, Centre Antoine Lacassagne, Nice, France;
[e] Department of Orthopaedic, Trauma, and Spine Surgery, Institut Universitaire de l'Appareil Locomoteur et du Sport, Hôpital Pasteur 2, CHU de Nice, France.

**Conflict of interest statement:**
The authors have no conflicts of interest to declare.

**Acknowledgments:** The authors thank the ParisTech BiomecAM chair program on subject-specific musculo-skeletal modeling, and in particular COVEA and Société Générale. The authors thank the support received from the Anatomy association from Nice, France (Association d'Anatomie Niçoise). The authors also thank the support received from the Fulbright Program as a Fulbright PhD scholarship.

# 7 - 1 Abstract

## 7 - 1.1 Purpose

Muscles have been proved to be a major component in postural regulation during pathological evolution or aging. Particularly, spino-pelvic muscles are recruited for compensatory mechanisms such as pelvic retroversion, or knee flexion. Change in muscles' volume could therefore be a marker of greater postural degradation. Yet, it is difficult to interpret muscular degradation as there are few reported values for young asymptomatic adults to compare to. The objective was to provide such reference values on spino-pelvic muscles. A model predicting the muscular volume from reduced set of MRI segmented images was investigated.

## 7 - 1.2 Methods

A total of 23 asymptomatic subjects younger than 24 years old underwent an MRI acquisition from T12 to the knee. Spino-pelvic muscles were segmented to obtain an accurate 3D reconstruction, allowing precise computation of muscle's volume. A model computing the volume of muscular groups from less than 6 MRI segmented slices was investigated.

## 7 - 1.3 Results

Baseline values have been reported in tables. For all muscles, invariance was found for the shape factor (ratio of volume over [area times length]: $SD<0.04$) and volume ratio over total volume ($SD<1.2\%$). A model computing the muscular volume from a combination of 2 to 5 slices has been evaluated. The 5 slices model prediction error (in % of the real volume from 3D reconstruction) ranged from 6% (Knee flexors and extensors and Spine flexors) to 11% (Spine extensors).

## 7 - 1.4 Conclusion

Spino-pelvic muscles' values for a reference population have been reported. A new model predicting the muscles' volumes from a reduced set of MRI slices is proposed. While this model still needs to be validated on other populations, the current study appears promising for clinical use to determine quantitatively the muscular degradation.


**Keywords:** Muscles, MRI, volume, asymptomatic subjects, young.

## 7 - 2 Introduction

While skeletal postural alignment has been widely investigated based on X-rays analysis (Barrey *et al.*, 2013), quantification of the muscles' degradation is not yet fully documented. As muscular degradation (mainly in terms of decrease of cross sectional area) has been correlated to back pain (Gildea *et al.*, 2013; Lee *et al.*, 2008; Parkkola *et al.*, 1993; Rasch *et al.*, 2007) and to aging (Ahmed *et al.*, 2005; Frontera *et al.*, 2000; Takahashi *et al.*, 2006; Takayama *et al.*, 2016), there is a need for quantitative analysis of muscular system in relation to skeleton aging (bone quality degradation and postural alignment modifications). As a first step, to differentiate pathological changes in the muscular system from the one associated with aging, it is of primary importance to review reference values for young asymptomatic adults. However literature lacks descriptive values (particularly on volumes) of the muscular system, specifically on the L1 to knee area, particularly involved in compensatory mechanisms.

Muscles' geometry has been explored using Computed Tomography (CT) (Danneels *et al.*, 2000; Rasch *et al.*, 2007). However, CT involves a significant ionizing dose: covering a specific part of the body extensively (significant number of slices) involves a moderate to high radiation dose for the patient (1.5mSv for a lumbar spine CT vs 0.02mSv for a Chest X-ray (Food and Drug Administration, 2015)). Most frequently, for CT, to avoid repeated acquisitions, only a reduced set of slices is acquired, only at specific locations of interest (Danneels *et al.*, 2000; Rasch *et al.*, 2007).

Another method used to investigate muscles is ultrasound (non-invasive). However, deep muscles can be more difficult to explore as it is a surface technique, and studies mainly focused on dynamic (muscle contraction) (Nuzzo and Mayer, 2013; Skeie *et al.*, 2015).

Finally, the most common imaging modality for the analysis of the muscular system is the MRI (Crawford *et al.*, 2016; Fortin *et al.*, 2014, 2016; Gildea *et al.*, 2013; Kjaer *et al.*, 2007; Lee *et al.*, 2008; Niemeläinen *et al.*, 2011; Parkkola *et al.*, 1993; Pezolato *et al.*, 2012; Savage *et al.*, 1991; Takahashi *et al.*, 2006). For example, different studies conducted by Fortin *et al.* reported CSA values and fat infiltration quantification (Fortin *et al.*, 2014, 2015, 2016) on various populations. Particularly, these studies provided valuable insights on the relation between muscular asymmetry, fat infiltration and low back pain (Fortin *et al.*, 2015). Most of these studies reported only 2D parameters such as cross-sectional area (Fortin *et al.*, 2014; Gildea *et al.*, 2013; Lee *et al.*, 2009; Niemeläinen *et al.*, 2011; Parkkola *et al.*, 1993; Pezolato *et al.*, 2012; Savage *et al.*, 1991; Takahashi *et al.*, 2006), and/or information on fat infiltration of muscles considered (Crawford *et al.*, 2016; Fortin *et al.*, 2014, 2015; Kjaer *et al.*, 2007; Lee *et al.*, 2009; Parkkola *et al.*, 1993; Pezolato *et al.*, 2012; Valentin *et al.*, 2015). Muscular volume has been however reported for the quadriceps femoris components (Barnouin *et al.*, 2014), pelvic and/or lower limbs muscles (Lube *et al.*, 2016; Handsfield *et al.*, 2014; Belavý *et al.*, 2011). The three last studies either included only a limited number of subjects (3 females and 3 males (Lube *et al.*, 2016)), or a wide range of age in the population considered (from 12 to 51 years old (Handsfield *et al.*, 2014)), or lastly, focused on the effect of bed-resting (Belavý *et al.*, 2011) (thus not considering daily representative condition). While fat infiltration gives an insight on the muscle quality (Fortin *et al.*, 2014, 2015), calibration may be an issue and this study focuses on the volume computation and 3D geometrical parameters of the muscles only.

Computing muscular volume can be done by interpolation or by 3D reconstruction of the muscle. In particular, MRI based 3D reconstruction and volume computation method has been reported as accurate (Jolivet *et al.*, 2008) and repeatable (Moal *et al.*, 2014). Still, quantitative analysis of MRI images can be time consuming. The deformation of a parametric specific object (DPSO) method (Jolivet *et al.*, 2008, 2014) allows for an accurate and precise 3D reconstruction of individual muscles, from segmentation on a selected set of MRI images, leading to an accurate volume computation in a fairly reduced amount of time. This method had been used on adults with spinal deformities for the spino-pelvic area (Moal *et al.*, 2014) and on volunteers younger than 40yrs old, for the cervical spine (Li *et al.*, 2014) and for lower limbs (Hausselle *et al.*, 2014; Südhoff *et al.*, 2009). While DPSO method provides time reduction by reducing the number of slices to consider per muscle, this method involves different slices for each muscle which may still be long when numerous muscles are considered. In addition to characterize spino-pelvic muscles' 3D geometry (cross sectional area as well as volume), on young asymptomatic volunteers, our aim is to propose a model quantifying rapidly muscular groups' volume from less than 6 MRI segmented images for all muscles.

# 7 - 3 Methods

## 7 - 3.1 Study Design

This is a prospective, single center study, recruiting subjects from September 2014 to March 2015. All participants signed an informed consent prior enrollment. This study has been reviewed and approved by Comité de Protection des Personnes (CPP 14.013), and included asymptomatic adults younger than 24 years old. Exclusion criteria included: previous surgery on lower limbs or spine, pregnancy, postural disorder, MRI contraindication (mainly linked to magnetic field).

## 7 - 3.2 Data collection

Information collected included: age, body mass index (BMI), sex. History of musculo-skeletal injury was also documented. Each subject undertook an MRI exam (General Electric 1.5T, Fairfield, USA), collecting axial images from vertebra T12 to the patella distal insertion. The protocol used was the same as the one described in a previous study (Moal *et al.*, 2015).The MRI machine was set with the following parameters: TR/TE = 427/11.3ms, acquisition matrix = 416*416pixels, phase oversampling = 100%, in plane resolution = $0.82\times0.82\text{mm}^2$, 8 stages, 40 slices by stage, slice thickness = 5mm, slice gap = 0mm, flip angle = 160°, parallel imaging acceleration factor(iPat) = 2, bandwidth = 391Hz/pixel, echo spacing = 11.3ms, acquisition time per stage = 7min, Total acquisition time = 50min.

3D reconstruction of the muscles (with information from all MRI slices) was carried out with software developed in our institution, using the DPSO method (Jolivet *et al.*, 2008; Moal *et al.*, 2014). Muscles of interest are represented in Figure 7.1, analysis was performed on the left and right muscles.

Because the border between specific muscles can be challenging to identify, some muscles were segmented together:

- the "adductor" includes the adductor brevis, the adductor longus, the adductor magnus as well as the obturatorius internus and the pectineus;
- the "erector spinae" includes the tractus medialis (multifidi and interspinales) and lateralis (iliocostalis and longissimus);
- the "iliopsoas" includes the iliacus and the psoas;
- the "vastus lateralis inter" includes the vastus lateralis and intermedius.

For each muscle, the following geometric parameters were computed: length of the muscle (L), maximal anatomical cross-sectional area ($A_{max}$) and volume of the muscle normalized (divided) by the height of the subject ($V_H$).

## 7 - 3.3 Statistical Analysis

Normality of each parameter studied ($V_H$, L, $S_p$, $A_{max}$), for individual muscles, was tested with a Lilliefors test (Lilliefors, 1967). For each muscle, differences were investigated between right and left sides and between females and males, for the geometric parameters ($V_H$, L, $A_{max}$): using a T-test if it was found to be drawn from a normal distribution; using a Mann-Whitney test otherwise. For each side (right and left), the ratio ($RV_{tot}$) of each muscle's volume over the total muscle of the side was computed as well. For $RV_{tot}$, mean, standard deviation (SD) and coefficient of variation (CV) [SD*100 / Mean] have been calculated.

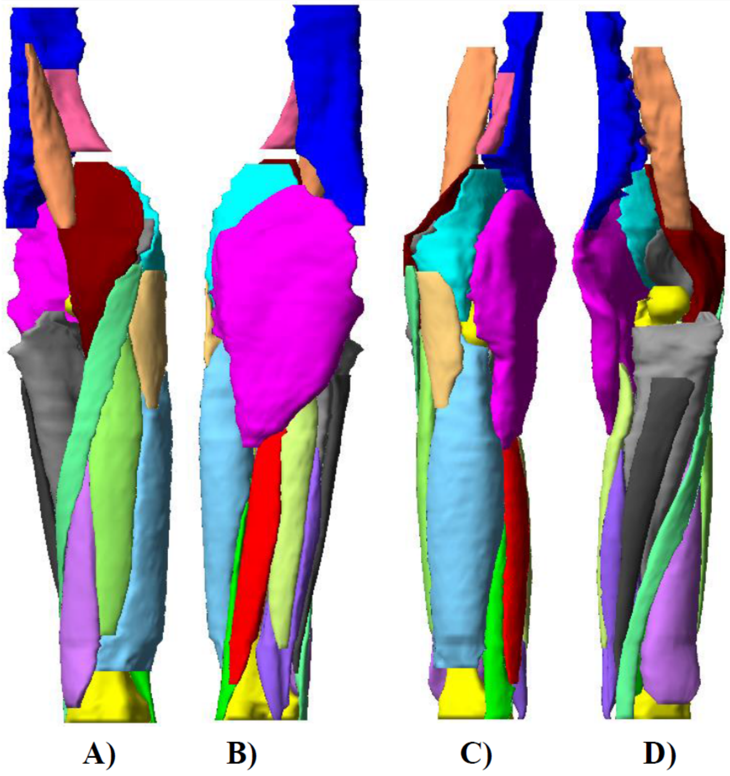


| | Spine | | Hip | | Knee | |
|---|---|---|---|---|---|---|
| *F: flexors / E: extensors* | F | E | F | E | F | E |
| Adductor | | | X | | | |
| Biceps femoris longum | | | | X | X | |
| Biceps femoris breve | | | | X | X | |
| Erectus spinae | | X | | | | |
| Femur | | | | | | |
| Gluteus maximus | | | | X | | |
| Gluteus medius | | | | | | |
| Gluteus minimus | | | | | | |
| Gracilis | | | X | | X | |
| Iliacus | X | | X | | | |
| Psoas | X | | X | | | |
| Quadratus lumborum | | X | | | | |
| Rectus femoris | | | X | | | X |
| Sartorius | | | X | | X | |
| Semimembranosus | | | | X | X | |
| Semitendinosus | | | | X | X | |
| Tensor fasciae lata | | | X | | | |
| Vastus lateralis inter | | | | | | X |
| Vastus medialis | | | | | | X |

Figure 7.1. : Muscles considered in the study (mesh obtained with DPSO method (Jolivet *et al.*, 2008)), represented on a 3D reconstruction of a left leg. **A)** Anterior view. **B)** Posterior view. **C)** Lateral view. **D)** Medial view. The table on the right describes the different functional groups considered for the analysis: Spine Flexors (Spine F), Spine Extensors (Spine E), Hip Flexors (Hip F), Hip Extensors (Hip E), Knee Flexors (Knee F) and Knee Extensors (Knee E).

In the following, muscles were grouped in functional groups per joint, respectively as flexors and extensors of the spine, hip and knee as detailed in Figure 7.1. For each group, the total muscular volume ($V^{gp}$) was computed. In addition, for each joint studied (knee, spine, hip), the ratio of flexors over extensors, $R_{flex\_ext}$, was computed as the volume ratio of flexors over extensors muscles of the joint. Normality of $V^{gp}$ and $R_{flex\_ext}$ was tested with a Lilliefors test. Level of significance, for all statistical tests, was set to 0.05.

### 7 - 3.4 Alternative estimations of the muscular volume

#### 7 - 3.4.1 Maximal Section Method

As described in Mersmann's study on the lower leg muscles (Mersmann *et al.*, 2014), the volume of each muscle was computed from the length and maximal cross sectional area of the muscle, using a factor of shape $S_p$. This factor was computed as the ratio of the volume (V) over the product [muscle length by muscle's maximal sectional area]: $S_p = V/((L*A_{max}))$. Validation of this factor of shape was done with a leave-one-out method.

#### 7 - 3.4.2 Reduced MRI set Method

Estimation of the volume from a reduced set of MRI segmented slices was investigated to reduce segmentation time and offer a tool applicable in a clinical setting. In order to quantify muscular volume more rapidly, a model using the DPSO method (Jolivet *et al.*, 2014; Moal *et al.*, 2014), with less than 6 segmented slices was investigated.

The volumes of all functional groups were predicted from a multilinear regression using information of a limited number of slices (from 2 to 5 slices). The following predictors were used in the model: Age, BMI, Femoral Length and the sum of the areas of the muscles contained in the group considered, on the slice considered. A principal component analysis (PCA) was performed to retain only relevant predictors (linear combination of the initially considered predictors). Each computed PCA predictor was replaced by the initial predictor most correlated with it, to obtain a clear and understandable prediction equation. Even if the sum of the areas of the muscles was not retained by this procedure as a predictor, it was added as such for its relevance as a global indicator.

The model was built on data from right side of the subjects. The slices were numbered upward from 0 to 150: slice 0 as the first slice with the posterior part of the femoral condyles visible, and slice 100 as the last slice with the femoral head visible.

The Spine Flexors' ($Spine_{flex}$) and Spine Extensors' ($Spine_{ext}$) muscles were segmented on slices from T12 to the greater trochanter ("proximal slices"), while the Knee and Hip, Flexors and Extensors ($Hip_{flex}$, $Hip_{ext}$, $Knee_{flex}$, $Knee_{ext}$), were segmented on slices from S1 to the femoral condyles ("distal slices"). Therefore, at least 1 slice from the "proximal slices" was included in the slices' combinations. A slice was considered only if it contained the muscles segmentation for at least 90% of the subjects. For each slices' combination, each muscles' functional group, the root mean square (RMS) was computed as the root mean square of the difference (in % of the real volume) between predicted volume (from the leave one out method) and real volume.

Combinatory analysis was performed to find the best combination of "proximal slices" (respectively "distal slices"), as the one presenting the smallest average RMS over $Spine_{ext}$ and $Spine_{flex}$ (respectively over $Hip_{flex}$, $Hip_{ext}$, $Knee_{flex}$ and $Knee_{ext}$). Lastly, the prediction of this model has been evaluated by computing the RMS for each functional group.

# 7 - 4 Results

## 7 - 4.1 Demographics

The sample studied included 12 females and 11 males. Age (respectively BMI) ranged from 18 to 21years (resp. 17.4 to 24.8kg/m$^2$). Mean age was 19.3years old (SD: 0.8). Mean BMI was 20.9kg/m$^2$ (SD: 2.0). Females' height ranged from 155 to 169cm vs 171 to 185cm for men.

## 7 - 4.2 Statistical Analysis

Tables 7.1 and 7.2 present means and SD of L, $A_{max}$, $S_p$, $V_H$, V, $RV_{tot}$ and CV of $RV_{tot}$.
No significant difference was found between right/left sides parameters ($V_H$, V, L, $A_{max}$), except for the following: V, $V_H$ and $RV_{tot}$ of the quadratus lumborum, rectus femoris and semi-tendinosus; L of the gluteus maximus and $A_{max}$ of quadratus lumborum, adductor and semi-tendinosus. Difference between right and left sides for these muscles/parameters was in average less than 11% of the mean value right/left (Tables 7.1 and 7.2). Values were averaged right/left when no significant difference was found (Tables 7.1 and 7.2).

The major part of the geometrical parameters considered followed a normal distribution except for the following muscles and parameters: for example the $V_H$ of right iliopsoas, the V of right adductor, the L of left erectus spinae, the $A_{max}$ of right gluteus minimus, the $RV_{tot}$ of left sartorius or the $S_p$ of both sides of quadratus lumborum.

Statistical differences between right/left $S_p$ were found for specific muscles, for which the difference was less than 3% of the mean value right/left (Table 7.2).

| Muscle | | V ($cm^3$) F | | V ($cm^3$) M | | $V_H$ ($cm^2$) F | | $V_H$ ($cm^2$) M | | $RV_{tot}$ (%) F | | | $RV_{tot}$ (%) M | | |
|---|---|---|---|---|---|---|---|---|---|---|---|---|---|---|---|
| | | Mean | SD | Mean | SD | Mean | SD | Mean | SD | Mean | SD | CV | Mean | SD | CV |
| [a] [b] **Iliopsoas** | | 290.9 | 36.2 | 514.8 | 43.6 | 1.8 | 0.2 | 2.9 | 0.3 | 6.9 | 0.6 | 8.6 | 8.2 | 0.5 | 5.8 |
| [b] **Quadratus lumborum** | **R:** | 33.7 | 9.2 | 62.0 | 7.8 | 0.2 | 0.1 | 0.3 | 0.0 | 0.8 | 0.2 | 22.2 | 1 | 0.1 | 12.7 |
| | **L:** | 35.9 | 7.8 | 67.8 | 9.8 | 0.2 | 0.0 | 0.4 | 0.1 | 0.8 | 0.1 | 15.4 | 1.1 | 0.2 | 15.7 |
| **Erectus spinae** | | 294.5 | 42.9 | 419.2 | 55.7 | 1.8 | 0.3 | 2.3 | 0.3 | 7 | 0.8 | 11.8 | 6.7 | 0.8 | 12.3 |
| [a] **Gluteus maximus** | | 606.1 | 80.4 | 829.2 | 97.0 | 3.7 | 0.5 | 4.6 | 0.5 | 14.4 | 1.1 | 7.9 | 13.2 | 1 | 7.5 |
| **Gluteus medius** | | 236.5 | 28.9 | 341.1 | 36.3 | 1.4 | 0.2 | 1.9 | 0.2 | 5.6 | 0.4 | 7.1 | 5.5 | 0.6 | 11.4 |
| **Gluteus minimus** | | 76.2 | 7.8 | 107.8 | 20.2 | 0.5 | 0.1 | 0.6 | 0.1 | 1.8 | 0.3 | 15.2 | 1.7 | 0.3 | 14.9 |
| **Adductor** | | 663.0 | 85.5 | 1028.5 | 81.6 | 4.1 | 0.5 | 5.8 | 0.5 | 15.7 | 1.2 | 7.4 | 16.4 | 0.7 | 4.3 |
| **Vastus lateralis inter** | | 824.9 | 93.2 | 1178.6 | 85.9 | 5.0 | 0.6 | 6.6 | 0.5 | 19.6 | 1.1 | 5.5 | 18.8 | 0.6 | 3.4 |
| **Vastus medialis** | | 314.9 | 37.4 | 465.1 | 49.3 | 1.9 | 0.2 | 2.6 | 0.3 | 7.5 | 0.6 | 7.9 | 7.4 | 0.7 | 9.4 |
| **Tensor Fasciae Lata** | | 45.8 | 10.6 | 69.8 | 21.8 | 0.3 | 0.1 | 0.4 | 0.1 | 1.1 | 0.2 | 21.5 | 1.1 | 0.3 | 28.8 |
| **Rectus femoris** | **R:** | 190.4 | 26.0 | 280.0 | 24.8 | 1.2 | 0.2 | 1.6 | 0.1 | 4.5 | 0.4 | 9 | 4.5 | 0.4 | 9 |
| | **L:** | 187.4 | 28.2 | 267.5 | 24.2 | 1.1 | 0.2 | 1.5 | 0.1 | 4.4 | 0.4 | 9.7 | 4.3 | 0.3 | 7.9 |
| **Gracilis** | | 66.5 | 9.8 | 104.8 | 18.3 | 0.4 | 0.1 | 0.6 | 0.1 | 1.6 | 0.2 | 12.5 | 1.7 | 0.2 | 13.4 |
| **Sartorius** | | 100.3 | 17.5 | 161.8 | 24.1 | 0.6 | 0.1 | 0.9 | 0.1 | 2.4 | 0.3 | 12.5 | 2.6 | 0.3 | 10.7 |
| [a] **Biceps femoris breve** | **R:** | 60.5 | 11.5 | 112.8 | 25.0 | 0.4 | 0.1 | 0.6 | 0.1 | 1.5 | 0.2 | 15.2 | 1.8 | 0.3 | 19.7 |
| | **L:** | 63.2 | 14.1 | 107.9 | 20.6 | 0.4 | 0.1 | 0.6 | 0.1 | | | | | | |
| **Biceps femoris longum** | | 128.1 | 17.9 | 184.1 | 23.8 | 0.8 | 0.1 | 1.0 | 0.1 | 3 | 0.3 | 9.6 | 2.9 | 0.3 | 10.1 |
| **Semi-membranosus** | | 154.2 | 22.6 | 223.4 | 31.7 | 0.9 | 0.1 | 1.2 | 0.2 | 3.7 | 0.4 | 12.1 | 3.6 | 0.4 | 12.2 |
| **Semi-tendinosus** | **R:** | 129.4 | 24.6 | 196.0 | 24.3 | 0.8 | 0.1 | 1.1 | 0.1 | 3.1 | 0.5 | 16.5 | 3.1 | 0.3 | 9.9 |
| | **L:** | 124.2 | 26.3 | 183.5 | 20.2 | 0.8 | 0.2 | 1.0 | 0.1 | 2.9 | 0.4 | 15.1 | 2.9 | 0.2 | 6.8 |

Table 7.1. Means. standard deviations (1*SD) and coefficient of variation (CV=SD*100/mean) of volume (V). volume normalized by height ($V_H$). and volumic ratio ($RV_{tot}$ for females and males. Values were averaged over right and left sides when no significant difference was found. Males' and females' values were separated as significant differences were found for all muscles for V and $V_H$. [a] (respectively [b]) means that statistical differences between males and females were found for $RV_{tot}$, for the right side of the muscle (resp. for the left side of the muscle).

| Muscle | | L (cm) F | | L (cm) M | | $A_{max}$ ($cm^2$) F | | $A_{max}$ ($cm^2$) M | | $S_p$ | | |
|---|---|---|---|---|---|---|---|---|---|---|---|---|
| | | *Mean* | *SD* | *Mean* | *SD* | *Mean* | *SD* | *Mean* | *SD* | *Mean* | *SD* | *RMSE (%)* |
| **Quadratus lumborum** | **R:** | 13.1 | 2.3 | 13.6 | 2.1 | 5.8 | 1.2 | 8.8 | 1.4 | 0.49 | 0.04 | 17.7 |
| | **L:** | | | | | 6.0 | 1.2 | 9.7 | 1.8 | | | |
| [b] **Erectus spinae** | | 22.1 | 2.0 | 23.6 | 2.1 | 22.5 | 2.5 | 29.8 | 2.8 | 0.59 | 0.00 | 5.2 |
| [a] [b] **Gluteus maximus** | **R:** | 27.9 | 2.0 | 30.3 | 1.9 | 40.1 | 4.9 | 49.2 | 4.2 | 0.55 | 0.00 | 5.9 |
| | **L:** | 26.9 | 1.6 | 30.3 | 1.5 | | | | | | | |
| [a] [b] **Gluteus medius** | | 18.1 | 0.8 | 20.6 | 1.0 | 25.6 | 3.8 | 33.7 | 2.4 | 0.5 | 0.01 | 6.6 |
| [a] **Gluteus minimus** | | 13.1 | 1.4 | 14.7 | 1.2 | 12.3 | 1.5 | 15.8 | 2.7 | 0.48 | 0.01 | 11.9 |
| **Adductor** | **R:** | 36.0 | 2.8 | 38.3 | 3.1 | 39.6 | 4.5 | 58.3 | 4.1 | 0.47 | 0.00 | 7.1 |
| | **L:** | | | | | 39.2 | 5.0 | 55.8 | 3.9 | | | |
| [a] [b] **Vastus lateralis inter** | | 34.6 | 1.2 | 37.8 | 1.5 | 40.4 | 4.9 | 52.8 | 4.5 | 0.59 | 0.00 | 4.8 |
| [b] **Vastus medialis** | | 31.2 | 1.7 | 33.5 | 2.1 | 17.4 | 2.2 | 24.1 | 2.7 | 0.58 | 0.00 | 5.2 |
| **Tensor Fasciae Lata** | | 15.7 | 1.6 | 16.1 | 2.4 | 4.9 | 1.1 | 7.2 | 2.2 | 0.60 | 0.01 | 9.0 |
| [a] **Rectus femoris** | | 31.1 | 2.1 | 33.3 | 1.7 | 10.6 | 1.6 | 14.2 | 1.6 | 0.58 | 0.00 | 4.6 |
| [a] [b] **Gracilis** | | 31.0 | 2.7 | 33.8 | 2.5 | 3.4 | 0.6 | 4.7 | 0.8 | 0.65 | 0.01 | 5.0 |
| [a] [b] **Sartorius** | | 46.5 | 1.4 | 50.8 | 2.1 | 2.8 | 0.5 | 4.1 | 0.6 | 0.77 | 0.00 | 4.7 |
| [a] [b] **Biceps femoris breve** | | 21.5 | 1.9 | 24.5 | 2.0 | 5.0 | 0.8 | 8.2 | 1.5 | 0.57 | 0.01 | 8.8 |
| [b] **Biceps femoris longum** | | 26.0 | 2.6 | 27.1 | 2.2 | 9.3 | 1.4 | 12.8 | 1.7 | 0.53 | 0.00 | 7.1 |
| [a] [b] **Semi-membranosus** | | 26.1 | 1.6 | 28.4 | 1.1 | 10.1 | 1.6 | 13.0 | 2.0 | 0.60 | 0.01 | 6.7 |
| **Semi-tendinosus** | **R:** | 30.7 | 2.9 | 31.6 | 3.4 | 7.1 | 1.3 | 11.0 | 1.8 | 0.58 | 0.01 | 7.4 |
| | **L:** | | | | | 7.0 | 1.8 | 10.1 | 1.2 | | | |
| [a] [b] **Femur** | | 44.5 | 1.5 | 49.1 | 1.7 | 33.8 | 3.5 | 42.6 | 3.5 | - | - | - |

Table 7.2. Means and standard deviations (1*SD) of length (L), maximal axial cross-sectional area ($A_{max}$) and shape factor ($S_p$), for females and males. [a] (respectively [b]) means that statistical differences between males and females were found for L , for the right side of the muscle (resp. for the left side). Root mean square error (RMSE), between estimated volume (from average shape factor) and real volume is in % of the real volume.

| | Group | | Females | | | Males | | |
|---|---|---|---|---|---|---|---|---|
| | | | Mean | SD | CV (%) | Mean | SD | CV (%) |
| **$V^{gp}$ ($cm^3$)** | **Spine Flex** | **R** | 287.4 | 38.0 | 13.2 | 518.4 | 49.0 | 9.5 |
| | | **L** | 294.4 | 36.5 | 12.4 | 511.2 | 40.1 | 7.9 |
| | **Spine Ext** | **R** | 328.1 | 48.2 | 14.7 | 482.5 | 53.7 | 11.1 |
| | | **L** | 330.6 | 52.4 | 15.8 | 485.7 | 61.4 | 12.6 |
| | **Hip Flex** | **R** | 1351.9 | 145.2 | 10.7 | 2176.7 | 160.6 | 7.4 |
| | | **L** | 1358.7 | 154.9 | 11.4 | 2130.2 | 190.0 | 8.9 |
| | **Hip Ext** | **R** | 1072.0 | 124.0 | 11.6 | 1538.0 | 138.8 | 9.0 |
| | | **L** | 1082.1 | 128.0 | 11.8 | 1535.7 | 144.7 | 9.4 |
| | **Knee Flex** | **R** | 636.1 | 76.6 | 12.0 | 980.3 | 96.1 | 9.8 |
| | | **L** | 639.5 | 78.3 | 12.3 | 968.0 | 104.7 | 10.8 |
| | **Knee Ext** | **R** | 1319.7 | 138.8 | 10.5 | 1927.1 | 162.0 | 8.4 |
| | | **L** | 1337.6 | 163.0 | 12.2 | 1907.8 | 103.0 | 5.4 |
| **$R_{flex\_ext}$** | **Spine** | **R** | 0.9 | 0.1 | 15.7 | 1.1 | 0.1 | 13.2 |
| | | **L** | 0.9 | 0.2 | 16.8 | 1.1 | 0.1 | 12.8 |
| | **Hip** | **R** | 1.3 | 0.1 | 7.8 | 1.4 | 0.1 | 6.9 |
| | | **L** | 1.3 | 0.1 | 8.6 | 1.4 | 0.1 | 5.2 |
| | **Knee** | **L** | 0.5 | 0.0 | 8.7 | 0.5 | 0.0 | 8.8 |
| | | **R** | 0.5 | 0.0 | 6.7 | 0.5 | 0.0 | 7.0 |

Table 7.3. Means; standard deviations (SD) and coefficient of variation (CV=SD*100/mean) of functional groups' volume ($V^{gp}$) and functional groups' ratio flexors/extensors ($R_{flex\_ext}$), for females and males, for right and left sides. No significant differences were found between right and left sides. Males' and females' values were reported separately to account for differences found in volume for each individual muscle.

Statistical differences between sexes were found for all muscles and femur, for $A_{max}$, V, $V_H$ (overall greater values for males). Even when considering normalized volume by the subject's height ($V_H$), males present greater volumes than females: average 1.9$cm^2$ vs 1.4$cm^2$; range 0.3-6.6$cm^2$ vs 0.2-5.0$cm^2$. For L (respectively $RV_{tot}$), significant differences were found between sexes for both sides for: gluteus maximus/medius, vastus lateralis inter, gracilis, sartorius, biceps femoris breve, semi-membranosus, femur; for the right gluteus minimus and rectus femoris; and for the left vastus medialis, biceps femoris longum, and erectus spinae, (respectively for both sides of the iliopsoas; for the right gluteus maximus and biceps femoris breve and for the left quadratus lumborum). No statistical differences between sexes were found for $S_p$.

Ratio of a given muscle's volume over the total volume ($RV_{tot}$) was found as quasi-invariant for all muscles (SD<1.2%).

Table 7.3 presents means, SD and CV of muscular groups' volumes $V^{gp}$ and ratio of flexors vs extensors $R_{flex\_ext}$. For each muscular functional group studied, for males and females separately, no statistical difference between right and left sides, was found for the volumes $V^{gp}$ (p>0.05 for Student T-test or Mann-Whitney test depending on normality of data).

### 7 - 4.3 Alternative estimations of the muscular volume

#### 7 - 4.3.1 Maximal Section Method

Table 7.2 presents mean and SD of $S_p$ for each muscle and the prediction error (RMS). For most muscles the RMS was less than 10%, except for gluteus minimus (11.9%) and quadratus lumborum (17.7%).

#### 7 - 4.3.2 Reduced MRI set Method

Figure 7.2 presents the best combination of slices. Single couple of slices, well chosen, at femoral and pelvic level, led to volume estimation with less than 15% of error. The 5 slices model prediction error (in % of the real volume computed from 3D reconstruction) ranged from 6% ($Knee_{flex}$, $Knee_{ext}$ and $Spine_{flex}$) to 11% ($Spine_{ext}$), this error being around 9-10% for $Hip_{flex}$ and $Hip_{ext}$. Equations predicting the volume are presented in Tables 7.4 and 7.5.

| **Coefficients** | **Hip** | | **Knee** | |
|---|---|---|---|---|
| | *Flexors* | *Extensors* | *Flexors* | *Extensors* |
| **Constant** | - 191.9 | - 73.0 | - 193.1 | - 294.8 |
| **A** | 40.2 | 36.6 | 21.6 | 21.6 |
| **B** | 33.4 | 33.4 | 18.2 | 22.5 |

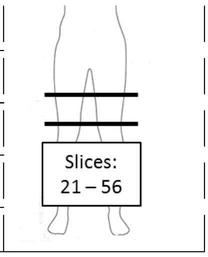


Table 7.4. For each muscular group, coefficients of the predictors in column. Equation to predict the muscular volume of a functional group using slices numbering as detailed in Figure 7.2 (Volume in $cm^3$; Area in $cm^2$; Constant in $cm^3$; A, B in cm): *Volume = **Constant** * 1 + **A** * Area_slice21 + **B*** Area_slice56*. Area_slice_N corresponds to the sum of the areas of the muscles labeled in the functional group studied, on the slice N (in $cm^2$).

| **Coefficients** | **Spine** | |
|---|---|---|
| | *Flexors* | *Extensors* |
| **Constant** | - 465.6 | - 24.4 |
| **A** | 11.3 | 0 |
| **B** | 8.0 | 5.5 |
| **C** | - 0.8 | 2.5 |
| **D** | 14.9 | 12.1 |

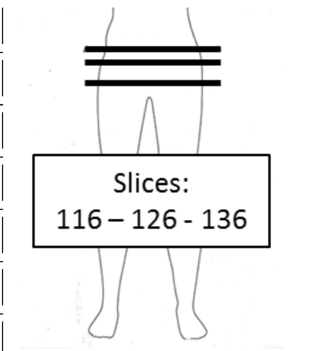


Table 7.5. For each muscular group, coefficients of the predictors in column. Equation to predict the muscular volume of a functional group using slices numbering as detailed in Figure 7.2 (Volume in $cm^3$; Area in $cm^2$; Constant in $cm^3$; A, B in cm): *Volume = **Constant** * 1 + **A** * Femoral_length + **B** * Area_slice116 + **C*** Area_slice126 + **D*** Area_slice136*. Area_slice_N corresponds to the sum of the areas of the muscles labeled in the functional group studied, on the slice N (in $cm^2$).

## 7 - 5 Discussion

This study reports reference values of muscular volume, length and cross-sectional areas for young asymptomatic subjects, providing baseline values for future studies and more additional findings. Ratio of a given muscle volume vs total volume was found quasi-invariant for asymptomatic young adults.

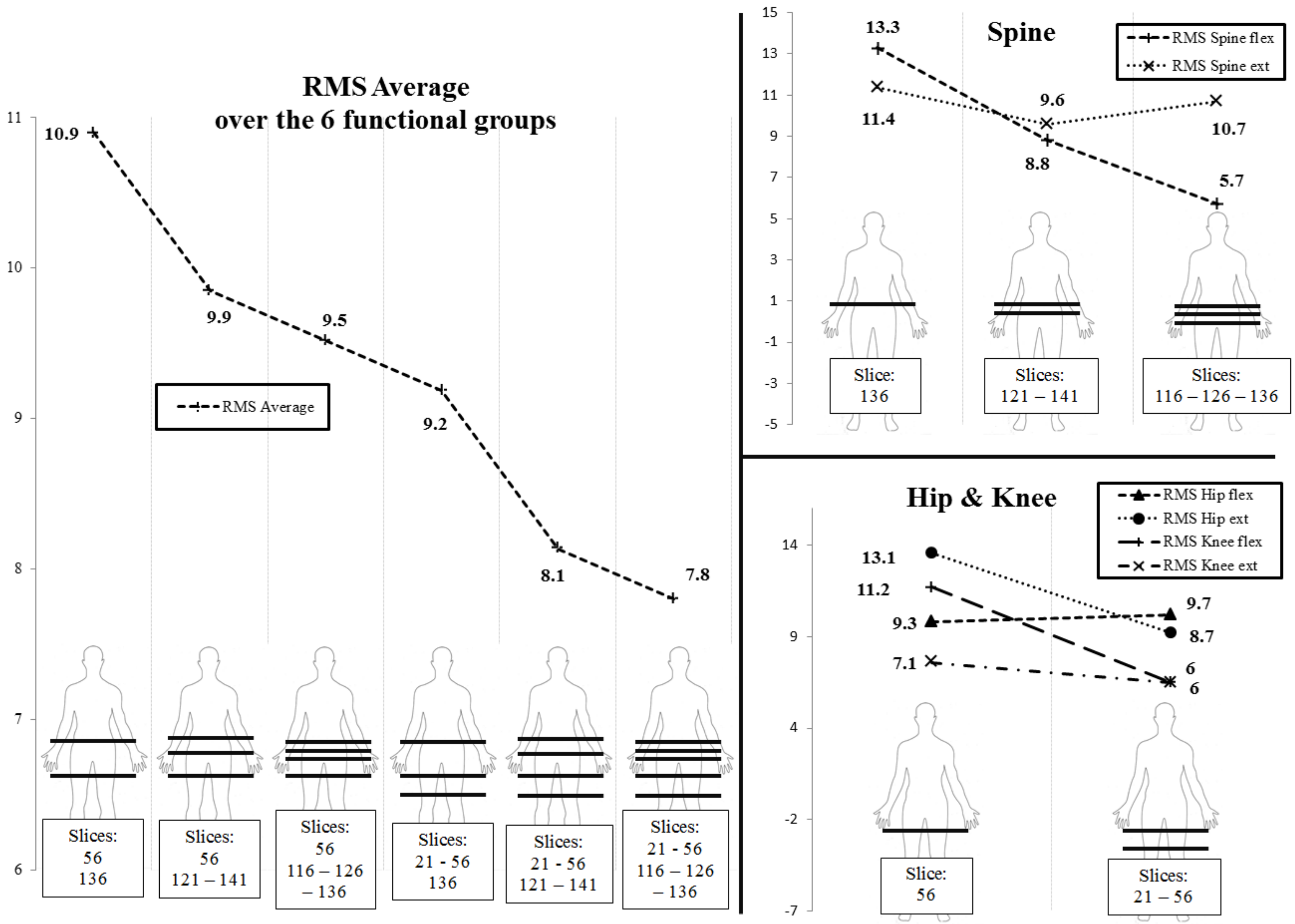


Figure 7.2. : RMS (root mean square) error for each functional group and on average over the 6 groups (« RMS Average »), for the different slices combinations.

A reduced set of 2 (respectively 5) segmented slices, well chosen, can be used to compute muscular volume with less than 14% of error (respectively 11%) (Figure 7.2).

This work comes with limitations. First, only 23 subjects were included in the study however as they were all aged between 18 and 24 years old, and as they all come from the same environment (medical students), the variability in their muscular system should be low. The small age range was an objective to better characterize the young asymptomatic population, however further studies should quantify age-related changes by recruiting volunteers from different age groups. A second limitation is the focus made on the characterization of the muscles' geometry, not considering the muscle quality, measured by the fat infiltration for example that remains an important parameter to describe the muscular system. Fat infiltration can be evaluated from MRI images acquired with the Dixon method (Moal *et al.*, 2015), this was the case in our study and associated data are currently under analysis. A third limitation is the consideration of the anatomical cross sectional area and not the physiological one: pennation angles of muscles were not considered as only axial slices were studied. In addition, some muscles were grouped because of borders' lack of visibility. Other studies reported this issue particularly considering the border between the vastus lateralis and vastus intermedius (Barnouin *et al.*, 2014) suggesting to group the two muscles together because of frequent fusion in young adults. Similar grouping was made to build up the adductor group, erector spinae group and iliopsoas group. While the last group is widely considered as such in the literature (Lube *et al.*, 2016; Sanchis-Moysi *et al.*, 2011; Ghiasi *et al.*, 2016), grouping muscles comes from the difficulty to identify proper border between muscles of this group, this difficulty is enhanced here by the inclusion of young healthy students presenting little fat between aponeurosis of different muscles (Barnouin *et al.*, 2014). This study did not include the small external hip rotators as choice was made to consider muscles frequently used in the sagittal postural maintenance as part of a wider project. These small muscles should however be included in a future finer study. It must be kept in mind however that grouping muscles will reduce the ability to quantify precisely these muscles' characteristics and therefore to provide basic values for comparison with other populations. Nevertheless, this study's objective was to provide a first global database for these muscles, and a clinical-user-friendly tool to estimate global muscular group's volume and estimate quantitatively muscular changes. The model using reduced set of MRI segmented slices has been built on right side data of subjects. The equations of the model have been applied on the left side and resulted in similar RMS errors (less than 1% difference), except for the spine flexors (13.5% for the left side vs 5.7% for the right side).

With these points in mind, the first objective of this study was to report reference values for spino-pelvic muscles' geometry, for young asymptomatic subjects, as few studies in the literature reported some of these values. Considering the cross-sectional area (CSA), our values are greater than the ones reported by Rasch *et al.* (Rasch *et al.*, 2007) but of the same order of magnitude: this can be due to the difference in the population studied: we included young asymptomatic subjects whereas their data come from the healthy limb of people planned for unilateral total hip replacement (Table 7.2). Another reason for the difference observed can be that we reported the maximal CSA, contrary to Rasch *et al.* reporting CSA at the distal femoral level (Rasch *et al.*, 2007). To our knowledge, no values were reported for the length of these muscles from axial images. The volume ratio, in percentage of total volume, was found similar to the values reported by Südhoff *et al.* (Südhoff *et al.*, 2009) for the lower limb's muscles. We also reported an invariance of this volume ratio between subjects (SD less than 1.2%) (Table 7.1). This parameter would be particularly interesting when studying altered muscles of elders or patients.

Considering muscular volume, comparison can be made with some previous studies from the literature (Barnouin *et al.*, 2014; Lube *et al.*, 2016; Handsfield *et al.*, 2014; Belavý *et al.*, 2011): overall our findings are in line with these results. Looking into more details to the iliopsoas, for the men, our findings are greater than those of Lube *et al.* (Lube *et al.*, 2016) and Handsfield *et al.* (Handsfield *et al.*, 2014): 515cm$^3$ vs between 442 and 452cm$^3$ for these studies. For the women, our results are greater (291cm$^3$) than Lube's (252 to 268cm$^3$) (Lube *et al.*, 2016) but lower than Handsfield's (452cm$^3$) (Handsfield *et al.*, 2014). Differences can be due to differences in the population studied (higher BMI, wider age range etc...): for example, Handsfield *et al.* reported values for 24 healthy participants (with only 8 females) (Handsfield *et al.*, 2014), and Lube *et al.*'s study (Lube *et al.*, 2016) included only 3 females and 3 males. All these comments could also apply to differences observed with these studies for the adductor group and biceps femoris. For the latter, Lube *et al.* already reported large variation of its volume across different populations, difference in the participants of each study could explain these differences (maximal difference of 47cm$^3$ for men) with Lube's data (Lube *et al.*, 2016).

Moal *et al.* (Moal *et al.*, 2015) reported muscular volume for the same functional groups as this study did, but including patients with adult spinal deformities: overall, the muscles studied presented a greater volume in the young asymptomatic group of this study. This agrees with the general and documented knowledge of sarcopenia (loss of skeletal mass) occurring with aging (Ahmed *et al.*, 2005; Frontera *et al.*, 2000; Narici *et al.*, 2003) as well as muscular degradation occurring with spinal pathologies (Gildea *et al.*, 2013; Parkkola *et al.*, 1993).

No major asymmetry was reported between right and left volumes of individual muscles. In comparison, previous studies have reported a limited role of multifidi volume asymmetry in prediction of low back pain syndrome (Fortin *et al.*, 2015). Fortin *et al.* reported a threshold of 10% of asymmetry to be the limit before abnormality (Fortin *et al.*, 2014): the asymmetries found in this study were less than 12% which confirm our population as a reference group, in addition to its young age.

Considering the muscular groups' volumes, sex's differences were found (Table 7.3). As for the shape factor, the methodology described here was based on the study of Mersmann *et al.* (Mersmann *et al.*, 2014) on lower leg's muscles. Still, we found similar variability of the shape factor as they did: maximum SD found here = 0.04 vs 0.04 (untrained subjects) and 0.05 (endurance athletes) as reported by Mersmann et al (Mersmann *et al.*, 2014) (Table 7.2). One can note that the maximal variability between subjects for the shape factor was reported here for the quadratus lumborum, this can be explained by its short length (Table 7.1): as it is visible on few slices with an irregular shape along the proximal-distal axis, it is difficult to characterize it by the same equation for all subjects. The use of this shape factor appears as adapted to compute muscle volume for most muscles (RMS <10%), but is not adapted for short muscles: gluteus minimus (RMS= 11.9%), quadratus lumborum (RMS= 17.7%) (Table 7.2).

Among all models studied (from 2 to 5 slices), the 2 slices model provided a gross estimation of muscular volume (Figure 7.2: average RMS=10.9%). The 5 slices model is a possible compromise between accuracy and analysis time in a routine environment, while the whole 3D model could be more appropriate for research, particularly when considering the spine extensors (RMS<8% for the average over the 6 functional groups (Figure 7.2)). This model uses a combination of 2 "distal slices" and 3 "proximal slices". Two "distal slices" are required: one near the distal end of the femur (slice 21) to estimate volume of specific muscles (semi-membranosus and biceps femoris breve for example); one mid-way on the diaphysis (slice 56) to better evaluate the great thigh muscles' (adductor, vastus, rectus femoris for example). The three "proximal" slices (slices 116, 126 and 136) are located between the acetabulum and T12 to estimate the volume of spine flexors and extensors: these slices are close to each other (10 slices apart) to focus on an area with segmentation for all the 3 muscles of interest (iliopsoas, erector spinae and quadratus lumborum) but also to estimate volume of a small and changing muscle in shape: the quadratus lumborum. In addition, the model is not sensitive to the exact position of the slice suggested in the model: using a slice positioned +/- 5 slices above or below, changes the averaged RMS by 1.5% maximum. Therefore, if validated on other populations, this method could be implemented in clinical routine for muscles characterization.

The two methods presented to compute muscular volume from little information are of same accuracy (RMS around 10% for both), but differ in their implementation: if the shape factor is useful for an individual muscle, the 5 slices model can compute volume of muscle groups. Both however gains time during analysis of MRI images (reconstruction time fairly reduced: 5 slices segmented vs more than 120 slices for total 3D reconstruction).

Different levels of analysis may be needed for characterizing muscular geometry: in clinical routine, a rapid method could provide a global insight of the patients' muscles, while in research, a longer method can be considered to obtain a finer analysis. If the DPSO method is the current method providing the most relevant estimation of each individual muscle's geometry, a new method has been proposed here for use in a clinical environment: it is less time-consuming and provides still a good estimation of functional groups' muscular volumes.

The current model appears promising for clinical routine to quantify muscular volume of functional groups. This model still needs to be validated on other populations (older adults, patients), and when validated, could provide a clinical-user-friendly tool to determine quantitatively the muscular degradation of patients / volunteers.

In conclusion, our study provided a database for geometrical parameters of spino-pelvic muscles for young asymptomatic adults. A new model computing the functional groups' muscular volume has been proposed and appears promising in estimating muscular volume of volunteers / patients.

## 7 - 6 Additional analysis and discussion

Prediction of gluteus minimus and gluteus medius volumes from a reduced set of slices was also investigated. As gluteus minimus is a short muscle, it was present only a limited number of slices: this required the addition of 1 slice to the model of 2 to 5 slices already presented.

As the gluteus medius was present on slices already included in the model no additional slice was required for this muscle. In addition, because the additional slice required for gluteus minimus could be a slice where gluteus medius was visible, the slice number 111 was chosen as the best one to combine best prediction of gluteus minimus volume (prediction error of 13.4% of the real 3D volume) and presence on the slice of gluteus medius. As for the gluteus medius, using only slice 111 lead to a prediction error of 7.1%; combination of slices 111 and 116 lead to a prediction error of 6.5% and combination of slices 111 and 121 lead to a prediction error of 6.0%. Table 7.6 presents the different reduced set of slices models with their respective prediction errors according to muscles considered.

No major increase of the mean prediction error was observed, when including the gluteus minimus and medius in the model: 10.7% now for the model at 3 slices (among which 1 is for gluteus minimus and gluteus medius) vs 10.9% before for the model with 2 slices. In addition, only 2 muscles were added: both reconstructed on 1 additional slice, and one of them reconstructed on 1 already included slice. Reconstruction of these 2 muscles on 1 or 2 slice(s) did not significantly increase reconstruction time.

Tables B.1, B.2, B.3, B.4, B.5, and B.6 (Appendix B) present the equations for the different models in order to predict the volumes of the different functional groups. For knee extensors, knee flexors, hip extensors and hip flexors, 1 or 2 slices are considered (56 or 21+56). For spine extensors and flexors, 1 to 3 slices are considered (136 or 121 + 141 or 116+126+136). For gluteus minimus, only one slice is considered (111). For gluteus medius, 1 or 2 slices are considered (111 or 111+116 or 111+121).
Therefore including the gluteus minimus and medius in the model from a reduced set of slices is not time-consuming, and can be used in the future. As presented in the next chapter, these two muscles are important when focusing on compensatory mechanisms occurring during aging or evolution of a pathology.

| **Slice(s)** | **56** | **56** | **56** | **21 + 56** | **21 + 56** | **21 + 56** |
|---|---|---|---|---|---|---|
| Hip flexors | 9.4 | 9.4 | 9.4 | 9.7 | 9.7 | 9.7 |
| Hip extensors | 13.1 | 13.1 | 13.1 | 8.7 | 8.7 | 8.7 |
| Knee flexors | 11.2 | 11.2 | 11.2 | 6.0 | 6.0 | 6.0 |
| Knee extensors | 7.1 | 7.1 | 7.1 | 6.0 | 6.0 | 6.0 |
| **Slice(s)** | **111** | **111** | **111** | **111** | **111** | **111** |
| Gluteus minimus | 13.4 | 13.4 | 13.4 | 13.4 | 13.4 | 13.4 |
| **Slice(s)** | **111** | **111 + 121** | **111 + 116** | **111** | **111 + 121** | **111 + 116** |
| Gluteus medius | 7.1 | 6.0 | 6.5 | 7.1 | 6.0 | 6.5 |
| **Slice(s)** | **136** | **121 + 141** | **116 + 126 + 136** | **136** | **121 + 141** | **116 + 126 + 136** |
| Spine flexors | 13.3 | 8.8 | 5.7 | 13.3 | 8.8 | 5.7 |
| Spine extensors | 11.4 | 9.6 | 10.7 | 11.4 | 9.6 | 10.7 |
| **Slice(s)** | **56 + 111 + 136** | **56 + 111 + 121 + 141** | **56 + 111 + 116 + 126 + 136** | **21 + 56 +111 + 136** | **21 + 56 + 111 + 121 + 141** | **21 + 56 + 111 + 116 + 126 + 136** |
| **Mean** | **10.7** | **9.8** | **9.6** | **9.5** | **8.5** | **8.3** |
| **# of slices** | **3** | **4** | **5** | **4** | **5** | **6** |

Table 7.6. : Prediction errors (in % of real 3D volume) for the different muscular groups and the different models from 3 to 6 slices

# CHAPTER 8

# SPINO-PELVIC MUSCLES OF ASD PATIENTS VS VOLUNTEERS

## 8 - 1 Introduction

While recent studies have demonstrated that muscles are crucial in the setting of postural regulation (Gildea *et al.*, 2013; Lee *et al.*, 2008; Parkkola *et al.*, 1993; Rasch *et al.*, 2007), most of these studies have been limited to specific muscles of symptomatic patients only. This study's objective is to compare spino-pelvic muscular volume of adults with spinal deformities (ASD) to a reference population. This would help to better understand potential compensatory mechanisms occurring during pathological evolution of the posture.

## 8 - 2 Methods

### 8 - 2.1 Participants

Group Y included young asymptomatic females (population studied in chapter 7). Group P included pre-operative female ASD patients over 35 years old with at least one of the following criteria concerning spinal deformity: Thoraco-lumbar or lumbar coronal Cobb angle >30°, Sagittal Vertical Axis >4cm, or Pelvic Tilt >20°. Group P have already been studied in a study published in 2015 (Moal *et al.*, 2015).

### 8 - 2.2 MRI analysis

All subjects underwent MRI acquisition from T12 to the knee, following the same protocol as described in chapter 7. Spino-pelvic muscles were segmented to compute muscle volume from 3D reconstruction, using the same method as described in chapter 7.

### 8 - 2.3 Statistical analysis

Muscles were grouped into functional groups (flexors and extensors) of spine, hip and knee (Figure 7.1). The volume of each functional group and the ratio ($R_{flex/ext}$) of the flexors' volume over the extensors' volume were computed for both Y and P groups. Normality of the volume and ratio ($RV_{tot}$) of each muscle's volume over total muscular volume, for muscles' groups and individual muscles were studied with a Lilliefors test (Lilliefors, 1967).
For each individual muscle, the volume and the ratio were compared between the Y and P groups, and statistical difference were investigated with a Student test when both Y and P groups' data were found to be drawn from a normal distribution, using the Mann-Whitney test otherwise.

## 8 - 3 Results

Group P included 19 female ASD patients: mean age: 60.1 years old (SD=12.7 years old); range: 37-80 years old. Group Y included 12 young asymptomatic females: mean age: 19.3 years old (SD=0.9 years old); range: 18-21 years old.

Patients of Group P presented a mean T2-T12 thoracic kyphosis of 51° (SD: 22°), a mean L1-S1 lordosis of -54° (SD: 15°), a mean SVA of 19mm (SD: 56mm), a mean pelvic incidence of 55° (SD: 14°), a mean pelvic tilt of 23° (SD: 12°), a mean maximal Cobb angle of 42° (SD: 16°).

All volumes and ratios were found to be drawn from a normal distribution with the exception of:

- for Group P, the volume of left gluteus maximus (p=0.02) and left gluteus minimus (p=0.02);
- for Group P, the $RV_{tot}$ of right vastus lateralis and intermedius (p=0.04), right biceps femoris breve (p=0.01) and right tensor fasciae lata (p=0.04); for Group Y of right iliopsoas (p=0.04) and left gluteus minimus (p=0.04).

For most of the muscles, means, standard deviations and Student t-test were used for sample's description. For the particular muscles listed above, medians, quartiles and Wilcoxon test were used.

## 8 - 3.1 Comparison for muscles functional groups

### 8 - 3.1.1 Volumes

Table 8.1 illustrates the comparison between subjects of Groups Y and P. Reported results are the differences, for each functional group considered, between mean volumes of Groups Y and P (expressed in % of the mean volume of Group Y). P-values of the Student t-test, to test for statistical difference of the means, are also reported in the table. Significant differences between both populations were reported for the left spine flexors (mean difference of -13.6%) and knee extensors (right :-18.1%; left: -21.5%).

| **RIGHT Functional Group** | **Spine Flexors** | **Spine Extensors** | **Hip Flexors** | **Hip Extensors** | **Knee Flexors** | **Knee Extensors** |
|---|---|---|---|---|---|---|
| **Mean (SD)** in $cm^3$ | 253.6 (48.9) % | 297.4 (60.8) % | 1224.6 (239.1) % | 994.8 (206.8) % | 591.1 (117.4) % | 1080.3 (253.1) % |
| **Difference of means** | - 11.8 % | - 9.4 % | - 9.4 % | - 7.2 % | - 7.1 % | - 18.1 % |
| **P-value of Student t-test** | 0.05 | 0.15 | 0.11 | 0.25 | 0.25 | 0.01 * |

| **LEFT Functional Group** | **Spine Flexors** | **Spine Extensors** | **Hip Flexors** | **Hip Extensors** | **Knee Flexors** | **Knee Extensors** |
|---|---|---|---|---|---|---|
| **Mean (SD)** in $cm^3$ | 254.2 (56.8) % | 293.5 (64.3) % | 1214.2 (243.2) % | 1003.8 (223.3) % | 603.8 (130.2) % | 1050.3 (257.5) % |
| **Difference of means** | - 13.6 % | - 11.2 % | - 10.6 % | - 7.2 % | - 5.6 % | - 21.5 % |
| **P-value of Student t-test** | 0.04 * | 0.10 | 0.08 | 0.28 | 0.40 | 0.00 * |

Table 8.1. : Comparisons of volumes of functional groups, between Groups P and Y: mean and standard deviation (SD) of Group P; difference of means (in % of Group Y mean) and p-values of the Student t-test (* means $p<0.05$, which means statistical difference).

### 8 - 3.1.2 Ratio of volume of flexors over volume of extensors: $R_{flex/ext}$

Table 8.2 reports the differences, for each functional group considered, between mean ratios ($R_{flex/ext}$) of Group Y and P (expressed in % of the mean ratio of Group Y). P-values of the Student t-test to test for statistical difference of the means are also reported in the table. Significant difference between both populations was reported for right (+15.1%) and left knee ratio (+22.3%).

| RIGHT Joint considered | Spine | Hip | Knee |
|---|---|---|---|
| **Mean (SD)** (no unit) | 0.9 (0.2) | 1.2 (0.1) | 0.6 (0.1) |
| **Difference of means** | - 2.1 % | - 1.9 % | 15.1 % |
| **P-value of Student t-test** | 0.74 | 0.60 | 0.01 * |

| LEFT Joint considered | Spine | Hip | Knee |
|---|---|---|---|
| **Mean (SD)** (no unit) | 0.9 (0.2) | 1.2 (0.1) | 0.6 (0.1) |
| **Difference of means** | - 2.5 % | - 3.0 % | 22.3 % |
| **P-value of Student t-test** | 0.73 | 0.42 | 0.00 * |

Table 8.2. Comparisons of Ratio of volume of flexors over volume of extensors ($R_{flex/ext}$) of functional groups, between Groups P and Y: mean and standard deviation (SD) of Group P; difference of means (in % of Group Y mean) and p-values of the Student t-test (* means $p<0.05$, which means statistical difference).

## 8 - 3.2 Comparison for each individual muscle

Table 8.4 and Table 8.3 report the differences, for each functional group considered, between mean volumes and ratios of Group Y and P (expressed in % of the mean volume/ratio of Group Y). P-values of the Student test to test for statistical difference of the means are also reported in the tables.

### 8 - 3.2.1 Volumes

When comparing Group P to Group Y, all muscles present a loss of volume except for gluteus medius right (mean difference of +2.6%) and left (+1.5%); gluteus minimus right (+8.6%) and left (+12.4%); tensor fasciae lata right (+2.9%) and left (+8.5%) and left biceps femoris breve (+0.4%).

### 8 - 3.2.2 Ratio of volume over total volume: $RV_{tot}$

Statistical differences ($p<0.05$) were found only for individual muscles' ratio $RV_{tot}$ of gluteus medius right and left (p=0.00); right gluteus minimus (p=0.02); vastus lateralis and intermedius right and left (p=0.00); left vastus medialis (p=0.01); rectus femoris right and left (p=0.00).

| | Muscle | Gluteus maximus | | Gluteus medius | | Gluteus minimus | |
|---|---|---|---|---|---|---|---|
| | **Side** | **Right** | **Left** | **Right** | **Left** | **Right** | **Left** |
| **Volume** | **Mean (SD) (cm$^3$)** | 553.8 (134.6) % | 555.1 (118.6) % # | 244.7 (51.1) % | 238.0 (49.2) % | 82.3 (21.8) % | 86.3 (14.1) % # |
| | **Diff. of Means** | -7.9 % | - 10.3 % # | 2.6 % | 1.5 % | 8.6 % | 12.4 % # |
| **$RV_{tot}$** | **Mean (SD)** | 14.6 (2.1) % | 14.7 (2.2) % | 6.5 (0.7) % | 6.4 (0.7) % | 2.2 (0.4) % | 2.0 (0.2) % # |
| | **Diff. of Means** | 2.2 % | 2.2 % | ***14.2 %*** | ***15.5 %*** | ***18.4 %*** | 10.2 % # |

Table 8.3. Results for gluteal muscles: differences (Diff.) of means, for both volume and volumic ratio $RV_{tot}$. # means the muscular group's volume or volumic ratio did not follow a normal distribution and therefore medians (respectively difference 3rd quartile - 1st quartile; resp. Mann-Whitney test) were used instead of means (resp. standard deviation; resp. Student t-test). Italic bold values means statistical difference ($p<0.05$).

| Muscle | | Iliopsoas | | Quadratus lumborum | | Erectus spinae | | Adductor | | Tensor fasciae lata | | Vastus lat. inter. | | Vastus medialis | |
|---|---|---|---|---|---|---|---|---|---|---|---|---|---|---|---|
| Side | | Right | Left | Right | Left | Right | Left | Right | Left | Right | Left | Right | Left | Right | Left |
| Volume | M. (SD) | 253.6 (48.9) % | 254.2 (56.8) % | 25.4 (7.4) % | 29.3 (7.9)% | 272.0 (57.8) % | 264.2 (60.1) % | 631.2 (140.7) % | 621.3 (134.8) % | 47.7 (19.0) % | 49.0 (18.6) % | 674.6 (150.3) % | 661.2 (162.2) % | 263.8 (76.0) % | 252.1 (68.7) % |
| Volume | Diff. of Means | - 11.8 % | - 13.6 % | ***- 24.7 %*** | ***- 18.5 %*** | - 7.6 % | - 10.3 % | - 4.7 % | - 6.3 % | 2.9 % | 8.5 % | ***- 17.4 %*** | ***- 20.6 %*** | - 15.6 % | ***- 20.5 %*** |
| $RV_{tot}$ | M. (SD) | 7.0 (0.3) % # | 6.8 (0.8) % | 0.7 (0.2) % | 0.8 (0.2) % | 7.3 (1.3) % | 7.2 (1.3) % | 16.6 (1.6) % | 16.6 (1.4) % | 1.3 (0.3) % # | 1.4 (0.6) % | 17.7 (1.7) % # | 17.6 (2.0) % | 6.9 (1.1) % | 6.7 (0.9) % |
| $RV_{tot}$ | Diff. of Means | 1.0 % # | - 2.2 % | - 14.4 % | - 6.0 % | 3.7 % | 2.7 % | 5.4 % | 6.1 % | 15.8 % # | 26.5 % | ***- 8.5 %*** # | ***- 10.4 %*** | - 7.1 % | ***- 11.1 %*** |

| Muscle | | Rectus femoris | | Gracilis | | Sartorius | | Biceps fem. breve | | Biceps fem. longum | | Semi-membranosus | | Semi-tendinosus | |
|---|---|---|---|---|---|---|---|---|---|---|---|---|---|---|---|
| Side | | Right | Left | Right | Left | Right | Left | Right | Left | Right | Left | Right | Left | Right | Left |
| Volume | M. (SD) | 141.8 (34.5) % | 136.9 (31.9) % | 58.6 (18.2) % | 58.0 (16.6) % | 91.5 (21.4) % | 94.7 (24.4) % | 59.5 (17.2) % | 63.5 (18.7) % | 122.3 (33.4) % | 130.0 (41.4) % | 145.1 (39.2) % | 141.0 (33.9) % | 114.1 (24.8) % | 116.7 (32.3) % |
| Volume | Diff. of Means | ***- 25.5*** % | ***- 26.9*** % | - 11.9 % | - 12.7 % | - 7.2 % | - 7.2 % | - 1.6 % | 0.4 % | - 3.0 % | 0.0 % | - 6.4 % | - 8.2 % | - 11.8 % | - 6.1 % |
| $RV_{tot}$ | M. (SD) | 3.8 (0.6) % | 3.7 (0.4) % | 1.5 (0.3) % | 1.5 (0.3) % | 2.4 (0.4) % | 2.5 (0.4) % | 1.4 (0.3) % # | 1.7 (0.4) % | 3.2 (0.6) % | 3.4 (0.8) % | 3.8 (0.7) % | 3.8 (0.6) % | 3.1 (0.6) % | 3.1 (0.6) % |
| $RV_{tot}$ | Diff. of Means | ***- 17.3*** % | ***- 17.2*** % | - 3.5 % | - 1.8 % | 3.6 % | 5.2 % | 2.3 % # | 14.8 % | 7.1 % | 12.0 % | 2.8 % | 3.6 % | - 1.1 % | 6.8 % |

Table 8.4. Results for specific muscles: mean (M.) and standard deviation (SD) (in $cm^3$); differences (Diff.) of means, for both volume and volumic ratio $RV_{tot}$. # means the muscular group's volume or volumic ratio did not follow a normal distribution and therefore medians (respectively difference 3rd quartile - 1st quartile; resp. Mann-Whitney test) were used instead of means (resp. standard deviation; resp. Student t-test). Italic bold values means statistical difference ($p<0.05$).

### 8 - 3.3 Correlation of muscles volumes and ratio with radiographic parameters

Severity of the spinal deformity can be quantified by radiographic parameters such as sagittal vertical axis, pelvic tilt, difference pelvic incidence with lumbar lordosis and Cobb angle. Table 8.5 lists the significant correlations found for ASD patients, between radiographic parameters and individual muscles' volume (V); and between radiographic parameters and volumic ratio ($RV_{tot}$) As the muscles' data (volume and ratio) were not found as drawn from a normal distribution for all muscles, Spearman correlation was performed.

| Radiographic parameter | | Muscle | Spearman coefficient |
|---|---|---|---|
| **Mismatch PI-LL** | $\mathbf{RV_{tot}}$ | Biceps Femoris Longum | L: - 0.50 |
| **Pelvic Tilt (PT)** | $\mathbf{RV_{tot}}$ | Biceps Femoris Longum | R: - 0.49 / L: - 0.49 |
| | | Tensor Fasciae Lata | L: 0.46 |
| | | Sartorius | L: 0.46 |
| **Sagittal Vertical Axis (SVA)** | $\mathbf{RV_{tot}}$ | Vastus Medialis | R: -0.46 / L: - 0.49 |
| | | Sartorius | R: 0.73 / L: 0.64 |
| | | Biceps femoris Longum | L: - 0.51 |
| **Maximal Cobb Angle** | $\mathbf{RV_{tot}}$ | Rectus Femoris | R: 0.66 |
| | | Gluteus Maximus | L: -0.50 |
| | | Semi-tendinosus | L: 0.51 |
| **Mismatch PI-LL** | **V** | Erectus Spinae | L: - 0.49 |
| **Pelvic Tilt (PT)** | **V** | Iliopsoas | L: - 0.52 |
| | | Biceps Femoris Longum | R: - 0.49 / L: - 0.46 |
| **Sagittal Vertical Axis (SVA)** | **V** | Iliopsoas | R: - 0.46 |
| | | Vastus Medialis | R: - 0.54 |
| | | Biceps femoris Longum | R: - 0.48 |
| **Maximal Cobb Angle** | **V** | Rectus femoris | R: 0.57 |

Table 8.5. Significant ($p<0.05$) Spearman correlations between radiographic parameters and muscular volume (V) and volumic ratio ($RV_{tot}$), for patients with spinal deformities of Group P. R (L) means Right (Left). PI-LL is the difference between pelvic incidence (PI) and lumbar lordosis (LL)

Worsening of the pathology can be evaluated by an increase in pelvic tilt accounting for retroversion of the pelvis, an increase in sagittal vertical axis accounting for a forward flexion of the trunk and/or a large mismatch between pelvic incidence and lumbar lordosis. These changes were significantly associated (Table 8.5) with:

- decrease in $RV_{tot}$ of vastus medialis (both sides), and biceps femoris longum (both sides);
- increase in $RV_{tot}$ of tensor fasciae lata (left side), and sartorius (both sides);
- increase in volume of tensor fasciae lata (both sides);
- decrease in volume of iliopsoas (both sides), vastus medialis (right side) and biceps femoris longum (both sides).

Severity of the deformation in the coronal plane (increase of the maximal Cobb angle) was significantly correlated with:

- increase in $RV_{tot}$ of rectus femoris (right side), and semi-tendinosus (left side);
- decrease in $RV_{tot}$ of gluteus maximus (left side);
- increase in volume of rectus femoris (right side);

# 8 - 4 Discussion

Sarcopenia is the volumic loss of muscles occurring with aging. The population studied here included ASD patients older than the population of reference (mean age: 60 years old vs 19.3 years old). Therefore both effects of sarcopenia and of pathological degradation should be observed in the results. The use of the ratio volume over total volume is thus interesting to rule out the effect of sarcopenia in the results' analysis.

## 8 - 4.1 Spine Flexors and Extensors

Spine extensors' volume of both sides, and right Spine flexors' volume were smaller for Group P (non-significant difference). The ratio $R_{flex/ext}$ does not vary significantly between groups, but was smaller for Group Y: difference of means of -2.1% for right side and of -2.5% for left side.

### 8 - 4.1.1 Spine Flexors

Smaller volume of the iliopsoas (-11.8% for right and -13.6% for left) associated with an unchanged ratio of volume $RV_{tot}$ (less than 3% absolute change), is a sign of sarcopenia (decrease of volume) but no change can be observed due to the pathological condition of patients of Group P.

### 8 - 4.1.2 Spine Extensors

Smaller volume of the erectus spinae (-7.6% for right and -10.3% for left) is associated with a larger ratio of volume ($RV_{tot}$) (3.7% for right and 2.7% for left) for Group P. This can be explained by the effect of sarcopenia (decrease of muscular volume) but the increase in proportion within the muscular system (larger $RV_{tot}$) is the sign of the increased recruitment of the back muscles in order to limit the forward flexion of the trunk for patients with ASD.
Smaller volume of the quadratus lumborum (-24.7% for right and -18.5% for left) is associated with a smaller ratio of volume ($RV_{tot}$) (-14.4% for right and -6.0% for left), for Group P. The effect of sarcopenia (decrease of volume) and of pathology (decrease of $RV_{tot}$) is thus observed.

## 8 - 4.2 Hip Flexors and Extensors

While smaller volumes were reported for both Hip flexors and Hip extensors for both sides, for Group P, the ratio $R_{flex/ext}$ does not vary significantly between both groups: difference of means of -1.9% for right side and of -3.0% for left side.

### 8 - 4.2.1 Hip Flexors

Smaller volume of the iliopsoas (-11.8% for right and -13.6% for left), for group P, associated with an unchanged ratio of volume $RV_{tot}$ (less than 3% absolute change between both populations), is the sign of sarcopenia (decrease of volume) but no change can be observed due to the pathological condition of patients of Group P.

Rectus femoris, vastus lateralis and intermedius and vastus medialis present a significantly smaller volume associated with a significantly smaller ratio of volume ($RV_{tot}$) (except for the volume and volumic ratio of vastus medialis right).

A non-significantly larger volume and ratio $RV_{tot}$ were observed for both sides of tensor fasciae lata. This can be associated with the smaller volume and ratio observed for the rectus femoris as the tensor fasciae lata can be recruited in order to increase the contraction power and efficiency of this thigh muscle.

Smaller volume of the adductor (-4.7% for right and -6.3% for left) was associated with a larger ratio of volume $RV_{tot}$ (+5.4% for right and +6.1% for left). This is a marker of an increased activity compared to Group Y, but also highlights the effect of sarcopenia: forward flexion of the trunk destabilizes the body and to increase lateral stability, adductor muscles are recruited (larger $RV_{tot}$).

Mean volumes of gracilis and sartorius were smaller for Group P (non significant differences ranging from -12.7% to -7.2%) and were associated with a non significantly larger ratio ($RV_{tot}$) for the sartorius (+3.6% for right side and +5.2% for left side); contrary to the smaller ratio observed for gracilis (-3.5% for right side and -1.8% for left side).

### 8 - 4.2.2 Hip Extensors

This group includes: gluteus maximus, semi-membranosus, semi-tendinosus, biceps femoris longum and biceps femoris breve. If the first muscle is a large muscle presenting a large volume, generating movements of large amplitude, the others are characterized as Knee Flexors (see next paragraph for more details). Gluteus maximus volume was smaller (-7.9% for right and -10.3% for left) while volumic ratio was a little larger: +2.2% for both sides: this muscle is only affected by sarcopenia. Patients with spinal deformities may present limited locomotion due to pain and discomfort, this could explain the decreased recruitment of gluteus maximus (smaller volume and slightly smaller $RV_{tot}$).

## 8 - 4.3 Knee Flexors and Extensors

Significantly smaller volume was observed (for mean volume of Group P vs Group Y) for Knee extensors (for both sides) and is responsible for the significantly larger the ratio $R_{flex/ext}$ for Group P: difference of means of +15.1% for right side and of +22.3% for left side.

### 8 - 4.3.1 Knee Flexors

This group includes: gracilis, sartorius, semi-membranosus, semi-tendinosus, biceps femoris longum and biceps femoris breve. For all, the mean volume of Group P was smaller when compared to Group Y, between -1.6% and -12.7%; except for left biceps femoris breve (+0.4%) and left biceps femoris longum (+0%). The effect of sarcopenia is therefore visible for most of these muscles. As for the ones presenting a larger volume, the difference was less than 2%.
A larger ratio ($RV_{tot}$) from +2.3% to 14.8% was reported for all the knee flexors considered, except for gracilis right (-3.5%) and left (-1.8%) and right semi-tendinosus (-1.1%). One can note that none of these differences of volume/ratio were found to be significant between Group P and Group Y.
The tendency observed is that these muscles gained importance with little loss of volume: it can be explained by an hyperactivity in order to hold back the body while trunk shifts anteriorly: knee flexors stabilize postural position of the body for patients of Group P.

### 8 - 4.3.2 Knee Extensors

Rectus femoris, vastus lateralis and intermedius and vastus medialis present a significantly smaller volume associated with a significantly smaller ratio of volume ($RV_{tot}$).
For these muscles, smaller volumes can be explained by the effect of age; while smaller ratio is linked to the trunk position shifted anteriorly for the patients. Because of this forward flexion of the trunk, these muscles are shortened, and contract less, thus little recruitment lead to a smaller ratio.

### 8 - 4.4 Gluteal group

The gluteal group includes the gluteus minimus, gluteus medius and gluteus maximus.

Larger volume was found for gluteus minimus and medius. Both can be assimilated as hip extensors, even though the commonly admitted function is a lateral control of the movement in the coronal plane.

The third muscle of the gluteal group is the gluteus maximus, also a hip extensor and qualified as a propulsion muscle used for locomotion and movements of large amplitude (because of its large length and volume, and of its distal insertion on the femur). The gluteus minimus and medius, because of their shorter length and more proximal insertions on the femur, seem to contribute to the regulation of the pelvic position by small movements and not to locomotion: both gluteus medius and minimus can be qualified as muscles of postural control.

Loss of volume observed for the gluteus maximus (mean difference of -7.9% for the right side and -10.3% for the left side) can then be interpreted as the effect of sarcopenia and/or as a marker of less activity (reduced amplitude of femoral movements compared to the pelvis) of the patients. Volumic gains (gain of nominal volume and of volumic ratio) observed for the gluteus medius and minimus suggest a need for postural regulation of the position of the pelvis, with movements of small amplitude of the pelvis compared to the femur.

### 8 - 4.5 Correlation of muscles volumes and ratio with radiographic parameters

ASD patients present, with worsening of postural alignment, a worse degradation of knee extensors, and increased recruitment of the knee flexors (Table 8.5). This reinforces the idea of the compensation with knee flexors to limit forward flexion of the trunk. Even if significant correlations with increase of maximal Cobb angle was reported only for a decrease of volumic ratio of right rectus femoris, left gluteus maximus and left semi-tendinosus; the severity of the spinal deformity in the coronal plane could be linked to differences observed between muscles of right and left sides. This would need further investigation to analyze into more details, the possible impacts of the coronal deformity on the muscular degradation observed.

### 8 - 4.6 Comparison with the literature

Pathological evolution of the area of the hip and knee muscles have been reported by Rasch *et al.* (Rasch *et al.*, 2007). They reported, in the limb with osteoarthritis, a decrease of 10 to 20% in cross-sectional area for gluteus maximus, psoas, rectus femoris, vastii (lateralis, medialis and intermedius), hamstrings (biceps femoris breve and longum, semi-membranosus, and semi-tendinosus), and adductors. The only muscles for which such a decrease has not been observed is the gluteus medius and minimus. Smaller volumes have been reported, in this study, for all muscles except gluteus medius and gluteus minimus.

Frontera *et al.* reported in 2000, in a longitudinal study over 12 years, the effect of sarcopenia on the thigh and its muscles: in 12 years, decrease of the CSA occurred for the total thigh (-12.5%), for all thigh muscles (-14.7%), for rectus femoris (-16.1%) and for knee flexors (-14.9%) (Frontera *et al.*, 2000). Similar results were found here for rectus femoris and knee flexors in terms of volume: -25% for the rectus femoris and -7.1% and -5.6% for the knee flexors. Greater decrease of volume was found here for the rectus femoris compared to the knee flexors muscles: this might be the sign of compensation via knee flexors in the setting of patients with forward flexion of the trunk. The smaller volume for the rectus femoris can be caused by both sarcopenia and pathological evolution as the ratio was smaller as well: this muscle is one of the first to degrade if the trunk is shifted forward (lesser length of contraction might imply smaller contractions and then loss of volume and ratio).

Concerning the psoas major and rectus femoris, Takahashi *et al.* (2006) reported evolution of CSA in different age groups from 20 to 80 years old, for asymptomatic women. For comparison, when retaining only subjects aged 20-29 years old versus 50-69 years old, evolution of the CSA during aging is similar to the volume's evolution reported here. The iliopsoas volume was 12.0% smaller compared to 19% smaller volume for the psoas major as reported by Takahashi *et al.* (CSA approximately decreased from 991 $mm^2$ to 800 $mm^2$). Concerning the rectus femoris, a volume 26% smaller was found here, compared to a 17% smaller CSA as reported by Takahashi *et al.* (CSA approximately decreased from 4096 $mm^2$ to 3400 $mm^2$). If for the psoas the difference is of same order magnitude, it is not the case for the rectus femoris: this can be explained by the effect of the pathological condition of the Group P studied here, that adds to the effect of aging, reported by Takahashi *et al.* (2006).

### 8 - 4.7 Limitations

This study focused on the analysis of volume and volumic ratio of individual muscles and functional groups, in two different populations. It did not take into account the fat infiltration of muscles. However, different studies reported either qualitative (Kjaer *et al.*, 2007) or quantitative measures (Fortin *et al.*, 2015; Antony *et al.*, 2014) of the fat component in muscles from MRI images. This is of special interest to characterize the efficient section of a muscle: a muscle can degrade in quality (increased fat infiltration) without any apparent change in muscular volume. The fat infiltration quantification was not reported in the present study as the calibration needed to ensure accurate fat infiltration quantification remained an issue at this stage. Nevertheless the information of the muscle quality (fat infiltration) will be included in the modeling part of this PhD (part D).
No information was collected for patients (recruited in a previous study during the PhD of Bertrand Moal) on the origin of the pathology, no information was therefore available to establish if the deformity developed as a result of back pain or as a result of postural change to maintain static balance.

## 8 - 5 Conclusion

In conclusion, this study focused on the comparison of young asymptomatic adults and older adults with spinal deformities. Values for individual muscles and functional groups have been reported and compared, highlighting differences for the older group with spinal deformities.

In particular, the reported atrophy of the knee extensors for the Patients group can result from inactivity due to pain and discomfort during walking for example. Meanwhile, the observed larger volume of pelvic muscles may imply increased activity due to the pelvic position's regulation in response to postural difficulty.

While this study attempted to draw conclusions from these preliminary results, further data are needed to consolidate these conclusions and interpretations. A larger and more diverse cohort in the future could help confirm these results. Further study is needed in order to differentiate properly compensatory mechanisms linked to an asymptomatic aging and troubles linked to spinal deformities. Such a study is currently undergoing in collaboration with Cédric Maillot within his Master project.

Future research will need to include the fat infiltration component for the different populations in order to assess the degradation of the muscular quality with aging and pathological evolution. Such study will bring important knowledge on the prevention of muscular degradation in elders and patients.

Overall, this study is the first of its kind and may allow researchers and clinicians better understand which muscles are involved in the compensatory mechanisms presented by ASD patients.

# CONCLUSION

This part of the PhD thesis focused on a refined analysis of the spino-pelvic muscles of two populations: a population of reference (young asymptomatic adults) and a population of older subjects with adult spinal deformities (ASD).

Firstly, reference values were reported for spino-pelvic muscles of healthy adults. A model computing accurately the muscular volume of functional groups, from only 6 MRI segmented slices, was proposed. This method allows an accurate computation of the volume in a clinical routine.

Secondly, description of spino-pelvic muscles was reported for adults with spinal deformities. Comparison was made with the population of reference. Significant differences can be identified as linked to compensatory mechanisms observed for ASD patients: pelvic retroversion can be linked to the observed larger volume of the gluteus minimus and medius; knee flexion can be linked to the smaller volumic ratio of knee extensors, and larger volumic ratio of knee flexors.

These compensatory mechanisms occur to limit effect of the anterior shift of the trunk observed in these patients, thus recruiting specific muscles to increase stability of this position, even if others muscles are therefore less requested.

This part focusing on muscles' analysis from MRI images, highlighted the link between postural alteration and muscular changes. If these alterations and changes have been described in the two first parts of this PhD, interactions between skeletal and muscular systems cannot be studied from these works. Biomechanical musculo-skeletal modeling would give insights on these interactions during the regulation of an efficient posture.

That is why the third part of this PhD will present the adaptation and personalization of a biomechanical musculo-skeletal model to investigate the muscular recruitment pattern in different subjects, for different postures.

# Part D

# Musculo-skeletal modeling

# INTRODUCTION

Quantification of the postural alignment and muscular system changes occurring with aging was performed in the first two parts of this PhD thesis. If strong interaction takes place between these two systems, it is difficult to draw conclusions on the relationship between the two from the previous two parts of the PhD thesis. Musculo-skeletal modeling offers the possibility to combine the postural information with the muscular geometry.

To reach this goal, a model of muscular regulation is used in this third part. It is an adaptation of the model developed by Vincent Pomero during his PhD in 1999-2002 (Pomero *et al.*, 2002, 2004). The main hypothesis is that muscles act to protect the inter-vertebral joint by reducing resulting forces and moments at the level of the inter-vertebral disc to an acceptable limit, during all daily activities.

This model of muscular regulation aims to estimate, with a control loop approach, the muscular recruitment and the resulting inter-vertebral (IV) loads, given the net reaction forces and moments (resulting from gravity). In the following, the term loads indicates the 6 components of the load: postero-anterior shear force, lateral shear force, compressive force, lateral bending moment, flexion moment and torsion moment.

The loads of the inter-vertebral joint (called $L_{IV\_joint}$) is equal to the net reaction forces and moments on the considered section ($L_{ext}$) minus the loads resulting from the muscles' action ($L_{muscles}$) (Equation 8.1):

$$L_{IV\_joint} = L_{ext} - L_{muscles} \tag{8.1}$$

$L_{ext}$ is the net reaction forces and moments obtained by direct or inverse free body diagram. The unknowns are $L_{IV\_joint}$ and $L_{muscles}$.

In order to estimate the loads generated by activated muscles, a control loop is used in this model (Figure 8.1) which aims to maintain the inter-vertebral loads within acceptable thresholds.

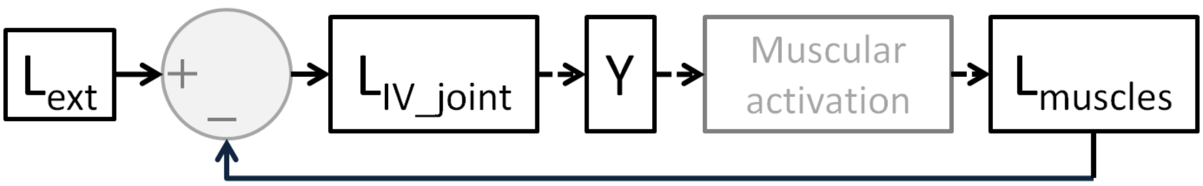


Figure 8.1. : Control loop of the Model of Muscular Regulation (MMR).

The regulation process considers two aspects:

- according to the net reaction forces and moments, a regulation command is computed to stimulate muscular activation (Equation 8.2). The regulation command, Y, is setting the amount of muscular recruitment needed: larger Y will result in a larger demand in muscular contraction in order to dramatically lower the resulting loads in the inter-vertebral joint.

$$Y = 10 * \frac{{L_{IV\_joint}}^3}{{Threshold_{IV\_joint}}^3} \tag{8.2}$$

- according to a muscle's cross-sectional area, line of action and position relative to the inter-vertebral joint, this muscle presents more or less the ability to reduce one or more components of the external forces and moments applied on the considered inter-vertebral joint. For example the quadratus lumborum will generate a lateral bending moment and lateral shear by its contraction and therefore can regulate these two load components (Figure 8.2).

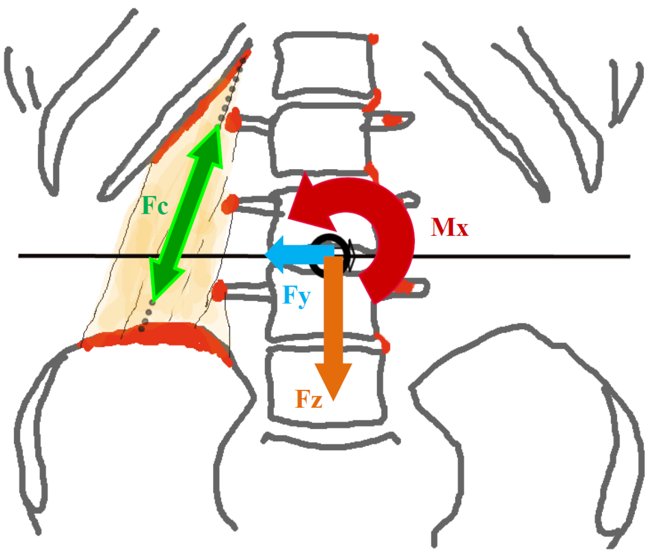


Figure 8.2. : Contraction of the quadratus lumborum (Fc in green) will generate a lateral bending moment (Mx in red) and a lateral shear (Fy in blue). Muscular contraction also generates a compression force (Fz in orange) [Adapted from (Pomero, 2002)].

A first estimation of the loads generated by muscles' activation is computed, leading to a decreased value of the loads in the IV joint from equation 8.1. This new value is then used as an input to compute the second estimation of $L_{muscles}$. This goes on, until further muscles recruitment does not change much the value of $L_{IV\_joint}$.

Model algorithm has been detailed in previously published articles (Pomero *et al.*, 2002, 2004) and is included in Appendix C. Input data are processed in Matlab® R2011b (The Mathworks Inc., Natick, MA, USA), before insertion into Simulink® (The Mathworks Inc., Natick, MA, USA). When developed in 2002, this model required: the use of a forceplate to estimate net reaction forces and moments; stereo-radiographs to reconstruct in 3D the bones, and MRI images for muscular geometry input. This model has been applied on four patients and one volunteer (Pomero *et al.*, 2002).

The main contribution of this PhD is to propose a process for subject-specific generation of musculo-skeletal model from EOS and MRI images, with new 3D reconstruction algorithms. The novelty resides in the computation of the net reaction forces and moments directly from the EOS radiographies, and the elaboration of a complete 3D geometry of both the spine, pelvis and muscles in the standing position. The following chapters will present this process and results obtained when applied to 20 subjects of various ages, with and without spinal deformities.

CHAPTER 9

# MMR MODELING INPUTS DETAILS

The model of muscular regulation (MMR) is based on personalized information of the patient. 3D reconstruction of the skeleton from EOS images, and muscles from MRI images will be used to access subject-specific information at the L3-L4 level. The MMR model requires the following entry data:

- Thresholds of admissible inter-vertebral joint loads for control loop regulation,
- Net reaction forces and moments at the inter-vertebral joint,
- Muscles' characteristics:
  - Muscles' geometry in the axial plane at mid-level of the inter-vertebral disc: area (CSA), coordinates of the centroid of the muscle ($Centroid\_i$, i=X,Y) and coordinates of the vector line of action ($Dir\_Muscle\_i$, i =X,Y,Z),
  - Muscles' maximal admissible stress in N/cm$^2$,

The outputs of the model are:

- resulting loads at the inter-vertebral joint,
- muscular forces.

Firstly, the threshold values of admissible inter-vertebral joint loads are detailed.
Secondly, details will be reported on the computation of the net reaction forces and moments from volumes, densities and locations of centers of mass of different segments using a direct free body diagram.
Finally, the process of obtaining the muscles' characteristics from MRI and EOS images, will be described.

## 9 - 1 Thresholds for inter-vertebral loads

As threshold values can be difficult to obtain *in vivo*, values were set according to the ones reported by Vincent Pomero (Pomero, 2002). The threshold values were set as follow: 75N for postero-anterior shear (Fx), 100N for lateral shear (Fy), 1500N for compression (Fz) and 4.9N for the different moments (Mx, My, Mz), based mainly on in-house based data from the Institute.

## 9 - 2 Net reaction forces and moments applied on the inter-vertebral joint

While most of the methods used a forceplate to apply inverse free body diagram and obtain the net reaction forces and moments resulting from gravity, here a direct free body diagram was combined with the 3D external envelope reconstructed on EOS images, and a density model. The density model included the different densities of each segment considered, values were set according to published data in the literature.

After 3D reconstruction of the external envelope from EOS images, this envelope is cut by the L3-L4 inter-vertebral disc plane. The center of mass and weight of each segment located above this plane can be computed from the different segments' volume (from the 3D external envelope (Nérot *et al.*, 2015)), with a density model (Figure 9.1). Then, the center of mass of the upper body, its mass and the vertical force resulting from gravity, can be easily calculated.

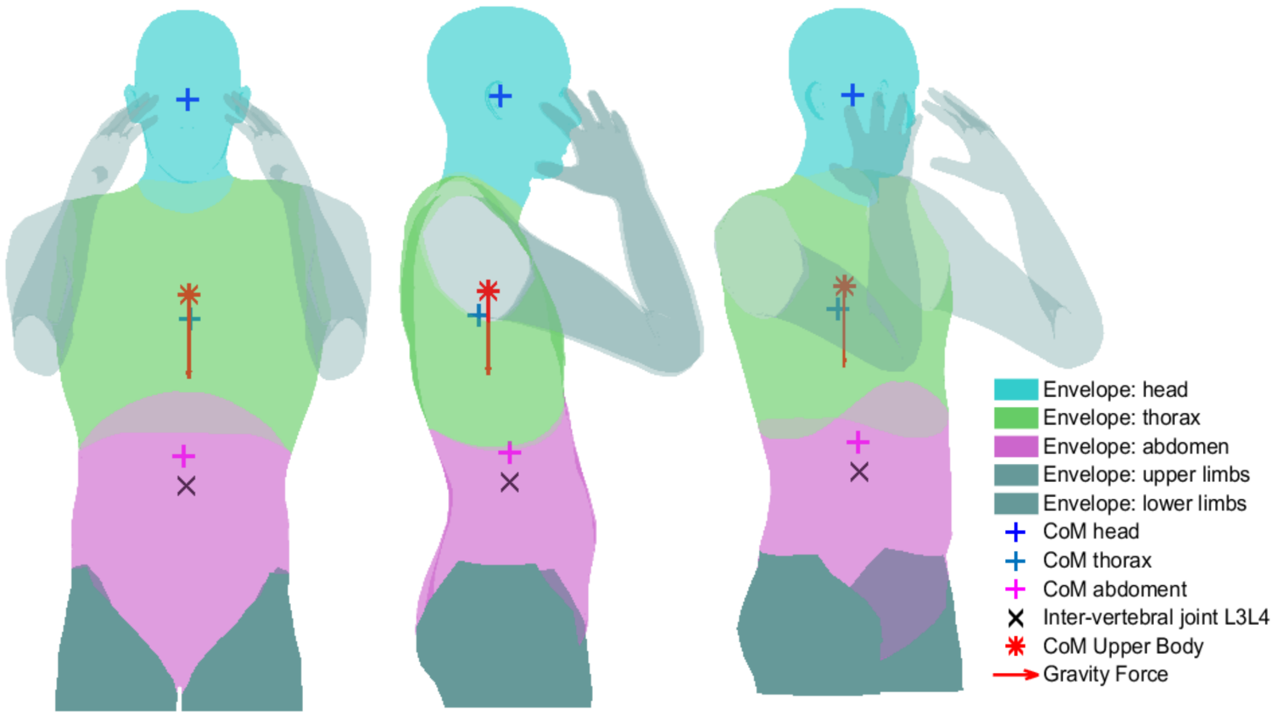


Figure 9.1. : 3D envelope with the different segments and their center of masses. Left: frontal view. Middle: sagittal view. Right: global view. CoM means center of mass.

Special focus was made on the density model conventionally used, based on cadaveric studies (Dempster, 1955; Chandler *et al.*, 1975). In order to improve accuracy of thorax density for a living population, a specific study has been conducted during this PhD. This work has been published in Journal of Biomechanics in 2016 (Amabile *et al.*, 2016c) and is reproduced hereafter.

## 9 - 3 Study on a new thorax density

The following was accepted for publication in Journal of Biomechanics in 2016 (Amabile *et al.*, 2016a), and is reproduced hereafter:

# DETERMINATION OF A NEW UNIFORM THORAX DENSITY REPRESENTATIVE OF THE LIVING POPULATION FROM 3D EXTERNAL BODY SHAPE MODELING.

**Authors:**

Celia Amabile[a, b], Julie Choisne[a], Agathe Nérot[a, c],Hélène Pillet[a], Wafa Skalli[a].

**Affiliations:**

[a] Arts et Métiers ParisTech, LBM/Institut de Biomécanique Humaine Georges Charpak, Paris, France;
[b] Spine Service, Hospital for Special Surgery, New York, NY 10021, USA;
[c] UMR_T9406, LBMC Laboratoire de Biomécanique et Mécanique des Chocs, IFSTTAR, Bron, France.

**Conflict of interest statement:**

The authors have no conflicts of interest to declare.

**Acknowledgments:**

The authors are grateful to the Banque Public d'Investissement for financial support through the dexEOS project part of the French FUI14 program. The authors also thank the ParisTech BiomecAM chair program on subject-specific musculo-skeletal modeling, and in particular COVEA and Société Générale.

### 9 - 3.1 Abstract

Body segment parameters (BSP) for each body's segment are needed for biomechanical analysis. To provide population-specific BSP, precise estimation of body's segments volume and density are needed. Widely used uniform densities, provided by cadavers' studies, did not consider the air present in the lungs when determining the thorax density.
The purpose of this study was to propose a new uniform thorax density representative of the living population from 3D external body shape modeling.
Bi-planar X-ray radiographs were acquired on 58 participants allowing 3D reconstructions of the spine, rib cage and human body shape. Three methods of computing the thorax mass were compared for 48 subjects: (1) the Dempster Uniform Density Method, currently in use for BSPs calculation, using Dempster density data, (2) the Personalized Method using full-description of the thorax based on 3D reconstruction of the rib cage and spine and (3) the Improved Uniform Density Method using a uniform thorax density resulting from the Personalized Method. For 10 participants, comparison was made between the body mass obtained from a force-plate and the body mass computed with each of the three methods.
The Dempster Uniform Density Method presented a mean error of 4.8% in the total body mass compared to the force-plate vs 0.2% for the Personalized Method and 0.4% for the Improved Uniform Density Method. The adjusted thorax density found from the 3D reconstruction was 0.74g/cm$^3$ for men and 0.73g/cm$^3$ for women instead of the one provided by Dempster (0.92g/cm$^3$), leading to a better estimate of the thorax mass and body mass.

**Keywords:** Thorax density; Body segment parameters; Rib cage volume; Thorax volume.

## 9 - 3.2 Introduction

The accuracy of the evaluation of the body mass and center of mass for each body's segment with specific geometric parameters is needed for biomechanical analysis in orthopedics, sports medicine, athletics' performance and ergonomics, and vehicle's design and safety. Body segment parameters are computed from each segment's volume estimated from proportional and geometrics methods (Hanavan, 1964; Hatze, 1980; Yeadon, 1990) or from photogrammetry (Davidson *et al.*, 2008; Jensen, 1978; Pillet *et al.*, 2010; Young *et al.*, 1983), radiography (Dumas *et al.*, 2005; Duval-Beaupère and Robain, 1987; Zatsiorsky and Seluyanov, 1985), DXA (Lee *et al.*, 2009), CT scans (Pearsall *et al.*, 1996) and MRI (Bauer *et al.*, 2007; Cheng *et al.*, 2000). To determine body segment's mass and center of mass, the density for each segment is needed.

Past studies widely used uniform densities based on studies on cadavers immersed in water (Chandler *et al.*, 1975; Dempster, 1955). The principal limitation with cadaver studies is the representation of a specific population group of elderly males which may differ from other subgroups body's densities such as young adults or females, and the poor size of the populations studied. For example, Chandler *et al.* presented results from 6 cadavers (mean age unknown) (Chandler *et al.*, 1975) vs 8 cadavers for Dempster *et al.* (mean age 72 years old (SD: 11)) (Dempster, 1955). The second limitation in immerging cadaver parts in water, is omitting the air in the lungs in the density determination of the thorax.

Most recent studies that investigated the mass and density of the thorax *in vivo* using MRI (Pearsall *et al.*, 1994) or computed tomography (Pearsall *et al.*, 1996) in the supine position highlighted inter-subject variability. Therefore, discrepancy exists in the definition of the thorax mass in term of percentage of the body mass ranging from 11% (Dempster, 1955) to 29.4% (Duval-Beaupère and Robain, 1987) and in density determination ranging from 0.82 (Pearsall *et al.*, 1994) to 0.92g/cm$^3$ (Dempster, 1955). Variation in population samples (age, gender, body type) can have an effect on the prediction of the thorax mass and density. Therefore there is a need for a new method to determine subject specific thorax density (and therefore mass) for each individual.

A new low-dose imaging system taking bi-planar radiographs (Dubousset *et al.*, 2010) combined with 3D reconstruction technique of the external body shape (Nérot *et al.*, 2015), spine (Humbert *et al.*, 2009b) and of rib cage (Aubert *et al.*, 2014) allows for volume estimation. Densities for each thorax tissues and segment have been well documented in the literature (Dempster, 1955; Erdmann and Gos, 1990; Hayashi *et al.*, 2011; Li *et al.*, 2010). The aim of this study was to combine those existing data to propose a new estimation of the thorax density.

## 9 - 3.3 Methods

### 9 - 3.3.1 Participants

58 asymptomatic participants (37 men, 21 women) were included in the study with a mean age of 35.5 years old [20–72 years old] and a mean body mass index (BMI) of 23.7kg/m$^2$ [17.2–30.5kg/m$^2$]. Participants were excluded if they presented spine pathologies or instrumentation anywhere in the upper body. All participants completed an informed consent document approved by the ethical committee of Hôpital Pitié Salpêtrière (Paris, France) (ethical committee approval CPP 06036).

Participants were divided into 2 groups. Group A included 48 participants (33 men, 15 women): mean age of 37.3 years old [20–72 years old] and a mean body mass index (BMI) of 23.8kg/m$^2$ [17.2–30.5kg/m$^2$]. Group B included 10 participants (4 men, 6 women): mean age of 27.0 years old [21–33 years old] and a mean body mass index (BMI) of 23.7kg/m$^2$ [20.0–29.5kg/m$^2$].

### 9 - 3.3.2 Quantification of the thorax mass

Low-dose bi-planar X-rays were acquired for all participants using the EOS® system (EOS imaging, Paris, France) which can simultaneously take a pair of X-rays from head to feet in the sagittal and frontal planes in upright position (Dubousset *et al.*, 2010). These bi-planar radiographs allow three

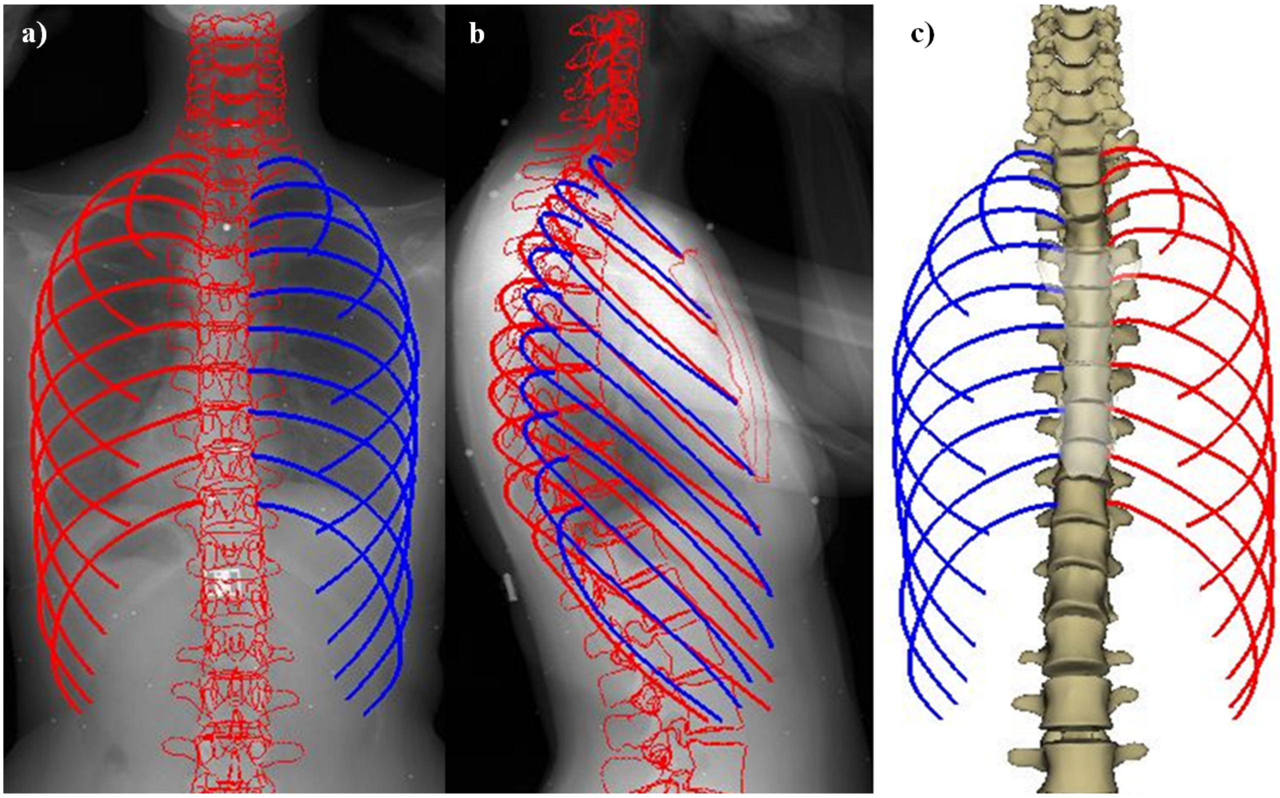


Figure 9.2. : 3D reconstruction of the rib cage. **a)** and **b)** Bi-planar radiographs with reconstructed spine and rib cage. **c)** 3D reconstruction of the spine and rib cage.

dimensional (3D) reconstructions of the bones and human body shape using well documented models (Aubert *et al.*, 2014; Humbert *et al.*, 2009b; Nérot *et al.*, 2015) (Figure 9.2 and figure 9.3). The spine, rib cage and body shape were reconstructed for all participants.

Body shape reconstruction was based on the deformation of a template which had been preliminarily segmented into 15 body segments, based on reference radiographs (Nérot *et al.*, 2015). During the envelope reconstruction process, the template was morphed to match the skin contours on the orthogonal radiographs and body segments were thereby adjusted to the anthropometry of the subject on the radiographs (by scaling using bony points, and surface deformation algorithm) (Nérot *et al.*, 2015).

The thorax was defined from templates' mesh proximal and distal limits with axilla as limits on the sides. The proximal limit was taken as the edge loop that best fits the basis of the neck along the rectangular mesh topology. Similarly, the distal limit was taken as the edge loop that best fits rib 10 (last "false rib", connected to cartilage of rib 7) along the rectangular mesh topology. The subject-specific volume of this body segment was calculated from the external envelope reconstruction. Rib cage volume from rib 1 to 10 was computed including the sternum.
Three methods used to compute the thorax mass ($M^T$) were compared for Group A and tested on Group B in terms of total body mass and center of pressure, against forceplate data:

1. the Dempster Uniform Density Method using Dempster density data (Dempster, 1955) ($M^T_{Dem}$),
2. the Personalized Method using full-description of the thorax components based on 3D reconstruction of the body shape, the spine and the rib cage ($M^T_{Perso}$)
3. the Improved Uniform Density Method using a uniform thorax density ($M^T_{Imp}$).

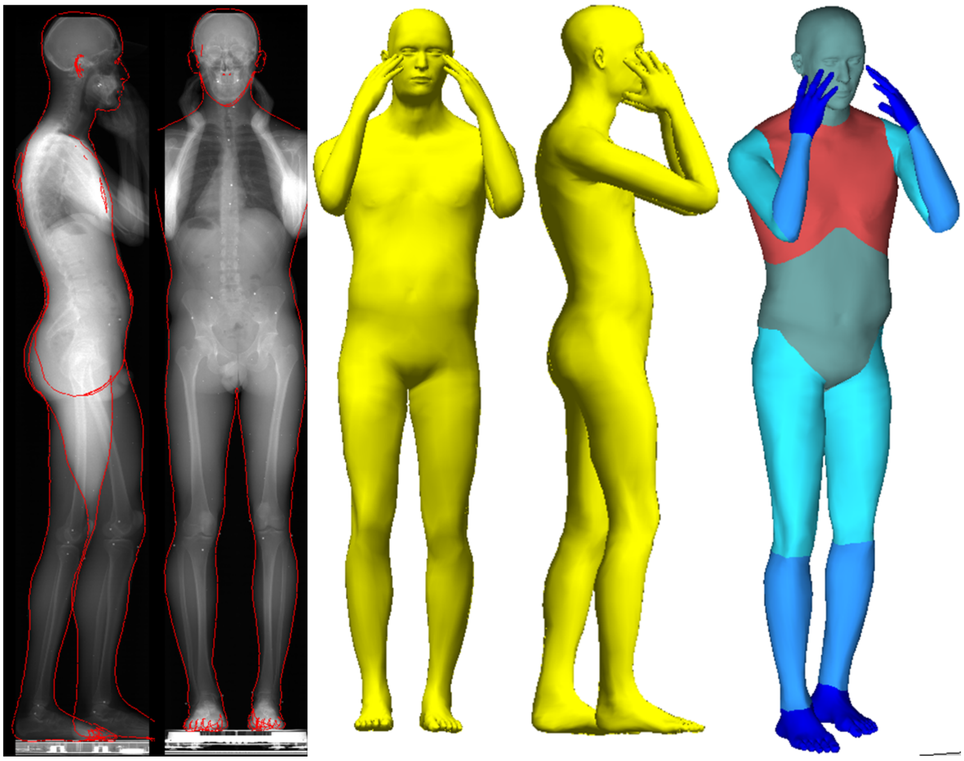

Figure 9.3. : 3D reconstruction of the body shape: projections on the bi-planar radiographs and 3D reconstruction of the body shape with the 15 considered segments (thorax highlighted in red).

**Dempster Uniform Density Method**

The Dempster Uniform Density Method is based on the density the most widely used in the literature for body segment density approximation which was described by Dempster in 1955 (Dempster, 1955). The Dempster Uniform Density Method computed the thorax mass ($M^T_{Dem}$) from the thorax volume ($V_{thorax}$) determined from the body shape 3D reconstruction and Dempster thorax density ($D_{thorax} = 0.92\text{g/cm}^3$). The thorax mass was computed as shown in Equation 9.1.

$$M^T_{Dem} = V_{thorax} * D_{thorax} \tag{9.1}$$

**Personalized Method based on 3D reconstructions**

The Personalized Method computed the thorax mass ($M^T_{Perso}$) by distinguishing different parts in the thorax. The rib cage volume ($V_{ribcage}$) was considered as containing the heart volume ($V_{heart}$), the lungs volume ($V_{lung}$) and the volume of the following bones ($V_{bone}$): T1–T12 vertebrae ($V_{Vert\_Ti}$, i = 1 to 12), the sternum and the 10 right and left ribs. The other tissues in the thorax, outside of the rib cage, were considered as soft tissues. The heart volume ($V_{heart}$) was computed in $\text{cm}^3$ from the age of the subject ($Age$) for both genders (Badouna *et al.*, 2012) according to Equation 9.2 and Equation 9.3.

$$^{men}V_{heart} = 738 * \frac{exp^{(-2.42+0.23*Age)}}{1 + exp^{(-2.42+0.23*Age)}} \tag{9.2}$$

$$^{women}V_{heart} = 572 * \frac{exp^{(-2.10+0.21*Age)}}{1 + exp^{(-2.10+0.21*Age)}} \tag{9.3}$$

The heart was considered as a soft tissue for its density: $D_{soft\_tissues} = 1.03\text{g/cm}^3$ (Dempster, 1955). Lung volume was computed as shown in Equation 9.4.

$$V_{lung} = V_{ribcage} - V_{heart} - V_{bone} \tag{9.4}$$

| | Mean volume ($cm^3$) | | SD of the volume ($cm^3$) | | Density applied ($g/cm^3$) |
|---|---|---|---|---|---|
| **Gender** | *F (n=15)* | *M (n=33)* | *F (n=15)* | *M (n=33)* | *F & M (n=48)* |
| **Thorax** | 13310.6 | 20341.5 | 2327.0 | 3330.9 | - |
| **Rib Cage** | 5912.6 | 8581.7 | 850.9 | 1162.1 | - |
| **Lungs** | 4874.8 | 7294.9 | 824.0 | 1138.9 | 0.28 |
| **Ribs cortical bone** | 137.4 | 155.6 | 5.6 | 8.3 | 2.00 |
| **Ribs trabecular bone** | 47.6 | 53.9 | 1.9 | 2.9 | 1.00 |
| **Sternum** | 40.9 | 44.3 | 7.4 | 6.2 | 1.00 |
| **Heart** | 566.8 | 719.9 | 6.4 | 19.5 | 1.03 |

Table 9.1. Means and standard deviations of the volumes (for Group A) used to compute the thorax mass, and density applied to each volume (Dempster, 1955; Li *et al.*, 2010; Shirotani, 1988). F: Female; M: Male.

During the X-ray acquisition, no breathing instruction was given to the participant. The density applied for the air volume in the lungs was $D_{lung} = 0.28 g/cm^3$ (Shirotani, 1988) (Table 9.1).
Bone volume was computed from the 3D reconstruction of the rib cage and spine. The reconstruction of the rib cage allows estimation of the volume of trabecular bone and of the cortical bone for each rib level and for each participant based on the rib length (Aubert *et al.*, 2014) (Equation 9.5).

$$V_{bone} = V_{sternum} + V_{ribs\_trabecular} + V_{ribs\_cortical} + \sum_{i=1}^{12} V_{Vert\_T_i} \tag{9.5}$$

Ribs' masses were computed using the following densities: $D_{cortical\_bone} = 2.00 g/cm^3$ and $D_{trabecular\_bone} = 1.00 g/cm^3$ (Li *et al.*, 2010). The vertebrae densities ($D_{T_i}$ i = 1 to 12) were differentiated depending on the gender and the age (Hayashi *et al.*, 2011) (Table 9.2). The sternum density was set to $D_{sternum} = 1.00 g/cm^3$. Therefore, the bone mass ($M_{bone}$), including the bone volume (Equation 9.5) and the bone densities mentioned above, was calculated as shown in Equation 9.6.

$$M_{bone} = (V_{sternum} + V_{ribs\_trabecular}) * D_{trabecular\_bone} + V_{ribs\_cortical} * D_{cortical\_bone} + \sum_{i=1}^{12} (V_{Vert\_T_i} * D_{T_i}) \tag{9.6}$$

The thorax mass with the Personalized Method ($M^T_{Perso}$) was computed as in Equation 9.7:

$$M^T_{Perso} = V_{lung} * D_{lung} + ((V_{thorax} - V_{ribcage}) + V_{heart}) * D_{soft\_tissues} + M_{bone} \tag{9.7}$$

With the purpose of developing an easier method to obtain the thorax mass, we computed a new average thorax density and predicted the rib cage volume from external data.

| | Age (yrs old) | Gender | T1 | T2 | T3 | T4 | T5 | T6 | T7 | T8 | T9 | T10 | T11 | T12 |
|---|---|---|---|---|---|---|---|---|---|---|---|---|---|---|
| **Mean volume ($cm^3$)** | **... - 40** | F (n=9) | 13.1 | 12.0 | 13.2 | 13.7 | 14.8 | 16.2 | 17.8 | 19.3 | 21.7 | 25.2 | 26.7 | 29.0 |
| | | M (n=22) | 18.4 | 18.3 | 18.3 | 18.4 | 19.7 | 21.8 | 23.6 | 24.7 | 27.8 | 31.3 | 34.1 | 37.4 |
| | **41 - 55** | F (n=2) | 12.9 | 15.0 | 15.1 | 15.1 | 15.6 | 18.4 | 19.5 | 20.7 | 23.9 | 28.4 | 27.9 | 29.8 |
| | | M (n=5) | 20.8 | 21.1 | 22.8 | 24.4 | 24.9 | 27.8 | 32.2 | 33.1 | 36.7 | 40.9 | 46.4 | 49.8 |
| | **56 - 70** | F (n=2) | 17.1 | 14.6 | 15.7 | 18.5 | 19.5 | 21.4 | 22.9 | 24.0 | 28.1 | 32.7 | 37.1 | 37.9 |
| | | M (n=2 | 17.7 | 18.2 | 18.6 | 20.7 | 22.9 | 26.0 | 27.6 | 30.8 | 33.0 | 35.3 | 39.4 | 43.0 |
| | **71 - ...** | F (n=2) | 19.0 | 18.6 | 17.7 | 19.9 | 22.0 | 22.8 | 25.1 | 25.1 | 30.2 | 33.0 | 36.0 | 35.2 |
| | | M (n=4) | 20.5 | 18.8 | 20.4 | 18.3 | 20.2 | 23.5 | 25.3 | 28.6 | 31.8 | 36.7 | 37.9 | 43.0 |
| **Density applied ($g/cm^3$)** | **... - 40** | F (n=9) | 0.24 | 0.22 | 0.22 | 0.21 | 0.21 | 0.20 | 0.20 | 0.19 | 0.20 | 0.20 | 0.19 | 0.18 |
| | | M (n=22) | 0.21 | 0.21 | 0.21 | 0.21 | 0.20 | 0.20 | 0.19 | 0.19 | 0.19 | 0.19 | 0.18 | 0.18 |
| | **41 - 55** | F (n=2) | 0.21 | 0.20 | 0.20 | 0.20 | 0.19 | 0.18 | 0.17 | 0.17 | 0.18 | 0.17 | 0.16 | 0.15 |
| | | M (n=5) | 0.19 | 0.19 | 0.19 | 0.18 | 0.18 | 0.17 | 0.16 | 0.15 | 0.16 | 0.16 | 0.15 | 0.14 |
| | **55 - 70** | F (n=2) | 0.17 | 0.16 | 0.16 | 0.16 | 0.15 | 0.14 | 0.14 | 0.13 | 0.14 | 0.13 | 0.12 | 0.11 |
| | | M (n=2) | 0.19 | 0.19 | 0.20 | 0.18 | 0.17 | 0.16 | 0.15 | 0.15 | 0.15 | 0.15 | 0.13 | 0.12 |
| | **71 - ...** | F (n=2) | 0.14 | 0.14 | 0.13 | 0.12 | 0.11 | 0.11 | 0.10 | 0.10 | 0.10 | 0.10 | 0.09 | 0.08 |
| | | M (n=4) | 0.17 | 0.17 | 0.16 | 0.15 | 0.14 | 0.13 | 0.12 | 0.12 | 0.13 | 0.12 | 0.11 | 0.10 |

Table 9.2. Means, for Group A, of the volumes of the vertebrae used to compute the thorax mass, and density applied to each vertebra (Hayashi *et al.*, 2011). F: Female; M: Male.

**Basic estimation for the routine use: Improved Uniform Density Method**
The Improved Uniform Density Method computed the thorax mass ($M^T_{Imp}$) from its external volume ($V_{thorax}$) and from a mean density computed from the Personalized Method ($D_{thorax\_Perso}$) as shown in Equation 9.8. This density was computed as the ratio between the thorax mass ($M^T_{Perso}$) determined in Equation 9.7 and the thorax volume ($V_{thorax}$) averaged for Group A's participants (Equation 9.9).

$$M^T_{Imp} = V_{thorax} * D_{thorax\_Perso} \tag{9.8}$$

$$D_{thorax\_Perso} = \frac{1}{48} * \sum_{j=1}^{48} \frac{M^T_{Perso}(j)}{V_{thorax}(j)} \tag{9.9}$$

### 9 - 3.3.3 Evaluation of the methods

**Estimation of the body mass**
As the thorax cannot be isolated, global body mass and center of pressure position were used as control parameters. For Group B, a force plate (Wii Balance Board (WBB), Nintendo, Kyoto, Japan) was placed in the EOS cabin during the stereo-radiography acquisition and recorded the mass and center of pressure (CoP) during the acquisition time. The WBB has been shown to be comparable to other usual forceplates in terms of comparison of balance tests and in terms of CoP estimation as its estimation presents an error less than 3% for both coordinates (Clark *et al.*, 2010).

Body mass and center of pressure were computed for each of the three methods and compared. In order to compute these, the individual subject-specific volume and barycenter of each 15 body segment of the reconstructed envelopes were calculated. Densities determined by Dempster (Dempster, 1955) were used for all segments' mass calculation except for the arms and thorax. For the arms, using regressions from Dempster, their masses were computed using ratios of all other body segments' masses (Dempster, 1955).

For the thorax, the three detailed methods were applied for determination of the thorax mass. Total body mass was computed as the sum of individual segments' masses. Center of pressure was computed as the weighted sum of segments' barycenters. Body mass and center of pressure were then compared for each method with the ones obtained from the WBB (considered as the gold standard) for Group B.

**Prediction of the rib cage volume, thorax mass and thorax volume**
Multi-linear regression was searched for to simplify computation of the rib cage volume from the reconstructed external thorax volume, the BMI, the Age and the Gender of the subject. Multi-linear regressions were computed using one or more of these regressors. Additional multi-linear regressions were searched for to estimate thorax mass (from the Personalized Method) and thorax volume from the BMI, the age and gender to see if demographic parameters alone were sufficient to evaluate thorax parameters.

Evaluation of the rib cage volume, thorax mass and thorax volume estimations were made by calculating the leave-one-out-error (LOOE) (i.e. the regression model is built on all patients except one, and tested on this one, and this is made for all patients), the R-squared statistics ($R^2$), the p-value (p-val) and the standard error of estimate (SEE) for each multi-linear regression.

## 9 - 3.4 Results

### 9 - 3.4.1 Quantification of the thorax mass

Mean and standard deviation of the volumes of the considered bones and segments can be found in Table 9.1 and Table 9.2.

The mean density used in the Improved Uniform Density Method was 0.74g/cm$^3$ (SD: 0.03g/cm$^3$) for men and 0.73g/cm$^3$ (SD: 0.03g/cm$^3$) for women.

Mean and standard deviations of the thorax mass computed with the three Methods can be found in Table 9.3. The mean difference between the thorax mass determined with the Personalized Method (respectively the Improved Uniform Density Method), and the thorax mass calculated with the Dempster Uniform Density Method, was 3.3kg (SD: 0.8) (respectively 3.3kg (SD: 0.8)). The mean difference between the thorax mass determined with the Personalized Method and calculated with the Improved Uniform Density Method was 0.0kg (SD: 0.5) (Figure 9.4).

| Thorax Mass (kg) | Male Subjects | | Female Subjects | |
|---|---|---|---|---|
| | Mean (1*SD) | 95% CI | Mean (1*SD) | 95% CI |
| Dempster Uniform Density Method | 18.7 (3.1) | [ 12.6 ; 24.8 ] | 12.2 (2.1) | [ 8.0 ; 16.5 ] |
| Personalized Method | 15.1 (2.7) | [ 9.6 ; 20.5 ] | 9.7 (1.9) | [ 6.0 ; 13.5 ] |
| Improved Uniform Density Method | 15.1 (2.5) | [ 10.1 ; 20.0 ] | 9.7 (1.7) | [ 6.3 ; 13.1 ] |

Table 9.3. Means, standard deviations and range of the thorax mass (in kg) obtained with the Dempster Uniform Density, Personalized and Improved Uniform Density Methods for Group A. 95%CI means: 95% confidence interval.

### 9 - 3.4.2 Evaluation of the methods

**Estimation of the body mass and CoP**

Individual differences between the body masses given by the WBB, the Dempster Uniform Density Method, the Personalized Method, and the Improved Uniform Density Method are displayed, for Group B, in Figure 9.5. For Group B, the average body mass was 71.0kg (SD: 15.0) from the WBB, and 74.4kg (SD: 15.6); 71.1kg (SD: 14.8) and 71.3kg (SD: 14.8) using the Dempster Uniform Density Method, the Personalized Method and the Improved Uniform Density Method respectively.
Differences between the CoP positions estimated by the Dempster Uniform Density Method, the Personalized Method and the Improved Uniform Density Method, compared to the WBB data were less than 4.8mm (Table 9.4).

| Differences between CoPs | X: postero-anterior direction (mm) | Y: medio-lateral direction (mm) | Norm (mm) |
|---|---|---|---|
| $CoP_{Dem} - CoP_{wii}$ | -0.7 (4.7) | 1.8 (1.8) | 4.4 (2.7) |
| | [ - 9.5 ; 4.5 ] | [ - 1.8 ; 3.9 ] | [ 0.2 ; 9.6 ] |
| $CoP_{Perso} - CoP_{wii}$ | 0.8 (5.0) | 1.5 (1.9) | 4.8 (2.5) |
| | [ - 8.6 ; 6.5 ] | [ - 2.1 ; 3.6 ] | [ 1.0 ; 8.7 ] |
| $CoP_{Imp} - CoP_{wii}$ | 0.7 (4.9) | 1.5 (1.9) | 4.7 (2.5) |
| | [ - 8.4 ; 6.4 ] | [ - 2.1 ; 3.7 ] | [ 1.0 ; 8.5 ] |

Table 9.4. Mean (1*SD) [min; max] of the differences between the CoP position evaluated by the WBB ($CoP_{wii}$), the Dempster Uniform Density Method ($CoP_{Dem}$), the Personalized Method ($CoP_{Perso}$) and the Improved Uniform Density Method ($CoP_{Imp}$); for Group B.

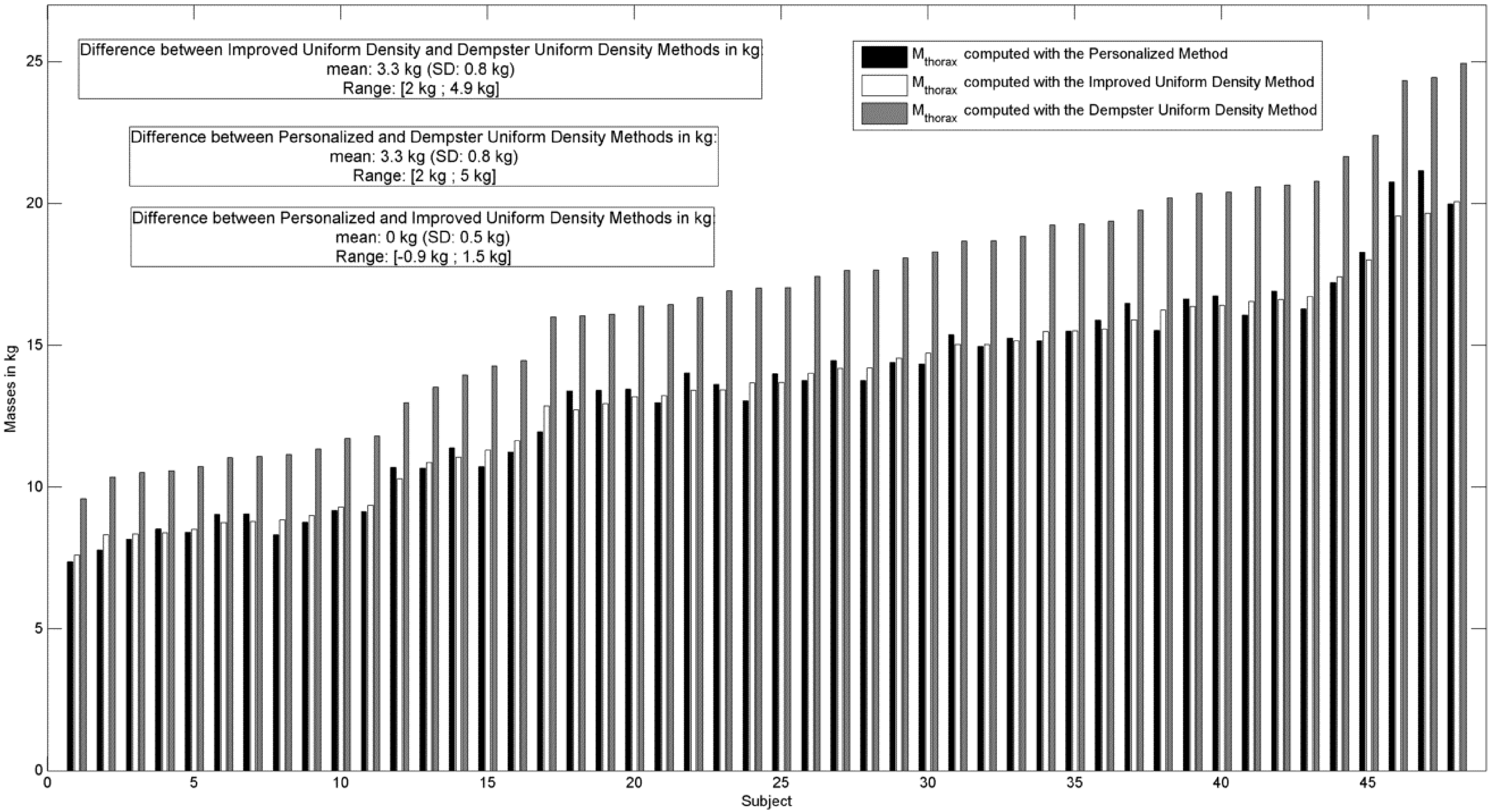


Figure 9.4. : Histogram comparing the mass of the thorax computed with the Dempster Method (in grey), the Personalized Method (in white) and the Estimation Method (in black), for Group A.

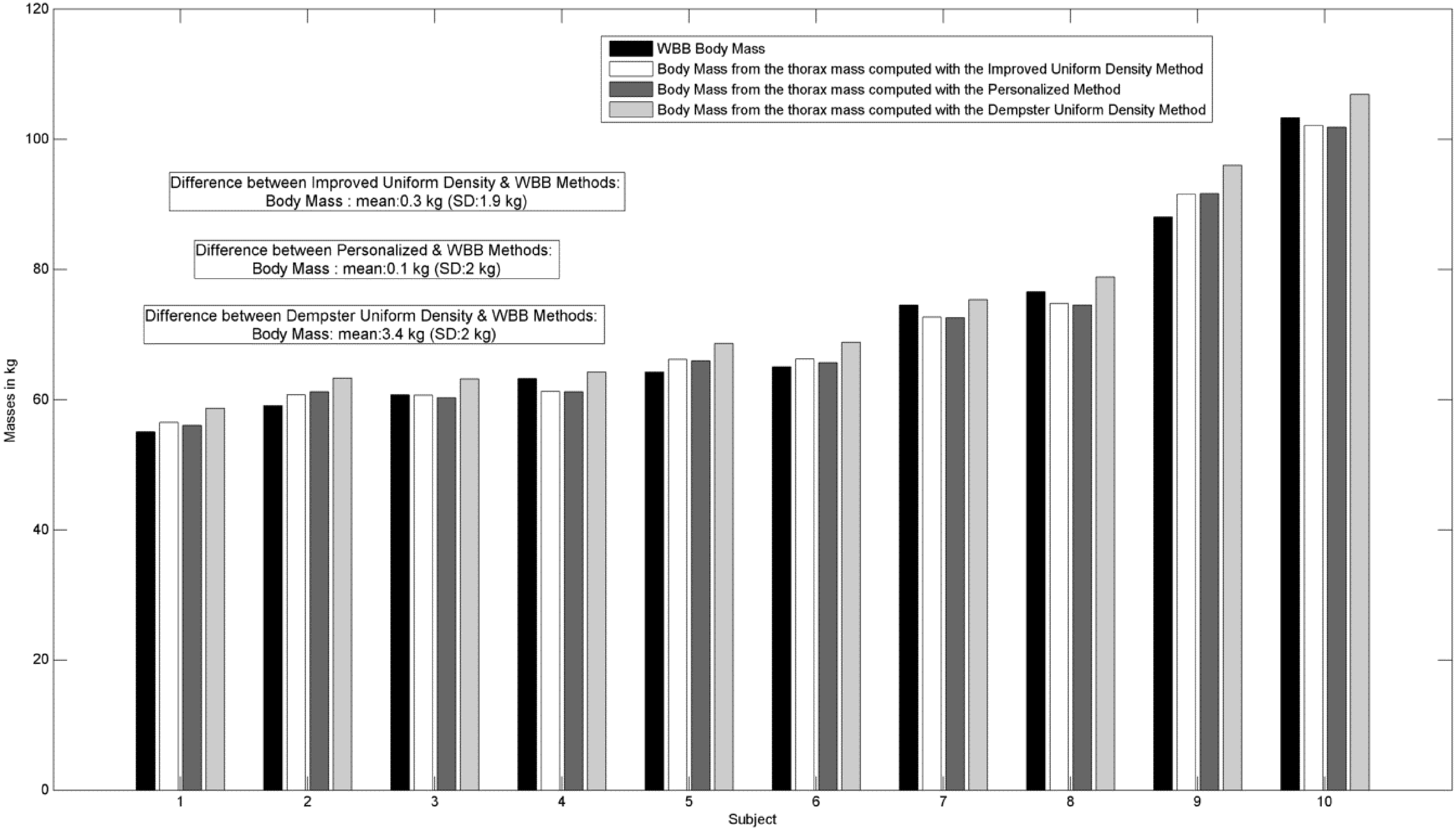


Figure 9.5. : Histogram comparing the body mass obtained from (1) the WBB (in black), (2) including the thorax mass from the Dempster Uniform Density Method (in light gray), (3) including the thorax mass from the Personalized Method (in gray), and (4) including the thorax mass from the Improved Uniform Density Method (in white), for Group B.

**Prediction of the rib cage volume, thorax mass and thorax volume from multi-linear regressions**

The model predicting the rib cage volume and presenting the smallest Leave-One-Out-Error (LOOE: 7.8% of the mean rib cage volume), the greatest $R^2$ (0.88) and the lowest Standard Error of the Estimate (SEE: 7.2% of the mean rib cage volume) was the one using 2 regressors (reconstructed external thorax volume ($V_{thorax}$) and Gender (0 for women and 1 for men)). The prediction of the rib cage volume (${}^{reg}V_{ribcage}$ in $cm^3$) based on the 2 regressors was significant ($p<0.05$) and relies on Equation 9.10.

$$ {}^{reg}V_{ribcage} = 0.298 * V_{thorax} + 572.7 * Gender + 1943.6 \tag{9.10} $$

This equation was tested on the Group B and differences between the predicted rib cage volume and the reconstructed rib cage volume was in average - 4.2% (SD: 5.9) of the mean rib cage volume.
The best predictors of the thorax volume and mass were the age, BMI and gender respectively leading to a LOOE of 12.1% and 14.1%; and to a SEE of 11.2% and 13.0% (both in % of the mean thorax mass or thorax volume) with high determination coefficient (Table 9.5). Thorax volume regression analysis was tested on the Group B and difference between the 3D reconstructed thorax volume and the predicted thorax volume was in average 5% of the mean thorax volume (SD: 11.5%). Thorax mass regression analysis was also tested on Group B and difference between the predicted thorax mass and the thorax mass determined with the Personalized Method was 3.8% of the mean thorax mass of the Personalized Method (SD: 12.5%).

| Value to predict | Correlation coefficient $\mathbf{R^2}$ | Equation |
|---|---|---|
| **Thorax Volume** $V_{thorax}$ **($\mathbf{cm^3}$)** | **0.79** | $V_{thorax}$ = (- 4.94 + 0.01 * **Age** + 0.76 * **BMI** + 6.55 * **Gender**) * $10^6$ |
| **Thorax Mass** $M^T_{Perso}$ **(kg)** | **0.75** | $M^T_{Perso}$ = - 4.65 + 0.01 * **Age** + 0.60 * **BMI** + 4.96 * **Gender** |

Table 9.5. Multilinear significant regressions (p-val<0.01) to predict thorax volume $V_{thorax}$ or thorax mass $M^T_{Perso}$ (Personalized Method) with demographic parameters as predictors: Age (years), BMI ($kg/m^2$), Gender (0 for Female and 1 for Male).

## 9 - 3.5 Discussion

The purpose of this study was to propose an improved uniform thorax density representative of the living population from 3D external body shape modeling. The currently used method (Dempster Uniform Density Method) was compared to two newly presented methods (Personalized and Improved Uniform Density Methods) for the thorax mass computation. The Improved Uniform Density Method introduced a new uniform density ($0.73 g/cm^3$ and $0.74 g/cm^3$ vs $0.92 g/cm^3$ for Dempster (Dempster, 1955)). This method is a compromise between accuracy and ease to implement: it is less complex to use but as accurate as the method considered as reference here: the Personalized Method.

The three methods were evaluated on Group A for calculation of the thorax mass based on the thorax volume and density. Overall, the Dempster Uniform Density Method over-estimated the thorax mass compared to the Personalized Method and the Improved Uniform Density Method. The main reason for this over-estimation is the change in thorax density between cadavers (Dempster Uniform Density Method) and living population (Personalized and Improved Uniform Density Method) due to the lung tissue. Reported lung densities on cadavers ranged from $0.563 g/cm^3$ (Erdmann and Gos, 1990) to $1.050 g/cm^3$ (Woodard and White, 1986) while *in vivo* measures were found to be $0.254 g/cm^3$ during expiration (Kohda and Shigematsu, 1989) and the mean lung density used for the Personalized method was $0.28 g/cm^3$. Therefore, *in vivo* density of the thorax computed with the Personalized Method was in average lower than the density calculated by Dempster (Dempster, 1955) and used in the Dempster Uniform Density Method.

The thorax density reported from *in vivo* studies on four adults using CT scan (Pearsall *et al.*, 1996) and on 26 males using MRI (Pearsall *et al.*, 1994) can vary substantially from 0.73–0.74 g/cm$^3$ in our study to 0.82g/cm$^3$ (Pearsall *et al.*, 1994) and 0.87g/cm$^3$ (Pearsall *et al.*, 1996). These differences can be attributed to variation in measurement techniques and in the population studied. A large range of males and females population ranging from 20 to 72 years old was considered in the present study while others used only males or just few individuals. Therefore discrepancies exist in the estimation of the thorax mass between *in vivo* studies ranging from 9.99kg (Jensen and Fletcher, 1994) to 20.48kg (Duval-Beaupère and Robain, 1987). The Personalized Method approximated an average thorax mass of 9.7kg for females and 15.1kg for males which is in the range of what was previously published (Duval-Beaupère and Robain, 1987; Jensen and Fletcher, 1994; Pearsall *et al.*, 1996, 1994).

In order to validate the new thorax density, choice was made to compare center of pressure and total body mass using the different methods to compute the thorax mass against forceplate data, for each subject of Group B. While thorax mass will be different for each method, the 14 other segments' mass used to compute the total body mass are based on Dempster density (Dempster, 1955) and the 3D body envelope for volume calculation. That way the only variant in the total body mass and COP calculation for each method is the thorax density. Despite its limitations, this validation method was considered as a realistic option available for evaluation. Further validation could consider *in vivo* calibrated whole body CT scans, but such data is difficult to obtain because of irradiation issues. Volumetric techniques tended to over-estimate the whole body mass which may be attributed to the use of uniform segment density from cadaver studies such as Dempster (body mass error estimation of 3.4kg in average). Body mass estimation error could vary from 0.2% to 5.9% on young volunteers (Pillet *et al.*, 2010) and from 1.1% to 4.6% on children and adults males (Sandoz *et al.*, 2010). A mean error of 4.8% [1.2–11.2%] in the total body mass was found in the present study using the Dempster Uniform Density Method which is concordant with the previous studies (Pillet *et al.*, 2010; Sandoz *et al.*, 2010).

These results demonstrated the need to incorporate improved density profiles representative of the living population. The Personalized Method used detailed differentiation in the thorax entities' volumes and densities and found a total body mass error of only 0.2%. However this method requires reconstructing the rib cage and spine which can be long and intricate. That is why the present study proposed the Improved Uniform Density Method based on a new average thorax density applicable to all *in vivo* studies. A body mass error of 0.4% was found between the Improved Uniform Density Method and the WBB. This error is less than the Dempster Uniform Density Method and equivalent to the Personalized Method. This new thorax density of 0.74g/cm$^3$ for men and 0.73g/cm$^3$ for women presented here showed a good estimation of the overall body mass. Moreover, a low SD of 0.03g/cm$^3$ for both genders demonstrated that the density does not vary much between individuals. Therefore, when computing the thorax mass, the thorax volume remains the most inter-subject variable parameter compared to the density.

The CoP was also estimated using the three methods and compared to the force plate. All methods gave a CoP error less than 4.8mm which is in the range of the WBB magnitude error (Clark *et al.*, 2010). The thorax density used to approximate the CoP did not influence on the determination of the CoP of asymptomatic adults. However these errors might change if the estimation was made on a population with postural disorders, especially patients with hyper kyphosis.

For investigators who wish to estimate a subject specific thorax density by differentiating the lungs density in the rib cage, the present study proposed rib cage volume estimation from the volume of the thorax and gender. The estimated rib cage volume approximated the reconstructed rib cage volume very well with a mean error of - 4.2% for Group B. Moreover, the present study used multi-linear regression analysis to estimate thorax volume and thorax mass from easily available demographic parameters such as age, gender and BMI. However this regression analysis could only predict thorax volume and mass with errors respectively of 11.2% and 13.0% (SEE errors) when compared to the real thorax volume from 3D thorax reconstruction and to the thorax mass estimated with the Personalized method.

This study's novelty resides in the differentiation of the lungs and heart, in the computation of the thorax density. Other segments' densities were not considered in this study as all of them, except the abdomen, are mainly composed of fat, muscle and bone. The thorax density only was considered for improvements in this study to focus on the influence of the air present in the lungs on the thorax density in the living population. Further improvements could include the liver and the shoulder girdle in the thorax description, and a more accurate sternum's density. Such enhancements are not straight forward as these organs/bones have subject variable masses and positions in the thorax. However, the authors are confident that these limitations will not significantly influence the total body mass as the present estimation of the total body mass is more realistic than the conventional one provided by Dempster (Dempster, 1955). No breathing instruction was given to the participants during the X-ray acquisition, as with the acquisition time of 30s, participants were not able to hold their breath. Another limitation of the presented study resides in the use of constants/equations to predict for example the heart volume (Badouna *et al.*, 2012), and the vertebrae densities (Hayashi *et al.*, 2011), which could contribute to the uncertainty of the estimated thorax mass. Nevertheless, despite these approximations, the Personalized Method provides a total body mass more accurate than the one computed with the Dempster Uniform Density Method (Dempster, 1955) (mean difference with the WBB total body mass: 0.1kg vs 3.4kg (Figure 9.5)). Therefore what seems important is to differentiate thorax structures of very different densities such as lungs and heart. While such detailed modeling could be uneasy to implement in routine studies, the Improved Uniform Density Method appears as a relevant alternative being as accurate and less complex. This reinforces the validity of the newly found thorax density, as it accounts for various approximations, and is still little variable between subjects. The last limitation of this study is the inability to validate the thorax mass estimation. However, total body mass was computed with the same body segments' densities except for the thorax, therefore differences observed, in the total body masses, come from differences in the thorax density.

### 9 - 3.6 Conclusion

Overall, this study provides a new density for the thorax segment (0.74g/cm$^3$ for men and 0.73g/cm$^3$ women) instead of the one provided by Dempster (0.92g/cm$^3$). This density leads to a better estimate of the thorax mass and therefore of the body mass from body segments' volume.

In light of the musculo-skeletal model introduced at the beginning of this part, this new thorax density appears as relevant, improving the thorax density of the density model when estimating the net reaction forces and moments at the inter-vertebral joint center. This section focused on the personalization of the computation of the net reaction forces and moments, as these are one of the input of the musculo-skeletal model used. The next section will provide details on the personalization of the muscles' characteristics used in the model.

## 9 - 4 Muscles considered

The MMR model considers a section at the lumbar level, precisely at the L3-L4 inter-vertebral disc level (Figure 9.6). To access personalized muscles' characteristics needed for the model, the global pelvis-spine-rib-cage system will be considered.

Muscles considered in the model included: the psoas; the quadratus lumborum; the latissimus dorsi; the erector spinae group (ilicostalis, longissimus dorsi, spinalis and multifidus group); and the abdominal group (obliquus externus, obliquus internus, transversus abdominis, rectus abdominis) (all muscles' anatomy are detailed in Appendix A).

The multifidus is a group of small and indistinguishable muscles (for more details see Table A.1). Because the muscle spinalis is not present at the considered level (disc L3-L4), it will not be considered in the following 3D reconstructions performed for the use in the MMR model.

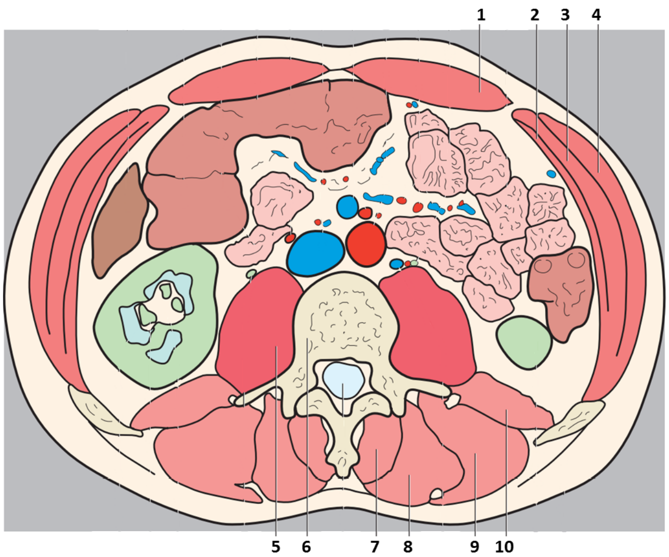


1. Rectus abdominis
2. Transversus abdominis
3. Obliquus internus
4. Obliquus externus
5. Psoas
6. Lumbar vertebra
7. Multifidus
8. Longissimus dorsi
9. Iliocostalis
10. Quadratus lumborum

Figure 9.6. : Axial slice at lumbar level. [Adapted from (Moeller and Reif, 2001)]

## 9 - 5 Muscles' geometry in the plane of the inter-vertebral disc

The model requires detailed muscular geometry at the inter-vertebral level of interest. This information can be extracted from MRI images but needs further processing in order to fully represent muscles' geometry in the standing neutral position, as patients are in the supine position during MRI acquisitions. First, the patient undergoes an EOS exam in the standing position, allowing to reconstruct in 3D the spine and the pelvis. Then, muscles are reconstructed in 3D from MRI images, using the DPSO method presented in the section 7. Finally, both 3D geometries are combined as explained hereafter.

### 9 - 5.1 Setting 3D muscles' reconstructions in the standing position

The method used is similar to the one reported, on lower limbs, by Hausselle *et al.* (Hausselle *et al.*, 2014): on one hand are the 3D envelope and skeleton in standing position (from EOS radiographs), on the other hand are the muscles in 3D in supine position (from MRI images) (Figure 9.7). An elastic transformation is then used to transform the muscles in the standing position and to match the two envelopes.

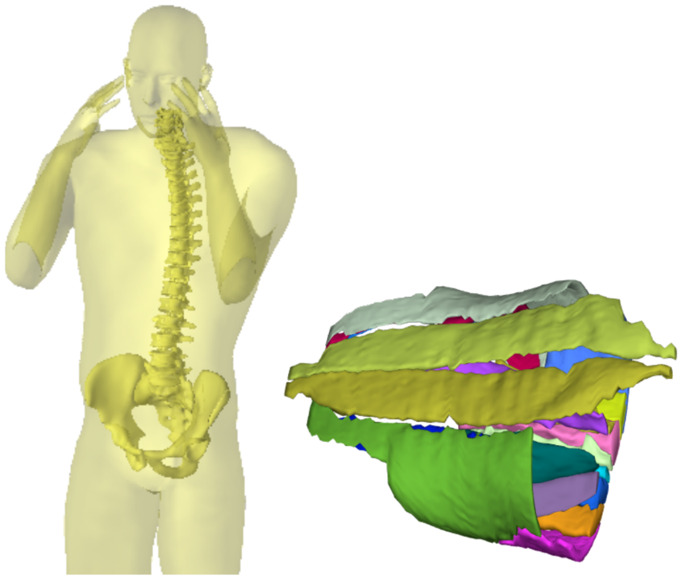

Figure 9.7. : Left, the pelvis, spine and envelope reconstructed in 3D in the standing position. Right: Muscles reconstructed in 3D in the supine position. The 3D external envelope reconstructed from MRI images was not represented for clarity.

As soft tissues deform under the action of the gravity, specific deformation of the 3D muscular reconstruction should be applied. To do so, control points are needed on both set of images to match the two reconstructions. A choice was made here to include the following control points: pelvic control points, spinal control points, and envelope control points.

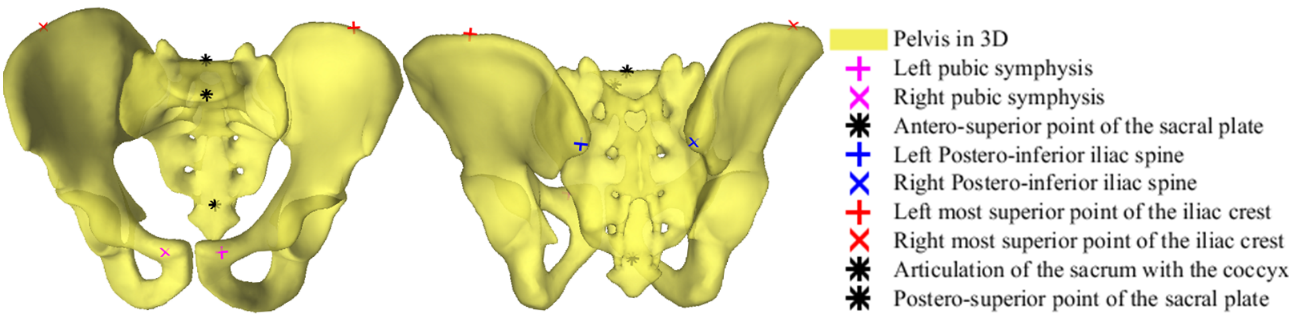


Figure 9.8. : Considered points on the pelvis for kriging MRI muscles on EOS skeleton. Anterior (left image) and posterior (right image) views.

Pelvic control points (Figure 9.8) included:

- the pubic symphysis at the extremity of the inferior right and left ramus of the pubis,
- the postero-inferior of the right and left iliac spine
- the most superior point of the right and left iliac crest,
- the postero-superior point of the sacral plate,
- the antero-superior point of the sacral plate,
- the articulation of the sacrum with the coccyx.

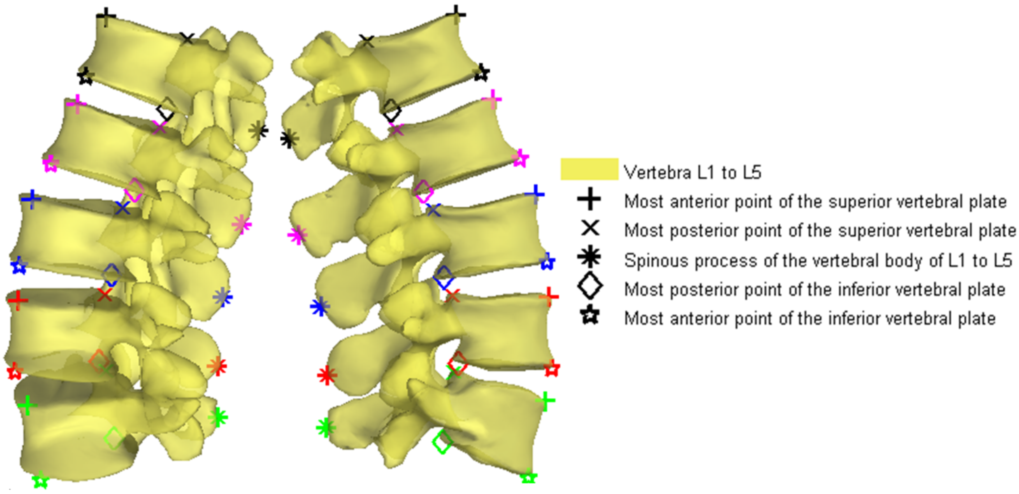


Figure 9.9. : Considered points on the spine for kriging MRI muscles on EOS skeleton. Medial and lateral views.

Spinal control points (Figure 9.9) included:

- the inter-vertebral joint center at the L1-L2, L2-L3, L3-L4 and L4-L5 levels,
- in the sagittal plane:
  - the most antero-superior point of the vertebral body of L1 to L5,
  - the most postero-superior point of the vertebral body of L1 to L5,
  - the most antero-inferior point of the vertebral body of L1 to L5,
  - the most postero-inferior point of the vertebral body of L1 to L5,
  - the spinous process of the vertebral body of L1 to L5.

Envelope control points (Figure 9.10) included the points of the external envelope contour on the axial section at the mid-levels of L1-L2, L2-L3, L3-L4 and L4-L5 inter-vertebral discs.

Kriging 3D MRI muscles and envelope reconstruction on the 3D EOS reconstruction allowed to obtain muscles' geometry in the standing position (Figure 9.11).

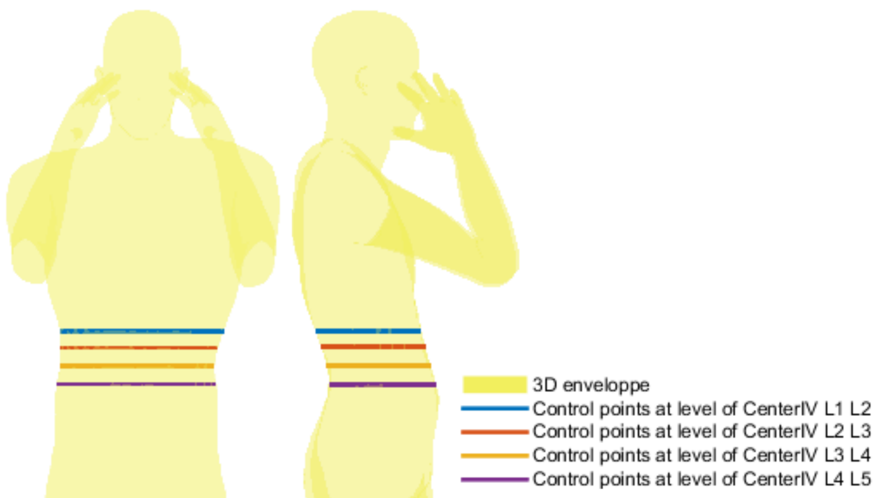


Figure 9.10. : Considered points on the envelope for kriging MRI muscles on EOS skeleton. CenterIV L3 L4 means the center of the L3-L4 inter-vertebral disc. Frontal and sagittal views.

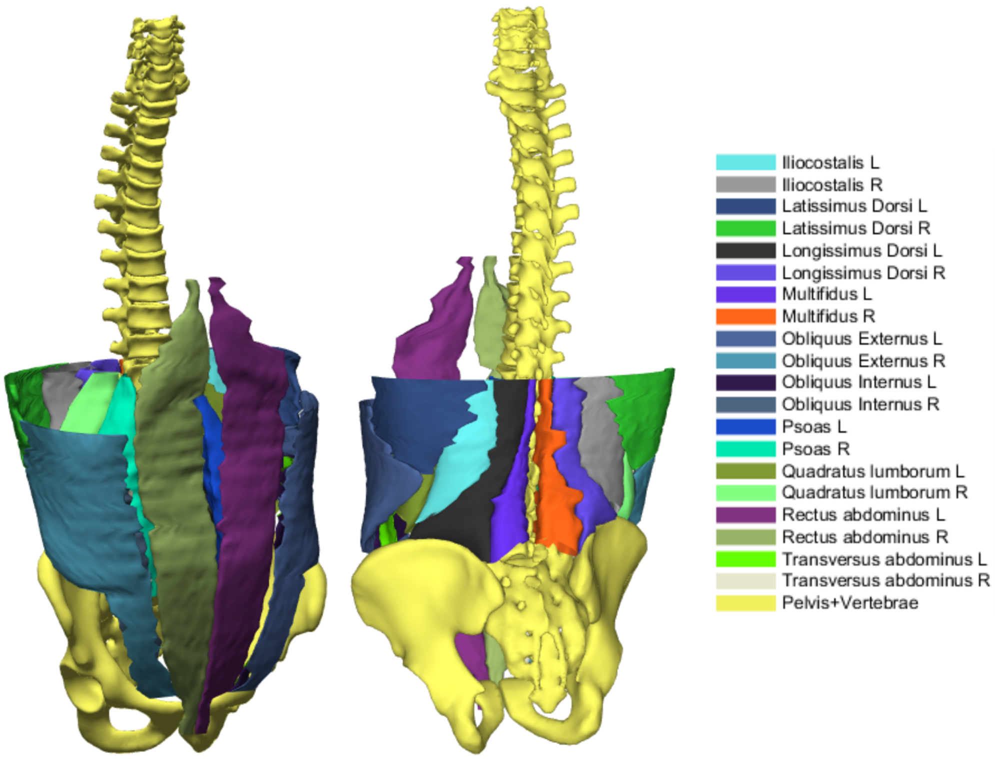


Figure 9.11. : 3D reconstruction of the muscles obtained from MRI segmentation, kriged on the EOS 3D skeleton model.

### 9 - 5.2 Section of interest

Once the 3D muscles' reconstructions have been set in the standing position, the 3D model is cut by an axial plane at mid-level of the inter-vertebral disc. This axial plane is the plane containing the L3-L4 inter-vertebral joint center.

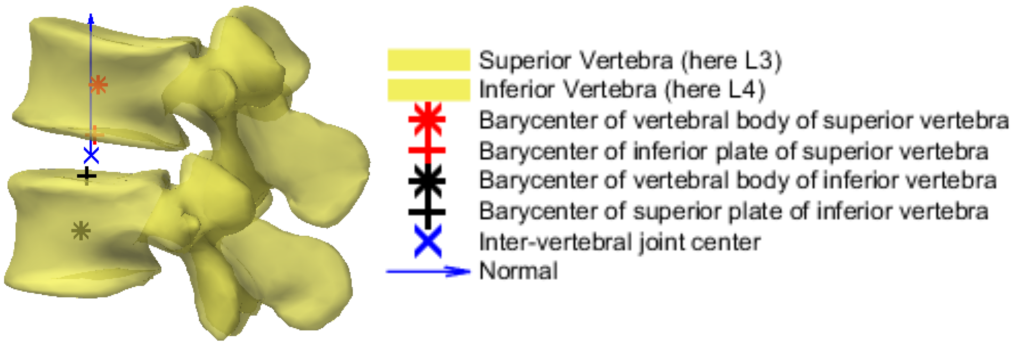


Figure 9.12. : Definition of the axial plane at mid level of the inter-vertebral disc in the EOS environment.

This axial plane, (Figure 9.12), is defined by:

- the normal, being defined as the vertical vector oriented upward;
- the inter-vertebral joint center, being defined as the middle point between the barycenter of the inferior plate of the superior vertebra and the barycenter of the superior plate of the inferior vertebra.

### 9 - 5.3 Muscular area on section

On the axial slice obtained, intersection of the 3D reconstructions of the muscles and the axial plane considered, results in the contour of each muscle on the slice. The muscle's area on the slice is computed from the number of pixels inside the muscle's contour and the pixel size. This area is called cross-sectional area (CSA).

### 9 - 5.4 Centroid of the muscle ($Centroid\_i$, i=X,Y)

The position of the barycenter of the muscle's contour is computed to give access to the muscles' centroids ($Centroid\_i$, i=X,Y).

### 9 - 5.5 Vector line of action

The main hypothesis is that for all considered muscles, the muscle's force (and therefore line of action) is oriented parallel to the principal direction of the muscle. A cubic spline (dark blue line on Figure 9.13) is computed as the cubic spline joining the successive centroids of each consecutive axial slices defining the muscle of interest (light blue points on Figure 9.13).

The vector line of action on the considered slice for the model MMR is the vector oriented upward that follows the direction of the line that best fits (in the least-square sense) all the axial centroids located more cranial that the centroid on the considered slice (red line on Figure 9.13). An example can be seen on Figure 9.13, for the psoas left muscle: green points represent the points on the muscle's contour being at the intersection with the considered inter-vertebral disc plane.

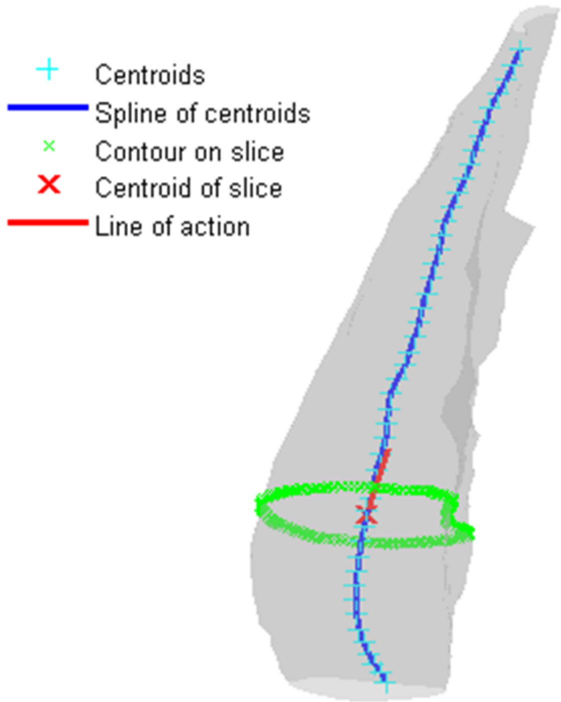


Figure 9.13. : Line of action of left psoas.

An example of the resulting muscular geometry information needed can be visualized on Figure 9.14: cross-sectional area, centroid, and line of action of each muscle is represented at the L3-L4 inter-vertebral disc level.

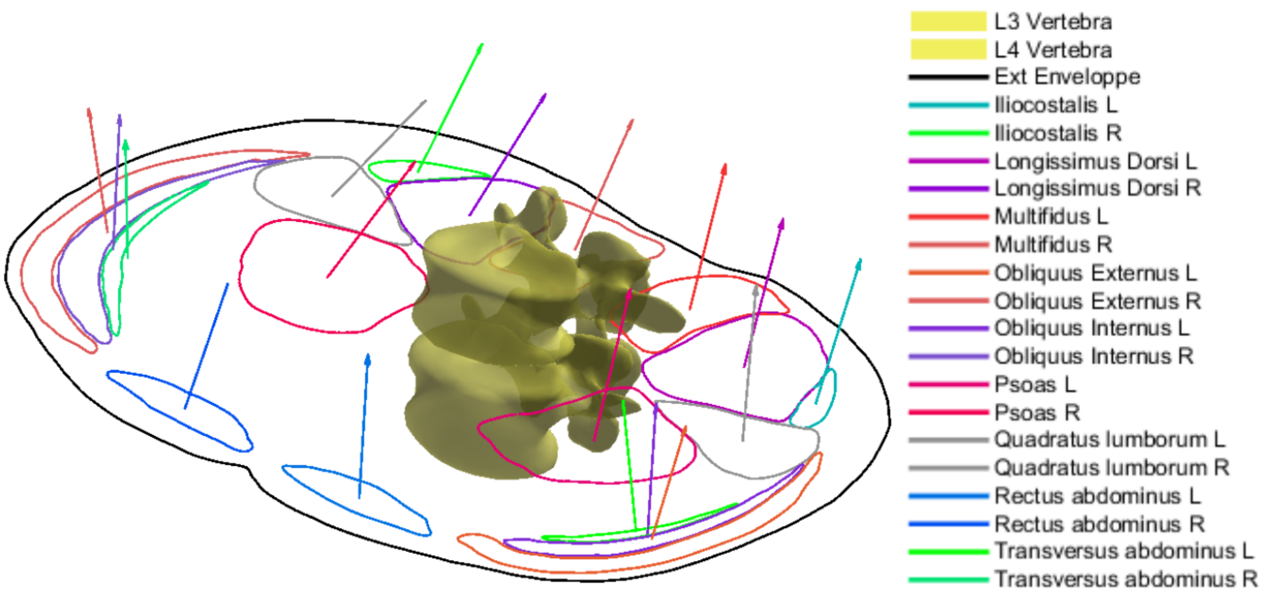


Figure 9.14. : Axial slice of the considered inter-vertebral disc (L3-L4 here), with, for each muscle: contour, centroid and vector of the line of action.

## 9 - 6 Muscles' maximal admissible stress

The maximal muscle stress is linked to the maximal force per unit surface area a muscle can generate. A decreased value, compared to normative data, indicates a general fatigue or muscular injury.

Studies reported in the literature values from 0.3 MPa to 1.0 MPa, equivalent to values from 30 N/cm$^2$ to 100 N/cm$^2$. Table 9.6 reports values used in the literature for biomechanical modeling of the trunk.

| | **Chole--wicki *et al.* 1996** | **Granata *et al.* 2001** | **Brown *et al.* 2005** | **El Ouaaid *et al.* 2013** | **Hajihos--seinali *et al.* 2014** | **Shahvar--pour *et al.* 2016** | **Bruno *et al.* 2015** |
|---|---|---|---|---|---|---|---|
| **MPa** | 0.35 | 0.5 | 0.5 | 0.6 | 0.6 | 0.6 | 1.0 |
| **N/cm$^2$** | 35 | 50 | 50 | 60 | 60 | 60 | 100 |

Table 9.6. Values reported in the literature for maximal admissible stress in muscle.

The value of 50N/cm$^2$ has been chosen here as representative of the overall values used in the literature. This value was also used by Pomero *et al.* (Pomero *et al.*, 2002, 2004).

## 9 - 7 Antagonist excitation from antagonist law

Antagonist muscles can be activated to control the posture and/or movement and to protect the joint by stabilizing it. In the setting of postural control, antagonist muscles are of great interest. The question is how antagonist excitation is implemented in the model?
The antagonist law reported in 1996 by Zhou *et al.* (Figure 9.15), was implemented by Vincent Pomero in 2002 in the model (Pomero *et al.*, 2002, 2004). This antagonist law provides the excitation of the antagonist muscles according to the resulting moment at the joint.

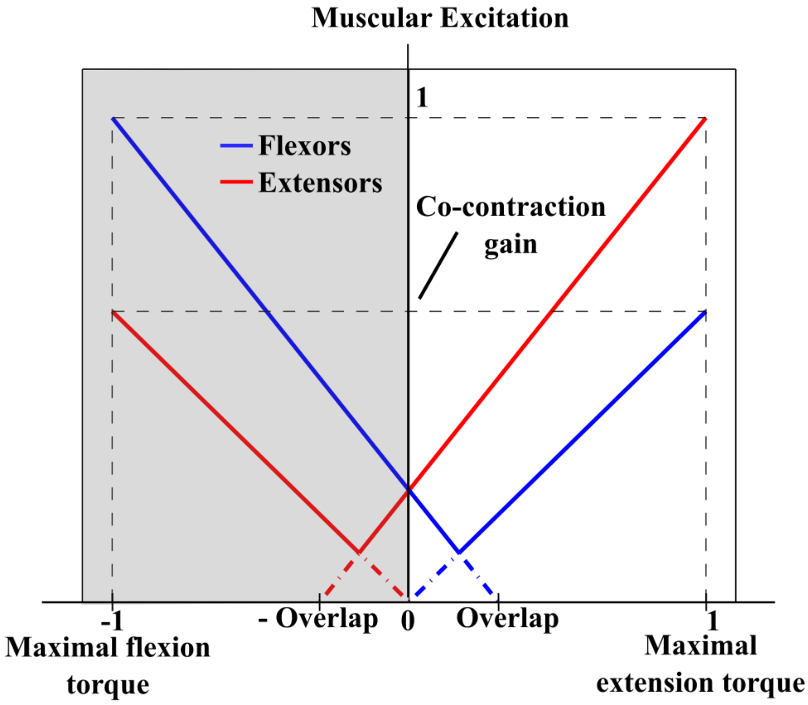


Figure 9.15. : Antagonist law (Zhou *et al.*, 1996).

If the *Overlap* for both muscles is set at 50%, "this means that if the command input changes linearly from maximal flexion torque (-1) to maximal extension torque (+1), the flexor starts fully active and decreases its activity linearly, reaching zero at the 50% of extension command. At a 50% flexion torque input command, the extensor is minimally activated, linearly increasing its activity until the maximum extension torque point.", cited from Zhou *et al.* (1996).

The *Co-contraction Gain* is defined as "the slope of the antagonist linear activation function" cited from Zhou *et al.* (1996).

Parameters Overlap and Co-contraction Gain, were fixed after a case study (Appendix D): the Overlap value was set at 25% while the Co-contraction was set at 20%.

# CHAPTER 10

# CLINICAL APPLICATION OF MMR MODELING

This chapter focuses on the use of the previously described biomechanical musculo-skeletal model on young and older adults with and without spinal deformities. The aim of this study was to compare resulting inter-vertebral loads for different subjects / patients with different postures.

## 10 - 1 Methods

### 10 - 1.1 Population

Three different groups of subjects/patients were considered, for whom both EOS radiographs and MRI images were acquired:

- the **Control** group: asymptomatic young adults (N=1),
- the **Aging** group: asymptomatic adults older than 50 years old (N=11),
- the **Patients** group: female patients with adult spinal deformities (N=8).

For the Control and Aging groups, inclusion in the study required: full body MRI with Dixon method, head to feet EOS radiographs, no previous musculo-skeletal surgery and no current disability. For the Patients group, inclusion in the study required being older than 35 years old, no history of spine surgery, no existing instrumentation and at least one of the following radiographic parameters: thoraco-lumbar or lumbar coronal Cobb angle greater than 30°, Sagittal Vertical Axis (SVA) greater than 4 cm, or Pelvic Tilt (PT) greater than 20° (for more details see study of Moal *et al.* (Moal *et al.*, 2015)).

All patients/subjects provided informed consent prior participating in the study after IRB and CCP approval. Data for the Control subject were collected during this PhD. The Aging Group subjects were prospectively recruited and collected in Hôpital Raymond Poincaré (Garches, France), during this PhD. The Patients Group subjects were extracted from a previous study in Hospital of Joint Diseases, (New York City, USA), during the PhD of Bertrand Moal (Moal, 2014).

### 10 - 1.2 Bi-planar radiographs

All subjects/patients underwent a head to feet EOS exam. 3D reconstructions of the spine (C3-L5) (Humbert *et al.*, 2009b), pelvis (Mitton *et al.*, 2006) and external body shape (Nérot *et al.*, 2015), were performed on bi-planar radiographs.

### 10 - 1.3 Magnetic Resonance Imaging

All subjects/patients underwent a head to feet MRI exam. Details about the MRI acquisition can be found in a previous study (Moal *et al.*, 2015).

3D reconstruction of the considered spino-pelvic muscles was performed with the DPSO method (Jolivet *et al.*, 2014). Muscles considered are: back muscles (multifidus, longissimus, iliocostalis), latissimus dorsi, psoas, quadratus lumborum, obliquus externus, obliquus internus, transversus abdominis, rectus abdominis. From these reconstructions were computed for each muscle, the centroid location on the slice L3-L4, the vector line of action and the cross-sectional area (CSA).

In order to quantify the fat infiltration of muscles present on the considered L3-L4 slice, the method reported by Antony *et al.* was applied (Antony *et al.*, 2014). Firstly, distribution of the intensity of pixels inside circles of $1mm^2$, placed either in muscular or fat area on the L3-L4 slice (Gille, 2006), was analyzed (top graph in Figure 10.2). Secondly, a sigmoid was applied to discriminate pixels from muscle and fat (bottom graph in Figure 10.1). Parameters of the sigmoid such as the threshold (fixed at 50) and the sharpness (fixed at 5) were set to obtain the best distinction between fat and muscle pixels according to their pixel intensity distribution (top graph in Figure 10.1). An example of this discrimination of fat and muscle pixels, for the right psoas, can be seen in Figure 10.2. Fat percentage (Pfat) was computed as the ratio number of fat pixels over total number of pixels inside the muscle's contour. This percentage was introduced in the model by a factor multiplying the cross-sectional area measured on the MRI slice, in order to compute the efficient area of the muscle: Efficient_area = (1-Pfat)*CSA.

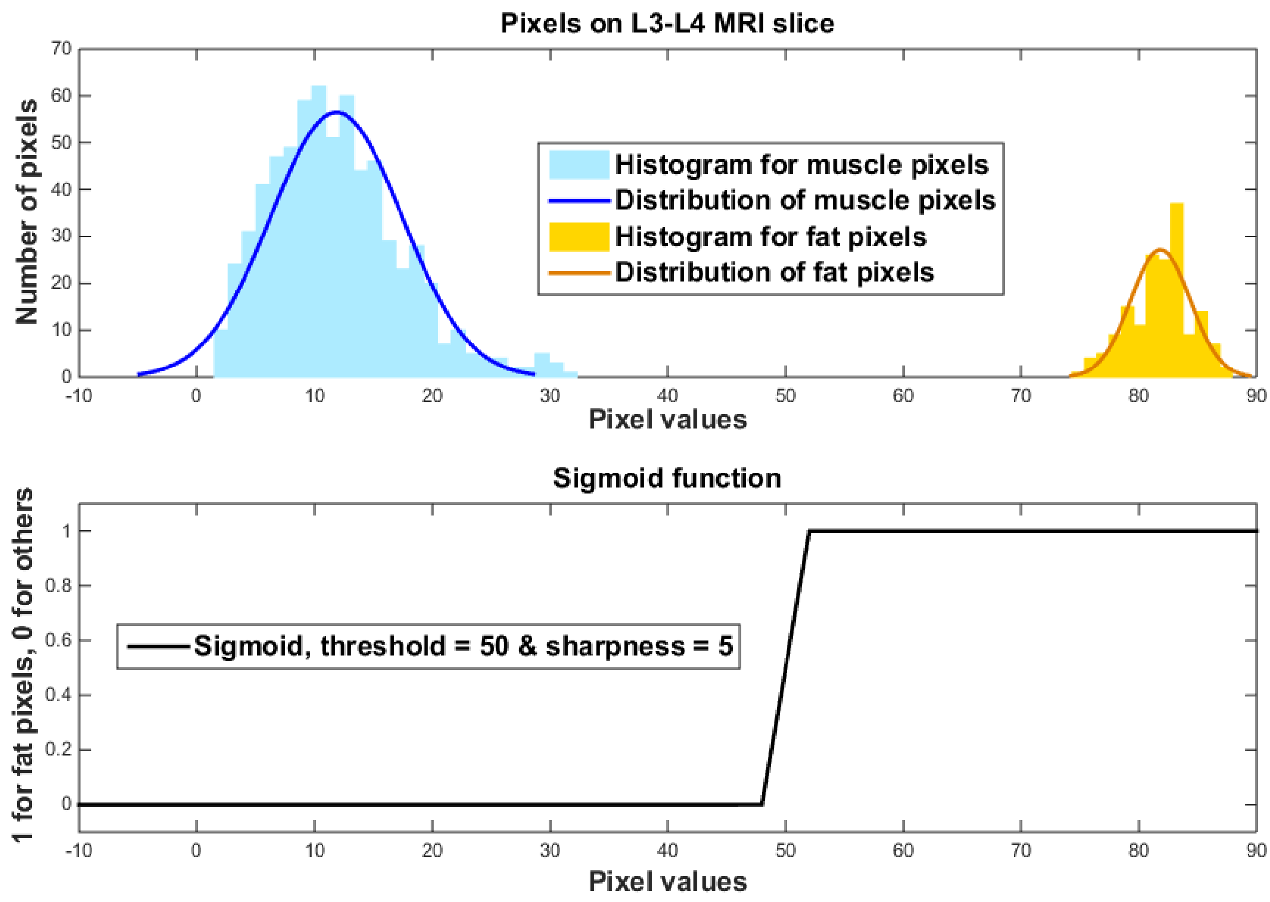


Figure 10.1. : **Top**: distribution of muscular pixels based on 4 circles of $1mm^2$ placed in darkest areas of right and left psoas and erector spinae or in area of subcutaneous fat. **Bottom**: sigmoid function applied for differentiation of fat and muscle pixels.

### 10 - 1.4 Biomechanical Model

The model algorithm is described elsewhere (Pomero *et al.* (2004), Appendix C), and process of medical images to obtain input details has already been described in a previous chapter (Chapter 9). Briefly, this

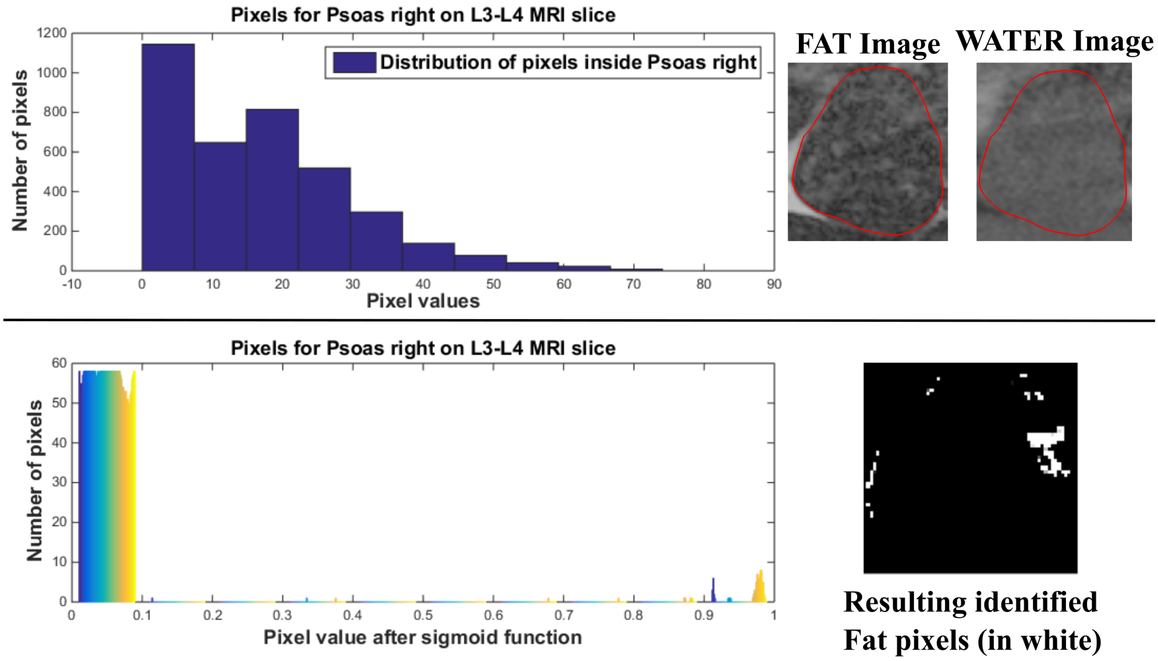


Figure 10.2. : Fat pixels detection in right psoas based on sigmoid discrimination (subject C1).

model takes as inputs 3D subject-specific geometry of the spine and pelvis (from 3D reconstruction based on bi-planar radiographs) and of the spino-pelvic muscles (from 3D reconstruction based on MRI images) (Figure 10.3). The inter-vertebral disc level L3-L4 was considered. By cutting the 3D reconstruction by an axial plane at this level, centroids, lines of actions and cross-sectional areas were obtained for each muscle present on the axial slice (Figure 10.4).

In this 3D reconstruction, the X axis is the postero-anterior axis; Y is the medio-lateral axis, oriented towards the left of the patient and Z is the caudo-cranial axis. In the following, Fx (respectively Fy and Fz) denotes the force on the X axis (resp. Y and Z axis); Mx (respectively My and Mz) denotes the moment on the X axis (resp. Y and Z axis).

The model computes the resulting loads at the L3-L4 inter-vertebral disc level by activating specific muscles in order to regulate and maintain the resulting loads within acceptable thresholds. More details can be found in the published study of Pomero *et al.* (Pomero *et al.*, 2004).

The net reaction forces and moments at the inter-vertebral joint can be computed for the 3D reconstruction of the external body envelope (Nérot *et al.*, 2015) and published segments densities (Dempster, 1955; Amabile *et al.*, 2016a). Figure 10.5, presents the 3D external envelope, the position of the center of mass of the upper body and the inter-vertebral joint center, for one Aging subject (A6). Figure 10.6, presents the coordinates of the center of mass of the upper body and its weight for all subjects and patients in the axial plane.

Threshold value of loads triggering muscular activation were set as follow: 75N for Fx; 100N for Fy; -1500N for Fz; 4.9Nm for Mx, My and Mz. Maximal admissible stress in muscles was set at 50N/cm$^2$ (Granata and Wilson, 2001; Brown and Potvin, 2005; Pomero *et al.*, 2004).

Antagonist activity was implemented in the model following the antagonist law described by Zhou *et al.* (Zhou *et al.*, 1996) with an overlap of 25% and a co-activity gain of 20%.

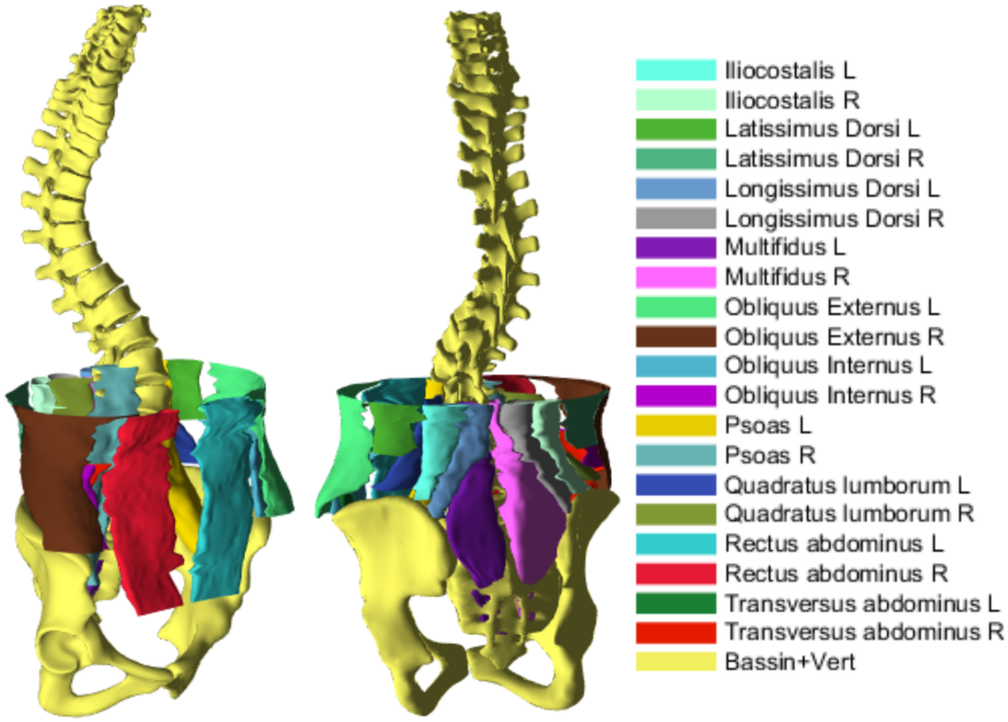


Figure 10.3. : 3D reconstruction of the muscles obtained from MRI segmentation, and skeleton from EOS radiographs, for the patient P1 of the Patients Group.

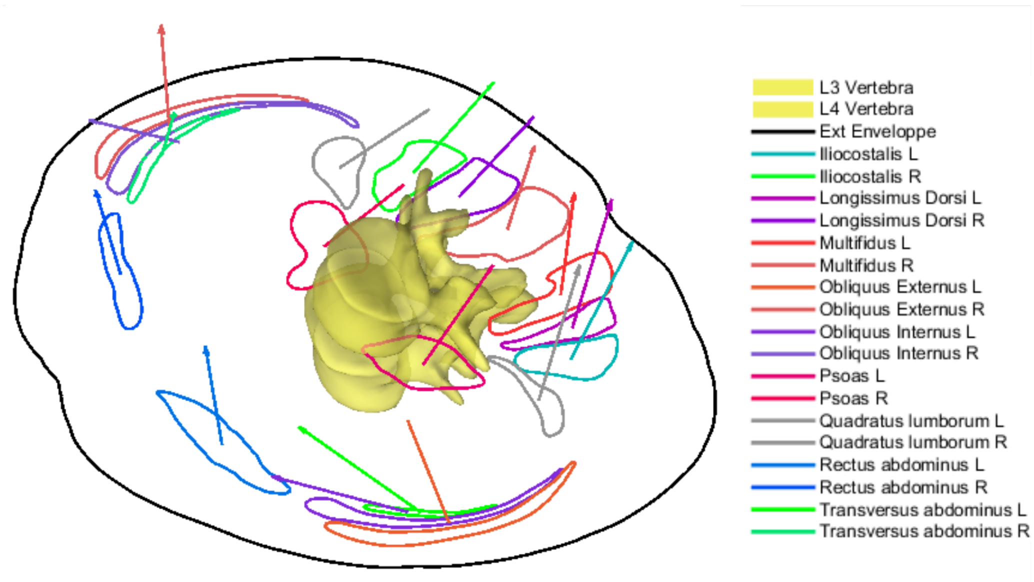


Figure 10.4. : Information obtained at the L3-L4 inter-vertebral disc level from 3D reconstruction of muscles and skeleton, for the patient P1 of the Patients Group.

### 10 - 1.5 Simulations

2 different static positions were considered:

- the standing position being the standardized free standing position described by Chaibi *et al.* (Chaibi *et al.*, 2012) held in the EOS cabin, called ***Neutral*** position;
- a simulated position with an anterior flexion of the trunk of 30°, called ***Flex30*** position.

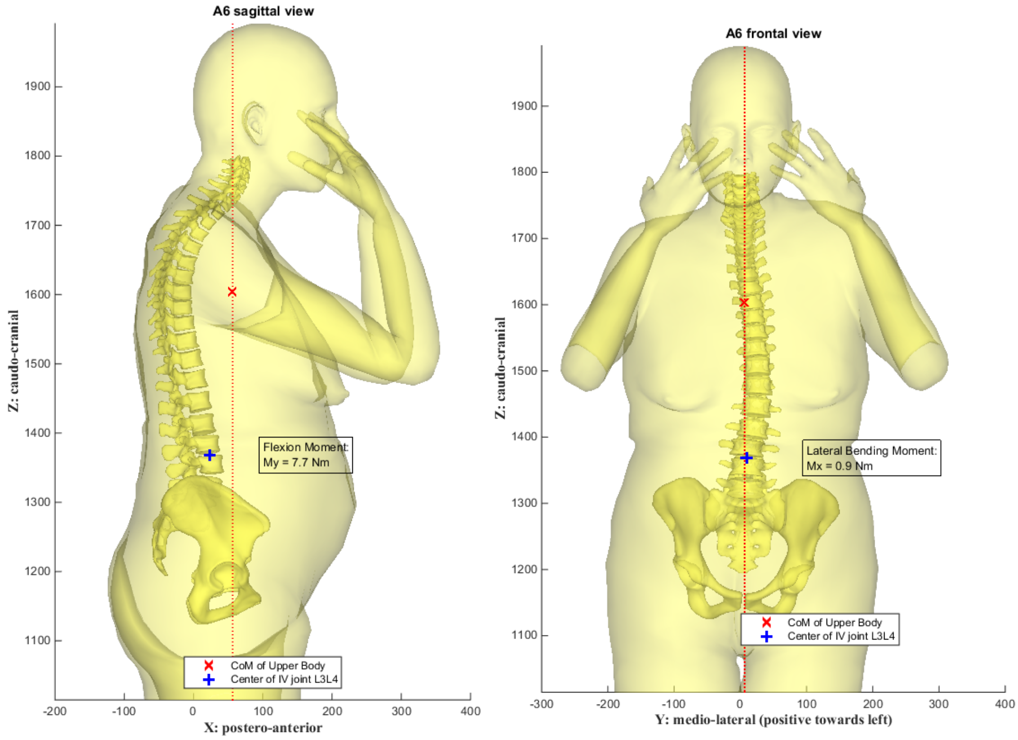


Figure 10.5. : Illustration of the computation of the net reaction forces and moments at the inter-vertebral joint center with position of the center of mass of the upper body for Aging subject A6 with net reaction forces and moments of: - 40.2N for Fx; 0.3N for Fy; -232.5N for Fz; 0.9Nm for Mx; 7.8Nm for My; - 0.1Nm for Mz, in the ***Neutral*** position.

The ***Flex30*** position was simulated by computing the net reaction forces and moments, when rotating the center of mass of the upper body (compared to the slice at the L3-L4 inter-vertebral joint level) of 30° anteriorly (rotation around the medio-lateral axis Y), with respect to the L3-L4 inter-vertebral joint center.
Three different configurations were tested for each position:

- All muscles were considered as not altered (no fat infiltration), with a maximal muscular stress of 50 N/cm$^2$, called ***No Alteration*** configuration;
- All muscles were considered to be altered with subject-specific fat tissue (fat infiltration computed from MRI slice as described by Antony *et al.* (2014)), with a maximal muscular stress of 50 N/cm$^2$, called ***Alteration*** configuration;
- All muscles were considered to be altered with subject-specific fat tissue (fat infiltration computed from MRI slice as described by Antony *et al.* (2014)), and maximal muscular contraction was reduced to 15 N/cm$^2$ to simulate muscular fatigue, called ***Fatigue*** configuration.

Altogether, 6 simulations were done for each patient (i.e. 2 positions * 3 configurations).

### 10 - 1.6 Analysis of net reaction forces and moments, and resulting loads

For each simulation, the net reaction forces and moments will be compared to the threshold values as the ratio of the two determine the regulation command Y stimulating muscular contraction (Equation 8.2). This will assess how much muscular contraction is needed to maintain the considered position. Then resulting loads will be compared to net reaction forces to evaluate the effect of the muscular contraction in limiting the resulting loads.

## 10 - 2 Results

Characteristics of each group can be found in Table 10.1.

| Group | N | Age (years) | BMI (kg/m$^2$) | Fat percentage (%) |
|---|---|---|---|---|
| **Control** | 1 | 28 | 24 | 2 (2) [0 - 9] |
| **Aging** | 11 | 63 (6) [52 - 71] | 25 (5) [20 - 38] | 4 (5) [0 - 35] |
| **Patients** | 8 | 63 (5) [54 - 70] | 22 (3) [20 - 28] | 6 (7) [0 - 36] |

Table 10.1. : For each group, age, BMI and fat percentage over all muscles. Mean (1*SD) [Range].

Figure 10.6 presents the axial position of the center of mass of the upper body from the inter-vertebral joint center, for each subject, for the ***Neutral*** position. The size of the point is proportional to the weight of the upper body. This figure allows to compare the different positions for the center of mass, directly linked to the net reaction forces and moments observed.

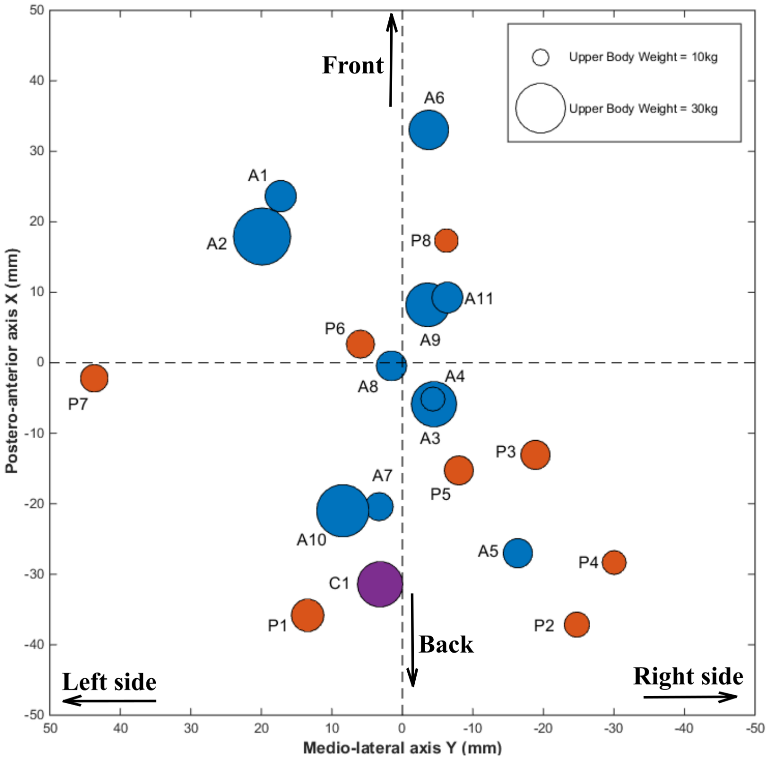


Figure 10.6. : Axial position of center of mass from inter-vertebral joint center and weight of the upper body, for each subject / patients in the ***Neutral*** position. The size of the circle is proportional to the upper body weight. The purple circle refers to the subject of the Control Group. Blue circles refer to subjects of the Aging Group. Orange circles refer to patients from the Patients Group.

### 10 - 2.1 *Neutral* position

Figures 10.8 and 10.9 present the forces and moments, for the ***Neutral*** position, for the net reaction forces and moments, and resulting loads obtained in the three simulated configurations. In the ***Neutral*** position, **net reaction forces and moments** larger than the threshold values were found for:

- postero-anterior shear force: for 2 in Aging Group (A3 and A9) and 1 in Patients Group (P8);
- lateral bending moment: for 1 in Aging Group (A2) and 1 in Patients Group (P7);
- flexion moment: for the Control subject (C1), 3 in Aging Group (A2, A6, A10) and 2 in Patients Group (P1 and P2).

For the Control subject (C1), five Aging subjects (A2, A3, A6, A9, A10) and 4 Patients (P1, P2, P7 and P8), regulation was needed by muscular activation in the ***Neutral*** Position (Figures 10.8 and 10.9). For all subjects / patients, for the three configurations simulated, muscular activation regulated the exceeding component by lowering the value below the threshold. Table 10.2 reports, for each force (Fx, Fy, Fz) and moment (Mx, My, Mz), the difference between resulting loads for each one of the three simulated configurations (No alteration, Alteration, Fatigue) and the net reaction forces and moments. Examples of muscular activation computed for one subject and one patient are presented in Figure 10.7.

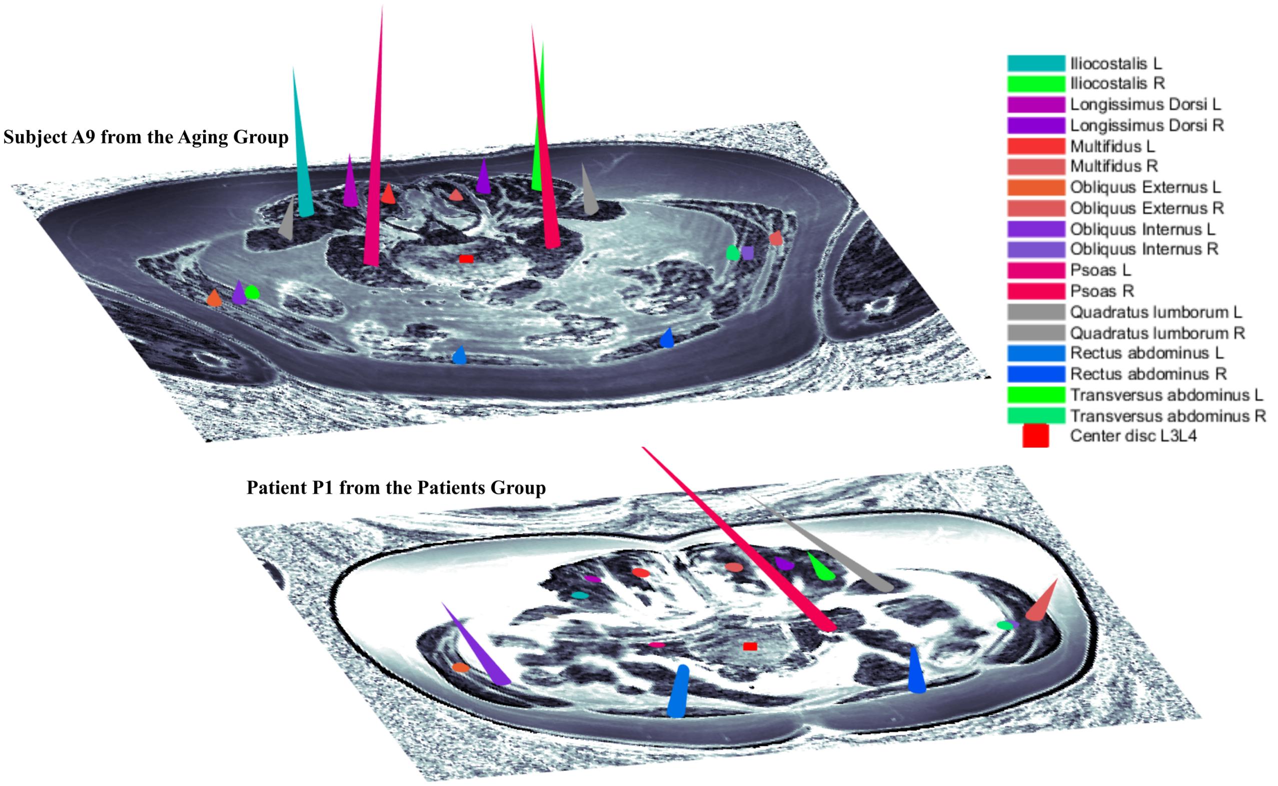


Figure 10.7. : Axial MRI slice at L3-L4 level with illustration of muscular activation. The height of cones is proportional to the activation of the muscle. Position of the center of the cone's basis is the centroid of the muscle, and direction of the cone is the line of action of the muscle. Subject A9 of Aging Group and patient P1 of the Patients Group are represented here in the ***Neutral*** position, with no alteration of muscles.

## 10 - 2.2 *Flex30* position

Figures 10.10 and 10.11 present the forces and moments, for the ***Flex30*** position, for the net reaction forces and moments, and resulting loads obtained in the three configurations simulated. In the ***Flex30*** position, **net reaction forces and moments** larger than the threshold values were found for:

- postero-anterior shear force: for 2 in Aging Group (A3 and A9) and 1 in Patients Group (P8);
- lateral bending moment: for 1 in Aging Group (A2) and 1 in Patients Group (P7);
- flexion moment, for all subjects / patients of all groups;
- torsion moment: for 2 in Aging Group (A1 and A2) and 7 in Patients Group (P1, P2, P3, P5, P6, P7 and P8).

Table 10.2 reports, for each force (Fx, Fy, Fz) and moment (Mx, My, Mz), the difference between resulting loads for each one of the three simulated configurations (No alteration, Alteration, Fatigue) and the net reaction forces and moments.

| **Neutral Position** | | | | | | |
|---|---|---|---|---|---|---|
| **No alteration** | **$F_x$ (N)** | **$F_y$ (N)** | **$F_z$ (N)** | **$M_x$ (Nm)** | **$M_y$ (Nm)** | **$M_z$ (Nm)** |
| **Control** | 46.0 | - 19.1 | - 200.7 | 1.7 | 4.9 | - 1.3 |
| **Aging** | - 5.7 / 71.2 | - 23.3 / 3.1 | - 176.9 / - 2.4 | - 1.3 / 4.9 | - 5.8 / 4.9 | - 0.8 / 0.5 |
| **Patients** | 5.5 / 40.0 | - 66.1 / 30.3 | - 162.1 / - 56.2 | - 2.6 / 5.2 | - 1.8 / 4.9 | - 1.2 / 1.9 |
| **Alteration** | **$F_x$ (N)** | **$F_y$ (N)** | **$F_z$ (N)** | **$M_x$ (Nm)** | **$M_y$ (Nm)** | **$M_z$ (Nm)** |
| **Control** | 47.0 | - 20.0 | - 208.2 | 1.8 | 4.8 | - 1.3 |
| **Aging** | - 6.0 / 70.9 | - 23.0 / 3.3 | - 171.4 / - 2.4 | - 1.3 / 4.8 | - 6.0 / 4.8 | - 0.8 / 0.5 |
| **Patients** | 4.3 / 40.7 | - 65.4 / 30.5 | - 164.0 / - 57.3 | - 2.7 / 5.3 | - 1.8 / 5.1 | - 1.2 / 1.9 |
| **Fatigue** | **$F_x$ (N)** | **$F_y$ (N)** | **$F_z$ (N)** | **$M_x$ (Nm)** | **$M_y$ (Nm)** | **$M_z$ (Nm)** |
| **Control** | 35.2 | - 13.0 | - 158.7 | 1.4 | 4.2 | - 1.3 |
| **Aging** | - 3.8 / 65.0 | - 19.4 / 2.6 | - 152.2 / - 1.3 | - 1.0 / 4.3 | - 5.5 / 4.4 | - 0.7 / 0.6 |
| **Patients** | 0.2 / 35.7 | - 56.9 / 24.1 | - 141.1 / - 45.7 | - 2.4 / 4.8 | - 1.6 / 4.6 | - 1.1 / 1.7 |

| **Flex30 Position** | | | | | | |
|---|---|---|---|---|---|---|
| **No alteration** | **$F_x$ (N)** | **$F_y$ (N)** | **$F_z$ (N)** | **$M_x$ (Nm)** | **$M_y$ (Nm)** | **$M_z$ (Nm)** |
| **Control** | 191.7 | - 60.8 | - 559.7 | - 0.4 | - 27.1 | 1.6 |
| **Aging** | 7.9 / 270.9 | - 68.8 / 39.3 | - 962.2 / - 278.9 | - 5.1 / 3.9 | - 36.0 /- 14.1 | - 5.8 / 1.9 |
| **Patients** | 3.8 / 226.4 | - 150.1 / 72.3 | - 563.5 / - 220.9 | - 1.6 / 4.4 | - 16.8 / - 11.4 | - 10.1 / 6.4 |
| **Alteration** | **$F_x$ (N)** | **$F_y$ (N)** | **$F_z$ (N)** | **$M_x$ (Nm)** | **$M_y$ (Nm)** | **$M_z$ (Nm)** |
| **Control** | 193.2 | - 61.0 | - 563.8 | - 0.5 | - 27.7 | 1.6 |
| **Aging** | 8.6 / 260.2 | - 69.6 / 39.8 | - 960.0 / - 277.6 | - 5.0 / 3.7 | - 36.3 /- 14.2 | - 5.8 / 1.7 |
| **Patients** | 4.1 / 226.3 | - 155.1 / 72.0 | - 576.2 / - 221.5 | - 1.7 / 4.8 | - 16.9 / - 11.4 | - 10.2 / 6.5 |
| **Fatigue** | **$F_x$ (N)** | **$F_y$ (N)** | **$F_z$ (N)** | **$M_x$ (Nm)** | **$M_y$ (Nm)** | **$M_z$ (Nm)** |
| **Control** | 217.6 | - 68.3 | - 589.7 | 0.0 | - 26.7 | 1.6 |
| **Aging** | 23.0 / 288.3 | - 53.0 / 38.3 | - 749.0 / - 281.6 | - 5.9 / 3.8 | - 24.6 / - 13.8 | - 3.7 / 1.4 |
| **Patients** | 18.9 / 240.0 | - 125.0 / 69.3 | - 489.1 / - 201.8 | - 0.2 / 3.7 | - 16.2 / - 11.1 | - 9.3 / 4.4 |

Table 10.2. Difference of resulting loads of different configurations with net reaction forces for the ***Neutral*** and ***Flex30*** Position. This difference reports the effect of the muscular activation on the resulting loads. For Control Group, value of the only suibject; for Aging and Patients Groups : min / max.

## 10 - 3 Discussion

This study aimed to investigate the effect of different postures and postural alterations on the muscular recruitment pattern, by looking into details at the inter-vertebral resulting loads for different positions and muscles states.

### 10 - 3.1 *Neutral* position

For the ***Neutral*** position, all load components were regulated after muscular activation (Figures 10.11 and 10.10). Alteration of the muscular quality did not increase loads over the threshold values, neither did the effect of fatigue combined with this alteration. This confirmed that the standing posture is economic in energy, even if for some subjects from the Patients Group, the lateral shear, bending moment and torsion moment were higher than in the Aging or Control groups: as spinal deformities of these patients were in 3D and principally in the coronal plane, the center of mass was not aligned with the considered inter-vertebral joint center, especially in the frontal plane, thus generating lateral shear force and associated moments (Figures 10.5 and 10.6).

Muscular activation reduced the loads compared to net reaction forces and moments (Table 10.2). However, when studying the effect of alteration of muscle quality with or without effect of fatigue, one can note that loads are increasing because of less efficient and powerful muscular contraction (Figures 10.11 and 10.10).

Compression values, for the ***Neutral*** position, ranged from 140N to 476N. Hajihosseinali *et al.* reported compressive values of 420N and 469N, at the L4-L5 level, for an adult of 1.7m for 68kg (Hajihosseinali *et al.*, 2014). A similar subject was considered by Gagnon *et al.* who reported a compressive value of 475N, at the L3-L4 level (Gagnon *et al.*, 2011). Similar subjects in our study are subjects A1 and A9 of the Aging Group for which compressive values ranged from 217N to 337N. Differences observed can come from the initial compression: while 344N compressive load was applied in these both studies, here only around 200N were computed as initial compression. This difference, while observing similar subjects, can come from the different densities applied on the segments while computing the upper body weight (Amabile *et al.*, 2016a), or from different morphologies considered. The net reaction compressive force used in this study was directly computed from the 3D subject-specific envelope of the subject.

Significantly higher values have been reported for compression from 800N to 1600N (Arshad *et al.*, 2016; Arjmand and Shirazi-Adl, 2006; Gagnon *et al.*, 2001; Granata and Wilson, 2001). These increased values again are influenced by the initial compression (net reaction force) that is around 350N for all these studies. Differences in the resulting compression can come from the algorithms governing models. However, in the neutral posture, supporting an upper body weight from 14kg to 45kg, as found here, seems reasonable and plausible.

Concerning the postero-anterior shear values, these are subject-specific as they are influenced by the initial posture of the patient and more particularly the distribution of the different segments above the considered slice. In this study, postero-anterior shear values ranged from -52N to 61N in the ***Neutral*** position. Reported values were 2N and 36N for Hajihosseinali *et al.* (Hajihosseinali *et al.*, 2014); -21N for Gagnon *et al.* (Gagnon *et al.*, 2011) and around 50N for Arshad *et al.* (Arshad *et al.*, 2016). Similar subjects in this study (A1 and A9) presented values between -33N and -52N in line with reported values in the literature. These postero-anterior shear values are strongly dependent on the location of the center of mass compared to the inter-vertebral joint center: because the L3-L4 disc plane presents a positive angle with the horizontal plane, the gravity force generates a negative value for postero-anterior shear. Only subjects for which L3-L4 was below the lordosis apex (disc plane oriented negatively compared to the horizontal) presented positive postero-anterior shear values.

One study reported flexion moment values of 4.1Nm, for the ***Neutral*** position (Hajihosseinali *et al.*, 2014), in line with our current findings (from -4 to 3 Nm). Positive or negative sign depended on

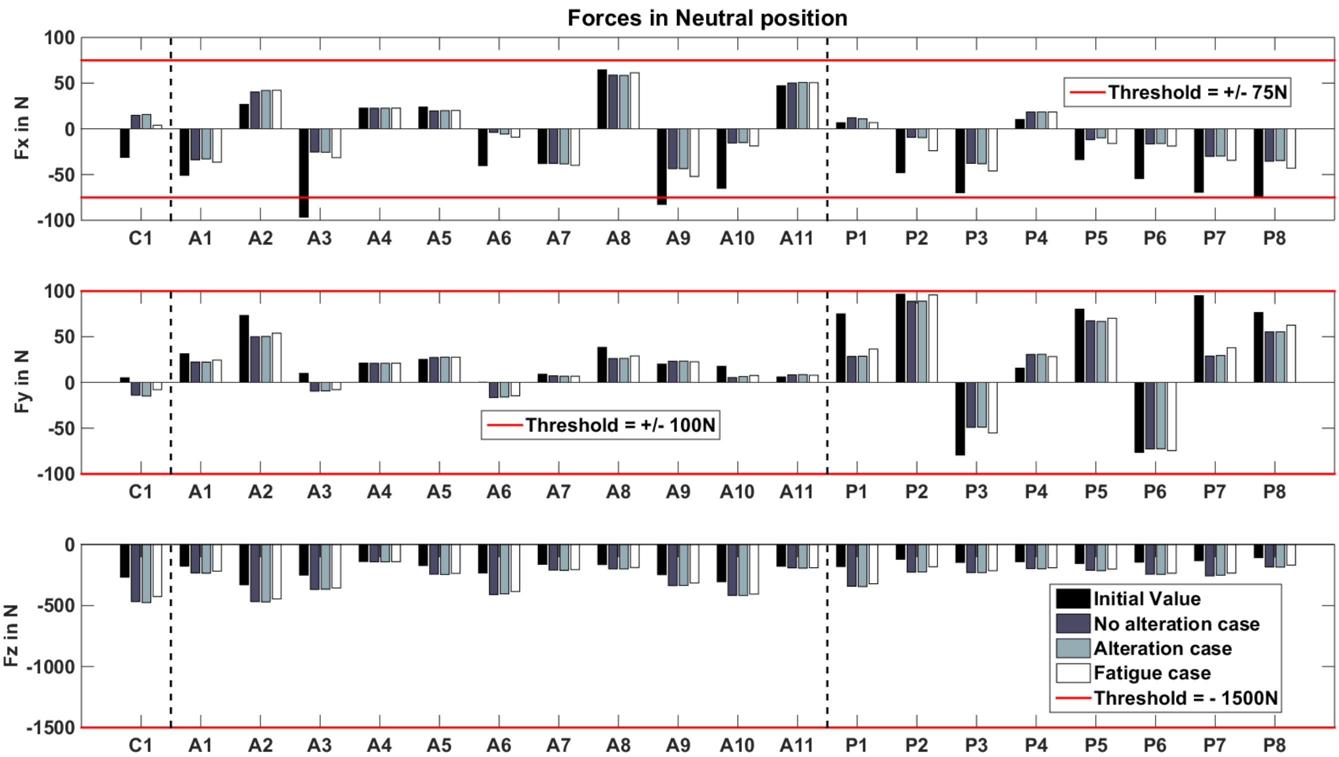


Figure 10.8. : Forces in the ***Neutral*** position for the net reaction forces (without muscular activation) and the three configurations simulated: No alteration; Alteration and Fatigue.

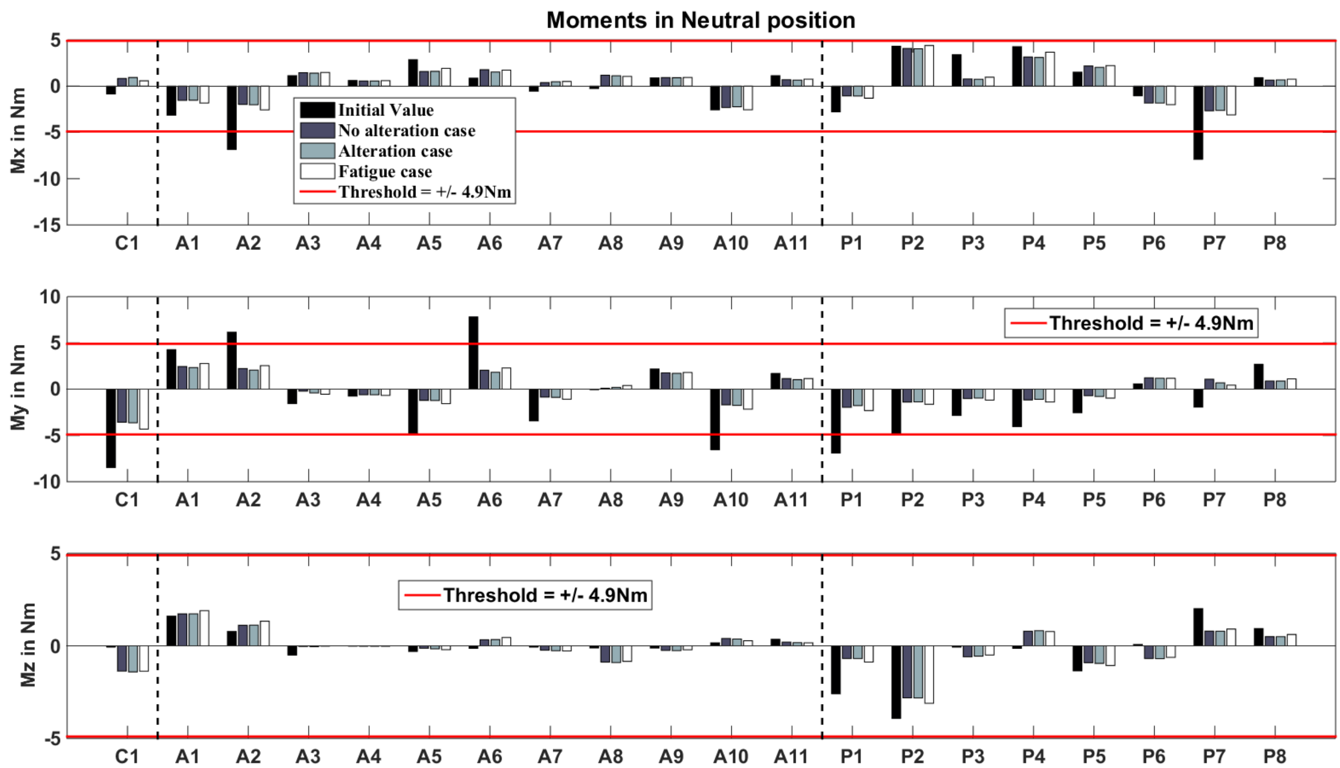


Figure 10.9. : Moments in the ***Neutral*** position for the net reaction moments (without muscular activation) and the three configurations simulated: No alteration; Alteration and Fatigue.

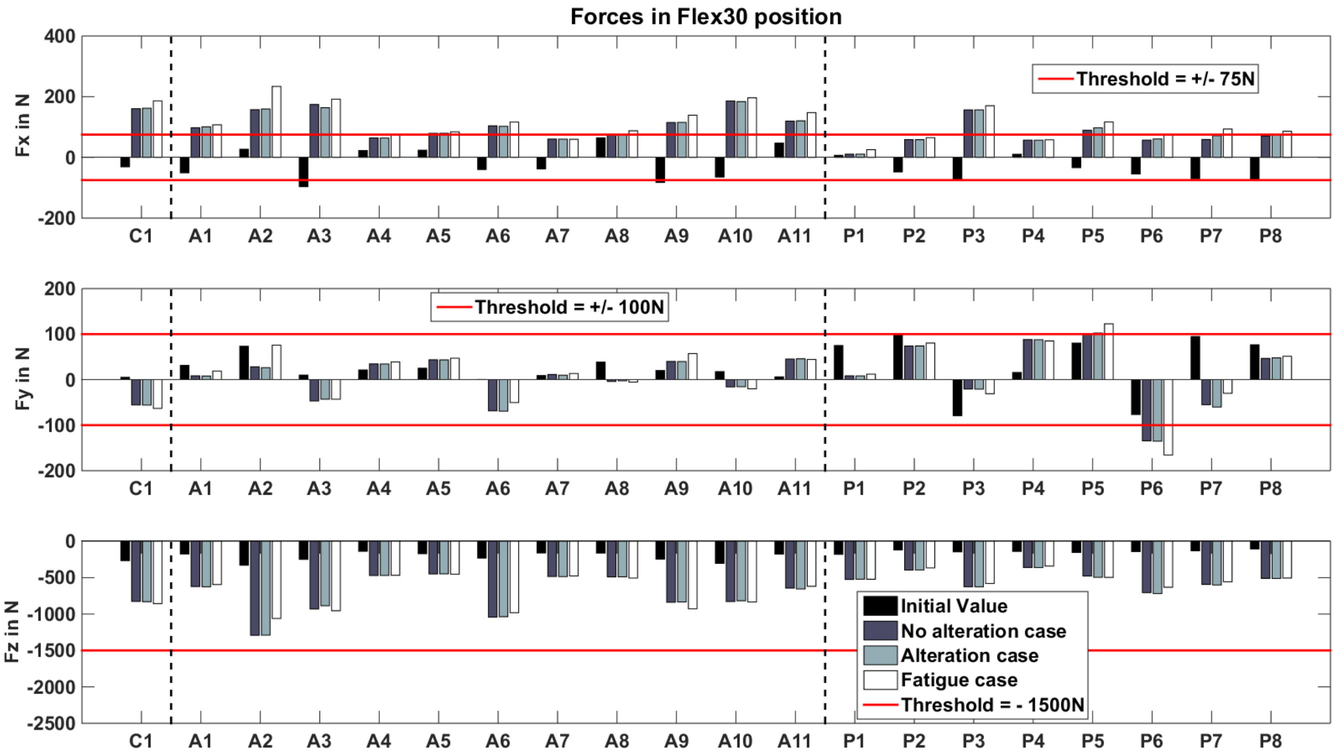


Figure 10.10. : Forces in the ***Flex30*** position for the net reaction forces (without muscular activation) and the three configurations simulated: No alteration; Alteration and Fatigue.

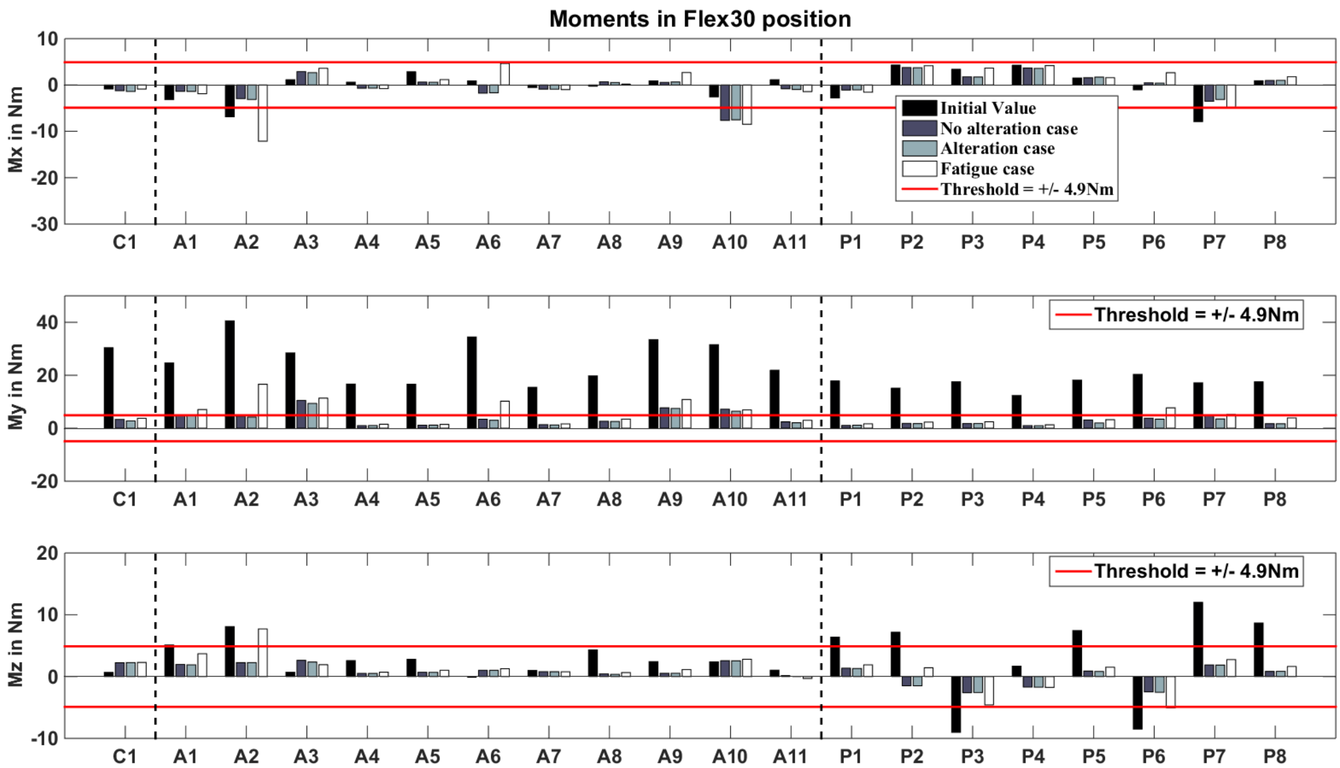


Figure 10.11. : Moments in the ***Flex30*** position for the net reaction moments (without muscular activation) and the three configurations simulated: No alteration; Alteration and Fatigue.

the relative position, in the sagittal plane, of the center of mass of the upper body compared to the inter-vertebral joint center (Figure 10.6).

### 10 - 3.2 *Flex30* position

The position of the trunk flexed anteriorly, was considered to stimulate a higher muscular response and increased net reaction forces and moments in the inter-vertebral joint compared to the ***Neutral*** position. As expected, the flexion moment (My) was above the threshold value for the net reaction forces and moments for all subjects; regulation demand was therefore high and greatly stimulated muscular activation. Out of the 8 patients with spinal deformities, 7 (88%) presented a higher torsion moment than the threshold, highlighting the 3D nature of the spinal deformities of those patients.

Concerning the flexion moment (My), muscular activation decreased the moment below the threshold except for 3 subjects from the Aging Group in the configuration ***No alteration*** and ***Alteration*** configuration. All these subjects exhibited high BMI value (24-28 kg/m$^2$) without presenting the largest BMI of the Aging Group. These subjects were not the ones with the largest fat infiltration in the back muscles. Lastly their initial shear and flexion moment were found in the range of other subjects' / patients' values.

Considering the ***Fatigue*** configuration, several subjects were not able to regulate this flexion moment (flexion moment exceeding 4.9 Nm) (Figure 10.11). Interestingly, these subjects / patients do not present higher fat infiltration in back muscles than others, but all presented a BMI greater than 23 kg/m$^2$. As the upper body is heavier, a small displacement in the axial plane will already introduce large moments in the inter-vertebral joint.

Only 2 studies to our knowledge reported values of resulting loads, for flexion of 30° of the trunk with no lift. Arshad *et al.* reported values of compression between 800 and 1100N reaching 1550N for a specific spinal rhythm (i.e. relative distribution of lumbar flexion at different lumbar levels) simulated; values of postero-anterior shear ranging from -50 to +50N or from 0N to 100N depending if the intra-abdominal pressure was considered or not (Arshad *et al.*, 2016). Gagnon *et al.* reported values of compression of 742N and postero-anterior shear values of 68N (Gagnon *et al.*, 2011). The postero-anterior shear values found here ranged from 11N to 234N and compressive force ranged from 342N to 1291N. Our values overall agree with those in the literature, the highest values for postero-anterior shear force were reported for subjects with high fat infiltration in the back muscles (even though this infiltration did not exceed 20%).

Surprisingly, the patient P7 presenting the highest fat infiltration of back muscles (iliocostalis, longissimus and multifidus) presented, in the ***Flex30*** position, a postero-anterior shear value of 72N when taking into account this muscular alteration (vs 59N with no alteration). Postero-anterior shear force reached 93N when considering the Fatigue configuration. This patient managed to limit the postero-anterior shear load even if the threshold at 75N was exceeded, at the expense of larger moments in the inter-vertebral joint (torsion moment of 1.9Nm with no alteration and with subject-specific alteration of muscles versus 2.8Nm when considering the Fatigue configuration).

Because an antagonist law has been implemented in the model, results predicted a certain amount of abdominal co-activity in the ***Flex30*** position. This co-activity is difficult to predict with optimization driven models (Arjmand *et al.*, 2009) but has been reported in studies using EMG-driven models (Gagnon *et al.*, 2001).

This model offers the possibility to study more precisely muscular activation for each muscle as reported in Figure 10.7. This type of figure could be useful to visualize which muscles need to be reinforced to limit more efficiently inter-vertebral loads.

### 10 - 3.3 Perspectives and limitations

One future improvement in this model would be to take into account the differences in muscular activation between young and older adults (Häkkinen *et al.*, 1998; Macaluso *et al.*, 2002). In particular, co-activity of antagonist muscles decreased in elderly, thus decreasing joint stability (Häkkinen *et al.*, 1998).

Another step towards a better representation would be to consider the arms in the computation of the net reaction forces and moments as this was not done here. If the arms are considered flexed with hands on the cheekbones such as in the Free Standing Position in the EOS cabin (Faro *et al.*, 2004), taking into account the arms would increase the compression as well as shear force and flexion moment, in the net reaction forces and moments. It might be also interesting to consider the arms along the body in a natural position such as when walking for example, this would in this case just impact the initial compression in the net reaction forces.

Another improvement would be to implement the deformation of the muscles in the ***Flex30*** position, and to provide the real 3D geometry of the spine and pelvis in such a position. This would lead to a more accurate computation of the net reaction forces and moments in such a position, and of the effects of muscular contraction on the resulting loads in the L3-L4 inter-vertebral joint. A related improvement would be to simulate posture and associated muscular geometry, for a non-compensated position for elders already recruiting compensatory mechanisms, using the protocol described in figure 6.2 of chapter 6.

One limitation of this study is the limited number of subjects in the Control Group, more young asymptomatic subjects would enhance results, by providing reference values of loads experienced in the inter-vertebral joints. Another limitation resides in the design of the model: currently, only one slice is considered for the control loop, therefore comparison between different disc levels cannot be made. The L3-L4 disc level was chosen here because it is located at the apex of the lordosis. Another interesting choice for future studies would be to consider the disc L5-S1 as it is the last level before the pelvic vertebra. If the sacral slope is large enough, this should result in high postero-anterior shear values to regulate. As with all optimization driven models, it is difficult to validate this model, except to compare to EMG values reported in the literature, and to *in-vivo* intra-discal pressure obtained with a pressure transducer inserted in a disc. However this comparison can be difficult due to the different morphologies and posture of subjects studied.

## 10 - 4 Conclusion

In conclusion, this study reported inter-vertebral loads for 2 different positions with different muscular alteration and muscular fatigue conditions. This study included a total of 20 subjects / patients of various ages, with different pathological conditions. In addition, the subject-specific 3D geometry of the spine, pelvis and muscles allowed for a refine analysis of the impact of postural alterations on muscular recruitment pattern.

The difficulty of specific subjects / patients to regulate one or more load component(s), could be used in the future, for design of specific exercises reinforcing specific muscles for example. This would allow a decrease of loads in the inter-vertebral joint and would reduce the probability of disc injury and back pain.

# CONCLUSION

This part focused on the computation of inter-vertebral loads for young and older adults with or without adult spinal deformities; with a biomechanical musculo-skeletal model.

Firstly, the adaptation and personalization of the input data of the previously published model (Pomero *et al.*, 2004) were described. The different steps to prepare input data from medical images such as radiographs and MRI images were reported. Computation of the net reaction forces and moments, at the inter-vertebral joint center at the L3-L4 disc level, was reported.

Secondly, this model was used to compute resulting loads in the inter-vertebral joint in different positions (standing and with flexion of the trunk); and with or without alteration of muscles (fat infiltration) and/or fatigue (decreased maximal muscular stress). Different populations were studied: one young asymptomatic adult, older asymptomatic adults and adults with spinal deformities.

The muscular recruitment pattern varied for each configuration, position, subject. Resulting loads were therefore subject-specific. Main results highlighted the ability for all to regulate the loads below a set threshold to protect the spinal cord, in standing position. Subjects with higher compressive force (higher body mass index), did not succeed in limiting the flexion moment for the position with the trunk flexed, when muscles were altered or experienced fatigue.

These results provide new insights on the work required by muscles to maintain an efficient posture, while preserving the spinal cord and inter-vertebral discs. Postural alterations have an impact on the resulting loads experienced in the inter-vertebral joint and different positions resulted in high differences in these loads.

This model identified specific muscles as essential for the maintenance of an economic posture, for each subject. Such findings could be used for surgical planning: for a specific subject, the best approach can be chosen as the one minimizing the impact on muscles essential for this subject.

This part focusing on the use of a biomechanical musculo-skeletal model, using 3D subject-specific data, highlighted the importance of such a personalization for the prediction of high resulting loads in the inter-vertebral joint in order to prevent injuries of spinal cord or inter-vertebral disc.

# GENERAL CONCLUSION

The objective of this PhD was to investigate age-related postural alignment and muscular changes.

The first part focused on the postural alignment changes over aging. A first study on young asymptomatic adults highlighted the quasi-invariant position of the head above the pelvis. This invariance provides a good distribution of the different segments above the pelvic vertebra, allowing for an efficient posture minimizing energy expenditure, inside the conus of economy, defined by Dubousset (Dubousset, 1994). Refine analysis of an older asymptomatic population concluded on the invariance of this alignment. However for 16 out of 41 subjects, this invariance was at the expense of other compensatory mechanisms such as pelvic retroversion and cervical hyperlordosis. Longitudinal study could assess if such biomarker could allow identification of such subjects at risk of degradation.

The second part of this PhD presented the work realized on MRI images, on the quantification of spino-pelvic muscles. Reference values have been calculated for young asymptomatic adults. A rapid and accurate method has been validated for the rough estimate of functional groups' volumes: this method could be implemented in clinical environment. A second chapter studied the spino-pelvic muscles of older adults with spinal deformities. Pathological aging affected muscles by a loss of volume for most muscles. However, gluteus muscles appeared as peculiar, as volumes and volumic ratios of gluteus muscles were larger than young asymptomatic adults'. This increase could be the marker of an increased stimulation to regulate finely the position of the pelvis supporting the whole upper body weight.

The third part focused on the adaptation and personalization of a spine and pelvis musculo-skeletal model in order to study the relationship between altered posture and muscular recruitment pattern (and therefore resulting inter-vertebral loads). By the study of various subjects in ages, pathological conditions and morphologies, preliminary results on the variability in muscular recruitment pattern have been reported. The ability to regulate the posture to limit inter-vertebral loads is subject-specific and suggests that future studies should emphasize the personalization of musculo-skeletal models to predict and analyze inter-vertebral loads for injury prevention. Preliminary work reported the difficulty of specific volunteers or patients to limit the flexion moment when the trunk is flexed about 30° anteriorly, when muscles are altered (fat infiltration quantified from MRI images) and under fatigue. These results highlight the importance of muscles' preservation during pathological evolution or aging, to resist the effect of fatigue the longest possible and better compensate postural alterations.

Overall, this PhD established reference values for asymptomatic adults in terms of postural alignment and muscular volumes. This provides a database for comparison when studying effect of aging or pathological evolution. Age-related changes were reported for the skeletal and muscular systems. Effect of an altered posture has been reported on muscular volume and muscular recruitment. An altered posture can be identified early, before a critical situation, by the assessment of the alignment of the head compared to the pelvis.

Another result was the rapid evaluation of muscular volumes of functional groups to quantify the muscular degradation occurring with aging, pathological evolution or post-operatively.

While the first two parts of this PhD quantified the changes occurring during aging, the musculo-skeletal model is a new tool to better understand the interaction between posture, spine and muscles. In this PhD, no concrete conclusion can be drawn on which from the postural alterations and the muscular changes cause the other. To do so, a larger cohort and a longitudinal study would bring significant knowledge on the changes occurring during aging or pathology's evolution. Indeed, this model has been used to study the process of aging but it could also be applied on various domains: for example to study evolution of spinal disorders, to investigate the development of low back pain, or to improve workstation ergonomics. Similarly, including patients with various pathologies and symptoms such as low back pain, ideally in a longitudinal study, would provide new elements on the understanding of these pathologies.

Short term perspectives include the global combination of the different results of this PhD: combining markers of the postural alignment alteration with quantification of the muscular degradation in the biomechanical model would improve this promising method and would open the way for different utilizations. Simplifying processing of medical images would allow user-friendly tools implementable in hospitals for clinical routine to quantify postural alignment with CAM-HA angle (or OD-HA angle); muscular degradation from MRI images; and impacts on the muscular recruitment pattern with the biomechanical model. Particularly, computing the resulting inter-vertebral loads, for elders presenting compensatory mechanisms at the pelvic and cervical levels, in a non-compensated position would be of special interest to evaluate the impact of these compensatory mechanisms.

Long term perspectives concerning biomechanical modelling include three different times in aging: the first one in prevention, the second one in back pain management and the third one in surgical planning and post-operative analysis.

Firstly, as the model presents the muscular pattern for the position chosen, clinical teams could identify specific muscles to reinforce, and design appropriate exercises to improve an efficient posture. This could also be used to reinforce specific muscles before surgery in order to enhance recovery and success of the surgical procedure.

Secondly, back pain management could be improved by providing real insights on the inter-vertebral loads, and muscular activation. Differentiation between high loads damaging the disc and hyper-stimulation of muscles and therefore their fatigue, could be made to improve diagnosis, prevention, and long-term care.

Thirdly, with this biomechanical model, different approaches for spinal surgical procedures (anterior approach, lateral or posterior approaches) can be simulated by reproducing the damages on muscles due to surgical procedure. This could give an insight on resulting loads in the inter-vertebral joint or implant after surgery. The best approach could then be chosen as the one minimizing these loads.

Overall, this model is original since it allows a complete 3D view of both muscles and skeleton. By providing the lines of action of muscles, impact of surgery or physical exercise can be directly imagined and modeled. This innovative view of the spino-pelvic complex provides a new promising instrument to improve spinal deformities care but also surgical planning.

# Part E

# List of Figures, Tables and References

# List of Figures

# List of Tables

# BIBLIOGRAPHY


Adams, M. A. (2015). Mechanical Properties of Aging Soft Tissues. In Derby, B., editor, *Mechanical Properties of Aging Soft Tissues*, pages 7–35. Springer International Publishing.

Adams, M. A., McNally, D. S., and Dolan, P. (1996). 'Stress' distributions inside intervertebral discs. The effects of age and degeneration. *The Journal of bone and joint surgery. British volume*, 78(6):965–972.

Ahmed, M. S., Matsumura, B., and Cristian, A. (2005). Age-related changes in muscles and joints. *Physical Medicine and Rehabilitation Clinics of North America*, 16(1):19–39.

Albracht, K., Arampatzis, A., and Baltzopoulos, V. (2008). Assessment of muscle volume and physiological cross-sectional area of the human triceps surae muscle in vivo. *Journal of Biomechanics*, 41(10):2211–8.

Amabile, C., Choisne, J., Nérot, A., Pillet, H., and Skalli, W. (2016a). Determination of a new uniform thorax density representative of the living population from 3D external body shape modeling. *Journal of Biomechanics*, 49(7):1162–1169.

Amabile, C., Moal, B., Chtara, O. A., Pillet, H., Raya, J. G., Iannessi, A., Skalli, W., Lafage, V., and Bronsard, N. (2016b). Estimation of spinopelvic muscles' volumes in young asymptomatic subjects: a quantitative analysis. *Surgical and radiologic anatomy*, pages 1–11.

Amabile, C., Pillet, H., Lafage, V., Barrey, C., Vital, J.-M., and Skalli, W. (2016c). A new invariant parameter characterizing the postural alignment of young healthy adults. *European Spine Journal*, pages 1–9.

Anders, C., Brose, G., Hofmann, G. O., and Scholle, H.-C. (2008). Evaluation of the EMG–force relationship of trunk muscles during whole body tilt. *Journal of Biomechanics*, 41(2):333–339.

Antony, J., McGuinness, K., Welch, N., Coyle, J., Franklyn-Miller, A., OConnor, N., and Moran, K. (2014). Fat Quantification in MRI-defined lumbar muscles. In *4th International Conference on Image Processing Theory, Tools and Applications.*

Arjmand, N., Gagnon, D., Plamondon, A., Shirazi-Adl, A., and Larivière, C. (2009). Comparison of trunk muscle forces and spinal loads estimated by two biomechanical models. *Clinical Biomechanics*, 24(7):533–41.

Arjmand, N., Gagnon, D., Plamondon, A., Shirazi-Adl, A., and Larivière, C. (2010). A comparative study of two trunk biomechanical models under symmetric and asymmetric loadings. *Journal of Biomechanics*, 43(3):485–91.

Arjmand, N. and Shirazi-Adl, A. (2006). Sensitivity of kinematics-based model predictions to optimization criteria in static lifting tasks. *Medical Engineering & Physics*, 28(6):504–514.

Arshad, R., Zander, T., Dreischarf, M., and Schmidt, H. (2016). Influence of lumbar spine rhythms and intra-abdominal pressure on spinal loads and trunk muscle forces during upper body inclination. *Medical engineering & Physics*, 38(4):333–8.

Aubert, B., Vergari, C., Ilharreborde, B., Courvoisier, A., and Skalli, W. (2014). 3D reconstruction of rib cage geometry from biplanar radiographs using a statistical parametric model approach. *Computer Methods in Biomechanics and Biomedical Engineering: Imaging & Visualization*, pages 1–15.

Badouna, A. N. I., Veres, C., Haddy, N., Bidault, F., Lefkopoulos, D., Chavaudra, J., Bridier, A., de Vathaire, F., and Diallo, I. (2012). Total heart volume as a function of clinical and anthropometric parameters in a population of external beam radiation therapy patients. *Physics in medicine and biology*, 57(2):473–84.

Barnouin, Y., Butler-Browne, G., Voit, T., Reversat, D., Azzabou, N., Leroux, G., Behin, A., McPhee, J. S., Carlier, P. G., and Hogrel, J.-Y. (2014). Manual segmentation of individual muscles of the quadriceps femoris using MRI: A reappraisal. *Journal of Magnetic Resonance Imaging*, 40(1):239–247.

Barrey, C., Roussouly, P., Le Huec, J.-C., D'Acunzi, G., and Perrin, G. (2013). Compensatory mechanisms contributing to keep the sagittal balance of the spine. *European Spine Journal*, 22(6):S834–841.

Barrey, C., Roussouly, P., Perrin, G., and Le Huec, J.-C. (2011). Sagittal balance disorders in severe degenerative spine. Can we identify the compensatory mechanisms? *European Spine Journal*, 20(5):626–33.

Baudoin, A., Skalli, W., de Guise, J. A., and Mitton, D. (2008). Parametric subject-specific model for in vivo 3D reconstruction using bi-planar X-rays: application to the upper femoral extremity. *Medical & biological engineering & computing*, 46(8):799–805.

Bauer, J. J., Pavol, M., Snow, C. M., and Hayes, W. C. (2007). MRI-derived body segment parameters of children differ from age-based estimates derived using photogrammetry. *Journal of Biomechanics*, 40:2904–2910.

Belavý, D. L., Miokovic, T., Rittweger, J., and Felsenberg, D. (2011). Estimation of changes in volume of individual lower-limb muscles using magnetic resonance imaging (during bed-rest). *Physiological Measurement*, 32(1):35–50.

Beneck, G. J. and Kulig, K. (2012). Multifidus atrophy is localized and bilateral in active persons with chronic unilateral low back pain. *Archives of Physical Medicine and Rehabilitation*, 93(2):300–306.

Berthonnaud, E., Dimnet, J., Roussouly, P., and Labelle, H. (2005). Analysis of the Sagittal Balance of the Spine and Pelvis Using Shape and Orientation Parameters. *Journal of Spinal Disorders Tehniques*, 18(1):40–47.

Bonneau, D. (2001). *Les muscles du rachis : de l'anatomie à la modélisation.* PhD thesis, Arts et Métiers ParisTech.

Boulay, C., Tardieu, C., Hecquet, J., Benaim, C., Mouilleseaux, B., Marty, C., Prat-Pradal, D., Legaye, J., Duval-Beaupère, G., and Pélissier, J. (2006). Sagittal alignment of spine and pelvis regulated by pelvic incidence: standard values and prediction of lordosis. *European Spine Journal*, 15(4):415–22.

Brown, S. H. M. and Potvin, J. R. (2005). Constraining spine stability levels in an optimization model leads to the prediction of trunk muscle cocontraction and improved spine compression force estimates. *Journal of Biomechanics*, 38(4):745–54.

Bruno, A. G., Bouxsein, M. L., and Anderson, D. E. (2015). Development and Validation of a Musculoskeletal Model of the Fully Articulated Thoracolumbar Spine and Rib Cage. *Journal of biomechanical engineering*, 137(8):081003.

Chaibi, Y., Cresson, T., Aubert, B., Hausselle, J., Neyret, P., Hauger, O., De Guise, J. A., and Skalli, W. (2012). Fast 3D reconstruction of the lower limb using a parametric model and statistical inferences and clinical measurements calculation from biplanar X-rays. *Computer methods in biomechanics and biomedical engineering*, 15(5):457–466.

Chandler, R. F., Clauser, C. E., Mcconville, J. T., Reynolds, H. M., and Young, J. W. (1975). Investigation of intertial properties of the human body. Technical report.

Cheng, C. K., Chen, H. H., Chen, C. S., Lee, C. L., and Chen, C. Y. (2000). Segment inertial properties of Chinese adults determined from magnetic resonance imaging. *Clinical Biomechanics*, 15:559–566.

Cholewicki, J. and McGill, S. M. (1996). Mechanical stability of the in vivo lumbar spine: implications for injury and chronic low back pain. *Clinical Biomechanics*, 11(1):1–15.

Christophy, M., Senan, N. A. F., Lotz, J. C., and O'Reilly, O. M. (2012). A Musculoskeletal model for the lumbar spine. *Biomechanics and Modeling in Mechanobiology*, 11(1-2):19–34.

Clark, R. A., Bryant, A. L., Pua, Y., McCrory, P., Bennell, K., and Hunt, M. (2010). Appendix A: Validity and reliability of the Nintendo Wii Balance Board for assessment of standing balance. *Gait & Posture*, 2010(3):307–310.

Crawford, R. J., Filli, L., Elliott, J. M., Nanz, D., Fischer, M. A., Marcon, M., and Ulbrich, E. J. (2016). Age- and level-dependence of fatty infiltration in lumbar paravertebral muscles of healthy volunteers. *American Journal of Neuroradiology*, 37(4):742–748.

Damet, J., Fournier, P., Monnin, P., Sans-Merce, M., Ceroni, D., Zand, T., Verdun, F. R., and Baechler, S. (2014). Occupational and patient exposure as well as image quality for full spine examinations with the EOS imaging system. *Medical Physics*, 41(6):063901.

Danneels, L. A., Vanderstraeten, G. G., Cambier, D. C., Witvrouw, E. E., and De Cuyper, H. J. (2000). CT imaging of trunk muscles in chronic low back pain patients and healthy control subjects. *European Spine Journal*, 9(4):266–72.

Davidson, P. L., Wilson, S. J., Wilson, B. D., and Chalmers, D. J. (2008). Estimating subject-specific body segment parameters using a 3-dimensional modeller program. *Journal of Biomechanics*, 41:3506–3510.

de Zee, M., Hansen, L., Wong, C., Rasmussen, J., and Simonsen, E. B. (2007). A generic detailed rigid-body lumbar spine model. *Journal of Biomechanics*, 40(6):1219–1227.

DeLeva, P. (1996). Adjustments to Zatsiorsky-Seluyanov's segment inertia parameters. *Journal of Biomechanics*, 29(9):1223–1230.

Dempster, W. T. (1955). Space Requirements of the seated operator. In *WADC Technical Report (TR-55-159), Wright Patterson Air Force Base, Ohio.*

Diebo, B., Ferrero, E., Lafage, R., Challier, V., Liabaud, B., Liu, S., Vital, J.-M., Errico, T., Schwab, F., and Lafage, V. (2015). Recruitment of compensatory mechanisms in sagittal spinal malalignment is age and regional deformity dependent: a full-standing axis analysis of key radiographical parameters. *Spine*, 40(9):642–649.

Disselhorst-Klug, C., Schmitz-Rode, T., and Rau, G. (2009). Surface electromyography and muscle force: Limits in sEMG–force relationship and new approaches for applications. *Clinical Biomechanics*, 24(3):225–235.

Dixon, W. T. (1984). Simple proton spectroscopic imaging. *Radiology*, 153(1):189–194.

Dolan, P. and Adams, M. A. (2001). Recent advances in lumbar spinal mechanics and their significance for modelling. *Clinical Biomechanics*, 16:S8–S16.

Dreischarf, M., Shirazi-Adl, A., Arjmand, N., Rohlmann, A., and Schmidt, H. (2016). Estimation of loads on human lumbar spine: A review of in vivo and computational model studies. *Journal of Biomechanics*, 49(6):833–845.

Dubois, G. (2014). *Contribution à la modélisation musculo-squelettique personnalisée du membre inférieur combinant stééoradiographie et ultrason.* PhD thesis, Arts et Métiers ParisTech.

Dubousset, J. (1994). Three-dimensional analysis of the scoliotic deformity. In Weinstein, S. L., editor, *The pediatric spine: principles and practice*, volume 22, chapter 22, pages 479–496. Raven Press ltd, wein- stei edition.

Dubousset, J., Charpak, G., Dorion, I., Skalli, W., Lavaste, F., De Guise, J. A., Kalifa, G., and Ferey, S. (2005). Une nouvelle imagerie ostéo-articulaire basse dose en position debout : le système EOS. *Radioprotection*, 40(2):245–255.

Dubousset, J., Charpak, G., Skalli, W., De Guise, J. A., Kalifa, G., and Wicart, P. (2008). Modélisation vertébrale et squelettique par le système EOS. *Archives de pédiatrie*, 15:665–666.

Dubousset, J., Charpak, G., Skalli, W., DeGuise, J. A., and Kalifa, G. (2010). EOS: A new imaging system with low dose radiation in standing position for spine and bone & joint disorders. *Journal of Musculoskeletal Research*, 13(01):1–12.

Dumas, R., Aissaoui, R., Mitton, D., Skalli, W., and De Guise, J. A. (2005). Personalized Body Segment Parameters From Biplanar Low-dose Radiography. *IEEE Transactions on biomedical engineering*, 52(10):1756–1763.

Duval-Beaupère, G. and Legaye, J. (2004). Composante sagittale de la statique rachidienne. *Revue du Rhumatisme*, 71(2):105–119.

Duval-Beaupère, G. and Robain, G. (1987). Visualization on full spine radiographs of the anatomical connections of the centres of the segmental body mass supported by each vertebra and measured in vivo. *International Orthopaedics*, 11:261–269.

Duval-Beaupère, G., Schmidt, C., and Cosson, P. (1992). A Barycentremetric study of the sagittal shape of spine and pelvis: the conditions required for an economic standing position. *Annals of biomedical engineering*, 20(4):451–462.

El Fegoun, A. B., Schwab, F., Gamez, L., Champain, N., Skalli, W., and Farcy, J.-P. (2005). Center of gravity and radiographic posture analysis: a preliminary review of adult volunteers and adult patients affected by scoliosis. *Spine*, 30(13):1535–1540.

El Helou, A. (2011). *Caractérisation biomécanique de la cheville et analyse de l'équilibre du sujet agé en reprise d'autonomie.* PhD thesis, Arts et Métiers ParisTech.

El Ouaaid, Z., Shirazi-Adl, A., Plamondon, A., and Larivière, C. (2013). Trunk strength, muscle activity and spinal loads in maximum isometric flexion and extension exertions: a combined in vivo-computational study. *Journal of Biomechanics*, 46(13):2228–35.

Erdmann, W. S. and Gos, T. (1990). Density of trunk tissues of young and medium age people. *Journal of Biomechanics*, 23(January):945–947.

Essendrop, M., Andersen, T. B., and Schibye, B. (2002). Increase in spinal stability obtained at levels of intra-abdominal pressure and back muscle activity realistic to work situations. *Applied Ergonomics*, 33(5):471–476.

Fairbank, J. C., Couper, J., Davies, J. B., and O'Brien, J. P. (1980). The Oswestry low back pain disability questionnaire. *Physiotherapy*, 66:271–273.

Faro, F. D., Marks, M. C., Pawelek, J., and Newton, P. O. (2004). Evaluation of a Functional Position for Lateral Radiograph Acquisition in Adolescent Idiopathic Scoliosis. *Spine*, 29(20):2284–2289.

Fechtenbaum, J., Etcheto, A., Kolta, S., Feydy, A., Roux, C., and Briot, K. (2015). Sagittal balance of the spine in patients with osteoporotic vertebral fractures. *Osteoporosis international*.

Fortin, M., Gibbons, L. E., Videman, T., and Battié, M. C. (2015). Do variations in paraspinal muscle morphology and composition predict low back pain in men? *Scandinavian Journal of Medicine and Science in Sports*, 25(6):880–887.

Fortin, M., Lazáry, À., Varga, P. P., McCall, I., and Battié, M. C. (2016). Paraspinal muscle asymmetry and fat infiltration in patients with symptomatic disc herniation. *European Spine Journal*, pages 1452–1459.

Fortin, M., Videman, T., Gibbons, L. E., and Battié, M. C. (2014). Paraspinal muscle morphology and composition: A 15-yr longitudinal magnetic resonance imaging study. *Medicine and Science in Sports and Exercise*, 46(5):893–901.

Frontera, W. R., Hughes, V. A., Fielding, R. A., Fiatarone, M. A., Evans, W. J., and Roubenoff, R. (2000). Aging of skeletal muscle: a 12-yr longitudinal study. *Journal of applied physiology*, 88(4):1321–1326.

Gagnon, D., Arjmand, N., Plamondon, A., Shirazi-Adl, A., and Larivière, C. (2011). An improved multi-joint EMG-assisted optimization approach to estimate joint and muscle forces in a musculoskeletal model of the lumbar spine. *Journal of Biomechanics*, 44(8):1521–1529.

Gagnon, D., Larivière, C., and Loisel, P. (2001). Comparative ability of EMG, optimization, and hybrid modelling approaches to predict trunk muscle forces and lumbar spine loading during dynamic sagittal plane lifting. *Clinical Biomechanics*, 16(5):359–372.

Galbusera, F., Wilke, H.-J., Brayda-Bruno, M., Costa, F., and Fornari, M. (2013). Influence of sagittal balance on spinal lumbar loads: a numerical approach. *Clinical Biomechanics*, 28(4):370–7.

Gangnet, N., Pomero, V., Dumas, R., Skalli, W., and Vital, J.-M. (2003). Variability of the spine and pelvis location with respect to the gravity line: a three-dimensional stereoradiographic study using a force platform. *Surgical and radiologic anatomy*, 25(5-6):424–433.

Gaumétou, E., Quijano, S., Ilharreborde, B., Presedo, A., Thoreux, P., Mazda, K., and Skalli, W. (2014). EOS analysis of lower extremity segmental torsion in children and young adults. *Orthopaedics & traumatology, surgery & research*, 100(1):147–151.

Gelb, D. E., Lenke, L. G., Bridwell, K. H., Blanke, K., and McEnery, K. W. (1995). An analysis of sagittal spinal alignment in 100 asymptomatic middle and older aged volunteers. *Spine*, 20(12):1351–1358.

Ghiasi, M. S., Arjmand, N., Shirazi-Adl, A., Farahmand, F., Hashemi, H., Bagheri, S., and Valizadeh, M. (2016). Cross-sectional area of human trunk paraspinal muscles before and after posterior lumbar surgery using magnetic resonance imaging. *European Spine Journal*, 25(3):774–82.

Gildea, J. E., Hides, J. A., and Hodges, P. W. (2013). Size and Symmetry of Trunk Muscles in Ballet Dancers With and Without Low Back Pain. *Journal of orthopaedic & sports physical therapy*, 43(8):525–533.

Gille, O. (2006). *Tool for evaluating trunk muscles using MRI: application to study of posture and muscular lesions secondary to surgery*. PhD thesis.

Granata, K. P., Lee, P. E., and Franklin, T. C. (2005). Co-contraction recruitment and spinal load during isometric trunk flexion and extension. *Clinical Biomechanics*, 20(10):1029–37.

Granata, K. P. and Orishimo, K. F. (2001). Response of trunk muscle coactivation to changes in spinal stability. *Journal of Biomechanics*, 34(9):1117–1123.

Granata, K. P. and Wilson, S. E. (2001). Trunk posture and spinal stability. *Clinical Biomechanics*, 16(8):650–659.

Hajihosseinali, M., Arjmand, N., and Shirazi-Adl, A. (2015). Effect of body weight on spinal loads in various activities: A personalized biomechanical modeling approach. *Journal of Biomechanics*, 48(2):276–282.

Hajihosseinali, M., Arjmand, N., Shirazi-Adl, A., Farahmand, F., and Ghiasi, M. S. (2014). A novel stability and kinematics-driven trunk biomechanical model to estimate muscle and spinal forces. *Medical engineering & Physics*, 36(10):1296–304.

Häkkinen, K., Kallinen, M., Izquierdo, M., Jokelainen, K., Lassila, H., Mälkiä, E., Kraemer, W. J., Newton, R. U., and Alen, M. (1998). Changes in agonist-antagonist EMG, muscle CSA, and force during strength training in middle-aged and older people. *Journal of applied physiology (Bethesda, Md. : 1985)*, 84(4):1341–9.

Han, J. S., Goel, V. K., Ahn, J. Y., Winterbottom, J., McGowan, D., Weinstein, J., and Cook, T. (1995). Loads in the spinal structures during lifting: development of a three-dimensional comprehensive biomechanical model. *European Spine Journal*, 4(3):153–168.

Han, K.-S., Rohlmann, A., Zander, T., and Taylor, W. R. (2013). Lumbar spinal loads vary with body height and weight. *Medical engineering & Physics*, 35(7):969–77.

Hanavan, E. (1964). A mathematical model of the human body. AMRL-TR-64-102. Technical report.

Handsfield, G. G., Meyer, C. H., Hart, J. M., Abel, M. F., and Blemker, S. S. (2014). Relationships of 35 lower limb muscles to height and body mass quantified using MRI. *Journal of Biomechanics*, 47(3):631–638.

Hatze, H. (1980). A mathematical model for the computational determination of parameter values of anthropomorphic segments. *Journal of Biomechanics*, 13:833–843.

Hausselle, J., Assi, A., El Helou, A., Jolivet, E., Pillet, H., Dion, E., Bonneau, D., and Skalli, W. (2014). Subject-specific musculoskeletal model of the lower limb in a lying and standing position. *Computer methods in biomechanics and biomedical engineering*, 17(5-8):480–487.

Hayashi, T., Chen, H., Miyamoto, K., Zhou, X., Hara, T., Yokoyama, R., Kanematsu, M., Hoshi, H., and Fujita, H. (2011). Analysis of bone mineral density distribution at trabecular bones in thoracic and lumbar vertebrae using X-ray CT images. *Journal of bone and mineral metabolism*, 29(2):174–185.

Hughes, R. E., Bean, J. C., and Chaffin, D. B. (1995). Evaluating the effect of co-contraction in optimization models. *Journal of Biomechanics*, 28(7):875–878.

Humbert, L., Carlioz, H., Baudoin, A., Skalli, W., and Mitton, D. (2008). 3D evaluation of the acetabular coverage by biplanar Xrays or single anteroposterior Xray compared with CT-scan. *Computer methods in biomechanics and biomedical engineering*, 11(3):257–262.

Humbert, L., De Guise, J. A., Aubert, B., Godbout, B., and Skalli, W. (2009a). 3D reconstruction of the spine from biplanar X-rays using parametric models based on transversal and longitudinal inferences. *Medical engineering & Physics*, 31(6):681–687.

Humbert, L., De Guise, J. A., Godbout, B., Cresson, T., Branchaud, D., Chav, R., Gravel, P., Parent, S., Dubousset, J., and Skalli, W. (2009b). Fast 3D reconstruction of the spine from biplanar radiography: a diagnosis tool for routine scoliosis diagnosis and research in biomechanics. *Computer methods in biomechanics and biomedical engineering*, 12(S1):151–163.

Illés, T. and Somoskeöy, S. (2012). The EOS™ imaging system and its uses in daily orthopaedic practice. *International Orthopaedics*, 36(7):1325–1331.

Iyer, S., Lenke, L. G., Nemani, V. M., Albert, T. J., Sides, B. A., Metz, L. N., Cunningham, M. E., and Kim, H. J. (2016). Variations in sagittal alignment parameters based on age: a prospective study of asymptomatic volunteers using full-body radiographs. *Spine*.

Izzo, R., Guarnieri, G., Guglielmi, G., and Muto, M. (2013). Biomechanics of the spine. Part I: spinal stability. *European journal of radiology*, 82(1):118–126.

Jensen, R. K. (1978). Estimation of the biomechanical properties of three body types using a photogrammetric method. *Journal of Biomechanics*, 11:349–358.

Jensen, R. K. and Fletcher, P. (1994). Distribution of mass to the segments of elderly males and females. *Journal of Biomechanics*, 27(1):89–96.

Jolivet, E., Daguet, E., Pomero, V., Bonneau, D., Laredo, J. D., and Skalli, W. (2008). Volumic patient-specific reconstruction of muscular system based on a reduced dataset of medical images. *Computer methods in biomechanics and biomedical engineering*, 11(3):281–290.

Jolivet, E., Dion, E., Rouch, P., Dubois, G., Charrier, R., Payan, C., and Skalli, W. (2014). Skeletal muscle segmentation from MRI dataset using a model-based approach. *Computer Methods in Biomechanics and Biomedical Engineering: Imaging & Visualization*, 2(3):138–145.

Kamina, P. (2006). *Anatomie Clinique*. 3rd edition.

Kiefer, A., Shirazi-Adl, A., and Parnianpour, M. (1998). Synergy of the human spine in neutral postures. *European Spine Journal*, 7(6):471–479.

Kim, J. S., Park, T. S., Park, S. B., and Kim, S. I. (2000). Measurement of femoral neck anteversion in 3D. Part 2:3D modelling method. *Medical & Biological Engineering & Computing*, 38(6):610–616.

Kim, Y. B., Kim, Y. J., Ahn, Y. J., Kang, G. B., Yang, J. H., Lim, H., and Lee, S. W. (2014). A comparative analysis of sagittal spinopelvic alignment between young and old men without localized disc degeneration. *European Spine Journal*, 23(7):1400–1406.

Kjaer, P., Bendix, T., Sorensen, J. S., Korsholm, L., and Leboeuf-yde, C. (2007). Are MRI-defined fat infiltrations in the multifidus muscles associated with low back pain ? *BioMed Central Medicine*, 5(2).

Kohda, E. and Shigematsu, N. (1989). Measurement of lung density by computed tomography: implication for radiotherapy. *Keio Journal of Medicine*, 38(4):454–463.

Kolta, S., Le Bras, A., Mitton, D., Bousson, V., De Guise, J. A., Fechtenbaum, J., Laredo, J. D., Roux, C., and Skalli, W. (2005). Three-dimensional X-ray absorptiometry (3D-XA): a method for reconstruction of human bones using a dual X-ray absorptiometry device. *Osteoporosis international*, 16(8):969–976.

Kristiansen, L. P., Gunderson, R. B., Steen, H., and Reikeras, O. (2001). The normal development of tibial torsion. *Skeletal radiology*, 30(9):519–522.

Lacour, M., Bernard-Demanze, L., and Dumitrescu, M. (2008). Posture control, aging, and attention resources: models and posture-analysis methods. *Clinical neurophysiology*, 38(6):411–421.

Lafage, R., Challier, V., Liabaud, B., Vira, S., Ferrero, E., Diebo, B. G., Liu, S., Vital, J.-M., Mazda, K., Protopsaltis, T. S., Errico, T. J., Schwab, F., and Lafage, V. (2015). Natural Head Posture in the Setting of Sagittal Spinal Deformity : Validation of Chin - Brow Vertical Angle , Slope of Line of Sight , and McGregor ' s Slope With Health - Related Quality of Life. *Neurosurgery*, 0(0):1–8.

Lafage, V., Schwab, F., Skalli, W., Hawkinson, N., Gagey, P. M., Ondra, S., and Farcy, J.-P. (2008). Standing balance and sagittal plane spinal deformity: analysis of spinopelvic and gravity line parameters. *Spine*, 33(14):1572–1578.

Lafage, V., Schwab, F., Vira, S., Patel, A., Ungar, B., and Farcy, J.-P. (2011). Spino-pelvic parameters after surgery can be predicted: a preliminary formula and validation of standing alignment. *Spine*, 36(13):1037–45.

Laughton, C. A., Slavin, M., Katdare, K., Nolan, L., Bean, J. F., Kerrigan, D. C., Phillips, E., Lipsitz, L. A., and Collins, J. J. (2003). Aging, muscle activity, and balance control: physiologic changes associated with balance impairment. *Gait & Posture*, 18(2):101–108.

Le Huec, J.-C., Demezon, H., and Aunoble, S. (2014). Sagittal parameters of global cervical balance using EOS imaging: normative values from a prospective cohort of asymptomatic volunteers. *European Spine Journal*, 24(1):63–71.

Lee, J. C., Cha, J.-G., Kim, Y., Kim, Y.-I., and Shin, B.-J. (2008). Quantitative analysis of back muscle degeneration in the patients with the degenerative lumbar flat back using a digital image analysis: comparison with the normal controls. *Spine*, 33(3):318–325.

Lee, M. K., Le, N. S., Fang, A. C., and Koh, M. T. H. (2009). Measurement of body segment parameters using dual energy X-ray absorptiometry and three-dimensional geometry: An application in gait analysis. *Journal of Biomechanics*, 42:217–222.

Legaye, J. (2014). Influence of age and sagittal balance of the spine on the value of the pelvic incidence. *European Spine Journal*, 23(7):1394–9.

Legaye, J., Duval-Beaupère, G., Hecquet, J., and Marty, C. (1998). Pelvic incidence: a fundamental pelvic parameter for three-dimensional regulation of spinal sagittal curves. *European spine journal*, 7(2):99–103.

Lewis, B. J., McCall, M. J., Green, A. R., Bennett, L. G., Pierre, M., Schrewe, U. J., O'Brien, K., and Felsberger, E. (2001). Aircrew exposure from cosmic radiation on commercial airline routes. *Radiation protection dosimetry*, 93(4):293–314.

Li, F., Laville, A., Bonneau, D., Laporte, S., and Skalli, W. (2014). Study on cervical muscle volume by means of three-dimensional reconstruction. *Journal of magnetic resonance imaging*, 39(6):1411–6.

Li, Z., Kindig, M. W., Subit, D., and Kent, R. W. (2010). Influence of mesh density, cortical thickness and material properties on human rib fracture prediction. *Medical Engineering and Physics*, 32:998–1008.

Lilliefors, H. W. (1967). On the Kolmogorov-Smirnov Test for Normality with Mean and Variance. *Journal of the American Statistical Association*, 62(318):399–402.

Lube, J., Cotofana, S., Bechmann, I., Milani, T. L., Özkurtul, O., Sakai, T., Steinke, H., and Hammer, N. (2016). Reference data on muscle volumes of healthy human pelvis and lower extremity muscles: an in vivo magnetic resonance imaging feasibility study. *Surgical and Radiologic Anatomy*, 38(1):97–106.

Mac-Thiong, J.-M., Labelle, H., Berthonnaud, E., Betz, R. R., and Roussouly, P. (2007). Sagittal spinopelvic balance in normal children and adolescents. *European spine journal*, 16(2):227–34.

Mac-Thiong, J.-M., Roussouly, P., Berthonnaud, E., and Guigui, P. (2011). Age- and sex-related variations in sagittal sacropelvic morphology and balance in asymptomatic adults. *European Spine Journal*, 20 Suppl 5:572–7.

Macaluso, A. and De Vito, G. (2004). Muscle strength, power and adaptations to resistance training in older people. *European Journal of Applied Physiology*, 91(4):450–72.

Macaluso, A., Nimmo, M. A., Foster, J. E., Cockburn, M., McMillan, N. C., and De Vito, G. (2002). Contractile muscle volume and agonist-antagonist coactivation account for differences in torque between young and older women. *Muscle & nerve*, 25(6):858–863.

Mangione, P., Gomez, D., and Senegas, J. (1997). Study of the course of the incidence angle during growth. *European Spine Journal*, 6(3):163–7.

Marras, W. S. and Sommerich, C. M. (1991). A Three-Dimensional Motion Model of Loads on the Lumbar Spine: I. Model Structure. *Human Factors: The Journal of the Human Factors and Ergonomics Society*, 33(2):123–137.

McDonald, J. H. (2009). *Handbook of Biological Statistics*. Sparky House Publishing, 2nd edition.

Mersmann, F., Bohm, S., Schroll, A., and Arampatzis, A. (2014). Validation of a simplified method for muscle volume assessment. *Journal of Biomechanics*, 47(6):1348–1352.

Million, R., Hall, R., Nilsen, K., and Baker, R. (1982). Assessment of the progress of the back-pain patient. *Spine*, 7:204–212.

Mitton, D., Deschênes, S., Laporte, S., Godbout, B., Bertrand, S., DeGuise, J. A., and Skalli, W. (2006). 3D reconstruction of the pelvis from biplanar radiography. *Computer methods in biomechanics and biomedical engineering*, 9(1):1–5.

Moal, B. (2014). *Adultes avec déformation rachidienne : traitement chirurgical et évaluation musculaire*. PhD thesis, Arts et Métiers ParisTech / New York University / Centre Hospitalier Universitaire de Bordeaux.

Moal, B., Bronsard, N., Raya, J. G., Vital, J.-M., Schwab, F., and Lafage, V. (2015). Volume and fat infiltration of spino-pelvic musculature in adults with spinal deformity. *World Journal of Orthopaedics*, 6(9):727–737.

Moal, B., Raya, J. G., Jolivet, E., Schwab, F., Blondel, B., Lafage, V., and Skalli, W. (2014). Validation of 3D spino-pelvic muscle reconstructions based on dedicated MRI sequences for fat- water quantification. *Innovation and Research in BioMedical Engineering*, 35(3):119–127.

Modenese, L., Phillips, A. T. M., and Bull, A. M. J. (2011). An open source lower limb model: Hip joint validation. *Journal of Biomechanics*, 44(12):2185–2193.

Moeller, T. B. and Reif, E. (2001). Volume 2. Thorax, abdomen, and pelvis. In Thieme, editor, *Pocket atlas of cross-sectional anatomy: Computed tomography and magnetic resonance imaging.* 2nd edition.

Mohammadi, Y., Arjmand, N., and Shirazi-Adl, A. (2015). Comparison of trunk muscle forces, spinal loads and stability estimated by one stability- and three EMG-assisted optimization approaches. *Medical Engineering and Physics*, 37(8):792–800.

Morasso, P. G. and Schieppati, M. (1999). Can muscle stiffness alone stabilize upright standing? *Journal of neurophysiology*, 82(3):1622–6.

Nachemson, A. (1975). Towards a better understanding of low-back pain: a review of the mechanics of the lumbar disc. *Rheumatology*, 14(3):129–143.

Narici, M. V., Maganaris, C. N., Reeves, N. D., and Capodaglio, P. (2003). Effect of aging on human muscle architecture. *Journal of applied physiology*, 95(6):2229–2234.

Nérot, A., Choisne, J., Amabile, C., Travert, C., Pillet, H., Wang, X., and Skalli, W. (2015). A 3D reconstruction method of the body envelope from biplanar X-rays: Evaluation of its accuracy and reliability. *Journal of Biomechanics*, 48(16):4322–4326.

Niemeläinen, R., Briand, M. M., and Battié, M. C. (2011). Substantial asymmetry in paraspinal muscle cross-sectional area in healthy adults questions its value as a marker of low back pain and pathology. *Spine*, 36(25):2152–2157.

Nuzzo, J. L. and Mayer, J. M. (2013). Body mass normalisation for ultrasound measurements of lumbar multifidus and abdominal muscle size. *Manual therapy*, 18(3):237–42.

Pajarinen, J., Lindahl, J., Savolainen, V., Michelsson, O., and Hirvensalo, E. (2004). Femoral shaft medialisation and neck-shaft angle in unstable pertrochanteric femoral fractures. *International Orthopaedics*, 28(6):347–353.

Parkkola, R., Rytökoski, U., and Kormano, M. (1993). Magnetic resonance imaging of the discs and trunk muscles in patients with chronic low back pain and healthy control subjects. *Spine*, 18(7):830–836.

Pearsall, D. J., Reid, J. G., and Livingston, L. A. (1996). Segmental Inertial Parameters of the Human Trunk as Determined from Computed Tomography. *Annals of biomedical engineering*, 24(26):198–210.

Pearsall, D. J., Reid, J. G., and Ross, R. (1994). Inertial properties of the human trunk of males determined from magnetic resonance imaging. *Annals of biomedical engineering*, 22(6):692–706.

Pezolato, A., de Vasconcelos, E. E., Defino, H. L., and Nogueira-Barbosa, M. H. (2012). Fat infiltration in the lumbar multifidus and erector spinae muscles in subjects with sway-back posture. *European spine journal*, 21:2158–2164.

Pillet, H., Bonnet, X., Lavaste, F., and Skalli, W. (2010). Evaluation of force plate-less estimation of the trajectory of the centre of pressure during gait. Comparison of two anthropometric models. *Gait & posture*, 31(2):147–152.

Pomero, V. (2002). *Modélisation géométrique et mécanique des muscles du tronc, relation entre musculature, troubles posturaux et surcharges vertébrales*. PhD thesis, Arts et Métiers ParisTech.

Pomero, V., Lavaste, F., Imbert, G., and Skalli, W. (2004). A proprioception based regulation model to estimate the trunk muscle forces. *Computer methods in biomechanics and biomedical engineering*, 7(6):331–338.

Pomero, V., Vital, J.-M., Lavaste, F., Imbert, G., and Skalli, W. (2002). Muscular Modelling: Relationship between postural default and spine overloading. *Research into Spinal Deformities*, 88:321–325.

Porter, M. M., Vandervoort, A. A., and Lexell, J. (1995). Aging of human muscle: structure, function and adaptability. *Scandinavian Journal of Medicine and Science in Sports*, 5(3):129–142.

Quijano, S., Serrurier, A., Aubert, B., Laporte, S., Thoreux, P., and Skalli, W. (2013). Three-dimensional reconstruction of the lower limb from biplanar calibrated radiographs. *Medical engineering & Physics*, 35(12):1703–12.

Rajnics, P., Pomero, V., Templier, A., Lavaste, F., and Illes, T. (2001). Computer-Assisted Assessment of Spinal Sagittal Plane Radiographs. *Journal of Spinal Disorders*, 14(2):135–142.

Rasch, A., Byström, A. H., Dalen, N., and Berg, H. E. (2007). Reduced muscle radiological density , cross- sectional area , and strength of major hip and knee muscles in 22 patients with hip osteoarthritis. *Acta Medica Iranica*, 78(4):505–510.

Rohlmann, A., Pohl, D., Bender, A., Graichen, F., Dymke, J., Schmidt, H., and Bergmann, G. (2014). Activities of everyday life with high spinal loads. *PLoS ONE*, 9(5):e98510.

Roudsari, B. S., Ebel, B. E., Corso, P. S., Molinari, N.-A. M., and Koepsell, T. D. (2005). The acute medical care costs of fall-related injuries among the U.S. older adults. *Injury*, 36(11):1316–22.

Roussouly, P., Gollogly, S., Berthonnaud, E., and Dimnet, J. (2005). Classification of the normal variation in the sagittal alignment of the human lumbar spine and pelvis in the standing position. *Spine*, 30(3):436–353.

Roussouly, P., Gollogly, S., Noseda, O., Berthonnaud, E., and Dimnet, J. (2006). The vertical projection of the sum of the ground reactive forces of a standing patient is not the same as the C7 plumb line: a radiographic study of the sagittal alignment of 153 asymptomatic volunteers. *Spine*, 31(11):E320–325.

Rubin, R. J., Leyvraz, P. F., Aubaniac, J. M., and Argenson, J. N. (1992). The morphology of the proximal femur: a threedimensional radiographic analysis. *Journal of bone and joint surgery*, 74-B:28–32.

Ryan, D. J., Protopsaltis, T. S., Ames, C. P., Hostin, R., Klineberg, E., Mundis, G. M., Obeid, I., Kebaish, K., Smith, J. S., Boachie-Adjei, O., Burton, D. C., Hart, R. A., Gupta, M., Schwab, F., and Lafage, V. (2014). T1 Pelvic Angle (TPA) Effectively Evaluates Sagittal Deformity and Assesses Radiographical Surgical Outcomes Longitudinally. *Spine*, 39(15):1203–1210.

Sanchis-Moysi, J., Idoate, F., Izquierdo, M., Calbet, J. A. L., and Dorado, C. (2011). Iliopsoas and gluteal muscles are asymmetric in tennis players but not in soccer players. *PLoS ONE*, 6(7):6–15.

Sandoz, B., Laporte, S., Skalli, W., and Mitton, D. (2010). Subject-specific body segment parameters' estimation using biplanar X-rays: a feasibility study. *Computer methods in biomechanics and biomedical engineering*, 13(6):649–54.

Savage, R. A., Millerchip, R., Whitehouse, G. H., and Edwards, R. H. T. (1991). Lumbar muscularity and its relationship with age, occupation and low back pain. *European Journal of Applied Physiology and Occupational Physiology*, 63(3-4):265–268.

Schnebel, B., Kingston, S., Watkins, R., and Dillin, W. (1989). Comparison of MRI to Contrast CT in the Diagnosis of Spinal Stenosis. *Spine*, 14(3):332–337.

Schultz, A. B., Andersson, G. B. J., Haderspeck, K., Ortengren, R., Nordin, M., and Björk, R. (1982). Analysis and measurement of lumbar trunk loads in tasks involving bends and twists. *Journal of Biomechanics*, 15(9):669–675.

Schwab, F., Lafage, V., Boyce, R., Skalli, W., and Farcy, J.-P. (2006). Gravity line analysis in adult volunteers: age-related correlation with spinal parameters, pelvic parameters, and foot position. *Spine*, 31(25):E959–E967.

Seber, S., Hazer, B., Köse, N., Göktürk, E., Günal, I., and Turgut, A. (2000). Rotational profile of the lower extremity and foot progression angle: computerized tomographic examination of 50 male adults. *Archives of orthopaedic and trauma surgery*, 120(5-6):255–258.

Shirotani, T. (1988). Realistic Torso Phantom for Calibration of in-vivo Transuranic-Nuclide Counting Facilities. *Journal of Nuclear Science and Technology*, 25(11):875–883.

Skalli, W., Champain, S., and Mosnier, T. (2007). Biomécanique du rachis. *Cahiers d'enseignement de la SOFCOT*, 96:8–17.

Skeie, E. J., Borge, J. A., Leboeuf-Yde, C., Bolton, J., and Wedderkopp, N. (2015). Reliability of diagnostic ultrasound in measuring the multifidus muscle. *Chiropractic & Manual Therapies*, 23(1):1–12.

Steffen, J.-S., Obeid, I., Aurouer, N., Hauger, O., Vital, J.-M., Dubousset, J., and Skalli, W. (2010). 3D postural balance with regard to gravity line: an evaluation in the transversal plane on 93 patients and 23 asymptomatic volunteers. *European spine journal*, 19(5):760–767.

Stokes, I. A. F., Aronson, D. D., Ronchetti, P. J., Labelle, H., and Dansereau, J. (1993). Reexamination of the Cobb and Ferguson Angles: Bigger is not always better. *Journal of Spinal Disorders*, 6(4):333–338.

Stokes, I. A. F. and Gardner-Morse, M. (2001). Lumbar spinal muscle activation synergies predicted by multi-criteria cost function. *Journal of Biomechanics*, 34(6):733–740.

Südhoff, I., de Guise, J. A., Nordez, A., Jolivet, E., Bonneau, D., Khoury, V., and Skalli, W. (2009). 3D-patient-specific geometry of the muscles involved in knee motion from selected MRI images. *Medical & biological engineering & computing*, 47(6):579–587.

Sugrue, P. A., McClendon, J., Smith, T. R., Halpin, R. J., Nasr, F. F., OShaughnessy, B. A., and Koski, T. R. (2013). Redefining Global Spinal Balance: normative values of cranial center of mass from a prospective cohort of asymptomatic individuals. *Spine*, 38(6):484–489.

Takahashi, K., Takahashi, H. E., Nakadaira, H., and Yamamoto, M. (2006). Different changes of quantity due to aging in the psoas major and quadriceps femoris muscles in women. *Journal of Musculoskeletal Neuronal Interactions*, 6(2):201–205.

Takayama, K., Kita, T., Nakamura, H., Kanematsu, F., Yasunami, T., Sakanaka, H., and Yamano, Y. (2016). A new predictive index for lumbar paraspinal muscle degeneration associated with aging. *Spine*, 41(2):E84–90.

Than, P., Szuper, K., Somoskeöy, S., Warta, V., and Illés, T. (2012). Geometrical values of the normal and arthritic hip and knee detected with the EOS imaging system. *International Orthopaedics*, 36(6):1291–1297.

Tinetti, M. E., Baker, D. I., McAvay, G., Claus, E. B., Garrett, P., Gottschalk, M., Koch, M. L., Trainor, K., and Horwitz, R. I. (1994). A multifactorial intervention to reduce the risk of falling among eldery people living in the community. *The New England Journal of Medicine*, 331(13):821–827.

Valentin, S., Licka, T., and Elliott, J. (2015). Age and side-related morphometric MRI evaluation of trunk muscles in people without back pain. *Manual Therapy*, 20(1):90–95.

van Dieën, J. H., Cholewicki, J., and Radebold, A. (2003). Trunk muscle recruitment patterns in patients with low back pain enhance the stability of the lumbar spine. *Spine*, 28(8):834–841.

Vaz, G., Roussouly, P., Berthonnaud, E., and Dimnet, J. (2002). Sagittal morphology and equilibrium of pelvis and spine. *European Spine Journal*, 11(1):80–7.

Vialle, R., Levassor, N., Rillardon, L., Templier, A., Skalli, W., and Guigui, P. (2005). Radiographic analysis of the sagittal alignment and balance of the spine in asymptomatic subjects. *The Journal of bone and joint surgery. American volume*, 87(2):260–267.

Vital, J.-M. and Senegas, J. (1986). Anatomical bases of the study of the constraints to which the cervical spine is subject in the sagittal plane. A study of the center of gravity of the head. *Surgical Radiologic Anatomy*, 8(3):169–173.

Vrtovec, T., Pernuš, F., and Likar, B. (2009). A review of methods for quantitative evaluation of spinal curvature. *European Spine Journal*, 18(5):593–607.

White, A. A., Johnson, R. M., Panjabi, M. M., and Southwick, W. O. (1975). Biomechanical analysis of clinical stability in the cervical spine. *Clinical orthopaedics and related research*, (109):85–96.

Wilke, H.-J., Neef, P., Caimi, M., Hoogland, T., and Claes, L. E. (1999). New in vivo measurements of pressures in the intervertebral disc in daily life. *Spine*, 24(8):755–762.

Winter, D. A., Patla, A. E., Frank, J. S., and Walt, S. E. (1990). Biomechanical Walking Pattern Changes in the Fit and Healthy Elderly. *Physical Therapy*, 70(6):340–347.

Wong, C., Rasmussen, J., Simonsen, E., Hansen, L., de Zee, M., and Dendorfer, S. (2011). The Influence of Muscle Forces on the Stress Distribution in the Lumbar Spine. *The Open Spine Journal*, 3:21–26.

Woodard, H. Q. and White, D. R. (1986). The composition of body tissues. *The British journal of radiology*, 59(708):1209–1218.

World Health Organization (2008). *World Health Organization global report on falls prevention in older age*. World Health Organization.

Yeadon, M. R. (1990). The simulation of aerial movement–II. A mathematical inertia model of the human body. *Journal of Biomechanics*, 23(1):67–74.

Yoganandan, N., Arun, M. W. J., Stemper, B. D., Pintar, F. A., and Maiman, D. J. (2013). Biomechanics of human thoracolumbar spinal column trauma from vertical impact loading. *Annals of advances in automotive medicine*, 57:155–66.

Young, J. W., Chandler, R. F., Ret, C. C. S., Robinette, K. M., and Zehner, G. F. (1983). Anthropometric and Mass Distribution Characteristics of the Adult Female. Technical report.

Zatsiorsky, V. M. and Seluyanov, V. N. (1985). Estimation of the mass and inertie characteristics of the human body by means of the best predictive regression equations. In *Biomechanics*, chapter IX-B, pages 233–239.

Zhou, B. H., Baratta, R. V., Solomonow, M., Olivier, L. J., and D'Ambrosia, R. D. (1996). Evaluation of isometric antagonist coactivation strategies of electrically stimulated muscles. *IEEE transactions on bio-medical engineering*, 43(2):150–60.

# Part F

# Publications and communications

## Publications

PAPERS ACCEPTED:

Nérot, A., Choisne, J., Amabile, C., Travert, C., Pillet, H., Wang, X., & Skalli, W. (2015). A 3D reconstruction method of the body envelope from biplanar X-rays: Evaluation of its accuracy and reliability. JOURNAL OF BIOMECHANICS, 48(16):4322-4326.

Amabile, C., Choisne, J., Nérot, A., Pillet, H., & Skalli, W. (2016). Determination of a new uniform thorax density representative of the living population from 3D external body shape modeling. JOURNAL OF BIOMECHANICS, 49(7):1162-1169.

Amabile, C., Pillet, H., Lafage, V., Barrey, C., Vital, J. M., & Skalli, W. (2016). A new quasi-invariant parameter characterizing the postural alignment of young asymptomatic adults. EUROPEAN SPINE JOURNAL, pages 1-9.

Amabile, C., Moal, B., Chtara, O. A., Pillet, H., Raya, J. G., Iannessi, A., Skalli, W., Lafage, V., & Bronsard, N. (2016). Estimation of spino-pelvic muscles' volume in young asymptomatic subjects: a quantitative analysis. SURGICAL AND RADIOLOGICAL ANATOMY, p1-11.

PAPERS UNDER REVISION:

Amabile, C., LeHuec, J.C & Skalli, W.(2016). Invariance of head-pelvis alignment and compensatory mechanisms for asymptomatic adults older than 49 years old. EUROPEAN SPINE JOURNAL.

## Congress Communications in an International Congress

ORAL COMMUNICATION WITH PEER-REVIEW SELECTION OF THE ABSTRACTS:

Amabile, C., Pillet, H., Lafage, V., & Skalli, W. (2015). A new invariant parameter characterizing the postural alignment of young healty adults. IN 25TH CONGRESS OF THE INTERNATIONAL SOCIETY OF BIOMECHANICS.

Amabile, C., Nérot, A., Choisne, J., Pillet, H., Lafage, V., & Skalli, W. (2015). Alignment of centers of mass of body segments with the gravity line. IN 40TH CONGRESS OF THE SOCIÉTÉ DE BIOMÉCANIQUE - PUBLISHED IN COMPUTER METHODS IN BIOMECHANICS AND BIOMEDICAL ENGINEERING, pages 1-2.

Amabile, C., Moal, B., Bronsard, N., Skalli, W., & Lafage, V. (2016). Prediction of Muscular Volume Of Functional Groups From A Reduced Set Of MRI Slices. IN 23RD INTERNATIONAL MEETING ON ADVANCED SPINE TECHNIQUES (IMAST) - PRESENTED BY NICOLAS BRONSARD.

Amabile, C., Moal, B., Bronsard, N., Skalli, W., & Lafage, V. (2016). Muscular Volume of Functional Groups from a reduced set of MRI slices. IN 40TH EUROPEAN SOCIETY BIOMECHANICS (ESB).

POSTER PRESENTATION WITH PEER-REVIEW SELECTION OF THE ABSTRACTS:

Amabile, C., Choisne, J., Nérot, A., Pillet, H., & Skalli, W. (2015). Prediction of the rib cage volume from anthropometric data. IN 21ST CONGRESS OF THE EUROPEAN SOCIETY OF BIOMECHANICS.

# Part G

# Appendices

APPENDIX A

# DETAILED ANATOMY OF MUSCLES STUDIED

This appendix presents the different muscles studied in this PhD.

| | | | | | |
|---|---|---|---|---|---|
| | 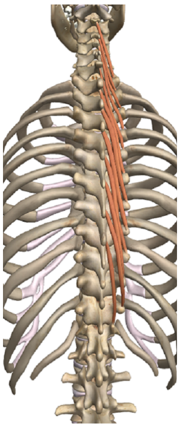 | 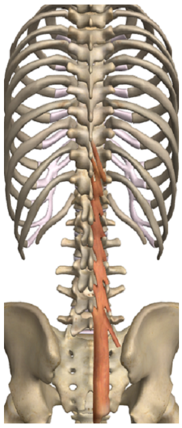 | 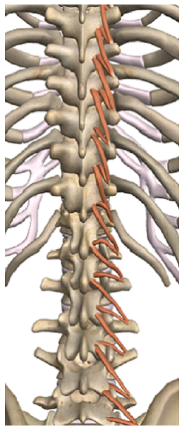 |  |  |
| **Name** | **Semi spinalis** | **Multifidus** | **Rotators** | **Interspinales** | **Intertransversarii** |
| | | **Grouped under the name of Multifidus** | | | |
| **Proximal Insertion** | Sp. processes of C2 to T4 and occipital bone | Sp. processes of vertebrae 2 to 4 levels superior to distal insertion | Tr. process of C1 to L5 | Sp. process of C1 to L5 | Tr. process of C1 to L5 |
| **Distal Insertion** | Tr. process of C4 to T10 | Sacrum, posterior sup. iliac spine and Iliac crest | Sp. process of inferior adjacent vertebra | Sp. process of adjacent vertebra | Tr. process of adjacent vertebra |
| **Function** | Spine extensor | Spine stabilizer | | | |

Table A.1. : Insertions and functions of spinal muscles (part 1 of 2). [Adapted from (Dubois, 2014; Bonneau, 2001) and from ZYGOTE BODY (`http://zygotebody.com/`)]. Abbreviations: Inf.: inferior; Sup.: superior; Tr.: transverse and Sp.: spinous.

| | | | | | |
|---|---|---|---|---|---|
| | 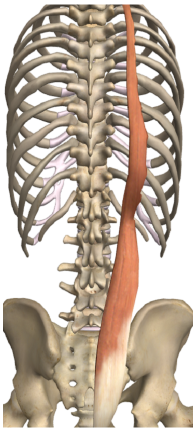 | 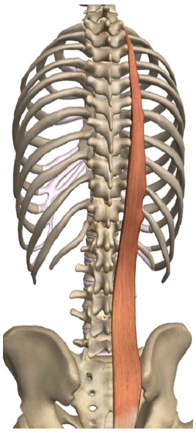 | 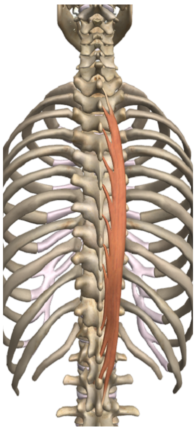 | 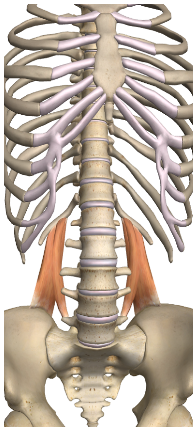 | 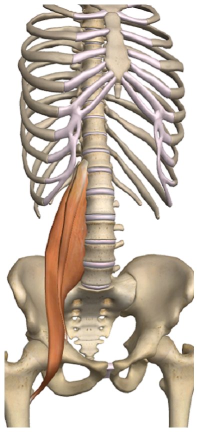 |
| **Name** | **Iliocostalis** | **Longissimus** | **Spinalis** | **Quadratus lumborum** | **Psoas** |
| | **Erector Spinae** | | | | |
| **Proximal Insertion** | Tr. processes of C4 to C7<br>Angles of the $1^{st}$ to $8^{th}$ ribs<br>Angles of the $5^{th}$ to $12^{th}$ ribs | Mastoid process<br>Tr. processes of C3 to C6<br>Tr. processes of T1 to T12 & inf border of the $4^{th}$ to $12^{th}$ ribs | Between sup. & inf. nuchal lines<br>Sp. processes of C2 to T4<br>Sp. processes of T2 to T9 | Lower border of the $12^{th}$ rib & tr. processes of L1 to L4 | Lateral faces of T12 to L5 & corresponding inter-vertebral discs |
| **Distal Insertion** | Angles of the $4^{th}$ to $8^{th}$ ribs<br>Angles of the $7^{th}$ to $12^{th}$ ribs<br>Lumbo-sacral fascia | Tr. processes of C3 to T3<br>Tr. processes of T1 to T5<br>Lumbo-sacral fascia & sp. processes of L2-L5 | Tr. processes of T3 to T5<br>Tr. processes of T2 to T11<br>Sp. processes of T11 to L1 | Iliac crest | Lesser trochanter |
| **Function** | Spine extensors | | | | Spine flexor<br>Hip flexor |

Table A.2. : Insertions and functions of spinal muscles (part 2 of 2). [Adapted from (Dubois, 2014; Bonneau, 2001) and from ZYGOTE BODY (`http://zygotebody.com/`)]. Abbreviations: Inf.: inferior; Sup.: superior; Tr.: transverse and Sp.: spinous.

| | | | | | | | | | |
|---|---|---|---|---|---|---|---|---|---|
| | 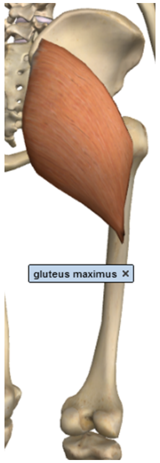 | 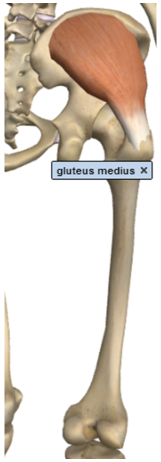 | 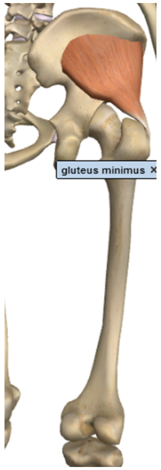 | 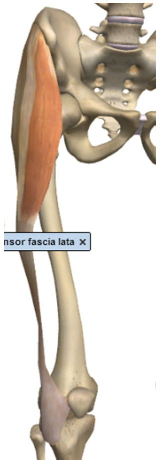 | 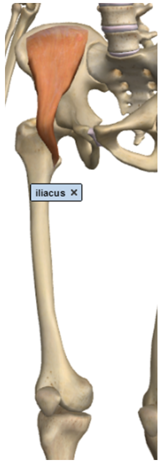 | 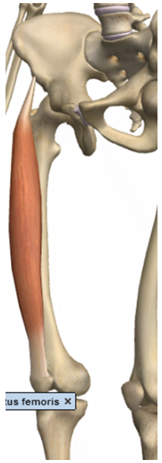 |  |  |  |
| **Name** | **Gluteus maximus** | **Gluteus medius** | **Gluteus minimus** | **Tensor fasciae lata** | **Iliacus** | **Rectus femoris** | **Vastus lateralis** | **Vastus medius** | **Vastus intermedius** |
| **Proximal Insertion** | Iliac crest | | | Iliac crest | Anterior inferior iliac spine | Antero-inferior iliac spine | Femoral linea aspera | | 3/4 superior of anterior-lateral part of the femur |
| | Sacrum Coccyx | Iliac fossa | | | Iliac fossa | | Great trochanter | | |
| **Distal Insertion** | Femoral linea aspera | Great trochanter | | Lateral tibial condyle | Lesser trochanter | The distal parts of the 4 muscles joined in a great tendon, called quadriceps tendon, inserting on the superior part of the patella. | | | |
| **Function** | Hip extensor | Hip adductor | | Hip adductor | Hip flexor | Knee extensor | | | |
| | Lateral rotator of the hip | | | Medial rotator of the hip | Lateral rotator of the hip | | | | |

Table A.3. : Insertions and functions of pelvic muscles and muscles of the anterior part of the thigh. [Adapted from (Dubois, 2014) and from ZYGOTE BODY (http://zygotebody.com/)]

| | | | | | | | | | |
|---|---|---|---|---|---|---|---|---|---|
| | 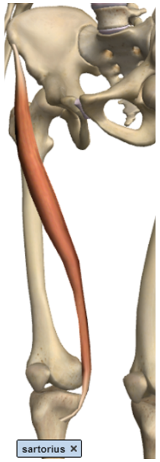 | 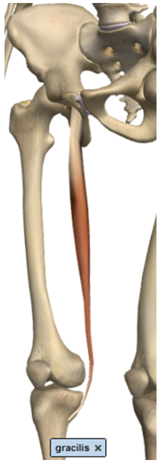 | 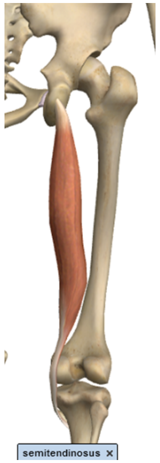 |  |  |  | 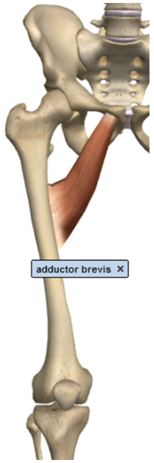 |  |  |
| **Name** | **Sartorius** | **Gracilis** | **Semi-tendinosus** | **Semi-membranosus** | **Biceps femoris longum** | **Biceps femoris breve** | **Adductor brevis** | **Adductor magnus** | **Adductor longus** |
| | | | | | | | | **Adductor** | |
| **Proximal Insertion** | Antero-superior iliac spine | Tuberosity of the ischium | | | | Femoral linea aspera | Pubis | Pubis<br>Tuberosity of the ischium | Pubis |
| **Distal Insertion** | 1/3rd superior of medial tibial condyle | | | Proximal part of medial tibial condyle | Fibula head and lateral tibial condyle | | Femoral linea aspera | | |
| **Function** | Knee flexor | | Hip extensor | | Knee flexor | | Adductor | | |
| | Knee flexor | | Knee flexor | | Internal rotator of the knee | | Lateral rotator of the hip | Medial rotation of the hip | Medial rotator of the hip |
| | External rotator of the hip | Internal rotator of the hip | Hip flexor | | Medial rotator of the knee | | Hip extensor with locked knee | | Hip flexor |

Table A.4. : Insertions and functions of muscles of the posterior and lateral part of the thigh. [Adapted from (Dubois, 2014) and from ZYGOTE BODY (`http://zygotebody.com/`)]

| Name | <br>**Obliquus externus** | 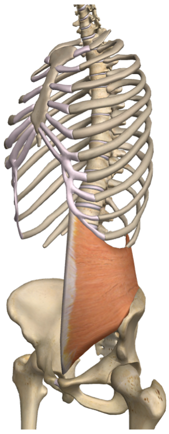<br>**Obliquus internus** | 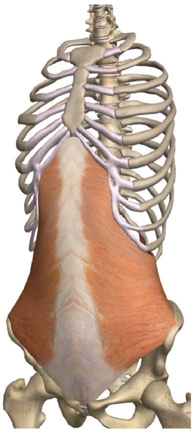<br>**Transversus abdominis** | 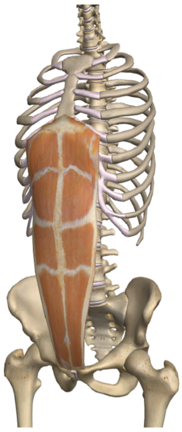<br>**Rectus abdominis** | 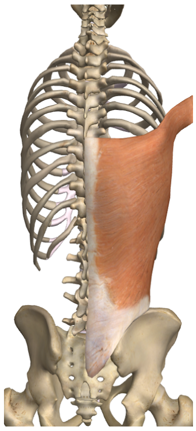<br>**Latissimus dorsi** |
|---|---|---|---|---|---|
| | **Abdominal Group** | | | | |
| **Proximal Insertion** | Lateral edges of the 5th to 12th ribs | Inferior borders edges of the 5th to 12th ribs<br>Linea alba | Linea alba & Xiphoid process of the sternum<br>Pubic crest | Inferior edges of the costal cartilages of the 5th to 7th ribs<br>Xiphoid process of the sternum | Posterior side of the humerus of the upper arm |
| **Distal Insertion** | Linea alba<br>Iliac crest<br>Pubis | Iliac crest | Iliac crest | Inner surfaces of the costal cartilages of the 7th to 12th ribs<br>Superior edge of the public bone<br>Pubic symphysis | Thoracolumbar fascia, iliac crest<br>Sp. processes of T7 to L5<br>Inferior 4 ribs and inferior angle of scapula |
| **Function** | Lateral flexor of the trunk<br>Rotator of the trunk | Rotator of the trunk | Compresses abdominal content<br>"corset muscle" | Spine flexor | Rotator of the trunk |

Table A.5. Insertions and functions of abdominal muscles. [Adapted from (Dubois, 2014; Bonneau, 2001) and from ZYGOTE BODY (`http://zygotebody.com/`)]. Abbreviations: Sp.: spinous.

APPENDIX B

# EQUATIONS FOR PREDICTION OF MUSCULAR VOLUME FROM REDUCED SET OF MRI SLICES

Coefficients of the equations used to compute volume of muscular functional groups from a reduced set of MRI slices are presented hereafter. Each coefficient (line of the table) is a vector of 1 line times N columns, N being equal to the number of slices considered plus 2 (for the constant and coefficient of femoral length).

"Group" can mean one of the following: Spine_flex; Spine_ext; Hip_flex; Hip_ext; Knee_flex; Knee_ext; Gluteus_minimus; Gluteus_medius.

## Model 3 slices:

For each Group, the equation for Model 3 MRI slices is:

$$Volume\_Group = Coeff\_Group * \begin{vmatrix} 1 \\ Femoral\_length \\ Area\_Group\_slice56 \\ Area\_Group\_slice111 \\ Area\_Group\_slice136 \end{vmatrix} \tag{B.1}$$

| **Model 3 slices** | **Constant** | $\mathbf{L_{Fem}}$ | **S. 56** | **S. 111** | **S. 136** |
|---|---|---|---|---|---|
| Coeff_Spine_flex | 23.6 | 0 | 0 | 0 | 33.4 |
| Coeff_Spine_ext | -46.0 | 0 | 0 | 0 | 15.3 |
| Coeff_Hip_flex | -144.2 | 0 | 36.2 | 0 | 0 |
| Coeff_Hip_ext | 287.6 | 0 | 60.4 | 0 | 0 |
| Coeff_Knee_flex | -2.6 | 0 | 34.3 | 0 | 0 |
| Coeff_Knee_ext | -282.4 | 0 | 295 | 0 | 0 |
| Coeff_Gluteus_minimus | -163.9 | 3.9 | 0 | 7.0 | 0 |
| Coeff_Gluteus_medius | -22.3 | 0 | 0 | 11.0 | 0 |

Table B.1. : Coefficients to compute the volume from few slices reconstructions with the model built on 3 MRI slices (Equation B.1): Volume and constant in $cm^3$; $L_{Fem}$ (femoral length) in cm; Area on slices in $cm^2$.

# Model 4-A slices:

For each Group, the equation for Model 4-A MRI slices is:

$$Volume\_Group = Coeff\_Group * \begin{vmatrix} 1 \\ Femoral\_length \\ Area\_Group\_slice56 \\ Area\_Group\_slice111 \\ Area\_Group\_slice121 \\ Area\_Group\_slice141 \end{vmatrix} \tag{B.2}$$

| **Model 4 slices** | **Constant** | $\mathbf{L_{Fem}}$ | **S. 56** | **S. 111** | **S. 121** | **S. 141** |
|---|---|---|---|---|---|---|
| Coeff_Spine_flex | 6.5 | 0 | 0 | 0 | 16.7 | 6.2 |
| Coeff_Spine_ext | 21.7 | 0 | 0 | 0 | 10.0 | 10.3 |
| Coeff_Hip_flex | -144.2 | 0 | 36.2 | 0 | 0 | 0 |
| Coeff_Hip_ext | 287.6 | 0 | 60.4 | 0 | 0 | 0 |
| Coeff_Knee_flex | -2.6 | 0 | 34.3 | 0 | 0 | 0 |
| Coeff_Knee_ext | -282.4 | 0 | 29.5 | 0 | 0 | 0 |
| Coeff_Gluteus_minimus | -163.9 | 3.9 | 0 | 7.0 | 0 | 0 |
| Coeff_Gluteus_medius | -223.2 | 5.6 | 0 | 6.1 | 4.1 | 0 |

Table B.2. : Coefficients to compute the volume from few slices reconstructions with the model built on 4-A MRI slices (Equation B.2): Volume and constant in $cm^3$; $L_{Fem}$ (femoral length) in cm; Area on slices in $cm^2$.

# Model 4-B slices:

For each Group, the equation for Model 4-B MRI slices is:

$$Volume\_Group = Coeff\_Group * \begin{vmatrix} 1 \\ Femoral\_length \\ Area\_Group\_slice21 \\ Area\_Group\_slice56 \\ Area\_Group\_slice111 \\ Area\_Group\_slice136 \end{vmatrix} \tag{B.3}$$

| **Model 4 slices** | **Constant** | $\mathbf{L_{Fem}}$ | **S. 21** | **S. 56** | **S. 111** | **S. 136** |
|---|---|---|---|---|---|---|
| Coeff_Spine_flex | 23.6 | 0 | 0 | 0 | 0 | 33.4 |
| Coeff_Spine_ext | -46.0 | 0 | 0 | 0 | 0 | 15.3 |
| Coeff_Hip_flex | -191.9 | 0 | 40.2 | 33.4 | 0 | 0 |
| Coeff_Hip_ext | -73.0 | 0 | 36.6 | 33.4 | 0 | 0 |
| Coeff_Knee_flex | -193.1 | 0 | 21.6 | 18.2 | 0 | 0 |
| Coeff_Knee_ext | -294.8 | 0 | 12.6 | 22.5 | 0 | 0 |
| Coeff_Gluteus_minimus | -163.9 | 3.9 | 0 | 0 | 7.0 | 0 |
| Coeff_Gluteus_medius | -22.3 | 0 | 0 | 0 | 11.0 | 0 |

Table B.3. : Coefficients to compute the volume from few slices reconstructions with the model built on 4-B MRI slices (Equation B.3): Volume and constant in $cm^3$; $L_{Fem}$ (femoral length) in cm; Area on slices in $cm^2$.

# Model 5-A slices:

For each Group, the equation for Model 5-A MRI slices is:

$$Volume\_Group = Coeff\_Group * \begin{vmatrix} 1 \\ Femoral\_length \\ Area\_Group\_slice56 \\ Area\_Group\_slice111 \\ Area\_Group\_slice116 \\ Area\_Group\_slice126 \\ Area\_Group\_slice136 \end{vmatrix} \tag{B.4}$$

| **Model 5 slices** | **Constant** | $\mathbf{L_{Fem}}$ | **S. 56** | **S. 111** | **S. 116** | **S. 126** | **S. 136** |
|---|---|---|---|---|---|---|---|
| Coeff_Spine_flex | -465.6 | 11.3 | 0 | 0 | 8.0 | -0.8 | 14.9 |
| Coeff_Spine_ext | -24.4 | 0 | 0 | 0 | 5.5 | 2.5 | 12.1 |
| Coeff_Hip_flex | -144.2 | 0 | 36.2 | 0 | 0 | 0 | 0 |
| Coeff_Hip_ext | 287.6 | 0 | 60.4 | 0 | 0 | 0 | 0 |
| Coeff_Knee_flex | -2.6 | 0 | 34.3 | 0 | 0 | 0 | 0 |
| Coeff_Knee_ext | -282.4 | 0 | 29.5 | 0 | 0 | 0 | 0 |
| Coeff_Gluteus_minimus | -163.9 | 3.9 | 0 | 7.0 | 0 | 0 | 0 |
| Coeff_Gluteus_medius | -172.3 | 4.1 | 0 | 5.3 | 4.6 | 0 | 0 |

Table B.4. : Coefficients to compute the volume from few slices reconstructions with the model built on 5-A MRI slices (Equation B.4): Volume and constant in $cm^3$; $L_{Fem}$ (femoral length) in cm; Area on slices in $cm^2$.

# Model 5-B slices:

For each Group, the equation for Model 5-B MRI slices is:

$$Volume\_Group = Coeff\_Group * \begin{vmatrix} 1 \\ Femoral\_length \\ Area\_Group\_slice21 \\ Area\_Group\_slice56 \\ Area\_Group\_slice111 \\ Area\_Group\_slice121 \\ Area\_Group\_slice141 \end{vmatrix} \tag{B.5}$$

| **Model 5 slices** | **Constant** | $\mathbf{L_{Fem}}$ | **S. 21** | **S. 56** | **S. 111** | **S. 121** | **S. 141** |
|---|---|---|---|---|---|---|---|
| Coeff_Spine_flex | 6.5 | 0 | 0 | 0 | 0 | 16.7 | 6.2 |
| Coeff_Spine_ext | 21.7 | 0 | 0 | 0 | 0 | 10.0 | 10.3 |
| Coeff_Hip_flex | -191.9 | 0 | 40.2 | 33.4 | 0 | 0 | 0 |
| Coeff_Hip_ext | -73.0 | 0 | 36.6 | 33.4 | 0 | 0 | 0 |
| Coeff_Knee_flex | -193.1 | 0 | 21.6 | 18.2 | 0 | 0 | 0 |
| Coeff_Knee_ext | -294.8 | 0 | 12.6 | 22.5 | 0 | 0 | 0 |
| Coeff_Gluteus_minimus | -163.9 | 3.9 | 0 | 0 | 7.0 | 0 | 0 |
| Coeff_Gluteus_medius | -223.2 | 5.6 | 0 | 0 | 6.1 | 4.1 | 0 |

Table B.5. : Coefficients to compute the volume from few slices reconstructions with the model built on 5-B MRI slices (Equation B.5): Volume and constant in $cm^3$; $L_{Fem}$ (femoral length) in cm; Area on slices in $cm^2$.

# Model 6 slices:

For each Group, the equation for computation of volume from 6 MRI slices is:

$$Volume\_Group = Coeff\_Group * \begin{vmatrix} 1 \\ Femoral\_length \\ Area\_Group\_slice21 \\ Area\_Group\_slice56 \\ Area\_Group\_slice111 \\ Area\_Group\_slice116 \\ Area\_Group\_slice126 \\ Area\_Group\_slice136 \end{vmatrix} \tag{B.6}$$

| **Model 6 slices** | **Cst** | $\mathbf{L_{Fem}}$ | **S. 21** | **S. 56** | **S. 111** | **S. 116** | **S. 126** | **S. 136** |
|---|---|---|---|---|---|---|---|---|
| Coeff_Spine_flex | -465.6 | 11.3 | 0 | 0 | 0 | 8.0 | -0.8 | 14.9 |
| Coeff_Spine_ext | -24.4 | 0 | 0 | 0 | 0 | 5.5 | 2.5 | 12.1 |
| Coeff_Hip_flex | -191.9 | 0 | 40.2 | 33.4 | 0 | 0 | 0 | 0 |
| Coeff_Hip_ext | -73.0 | 0 | 36.6 | 33.4 | 0 | 0 | 0 | 0 |
| Coeff_Knee_flex | -193.1 | 0 | 21.6 | 18.2 | 0 | 0 | 0 | 0 |
| Coeff_Knee_ext | -294.8 | 0 | 12.6 | 22.5 | 0 | 0 | 0 | 0 |
| Coeff_Gluteus_minimus | -163.9 | 3.9 | 0 | 0 | 7.0 | 0 | 0 | 0 |
| Coeff_Gluteus_medius | -172.3 | 4.1 | 0 | 0 | 5.3 | 4.6 | 0 | 0 |

Table B.6. : Coefficients to compute the volume from few slices reconstructions with the model built on 6 MRI slices (Equation B.6): Volume and constant (Cst) in $cm^3$; $L_{Fem}$ (femoral length) in cm; Area on slices in $cm^2$.

# APPENDIX C

# ALGORITHM OF THE MUSCULO-SKELETAL MODEL OF MUSCULAR ACTIVATION

The loads in the inter-vertebral joint (called $L_{IV\_joint}$) are equal to the net reaction forces and moments on the section considered ($L_{ext}$) minus the loads generated by the muscles' contraction ($L_{muscles}$) (Equation C.1 and Figure C.1):

$$L_{IV\_joint} = L_{ext} - L_{muscles} \tag{C.1}$$

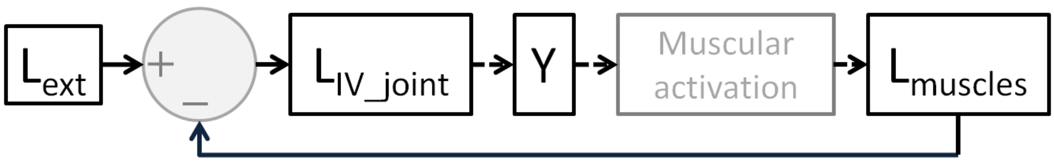


Figure C.1. : Control loop of the model of muscular regulation (MMR).

In the following, $N$ is the total number of muscles.

## 3 - 1 Regulation function

From the inter-vertebral joint load is estimated the regulation function Y:

$$Y = 10 * \frac{{L_{IV\_joint}}^3}{{Threshold_{IV\_joint}}^3} \tag{C.2}$$

$Threshold_{IV\_joint}$ refers to the values fixed in section 9 - 1. The exponent of the law is set at 3 as most of the models use this exponent in order to enhance entry signal by a power law (Brown and Potvin, 2005; Arjmand *et al.*, 2010; Wong *et al.*, 2011; El Ouaaid *et al.*, 2013; Hajihosseinali *et al.*, 2014; Bruno *et al.*, 2015). The constant 10 was chosen arbitrarily (Pomero *et al.*, 2004).

## 3 - 2 Ability of each muscle to contract, to regulate a load component

Each muscle, depending on its position and line of action, has the ability to contract in order to lower a load component. A scalar is computed for each muscle and for each load component, to represent this ability. The complete matrix with all scalars has 1 line per muscle and 1 column per load component; and is called *Ability_contract*.

The first three columns represent the ability to regulate the forces: scalars are equal to the product of the cross-sectional area times the vector line of action of the muscle. The last three columns represent the ability to regulate the moment: scalars are equal to the cross-sectional area ($CSA$) times the resulting cross product of the centroid vector (Centroid, being the plane of study, its Z component is therefore 0) by the vector line of action ($Dir\_muscle$). In equation C.3, $Ability\_contract(i\_muscle,:)$ represents one matrix line for one muscle.

$$Ability\_contract(i\_muscle,:) = \left|\begin{array}{c} Dir\_muscle_X \times CSA \\ Dir\_muscle_Y \times CSA \\ Dir\_muscle_Z \times CSA \\ Centroid_Y \times Dir\_muscle_Z \times CSA \\ -Centroid_X \times Dir\_muscle_Z \times CSA \\ \left[Centroid_X \times Dir\_muscle_Y - Centroid_Y \times Dir\_muscle_X\right] \times CSA \end{array}\right|^T \quad (C.3)$$

## 3 - 3 Identification of the antagonist muscles

Antagonist muscles are identified as such after computation of the $Mat\_ANTAG$ matrix which size is as follow: 1 line per muscle; 1 column per muscle; and 1 third dimension for each load component. In equation C.4, $Mat\_ANTAG(:,:,i\_load)$ represents one matrix for one load component and $Ability\_contract(:,i\_load)$ represents one column of the matrix $Ability\_contract$ (for one load component).

$$Mat\_ANTAG(:,:,i\_load) = Ability\_contract(:,i\_load) \times Ability\_contract(:,i\_load)^T \quad (C.4)$$

Muscles presenting a negative scalar do not have the ability to regulate this load component and are therefore labeled as antagonist; this is done for each load component.

## 3 - 4 Activation of the agonist muscles

Excitation of agonist muscles is computed from the ability of a muscle to regulate a load component and the regulation function of this load component. The product of the two represent how much agonist muscles are requested.

$$Excitation\_AG = Ability\_contract^T \times Y \quad (C.5)$$

Activation is then computed from the excitation with a sigmoid function, resulting in a scalar between 0 and 1.

$$Activation\_AG = Sigmoid(Excitation\_AG) \quad (C.6)$$

## 3 - 5 Activation of the antagonist muscles

Excitation of the antagonist muscles is computed from the antagonist law described by Zhou *et al.* in 1996 (Zhou *et al.*, 1996). This law was detailed in section 9 - 7. Excitation of the antagonist muscles is a function of the ratio $L_{IV\_joint}$ over $Max\_L_{muscles}$.

$Max\_L_{muscles}$ is the maximum load generated by muscles when all muscles are contracted simultaneously to their maximal stress: each component is computed as if all muscles contracted simultaneously to regulate only this component (Equation C.7). It is worth noting that in the antagonist law, only moments are considered to compute the antagonist muscles' excitation.

$$Max\_L_{muscles} = \begin{vmatrix} \sum_{i=1}^{N}\left(Dir\_muscle_X{}^i \times CSA^i \times S_{max}{}^i\right) \\ \sum_{i=1}^{N}\left(Dir\_muscle_Y{}^i \times CSA^i \times S_{max}{}^i\right) \\ \sum_{i=1}^{N}\left(Dir\_muscle_Z{}^i \times CSA^i \times S_{max}{}^i\right) \\ \sum_{i=1}^{N}\left(Centroid_Y{}^i \times Dir\_muscle_Z{}^i \times CSA^i \times S_{max}{}^i\right) \\ \sum_{i=1}^{N}\left(-Centroid_X{}^i \times Dir\_muscle_Z{}^i \times CSA^i \times S_{max}{}^i\right) \\ \sum_{i=1}^{N}\left(\left[Centroid_X{}^i \times Dir\_muscle_Y{}^i - Centroid_Y{}^i \times Dir\_muscle_X{}^i\right] \times CSA^i \times S_{max}{}^i\right) \end{vmatrix}^T \tag{C.7}$$

In equation C.7, $Dir\_muscle_X{}^i$ (respectively $Dir\_muscle_Y{}^i$ and $Dir\_muscle_Z{}^i$) is the X (respectively Y, and Z) component of the vector line of action of the muscle considered. $CSA^i$ is the cross-sectional area of the muscle considered and $Centroid_X{}^i$ and $Centroid_Y{}^i$ the X and Y coordinated of the centroid of the muscle considered. $N$ is the total number of muscles.

Activation of the antagonist muscles is then computed as follow:

$$Activation\_ANTAG = Antag\_Gain \times Activation\_AG \times Mat\_ANTAG \times Excitation\_ANTAG \tag{C.8}$$

Antag_Gain is a parameter of the antagonist law which value is set as described in Appendix D.

## 3 - 6 Activation of the agonist and antagonist muscles

Activation of all muscles ($Activation\_total$) is therefore calculated from adding the activation of the agonist muscles and the activation of the antagonist muscles:

$$Activation\_total = Activation\_ANTAG + Activation\_AG \tag{C.9}$$

## 3 - 7 Load generated by muscles

The load generated by muscles is computed from geometrical parameters and activation of muscles.

$$L_{muscles} = \sum_{i=1}^{N}\left(Activation\_total^i \times S_{max}{}^i \times CSA^i\right) \tag{C.10}$$

$S_{max}{}^i$ is the maximal admissible stress of the muscle considered, $CSA^i$ its cross-sectional area and $Activation\_total^i$ is the scalar corresponding to its activation. $N$ is the total number of muscles.

From there, a new inter-vertebral load ($L_{IV\_joint}$) is computed as the previous $L_{IV\_joint}$ minus the load generated by muscles $L_{muscles}$: all steps can be followed from the beginning in order to obtain a new load generated by muscles $L_{muscles}$.

APPENDIX D

# ANTAGONIST PARAMETERS

This appendix is a study aiming to fix values for the parameters relative to the antagonist excitation: the **Overlap** and **Co-contraction Gain** of the antagonist law (Figure D.1); but also the **Antagonist Gain** that multiplies the antagonist activation before adding it to the agonist activation (Equation C.8 in Appendix C).

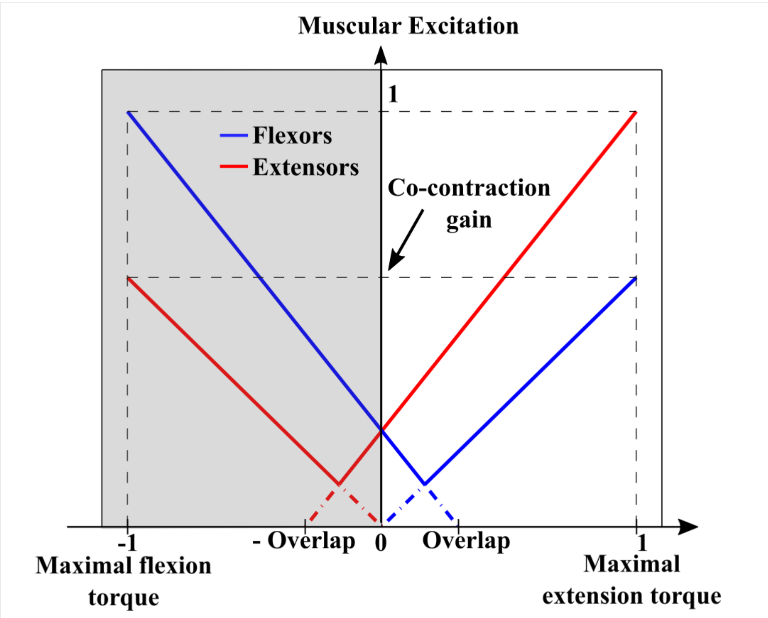


Figure D.1. : Antagonist law (Zhou *et al.*, 1996).

Zhou *et al.* reported ranges of values for Overlap and Co-contraction Gain, after an extensive study of multiple combinations on knee muscles of cats. Influence of the increase of these two parameters can be visualized in Figures D.2 and D.3.

A co-contraction gain below 10% was recommended by Zhou *et al.* (1996), in order to stabilize the joint but also to provide good input tracking (input being joint torque) (Zhou *et al.*, 1996). An overlap between 25% and 50% was recommended based on the optimum found for torque transmission efficiency (Zhou *et al.*, 1996). These recommendations were found after investigation of different combinations. The same methodology was followed here to fix these parameters.

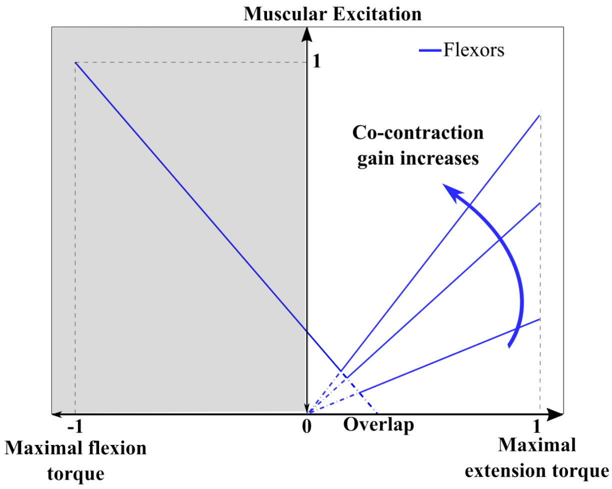


Figure D.2. : Antagonist law (Zhou *et al.*, 1996): influence of Co-contraction Gain.

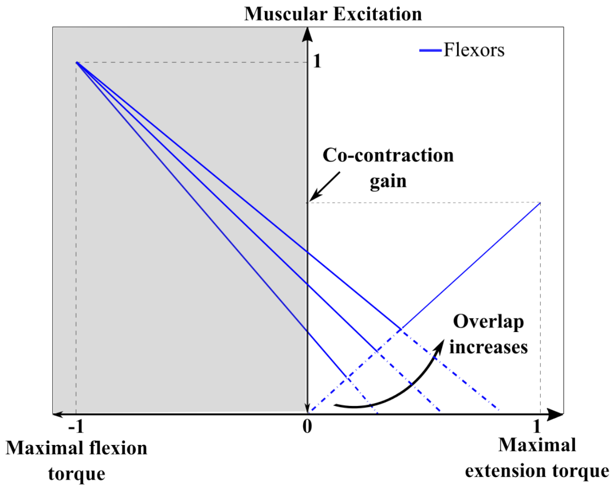


Figure D.3. : Antagonist law (Zhou *et al.*, 1996): influence of Overlap.

3D skeleton and muscular geometry were obtained from EOS and MRI exams for a young asymptomatic adult: 28 years old, 84.4kg, 1.88m, BMI = 23.9kg/m$^2$ (Figure 9.11). 4 static positions were considered:

- EOS standardized position (Faro *et al.*, 2004), called **Neutral**,
- Flexion of 30° of the trunk around the inter-vertebral disc considered (L3-L4), called **Flex_0N**,
- Flexion of 30° of the trunk around the inter-vertebral disc considered (L3-L4) with a weight of 9kg in the hands at 50cm of the abdomen, called **Flex_90N**,
- Flexion of 30° of the trunk around the inter-vertebral disc considered (L3-L4) with a weight of 180kg in the hands at 50cm of the abdomen, called **Flex_180N**.

For each position, the resulting loads after activation of muscles were computed with antagonist parameters taking one of each of the following values:

- Overlap: 0% / 25% / 50% / 75% / 100%,
- Co-contraction Gain: 0% / 25% / 50% / 75% / 100%,
- Antagonist Gain: 0% / 25% / 50% / 75% / 100%.

There were in the end 5*5*5 = 125 cases for each position, so in total 500 simulations ran.

In order to chose the best combination, careful study of the most critical position (Flex_180N) was performed. A criteria on the compression value was set in order to discriminate between the different parameters' combination: the compression was set to not exceed 4000N (50% risk of fractures have been reported at a peak force of 3700N by Yoganandan *et al.* (Yoganandan *et al.*, 2013)). Results in terms of compression force, Fz, for the different combinations, are presented in Figure D.4

In Figure D.4, cases with Overlap = 0% or Co-contraction Gain = 0% or Antagonist Gain = 0% were reported for comparison. However this value of 0% does not present any interest for studying antagonist excitation. Overlap of 0% means direct excitation of the antagonist muscles. Co-contraction Gain of 0% means maximal excitation of antagonist is 0%. Antagonist Gain of 0% means that the weight of antagonist activation compared to agonist activation is zero.

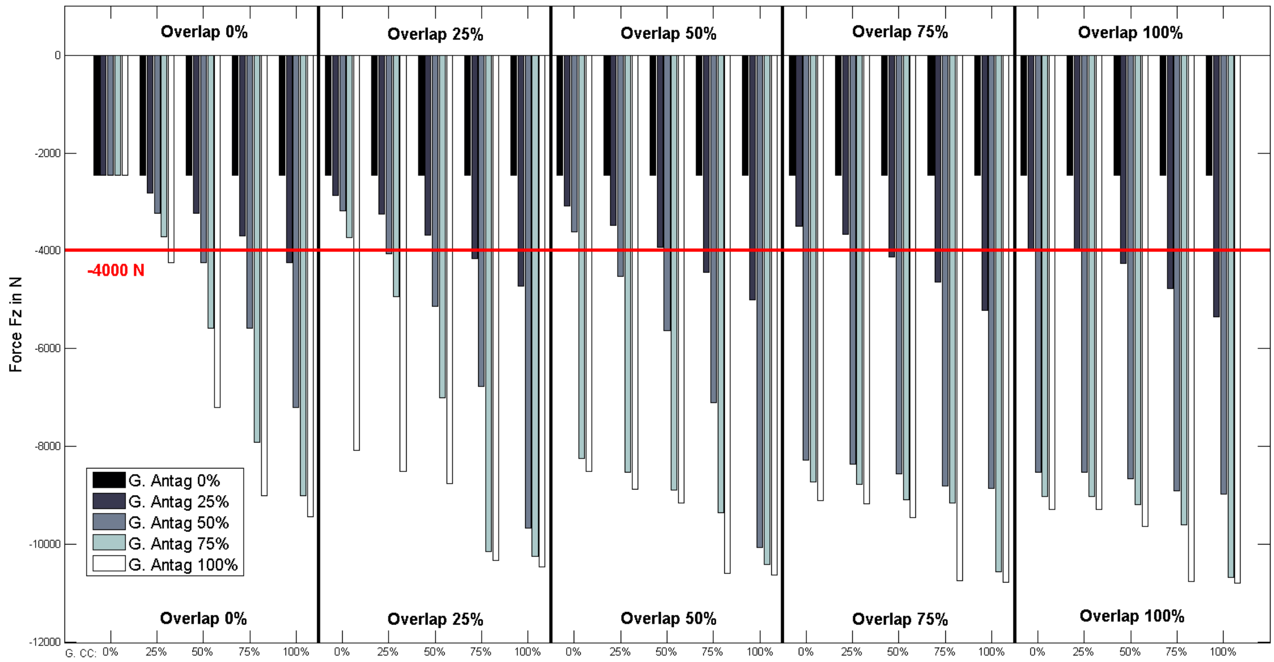


Figure D.4. : Compression force for Flex_180N. Results for different combinations of the antagonist parameters: Overlap; Co-contraction Gain (G. CC); Antagonist Gain (G. Antag). -4000 N was set as the value to not exceed.

As seen on Figure D.4, the only bars for which the - 4000N value is not exceeded, are:

- for Antagonist Gain = 0%, for whichever value of Overlap and Co-contraction Gain,
- for Antagonist Gain = 25%, Overlap = 0 %, for Co-contraction Gain ⩽ 75%,
- for Antagonist Gain = 25%, Overlap = 25 %, for Co-contraction Gain ⩽ 50%,
- for Antagonist Gain = 25%, Overlap = 50%, for Co-contraction Gain ⩽ 50%,
- for Antagonist Gain = 25%, Overlap = 75%, for Co-contraction Gain ⩽ 25%,
- for Antagonist Gain = 50%, Overlap = 0%, for Co-contraction Gain ⩽ 25%,
- for Antagonist Gain = 50%, Overlap = 25%, for Co-contraction Gain = 0%,
- for Antagonist Gain = 50%, Overlap = 50%, for Co-contraction Gain = 0%,
- for Antagonist Gain = 75%, Overlap = 0%, for Co-contraction Gain ⩽ 25%,
- for Antagonist Gain = 75%, Overlap = 25%, for Co-contraction Gain = 0%,
- for Antagonist Gain = 100%, Overlap = 0%, for Co-contraction Gain = 0%,

Taking out the combinations when one of the parameters if equal to 0%, the only value possible for the Antagonist Gain is 25%, with an Overlap between 25% and 75%, and a Co-contraction Gain different from 0%. Table D.1 reports values for each load component, for these combinations.

When looking into details in Table D.1, one can note that values obtained either with a Co-contraction Gain larger than 25%, either with an Overlap value larger than 25%; postero-anterior and lateral shear exceed values of respectively 1000N and 300N. 1000N in postero-anterior shear is four times the maximal value reported for 10 daily activities and 250N in lateral shear was reported as the maximal value for 10 daily activities (Rohlmann *et al.*, 2014). In addition, Zhou *et al.* reported an optimal value between 25% and 50% for the Overlap (Zhou *et al.*, 1996). The value for the Overlap was therefore set at 25%.

| **$F_x$ (N)** | *Co-contraction Gain* **0 %** | **25 %** | **50 %** | **75 %** | **100 %** |
|---|---|---|---|---|---|
| Overlap 25% | 870.0 | 1020.2 | 1188.5 | 1376.6 | 1592.3 |
| Overlap 50% | 974.1 | 1126.6 | 1306.5 | 1509.2 | 1737.1 |
| Overlap 75% | 1150.4 | 1213.0 | 1399.1 | 1607.0 | 1839.8 |

| **$F_y$ (N)** | *Co-contraction Gain* **0 %** | **25 %** | **50 %** | **75 %** | **100 %** |
|---|---|---|---|---|---|
| Overlap 25% | - 263.9 | - 314.7 | - 370.8 | - 433.0 | - 503.6 |
| Overlap 50% | - 296.8 | - 342.2 | - 390.7 | - 445.8 | - 507.7 |
| Overlap 75% | - 329.8 | - 344.6 | - 388.8 | - 438.5 | - 494.1 |

| **$F_z$ (N)** | *Co-contraction Gain* **0 %** | **25 %** | **50 %** | **75 %** | **100 %** |
|---|---|---|---|---|---|
| Overlap 25% | - 2863.8 | - 3249.3 | - 3680.4 | - 4162.3 | - 4714.2 |
| Overlap 50% | - 3088.5 | - 3473.4 | - 3924.8 | - 4433.1 | - 5004.6 |
| Overlap 75% | - 3501.2 | - 3656.8 | - 4118.4 | - 4634.1 | - 5211.6 |

| **$M_x$ (Nm)** | *Co-contraction Gain* **0 %** | **25 %** | **50 %** | **75 %** | **100 %** |
|---|---|---|---|---|---|
| Overlap 25% | -2.6 | 2.3 | 7.6 | 13.1 | 19.1 |
| Overlap 50% | 0.5 | 1.7 | 3.3 | 5.0 | 6.8 |
| Overlap 75% | - 1.6 | - 1.8 | - 2.3 | - 3.0 | - 3.8 |

| **$M_y$ (Nm)** | *Co-contraction Gain* **0 %** | **25 %** | **50 %** | **75 %** | **100 %** |
|---|---|---|---|---|---|
| Overlap 25% | 19.5 | 22.8 | 26.4 | 30.7 | 35.4 |
| Overlap 50% | 21.5 | 24.9 | 28.6 | 32.8 | 37.6 |
| Overlap 75% | 25.0 | 26.3 | 30.1 | 34.4 | 39.3 |

| **$M_z$ (Nm)** | *Co-contraction Gain* **0 %** | **25 %** | **50 %** | **75 %** | **100 %** |
|---|---|---|---|---|---|
| Overlap 25% | 15.0 | 17.6 | 20.4 | 23.2 | 26.3 |
| Overlap 50% | 16.8 | 18.0 | 18.7 | 19.5 | 20.4 |
| Overlap 75% | 15.3 | 15.2 | 14.8 | 14.3 | 13.7 |

Table D.1. : Comparison for position Flex_180N of different Co-contraction Gain and Overlap values.

Concerning the Co-contraction Gain, Zhou *et al.* reported an optimal value around 10% (Zhou *et al.*, 1996). Fine-tuning of the Co-contraction Gain value was done by computing the resulting loads for the 4 positions (Neutral, Flex_0N, Flex_90N, Flex_180N), with an Antagonist Gain of 25%, an Overlap of 25% and a Co-contraction Gain being 10%, 15%, 20% or 25%.

Table D.2 presents the resulting loads for each position and each value of Co-contraction tested. Co-contraction Gain variation did not influence any of the load components in the Neutral and Flex_0N positions, because of the low recruitment of antagonist muscles in these positions.

The Co-contraction Gain value is important to set carefully, in order to give weight to the antagonist excitation (D.2). As found here, the difference for each load component, between the different values of co-contraction grain are small. Therefore a Co-contraction gain of 20% was chosen here. This value is a little higher than the recommendation made by Zhou *et al.* (Zhou *et al.*, 1996), because hypothesis was made that antagonist muscles' excitation in the spine joint will be triggered for smaller ratio of moments in the antagonist law, than in the knee joint.

One can note the high values of loads for the position Flex_180N, it is important to note that this position cannot be maintained statically, and is therefore not physiological. It is equivalent to handle 3 packs of 6 liters of water at the same time with the back flexed at 30°. Such a position is never encountered in life, that is why high values cannot be taken as representative of a daily situation. This position was however taken into account in this analysis in order to account for a great critical situation for which antagonist activity will be large enough to observe difference with variation of each antagonist parameter.

| **Neutral** | $\mathbf{F_x}$ | $\mathbf{F_y}$ *in N* | $\mathbf{F_z}$ | $\mathbf{M_x}$ | $\mathbf{M_y}$ *in Nm* | $\mathbf{M_z}$ |
|---|---|---|---|---|---|---|
| Net reaction loads | - 31.2 | 5.1 | - 267.2 | - 0.9 | - 8.5 | - 0.1 |
| AG | - 5.1 | 0.2 | - 357.7 | - 0.5 | - 3.4 | - 0.6 |
| ANTAG G. CC 10-25% | 30.5 | - 9.3 | - 453.1 | - 0.1 | - 3.6 | - 0.6 |

| **Flex_0N** | $\mathbf{F_x}$ | $\mathbf{F_y}$ *in N* | $\mathbf{F_z}$ | $\mathbf{M_x}$ | $\mathbf{M_y}$ *in Nm* | $\mathbf{M_z}$ |
|---|---|---|---|---|---|---|
| Net reaction loads | - 31.2 | 5.1 | - 267.2 | - 0.9 | 30.4 | 0.7 |
| AG | 129.3 | - 42.9 | - 710.3 | - 3.2 | 3.0 | 2.8 |
| ANTAG G. CC 10-25% | - 170.5 | - 50.0 | - 830.1 | - 2.1 | 3.6 | 2.6 |

| **Flex_90N** | $\mathbf{F_x}$ | $\mathbf{F_y}$ *in N* | $\mathbf{F_z}$ | $\mathbf{M_x}$ | $\mathbf{M_y}$ *in Nm* | $\mathbf{M_z}$ |
|---|---|---|---|---|---|---|
| Net reaction loads | - 41.5 | 6.8 | - 354.9 | - 1.1 | 84.6 | 1.7 |
| AG | 364.9 | - 116.3 | - 1553.4 | - 8.7 | 7.2 | 6.9 |
| ANTAG G. CC 10% | 485.1 | - 139.5 | - 1823.0 | - 4.8 | 9.4 | 7.3 |
| ANTAG G. CC 15% | 494.9 | - 142.4 | - 1851.1 | - 4.6 | 9.5 | 7.3 |
| ANTAG G. CC 20% | 504.5 | - 145.4 | - 1878.7 | - 4.5 | 9.7 | 7.4 |
| ANTAG G. CC 25% | 514.3 | - 148.3 | - 1906.7 | - 4.3 | 9.8 | 7.4 |

| **Flex_180N** | $\mathbf{F_x}$ | $\mathbf{F_y}$ *in N* | $\mathbf{F_z}$ | $\mathbf{M_x}$ | $\mathbf{M_y}$ *in Nm* | $\mathbf{M_z}$ |
|---|---|---|---|---|---|---|
| Net reaction loads | - 51.7 | 8.5 | - 442.6 | - 1.4 | 138.7 | 2.8 |
| AG | 679.9 | - 216.1 | - 2447.7 | - 10.8 | 15.2 | 13.0 |
| ANTAG G. CC 10% | 928.7 | - 284.8 | - 3014.5 | - 0.5 | 20.7 | 16.2 |
| ANTAG G. CC 15% | 958.2 | - 294.4 | - 3090.3 | 0.4 | 21.4 | 16.7 |
| ANTAG G. CC 20% | 988.9 | - 304.3 | - 3168.9 | 1.3 | 22.1 | 17.1 |
| ANTAG G. CC 25% | 1020.2 | - 314.7 | - 3249.3 | 2.3 | 22.8 | 17.6 |

Table D.2. : Net reaction loads (forces and moments), resulting loads with agonist activity only (AG) and resulting loads with antagonist activity (ANTAG G. CC) with co-contraction gain being 10%, 15%, 20%, 25%.

**ANALYSE QUANTITATIVE ET MODELISATION BIOMECANIQUE DE L'ALTERATION DE L'EQUILIBRE DURANT LE VIEILLISSEMENT**

**RESUME :** Le vieillissement de la population mondiale pose la question : comment bien vieillir ? La chute de personnes âgées est connue pour être le point de départ d'un cercle vicieux conduisant trop souvent à la perte d'autonomie avec un réel coût de prise en charge pour la société et le patient. La chute est la conséquence de la perte d'un équilibre efficace et économe en énergie, résultant d'une synergie entre le squelette, les muscles et les capacités cognitives. L'objectif de cette thèse est de rechercher les premiers signes d'un vieillissement pathologique afin de repérer, en amont, les personnes à risque. La première partie présente la caractérisation de l'alignement postural d'adultes jeunes et vieillissants, par l'analyse de reconstructions 3D du squelette obtenues à partir de radiographies bi-planaires. Elle permet d'identifier un invariant et des stratégies de compensation chez les sujets vieillissants. La deuxième partie s'intéresse au système musculaire via la reconstruction 3D de muscles à partir d'images IRM, pour des adultes jeunes et vieillissants avec déformations rachidiennes. Elle permet de mettre en évidence des changements musculaires en lien avec l'altération de la posture. La dernière partie de cette thèse aborde l'adaptation et la personnalisation d'un modèle biomécanique musculo-squelettique calculant les efforts résultants au niveau inter-vertébral. Une boucle de contrôle vise à limiter ces efforts en activant les muscles requis. L'utilisation de la géométrie 3D personnalisée dans ce modèle, ouvre la voie à une compréhension fine des mécanismes de compensation se produisant au cours du vieillissement, normal ou pathologique. Cette partie révèle l'influence de l'altération de la posture sur le pattern de recrutement musculaire. Cette thèse met en évidence des altérations au cours du vieillissement, ce qui pourrait ouvrir la voie à l'identification de biomarqueurs permettant une meilleure prise en charge en amont des personnes vieillissantes à risque.

**Mots clés :** équilibre, vieillissement, alignement postural, système musculaire, modélisation biomécanique musculo-squelettique.

**QUANTITATIVE ANALYSIS AND BIOMECHANICAL MODELING OF THE BALANCE ALTERATION DURING AGING**

**ABSTRACT :** Aging of the global population challenges scientific community in finding ways to live longer, but also in better condition. Falling of the elderly is known to be the start of a vicious cycle leading to loss of autonomy, involving great costs for the society as well as for the patient. Falling is the consequence of the loss of an efficient balance involving skeleton, muscles and cognitive capacities. The objective of this PhD was to search for early changes leading to pathological aging, in order to detect people at risk. The first part reports the characterization of the postural alignment, of both young and older asymptomatic adults, from 3D reconstruction of their skeleton based on bi-planar X-rays. An invariant was found and compensatory strategies have been identified for aging adults. The second part focuses on the 3D reconstructions of the muscles, based on MRI images, both for young adults and older adults with spinal deformities. This part identifies muscular changes in relation with postural alterations. The last part of this PhD tackles the adjustment and personalization of a biomechanical musculo-skeletal model computing the resulting load in the inter-vertebral joint. The control loop approach of the model aims to limit these loads by activating appropriate muscles. The use of 3D personalized geometry as input of the model allows a better understanding of specific compensatory mechanisms occurring during aging or pathological evolution. This part reveals the influence of the postural alteration on the muscular recruitment pattern. This PhD brings to light aging alterations of the skeleton and muscles; this could lead to biomarkers' identification allowing a better identification of aging people at risk.

**Keywords** : balance, aging, postural alignment, muscular system, biomechanical musculo-skeletal modeling.

ARTS ET MÉTIERS ParisTech

ParisTech
INSTITUT DES SCIENCES ET TECHNOLOGIES
PARIS INSTITUTE OF TECHNOLOGY